

EVALUATING CONCRETE BRIDGE DECK PERFORMANCE

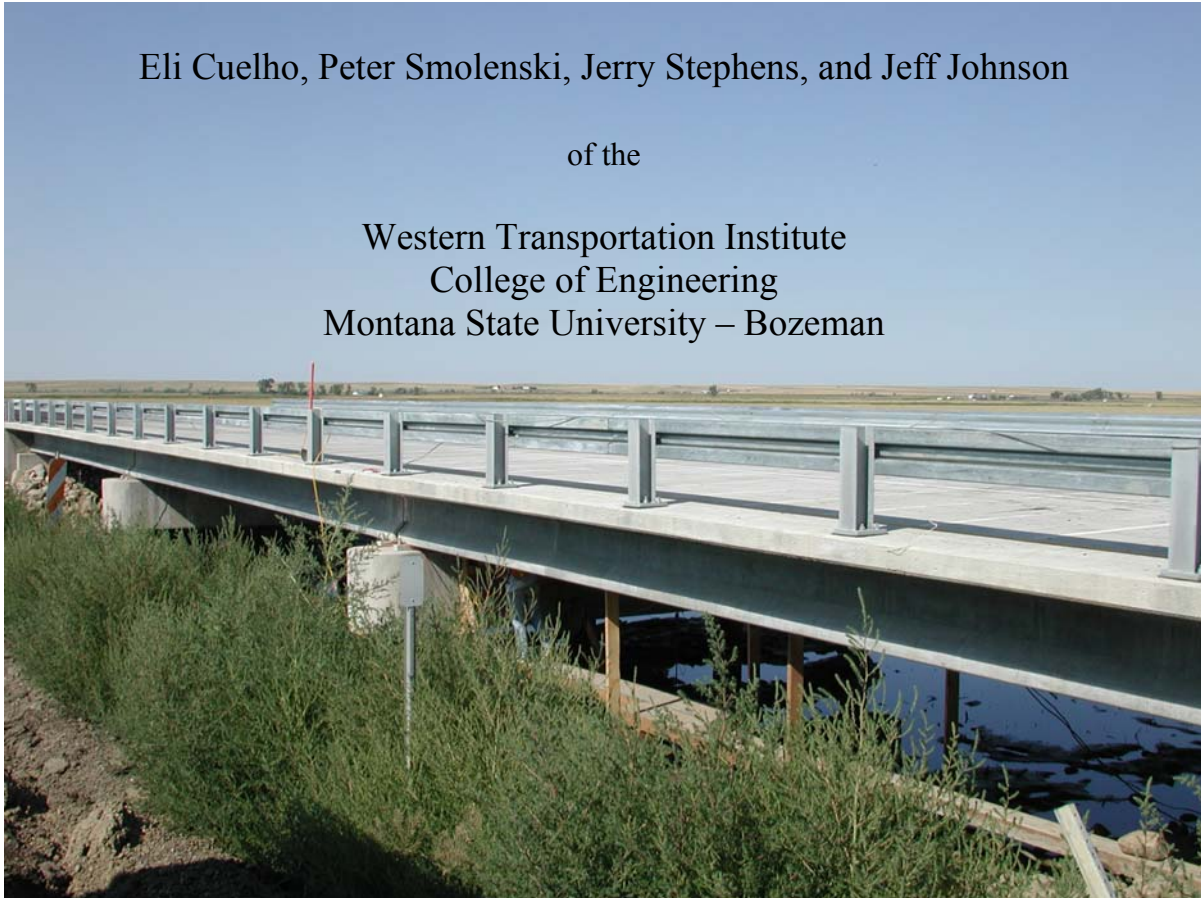
Interim Project Report

by

Eli Cuelho, Peter Smolenski, Jerry Stephens, and Jeff Johnson

of the

Western Transportation Institute
College of Engineering
Montana State University – Bozeman



prepared for the

State of Montana
Department of Transportation
Research Section

in cooperation with the

U.S. Department of Transportation
Federal Highway Administration

July 2004

TECHNICAL REPORT DOCUMENTATION PAGE

1. Report No.	2. Government Access No.	3. Recipient's Catalog No.	
4. Title and Subtitle Evaluating Concrete Bridge Deck Performance		5. Report Date July 2004	
		6. Performing Organization Code	
7. Author(s) Eli Cuelho, Peter Smolenski, Jerry Stephens & Jeff Johnson		8. Performing Organization Report Code	
9. Performing Organization Name and Address Western Transportation Institute PO Box 174250 Montana State University - Bozeman Bozeman, Montana 59717-4250		10. Work Unit No. (TRAIS)	
		11. Contract or Grant No. MSU G&C #426380 MDT Project #8156	
12. Sponsoring Agency Name and Address Montana Department of Transportation 2701 Prospect Avenue Helena, Montana 59620-1001		13. Type of Report and Period Covered Interim Report February 2002 – July 2004	
		14. Sponsoring Agency Code 5401	
15. Supplementary Notes Research performed in cooperation with the Montana Department of Transportation and the U.S. Department of Transportation, Federal Highway Administration.			
16. Abstract One major area of concern regarding concrete bridge deck performance is durability. It is generally acknowledged across the country that the service life of bridge decks designed by traditional procedures is often shorter than desired. The construction of three new bridges near Saco, Montana on Montana Route State 243 provides a unique opportunity for bridge engineers at the Montana Department of Transportation (MDT) to study various techniques for extending the service life of reinforced concrete bridge decks. The Western Transportation Institute at Montana State University was contracted to conduct a comparative study of the performance of three bridge decks in Saco, Montana and assess their long term durability. To accomplish the research objectives, an array of strain and temperature instrumentation was embedded in each of the bridge decks prior to placing the deck concrete. Basic structural behavior of the decks is being characterized by subjecting the decks to controlled live load tests in which vehicles with known characteristics and weights are driven across the bridges while simultaneously monitoring the strain response. During the live load tests conducted in July 2003, two heavily loaded three-axle dump trucks (~285 kN or ~64 kip) were used to load each of the bridge structures along nine longitudinal paths. The analysis of live load data concentrated on transverse deck response, since it was believed to be most significantly affected by the design configuration of each bridge deck. Because the bridges are relatively young, only subtle behavioral differences have emerged to date from the data collected and analyzed from the live load tests. Nevertheless, throughout the preceding analyses of live load test data, it was determined that all three decks exhibit similar global behaviors in the longitudinal direction, and that these behaviors agree with expected behaviors. Overall, for the parameters analyzed in this research, no difference in performance (i.e., occurrence of cracking, non-linear behavior, or possible indication of accumulating damage) was observed between the three bridge decks. In addition, approximately twelve months of long-term data has been collected from embedded sensors in each of the bridge decks. Baseline corrosion tests, topographic surveys, and crack and delamination surveys have been conducted on each of the bridge decks. As expected, obvious differences between the different deck designs have not been observed in the results of these activities, although, recent crack formations may be showing preliminary behaviors unique to each of the designs. The analysis presented herein serves as a baseline to establish the condition of the three bridges before further exposure to traffic and the environment. Data obtained from long term monitoring and the second live load test will help substantiate any conclusions made thus far, and will hopefully provide a more comprehensive body of evidence by which to judge deck design superiority.			
17. Key Words Bridge deck instrumentation, long term monitoring, live load testing, durability, corrosion, field evaluation		18. Distribution Statement No restrictions. This document is available to the public through NTIS, Springfield, Virginia 22161.	
19. Security Classif. (of this report) Unclassified	20. Security Classif. (of this page) Unclassified	21. No. of Pages 193	22. Price

ACKNOWLEDGMENTS

The authors would like to extend their appreciation to the Montana Department of Transportation (MDT) for their sponsorship and participation in this project and the Research and Special Programs Administration (RSPA) for helping fund the instrumentation. We also wanted to specifically thank the MDT Research Section and the technical panel; namely, Craig Abernathy, Sue Sillick, Joe Koleman, Kent Barnes, Miki Lloyd, Bill Fullerton, Mike Lynch, Devin Roberts, Mark Studt and Ted Burch for providing essential technical assistance throughout the project. The following list highlights some of the others who were not directly involved in the project, but who helped us accomplish the work described in this report.

- To Ed Bibeau, Lawrence (Jim) Garfield and John Hasler of the Montana Department of Transportation who drove the test trucks during the live load tests.
- Dan Bisom of the Montana Department of Transportation who organized the installation of the traffic classifier and annual deployment of the portable WIM equipment.
- Jeff Butler of Montana State University facilities services who helped us find a place to store the reinforcement until it was ready for shipment to Saco.
- Dwain Carter of the Montana Department of Transportation who hauled the instrumented rebar up to Saco on the maiden voyage with his truck and trailer.
- Dave Cox of the Montana State University welding and machine shop who allowed us to use the welding shop to instrument the reinforcement.
- Jay Fleming of the Montana Department of Transportation who conducted all of the slump and air entrainment tests and helped us collect concrete samples while the bridge decks were being poured.
- Larry Greufe and Mark Kurokawa of the Montana Department of Transportation who helped with the inspection and coordination of the construction activities.
- Ken Hembree, Bill Juve, and Jim Heikens of the Montana Department of Transportation who helped coordinate the test vehicles for the live load tests and who provided the wooden poles on which to mount the communication antennas and solar panels.
- The Saco Public Schools for allowing us to use their existing communication tower to mount our temporary weather station, as well as supplying a dedicated Internet connection and power for our data acquisition system.
- Jeff Shultz of Bridge Diagnostic Incorporated who allowed us to use the Intelliducers™ during the live load testing and associated laboratory tests.
- Roger Solberg who helped us collect data from the roadside traffic classifier.
- Jim Wickens (Project Manager), Jason Plouffe (Construction Supervisor) and Art Harding (Iron Worker) of Sletten Construction who worked around and with us to make this project a success.

DISCLAIMER

This document is disseminated under the sponsorship of the Montana Department of Transportation and the United States Department of Transportation in the interest of information exchange. The State of Montana and the United States Government assume no liability of its contents or use thereof.

The contents of this report reflect the views of the authors, who are responsible for the facts and accuracy of the data presented herein. The contents do not necessarily reflect the official policies of the Montana Department of Transportation or the United States Department of Transportation.

This report does not constitute a standard, specification, or regulation.

ALTERNATIVE FORMAT STATEMENT

The Montana Department of Transportation attempts to provide reasonable accommodations for any known disability that may interfere with a person participating in any service, program, or activity of the Department. Alternative accessible formats of this document will be provided upon request. For further information, call (406) 444-7693 or TTY (406) 444-7696.

EXECUTIVE SUMMARY

One major area of concern regarding concrete bridge deck performance is durability. It is generally acknowledged across the country that the service life of bridge decks designed by traditional procedures is often shorter than desired. Typically, the deck concrete cracks, allowing corrosive agents (notably deicers) to access the reinforcing steel. The steel subsequently corrodes and the expansive products of this corrosion further fracture the concrete. Cracks in the concrete also promote freeze-thaw damage, since moisture in the cracks can freeze, producing expansive and destructive forces in the deck surface. Customary approaches used to mitigate these problems include, but are not limited to, coating the reinforcing steel with epoxy, reducing the amount of steel reinforcement, using denser concrete mixes, cathodic protection, and sealing the concrete surface. While these measures have all been used for several years, instrumented field tests to determine their performance has been sparse, due in part to the costs involved in conducting such tests and the difficulties encountered in finding appropriate sites.

The construction of three new bridges near Saco, Montana on Montana Route 243 provides a unique opportunity for bridge engineers at the Montana Department of Transportation (MDT) to study various techniques for extending the service life of reinforced concrete bridge decks. Two alternative deck designs were used in addition to the standard bridge deck design used by MDT. The “Conventional” bridge deck (used as a control in this experiment) was designed using the standard practices of MDT’s Bridge Bureau, and utilizes a conventional deck concrete and standard reinforcement layout. The “Empirical” bridge deck was designed using the empirical design approach specified by the AASHTO LRFD Specification for Highway Bridges, which allows for a significant reduction in the steel reinforcement in conjunction with the standard deck concrete. The high performance concrete, “HPC,” bridge deck was designed using the standard reinforcement layout (as in the Conventional deck) but utilized a high performance concrete for the deck. Each of these bridges was constructed less than a mile from one another, so environmental and vehicle demands are the same on the three structures. The Western Transportation Institute was contracted to conduct a comparative study of the performance of three bridge decks in Saco, Montana and assess their long term durability.

To accomplish the research objectives, an array of strain and temperature instrumentation was embedded in each of the bridge decks prior to placing the deck concrete. Strains are measured both in the reinforcement and the concrete at strategic locations using two different technologies: resistance strain gages bonded directly to the reinforcing steel and embedded directly in the concrete, and vibrating wire strain gages embedded in the concrete. Resistance strain gages are very suitable for responding to immediate changes in strain during live load events, while the vibrating wire strain gages respond slower but are more stable over longer periods of time corresponding to diurnal or seasonal strain fluctuations.

Basic structural behavior of the decks is being characterized by subjecting the decks to controlled live load tests in which vehicles with known characteristics and weights are driven across the bridges while simultaneously monitoring the strain response. These tests will reveal how each type of deck structurally transfers wheel loads from their point of application into the supports and to determine the magnitudes of the stresses and strains that develop in the decks as they perform this function. Strain measurements are being used to establish both the manner in which the decks carry loads from their point of application into the supports, and the magnitude of the demands that these loads place on the decks relative to their capacity. This information will help determine the likelihood of immediate and/or long term crack development in the decks from vehicle loads.

During the live load tests conducted in July 2003, two heavily loaded three-axle dump trucks (~285 kN or ~64 kip) were used to load each of the bridge structures along nine longitudinal paths. Generally, tire loads were positioned to be either directly over a girder or at the midspan between girders to characterize deck response under the most critical load positions. Each bridge was subjected to 15 test runs: 8 low speed single-truck tests, 5 high speed single-truck tests, and 2 low speed two-truck tests.

The analysis of live load data concentrated on transverse deck response, since it was believed to be most significantly affected by the design configuration of each bridge deck. The aspects of bridge deck behavior that were investigated included formation of longitudinal cracks, the presence of in-plane stresses, how each bridge carries load, transverse deck integrity over the girders, and whether the decks exhibit non-linear behavior. These various items are indicative of deck condition relative to stiffness, cracking, and deformation behavior. Each of these behaviors was examined using data from the strain gages bonded to the reinforcement in the transverse direction. The height of the bending neutral axis within the deck, the relative magnitude of the bending moments experienced by the decks, and the validity of superposition for calculating deck demands under multiple vehicle events were used to study these behaviors.

Because the bridges are relatively young, only subtle behavioral differences have emerged to date from the data collected and analyzed from the live load tests. At this early date, it is difficult to assess what these differences indicate with regard to the overall durability and structural efficiency of each deck type. The significance of these differences in behavior relative to performance may become clearer as additional data is collected over the remainder of the project. Nevertheless, throughout the preceding analyses of live load test data, it was determined that all three decks exhibit similar global behaviors in the longitudinal direction, and that these behaviors agree with expected behaviors.

Analysis of the strain data collected in the transverse direction of the decks during the live load tests revealed the following conclusions:

- Positive moment regions of the decks do not reveal the presence of longitudinal cracks on the underside of the deck.
- Likewise, the existence of longitudinal cracks in the top surface of the decks is also unlikely in negative moment regions of the deck.
- In-plane axial forces (generally less than 10 $\mu\epsilon$) are inferred in each of the decks, according to an analysis related to the position of the bending neutral axis.
- Negative bending over the girders is not critical under live load demands.
- Analysis of the relative stiffness of each of the bridge decks showed that the Empirical deck is softest, both longitudinally and transversely, despite classic computation of Girder Distribution Factors, which gives the appearance that the Empirical deck is stiffer in the transverse direction.
- Linear superposition works well for all three bridge decks, indicating that all three decks are behaving linear-elastically.

Overall, for the parameters analyzed in this research, no difference in performance (i.e., occurrence of cracking, non-linear behavior, or possible indication of accumulating damage) was observed between the three bridge decks.

Approximately twelve months of long-term data has been collected from embedded sensors in each of the bridge decks. All the active sensors currently provide measurements once every hour. While the work up to this point has focused mainly on the analysis of the live load data, strain and temperature data from the long term monitoring effort will be studied to correlate changes in deck performance with the vehicle and environmental loads they experience.

Baseline corrosion tests, topographic surveys, and crack and delamination surveys have been conducted on each of the bridge decks. As expected, obvious differences between the different deck designs have not been observed in the results of these activities, although, recent crack formations may be showing preliminary behaviors unique to each of the designs.

The analysis presented herein serves as a baseline to establish the condition of the three bridges before further exposure to traffic and the environment. Data obtained from long term monitoring and the second live load test will help substantiate any conclusions made thus far, and will hopefully provide a more comprehensive body of evidence by which to judge deck design superiority.

TABLE OF CONTENTS

1	Introduction.....	1
1.1	Background	1
1.2	Objectives and Scope	2
1.3	Project Timeline	2
2	Literature Review.....	4
2.1	Bridge Deck Design Considerations	4
2.2	Live Load Testing of Bridges.....	6
2.3	Instrumentation.....	8
3	Description of the Bridges	11
3.1	Concrete Bridge Deck	12
3.2	Steel Reinforcement	18
3.3	Prestressed Girders	18
4	Development and Implementation of the Instrumentation Plan	20
4.1	Gage Locations.....	20
4.2	Position Referencing Nomenclature.....	22
4.3	Instrumentation.....	23
4.3.1	Resistance Strain Gages.....	23
4.3.2	Vibrating Wire Strain Gages.....	26
4.3.3	Concrete Embedment Strain Gages	27
4.3.4	Intelliducers™.....	28
4.4	Data Acquisition System	29
4.4.1	Data Acquisition Computer	30
4.4.2	Multiplexers	31
4.4.3	Communication and Power.....	31
4.4.4	Supporting Circuitry	32
4.4.5	Long-Term Monitoring Circuit Arrangement.....	38
4.4.6	Live Load Testing Arrangement.....	39
4.5	Installation and Assemblage.....	40
5	Weather Station.....	43
6	Live Load Testing	45
6.1	Test Vehicles	45
6.2	Testing Procedure.....	47
6.3	Data Processing	50

7	Results and Analysis of Live Load Test Data.....	51
7.1	General Behaviors	51
7.2	Deck Cracking and Axial Strain Analysis.....	56
7.2.1	Position of Neutral Axis in Bridge Decks.....	58
7.2.2	Deck Integrity over Girders	75
7.2.3	Deck Stiffness	80
7.2.4	Superposition	86
7.3	High Speed Live Load Tests	88
7.4	Review of Analysis Observations	89
8	Long Term Monitoring	91
8.1	Internal Strain Measurements.....	91
8.2	Internal Temperature Measurements.....	95
8.3	Large Event Monitoring	96
8.4	Corrosion Testing.....	98
8.4.1	Half-Cell Potential Tests.....	98
8.4.2	Carbonation Tests	100
8.5	Crack Mapping.....	100
8.6	Surveying.....	103
9	Summary and Conclusions	105
9.1	Summary	105
9.2	Conclusions	106
10	References.....	107
	Appendix A: Deck Concrete Material Properties	A-1
	Appendix B: ASTM Specification References	B-1
	Appendix C: Deck Rebar Material Properties	C-1
	Appendix D: Prestressed Girder Material Properties.....	D-1
	Appendix E: Instrumentation Plan.....	E-1
	Appendix F: Crack Survey Maps.....	F-1

LIST OF TABLES

Table 1: Average Slump and Air Content from Bridge Deck Concrete	13
Table 2: Concrete Samples Collected during Construction.....	14
Table 3: Concrete Sampling and Testing Matrix – Conventional Deck, Cast 6/05/03.....	15
Table 4: Concrete Sampling and Testing Matrix – Empirical Deck, Cast 6/02/03.	16
Table 5: Concrete Sampling and Testing Matrix – HPC Deck, Cast 5/28/03.	17
Table 6: Average 28-Day Concrete Strengths	18
Table 7: Modulus of Elasticity of Deck Concrete	18
Table 8: Average 28-day Prestressed Girder Concrete Compressive Strengths.....	19
Table 9: Actual Neutral Axis Positions for the Conventional Bridge Deck.....	64
Table 10: Actual Neutral Axis Positions for the Empirical Bridge Deck.....	65
Table 11: Actual Neutral Axis Positions for the HPC Bridge Deck.....	65
Table 12: Bending Neutral Axis Heights at Various Cracking Levels under Positive Moment.....	67
Table 13: Values of ϕ at Gage Location D-4.....	68
Table 14: Actual Neutral Axis Heights (Gage Location D-4)	69
Table 15: Back-Calculated Axial Strains for the Conventional Deck	71
Table 16: Back-Calculated Axial Strains for the Empirical Deck	71
Table 17: Back-Calculated Axial Strains for the HPC Deck.....	72
Table 18: Values of ϕ at 40 m during ST-U Test	80
Table 19: Summary of Transverse Stiffnesses for Each Deck	81
Table 20: Bridge Concrete Parameters	82
Table 21: AASHTO LRFD Distribution Factors.....	82
Table 22: Typical GDF Calculation, Single truck Test R (ST-R) on the Empirical Deck	84
Table 23: Summary of Saco Bridge Girder Distribution Factors	85
Table 24: Bridge Deck Stiffness Parameters	85
Table 25: Example Summary of Large Event Data Collected on Saco Bridges	97
Table 26: Categories of Corrosion Probability for the Half-Cell Test.....	99
Table 27: Results of First Series of Half-Cell Testing.....	100
Table 28: Date of Crack Surveys.....	101

LIST OF FIGURES

Figure 1: Completed Saco Bridge.....	3
Figure 2: Reported Deck Strains at Midspan (from Stallings and Porter, 2002).....	8
Figure 3: Plan View of Transverse Gage Lines (from Cao et al., 1994)	10
Figure 4: Typical Transverse Cross-Section Showing Gage Point Locations (from Cao et al., 1994)	10
Figure 5: Elevation View of One of the Bridges	11
Figure 6: End View of Conventional Bridge Deck.....	11
Figure 7: Example Reinforcement Densities of the Conventional and HPC Decks (a), and the Empirical Deck (b).....	12
Figure 8: Placing the Deck Concrete	13
Figure 9: Dimensioned Cross-Sectional View of Saco Bridge Girders.....	19
Figure 10: General Location of Strain Gages Oriented in the Longitudinal Direction (plan view)	21
Figure 11: General Location of Strain Gages Oriented in the Transverse Direction (plan view)	22
Figure 12: General Location of Intelliducer™ Gages Oriented in the Longitudinal Direction (plan view)	22
Figure 13: Gage Reference Numbering System	23
Figure 14: Resistance Strain Gage from Micro-Measurements Group, Inc. (CEA-06-250UN-350)	24
Figure 15: Strain Gage Bonded to the Reinforcement before (Top) and after (Bottom) Environmental Protection	25
Figure 16: Vibrating Wire Strain Gage (VCE-4200).....	26
Figure 17: Illustration of Finished Gage Location Showing All Three Embedded Gages	27
Figure 18: Concrete Embedment Strain Gage (EGP-5-350)	27
Figure 19: Intelliducer™ Mounted on Concrete Surface.....	28
Figure 20: Intelliducer™ Mounted to Bottom of Concrete Girder with Extensions	29
Figure 21: Various Components within a Data Acquisition Box	30
Figure 22: Communication Path for Long Term Monitoring	32
Figure 23: Ideal Wheatstone Bridge Circuit Arrangement	33
Figure 24: Wheatstone Bridge Arrangements Used on Saco Bridges	34
Figure 25: Diagram of Daughterboard Circuitry	36
Figure 26: Alternative Circuit Design for Single-Ended Measurements.....	37
Figure 27: Data Acquisition Layout during Long-Term Monitoring	39
Figure 28: Data Acquisition Layout during Live Load Testing	40
Figure 29: Example of Cable Run	41
Figure 30: Data Acquisition and Power Enclosure Arrangement under the Bridge Decks.....	42

Figure 31: Internet Screenshot of Real-Time Weather Data from the Saco Weather Station	44
Figure 32: Dimension and Weight of the Sterling 3-Axle Dump Truck Used during Live Load Tests	46
Figure 33: Dimension and Weight of the Volvo 3-Axle Dump Truck Used during Live Load Tests	46
Figure 34: Sterling 3-Axle Dump Truck.....	47
Figure 35: Photograph of Longitudinal Lines Used for Truck Positioning during Live Load Testing	48
Figure 36: Truck Positions for Live Load Tests	49
Figure 37: Illustration of Global Longitudinal Behavior.....	52
Figure 38: Strain History - Conventional Deck longitudinal Gage Location D-3 (ST-T Test)	53
Figure 39: Strain History - All Three Decks Longitudinal Gage Location D-3 (ST-T Test)	54
Figure 40: Strain History - Empirical Deck Longitudinal Gage Location F-1 (ST-T Test)	55
Figure 41: Strain history - all three decks longitudinal Gage Location F-1 (ST-T test).....	56
Figure 42: Transverse Gages of Interest (Gage Line D).....	58
Figure 43: Homogeneous Deck Cross-Section Geometry with Calculated Bending Neutral Axis and Expected Bending Strain Profile (uncracked)	59
Figure 44: Saco Bridge Deck Cross-Section Geometries with Calculated Bending Neutral Axes and Expected Bending Strain Profiles (uncracked)	61
Figure 45: Typical Positive Moment Response from Bonded Strain Gages (Gage Location D-4, ST-S Test).....	62
Figure 46: Illustration of How Actual Neutral Axis Height is Determined.....	63
Figure 47: 40 m and 42 m Truck Positions, Relative to Gage Line D.....	64
Figure 48: Theoretical Cracking Scenarios.....	67
Figure 49: Illustration of Neutral Axis Shift Due to In-Plane Axial Strains under a) Positive Moment and b) Negative Moment	70
Figure 50: Illustration of Axial Tension Behavior at Gage Location D-1	73
Figure 51: Transverse Strain Profile Revealing Axial Tension (ST-S Test at 40 m Truck Position)	74
Figure 52: Strain History at Gage Location D-5 during ST-U Test (Conventional Deck).....	76
Figure 53: Strain History at Gage Location D-5 during ST-U test (All Three Decks).....	77
Figure 54: Illustration of Global and Local Bridge Deck Behavior from Live Loads	78
Figure 55: Transverse Strain Profile Showing Tensile Shift under Negative Moment (ST-X Test at 40 m)	79
Figure 56: Bridge Profile at Center Span.....	83
Figure 58: Transverse Strain Profile Showing Superposition in the Conventional Deck from Gage Line D at the 40 m Truck Position.....	87

Figure 59: Transverse Strain Profile Showing Superposition in the Conventional Deck from Gage Line D at the 40 m Truck Position.....	88
Figure 60: Comparison of the Longitudinal Strain Response in Low and High Speed Tests for the Conventional Deck.....	89
Figure 61: Long Term Data Showing the Formation of Cracks in All Three Decks.....	92
Figure 62: Long Term Data Illustrating Non-Cracked Portion of the Deck.....	93
Figure 63: Comparison of Cracked and Non-cracked Position in the Conventional Deck.	94
Figure 64: Comparison of Bottom Deck Temperatures during the Cure Cycle.	96
Figure 65: Typical Strain Response during a Large Vehicle Event.....	98
Figure 66: Illustration of Half-Cell Test on Saco Bridges.....	99
Figure 67: Full-Depth Crack in Empirical Deck as Seen from Underside	102
Figure 68: Cracks in the Overhang of the HPC Deck.....	102
Figure 69: Surface Cracks on the Bottom of the HPC Deck	103
Figure 70: Survey Points Shown on Plan View of Bridge Deck	104

1 INTRODUCTION

1.1 Background

The durability of concrete bridge decks is a major concern for designers. It is generally acknowledged across the country that the service life of bridge decks designed by traditional procedures is often shorter than desired. Typically, the concrete in the decks cracks, which allows agents of corrosion (notably deicers) to penetrate to the reinforcing steel. The steel subsequently corrodes, and the expansive products of this corrosion further crack the concrete. Cracks in the concrete also contribute to freeze-thaw damage in the concrete, as moisture in the cracks can freeze, which also produces expansive and thus destructive forces in the material. Approaches to mitigating these problems include coating the reinforcing steel with epoxy, using less reinforcing steel, using less permeable concretes, and sealing the concrete surface. While these mitigating measures have all been used for several years, instrumented field tests on their performance has been sparse, in part due to the costs involved in conducting such tests and the difficulties encountered in finding appropriate sites.

While planning the replacement of three bridges on Highway 243 north of Saco, Montana, bridge engineers at the Montana Department of Transportation (MDT) recognized and seized a unique opportunity to evaluate different deck designs built by the same contractor and subsequently exposed to the same environmental and vehicular conditions. Thus, variability in test articles and conditions between test sites typically encountered in large-scale field investigations was minimized in this situation. The primary focus of this research project has been to compare the performance of three different bridge deck designs.

All three bridges utilized a concrete slab on prestressed stringer construction, but incorporated a different concrete deck design. One bridge deck was designed using standard practices of MDT's Bridge Bureau and built using conventional concrete and reinforcement layout. As such, it is referred to as the "Conventional" bridge deck. The second deck, known as the "Empirical" bridge deck, was designed using the empirical design approach presented in the AASHTO LRFD Specification for Highway Bridges. This design allowed for an overall reduction in the reinforcing steel, but still used a conventional concrete mix design. The third bridge deck, referred to as the "HPC" bridge deck, was designed in the same manner as the Conventional deck, but replaced the standard concrete with high performance concrete (HPC).

A variety of gages were embedded in the decks to monitor their relative performance. The instrumentation consists of strain gages bonded directly to the reinforcement and embedded in the concrete. Gages were placed at locations within the deck where critical levels of stress are expected to occur. The data collected from these gages were monitored during live-load events and are being continually monitored to capture long term environmental effects.

1.2 Objectives and Scope

The objective of this project is to investigate the performance of three different types of concrete bridge decks, namely:

1. a conventionally reinforced deck made with standard concrete, designed and constructed following standard practices of MDT's Bridge Bureau,
2. a deck with reduced reinforcement made with normal concrete, designed following the empirical design approach presented in the AASHTO LRFD Specifications for Highway Bridges and constructed following standard MDT practice, and
3. a conventionally reinforced deck made with high performance concrete (HPC) developed following FHWA guidelines.

The structural behavior of these decks under vehicle live loads and their long-term durability under environmental and vehicular demands will be studied using instrumentation embedded in the bridge deck. The performance of the decks is being compared and contrasted with due consideration of the known and projected costs for each type of deck.

1.3 Project Timeline

Prior to construction of the three new bridges on Route 243 near Saco, Montana, a temporary weather station was installed atop the Saco Public School in August 2002 to provide weather information during the life of the project, and provide a conduit for future data transmission from the bridges. Bridge construction at the Saco bridge site began during the winter of 2002-2003. While the old bridges were being removed and the new support structure for the replacement bridges was being constructed, an instrumentation plan was being developed to determine the layout of the embedded instrumentation. Immediately following, the reinforcement strain gages were bonded to rebar at Montana State University. Additionally, the data acquisition system was being programmed and associated circuitry was built. By April 2003, the bridge superstructure was in place and all deck forming was complete. The instrumented reinforcement was delivered to the Saco construction site and installed in the bridge decks. Soon after, the remaining instrumentation was tied in place, all instrumentation cabling was routed, the communication and power hardware was installed, and the instrumentation was activated. Specific locations of all the instrumentation were recorded prior to placement of the deck concrete.

The concrete was placed in the HPC deck on May 28, 2003; in the Empirical deck on June 3, 2003; and in the Conventional deck on June 5, 2003. Concrete samples were collected from several trucks in the instrumented section of the bridges. Over the next month, the bridges were allowed to cure, the deck forms were removed, the saw-cuts were made over the south bents, the decks were grooved, the guardrail was installed, and the bridge approaches were paved. Figure 1

shows one of the finished Saco bridges. The first live load tests were conducted in late July 2003, as well as the benchmark durability tests (i.e., half-cell tests and carbonation tests). Additionally, the first topographic survey of the bridge decks was conducted. All three bridges were then opened to public use in early August 2003.



Figure 1: Completed Saco Bridge

This report documents all of these activities, and includes an extensive analysis of the first set of live load tests. The second set of live load tests is scheduled for July 2005. Less work has been done with regard the analysis of the long term data collected since the decks were cast, but will be the focus of the analysis effort over the next year. Nevertheless, a preliminary examination of some of the early long term data is provided.

Prior to beginning the work outlined above, available literature on bridge deck performance was collected, reviewed and summarized. This report begins with a summary of this review.

2 LITERATURE REVIEW

Reinforced concrete has emerged as a highly versatile building material in the modern age. For certain applications, it has several advantages over other building materials. Due to the combination of the steel and the concrete, the structure is effectively strong under both tensile and compressive demands. This strength is offered at a significantly reduced cost from steel alone. Additionally, reinforced concrete may be formed into countless structural and aesthetic forms not readily available when using steel or other building materials. As with all materials, reinforced concrete's benefits are accompanied by disadvantages. Within the reinforced concrete matrix, concrete is susceptible to brittle fracture, and the steel is susceptible to corrosion damage.

Historically, as the use of reinforced concrete became more widespread, it was important to test and understand its physical properties and behaviors under specific loading conditions. Due to the deterioration of transportation infrastructure in the United States, a renewed interest has emerged toward understanding reinforced concrete specifically as it applies to highway bridges (Lenett et al., 2001).

Cao (1996) states that about one-third of the nation's bridges have deficient decks. In this regard, one of the major problems that bridge decks face is corrosion of the reinforcing steel. This damage is generally initiated by cracking of the concrete in the top of the deck. These cracks allow moisture, deicing chemicals, and air to reach the steel and sustain the oxidation process. As the reinforcing steel corrodes, it debonds from the surrounding concrete, thereby reducing composite action, as well as overall structural integrity. Furthermore, due to the expansive nature of the corroding steel and the relatively low tensile strength of concrete, portions of the deck may spall as the corrosive activity proceeds. Many possible solutions to this problem are currently under investigation and include: epoxy-coated rebar, fiber-reinforced polymer (FRP) reinforcement, fiber-reinforced concretes (FRC), low-permeability concretes, and reduced amounts of reinforcement (Cao, 1996; Bakht et al., 2000). To date, full-scale, instrumented field testing of these damage mitigation techniques, as applied to bridge decks, has been sparse.

2.1 Bridge Deck Design Considerations

The deck-on-girder design used in the Saco bridges is typically comprised of a reinforced concrete slab supported by two or more girders made of steel, timber, or prestressed concrete, and is one of the most common bridge designs in use today (Cao et al., 1994). In this configuration, the deck directly supports tire loads by transferring them transversely to the adjacent girders. The bridge deck is compositely attached to the girders using shear connectors to better resist longitudinal moments and transfer loads to the supporting substructure.

Traditionally, the AASHTO (2000) bridge deck design method assumes that slab-on-girder deck sections behave as one-way slabs acting in the transverse direction (perpendicular to

traffic). In 1930, Westergaard represented the bridge deck as a continuous beam supported by rigid girders which are unable to deflect vertically (Mourad and Tabsh, 1999; Csagoly and Lybas, 1989; and Cao et al., 1994). It is generally acknowledged that Westergaard's model yields conservative designs relative to strength and safety. More recently, research has sought to make deck design more efficient by modeling the actual load carrying mechanisms more accurately. The discovery of a mechanism called "internal arching" allows designers and researchers to develop sufficiently strong designs using less reinforcing steel than is required in conventionally designed decks. This has become a popular technique since reducing the amount of reinforcing steel reduces the probability of corrosion damage and increases efficiency.

Contrary to traditional models, the deck slab does not actually support wheel loads completely in flexure. Instead, a 'compressive dome' forms due to cracking in the positive moment regions (i.e., bottom fibers) of the deck concrete (Csagoly and Lybas, 1989; Fang et al., 1990; AASHTO, 2000). This 'compressive dome' supports wheel loads by relying upon the lateral restraint provided by the surrounding deck concrete and other structural elements such as girders and diaphragms. Additionally, remaining flexural loads are carried by the reinforcing steel in the bottom mat (Csagoly and Lybas, 1989). In-plane compressive membrane forces found in the concrete near the tire generally helped to establish the presence of the arching phenomenon.

Canada has developed a deck design that takes advantage of this arching behavior, commonly referred to as the 'Ontario' deck design. For bridge decks meeting certain geometric criteria, the Ontario approach allows the total amount of reinforcing steel to be reduced by approximately 30%. The primary design guideline requires a minimum steel area of 0.3% of the concrete area in both the top and bottom reinforcing mats to help control cracking and maintain confinement within the deck. Based on component testing and finite element analysis (FEA), AASHTO (2000) has included provisions for an 'empirical design,' which is similar to the Ontario deck design except that a further reduction in the top layer of reinforcing steel is allowed. Minimum top and bottom-mat steel areas of 0.2% and 0.3% of the concrete area, respectively, are required to improve crack control and maintain confinement within the deck.

To evaluate the validity of the internal arching behavior, Fang et al. (1990) tested a full-scale bridge specimen at the University of Texas at Austin. The deck concrete had a compressive strength of approximately 29 MPa. At wheel loads up to three times the AASHTO service wheel load of 92.5 kN, no compressive membrane stresses (indicative of internal arching) were observed, however, membrane tension was observed. Above this load, cracking began to occur in the positive moment regions of the slab, initiating internal arching. As expected, internal arching and failure in punching shear were also observed in the specimen at higher loads.

To further validate the credibility of the empirical deck design method, Csagoly and Lybas (1989) reviewed several research projects related to internal arching behavior in bridge decks.

One laboratory experiment proved that bridge decks with two mats of reinforcement fail in punching shear at loads six times larger than the design wheel load. All of the reviewed studies confirmed that the ultimate capacity and serviceability of the empirical deck design is comparable to the traditional deck design methods.

Fenwick and Dickson (1989) conducted laboratory tests on reinforced concrete slabs to investigate structural benefits from membrane action. Their results indicated increased strength in confined plates, suggesting membrane action was potentially contributing to load carrying capacity. However, without further testing they were unable to conclusively establish the relationship between membrane action and increased strength.

A more aggressive approach to mitigate steel corrosion is to completely remove all steel from the top mat, as proposed by Cao (1996). The slab theory of Westergaard requires the placement of reinforcing steel near the top of the deck to resist negative moments that occur over the girders. However, Cao (1996) concluded that slab theory alone was not sufficient for use in deck design. Due to the underlying differential deflections between girders, the negative moments incurred in the deck slab were less than those predicted by a slab supported on rigid girders. Cao et al. (1994) performed live load testing on the South Platte River Bridge near Commerce City, Colorado to evaluate this conclusion. Based on his results, the top mat of reinforcing steel was not necessary to withstand the negative bending moment over the girders induced by truck loads. Although these conclusions have not been included in the bridge design provisions of AASHTO (2000), his findings are important and may help others properly understand and interpret live load test results.

Even more recently, Canadian engineers have developed ‘steel-free’ concrete bridge deck designs, which take advantage of arching action to completely eliminate all of the reinforcing steel within the deck (Bakht and Lam, 2000; Sargent et al., 1999; Bakht and Mufti, 1998). In lieu of the internal steel reinforcement, exterior steel ‘straps’ are connected between adjacent girders to provide the lateral confinement necessary to maintain arching action. Other steel-free deck designs utilize fiber-reinforced polymer (FRP) bars or grids within the deck concrete in place of traditional steel rebar (Bakht et al., 2000). Both steel-free methods effectively mitigate any damage due to corrosion of the reinforcing steel by completely removing it from inside the deck.

2.2 Live Load Testing of Bridges

It is important to evaluate how bridge decks respond to vehicle loads (namely heavy vehicles) and how that response affects the expected durability of the deck over time. Changing the amount and/or configuration of the reinforcing steel may influence the bridge deck’s load-carrying capacity and/or load transfer path. Although the opportunity for cracking and corrosion may be reduced or eliminated, the overall stability and integrity of the bridge deck must not be

compromised. Live load tests are commonly used to evaluate the behavior and integrity of bridges. The majority of live load tests conducted on deck-on-girder bridges have focused mainly on the girder system to determine how loads are distributed among these members. Many studies generally attempt to quantify the load carrying capacity of the bridge based on properties of the girders, and how loads are globally transferred through the superstructure and substructure to the ground. Girder distribution factors (GDFs) are commonly reported as a measure of bridge performance (Nassif et al., 2003; Tabsh and Tabatabai, 2001; Yang and Myers, 2003; Amer et al., 1999).

Even though bridge decks are acknowledged as a primary source of deficiency, very few projects have focused specifically on the internal response and the durability of bridge decks under live and environmental loads. A limited number of projects have investigated bridge deck responses to these load types as part of a larger study. Lenett et al. (2001) installed instrumentation and conducted live load tests on the HAM-126-0881L bridge near Cincinnati, Ohio. The instrumentation for the project was extensive, monitoring nearly every aspect of the bridge – abutments, piles, stringers, and the deck. Most deck sensors were placed in the longitudinal direction to construct strain profiles in the deck-girder composite sections. Monitoring was conducted during construction of the bridge to evaluate what effects the bridge experienced prior to being commissioned. Before traffic was allowed on the bridge, it was subjected to live load tests (mostly static). Bending stresses in the girders and the distribution of longitudinal strains across transverse strips of the deck were the primary focus of the analysis. The response of the bridge to environmental fluctuations was then monitored over at least one full year.

Stallings and Porter (2002) performed live load tests on the Uphapee Creek Bridge in Alabama, in which some measurements of the deck response were made. This bridge deck was constructed using a high performance concrete (HPC) mix design. Comparisons of test results with AASHTO predictions were of greatest interest to the authors. Although deck strains recorded from strain gages attached to transverse reinforcement were measured and reported, little comment was offered with regard to their meaning. Typical deck strain results reported by Stallings and Porter (2002) are shown in Figure 2. Internal deck strains recorded from strain gages located at the longitudinal midspan and transversely between two girders are shown. The abbreviations “TT” and “BT” refer to top transverse and bottom transverse gages, respectively, and, “TL” and “BL” refer to top longitudinal and bottom longitudinal gages, respectively.

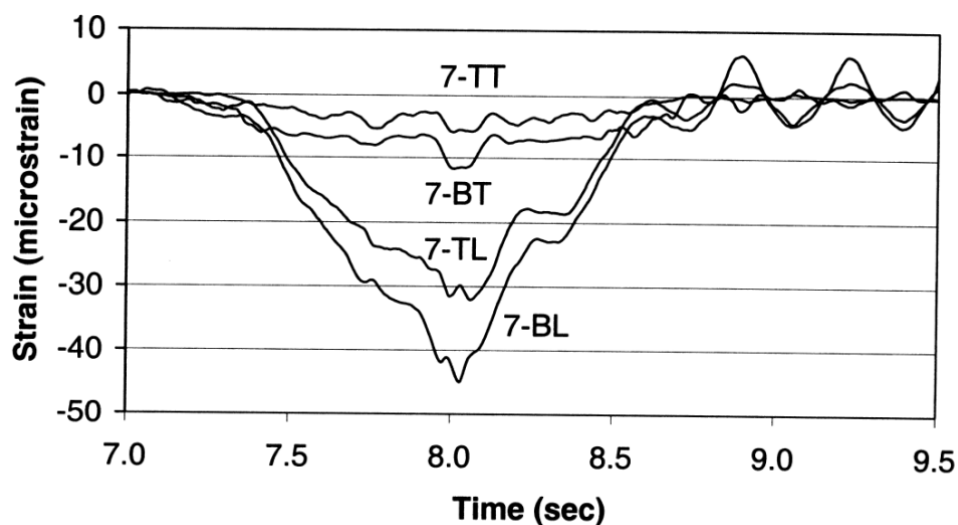


Figure 2: Reported Deck Strains at Midspan (from Stallings and Porter, 2002)

Cao (1996) performed live load testing on the South Platte River Bridge near Commerce City, Colorado to validate a simplified method to analyze and model the behaviors of reinforced concrete bridge decks. The test truck used by Cao (1996) had a front axle weight of 73.4 kN (16.5 kips), a combined rear tandem axle weight of 252 kN (56.7 kips), and a total trailing axle weight of 145.5 kN (32.7 kips). The total weight of the truck was 471.5 kN (106 kips), which is 47% more than a standard HS20 truck, however, the wheel and axle spacing were similar. The bending moments in the bridge deck were calculated from strain data. This analysis helped to verify his hypothesis that negative moments in the bridge deck are reduced by differential girder deflections.

2.3 Instrumentation

Instrumentation is commonly used to monitor and understand the behavior of various structures. On reinforced concrete structures, instrumentation may be placed internally or externally depending on what types of information are desired. Typical sensors include strain gages, temperature sensors, tilt meters, accelerometers and displacement gages. Strain gages may be embedded in the concrete or attached directly to the reinforcing steel using a variety of configurations and techniques. Many research projects have utilized instrumentation, yet few have focused their attention on strains within the bridge deck. Following are a few examples of such projects.

In a study by Buckler et al. (2001), researchers at the Virginia Transportation Research Council (VTRC) developed a computational model to represent the behavior of a reinforced concrete bridge deck. They successfully validated their model using experimental results from the Willis River Bridge, an instrumented bridge deck in Buckingham County, Virginia. Instrumentation was designed to measure the displacement of the four stringers, longitudinal

strains in the flanges of the four stringers, transverse deck strains midway between the three sets of stringers, and the natural frequency of the bridge (Buckler et al., 2001).

Cantilever deflection gages (CDG) were attached to the lower flanges of each stringer to determine the deflection of all four steel stringers. The CDGs used in this research consisted of a triangular steel plate instrumented with strain gage. The plate was attached to flange of the stringer at its midspan using C-clamps, and a weight suspended from the plate rested on the ground below. The suspended weight imparts an initial strain on the plate, so as the bridge deflects under a load the strain in the CDG decreases. Strain in the CDGs was converted into deflections of the stringer at midspan.

Resistance strain gages were bonded to the flanges of the stringers using an epoxy to measure longitudinal strain. Two stringers had both top and bottom flanges instrumented, while the remaining stringers only had gages on the bottom flanges.

Five weigh in motion gages (WIM) were used to measure strain in the bottom of the concrete. Three gages were placed on the underside of the deck midway between each set of stringers to measure transverse strain. A fourth WIM gage was oriented in the longitudinal direction near the interface between the top flange of the second stringer and the bottom of the concrete deck. The fifth WIM gage was placed in the same location, but oriented in the transverse direction.

Accelerometers were used to determine the natural frequency of the bridge. A single accelerometer was placed on the top surface of the bottom flange of each girder at their midspan. All of the data mentioned were recorded near the middle of the first span, between the abutment and first pier.

For the field investigation of the South Platte River Bridge near Commerce City, Colorado (Cao et al., 1994), bridge deck response was monitored using strain gages embedded at different locations within the deck concrete. The strain gages were welded onto pieces of #4 rebar having several bends to ensure good bonding with the surrounding concrete. Five transverse gage lines were selected; three in the experimental portion of the deck, and two in a control section (Figure 3). In the experimental portion of the deck, the first and third gage lines are located near the ends of the span. The second gage line was near, but not exactly at the center of the span. In the control portion of the deck, the same gage lines were used, except that the gage line near the pier was not included. There were seven gage points within each gage line, as shown in Figure 4. At each gage point, gages were typically placed near the top and bottom of the bridge deck in either the transverse or longitudinal direction.

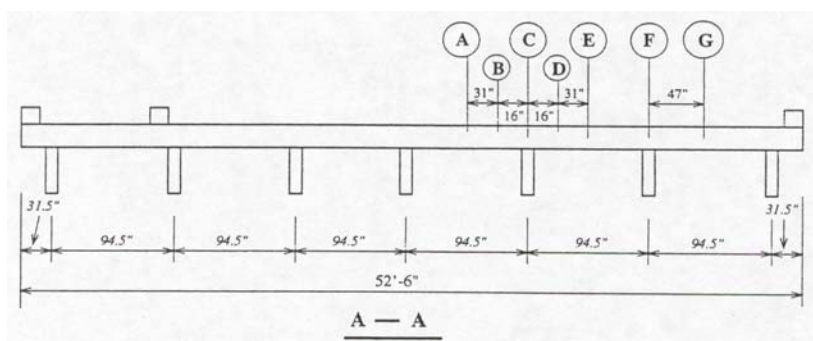


Figure 3: Plan View of Transverse Gage Lines (from Cao et al., 1994)

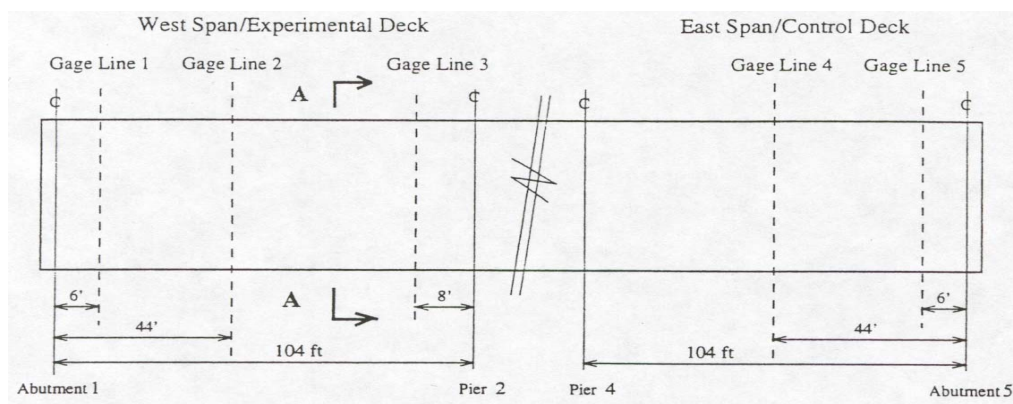


Figure 4: Typical Transverse Cross-Section Showing Gage Point Locations (from Cao et al., 1994)

3 DESCRIPTION OF THE BRIDGES

The three new bridges were constructed on Route 243 approximately one mile north of Saco, Montana. Route 243 is a local route that has an average annual daily traffic count of 220 (1998), with 11.5% being trucks. Much of the anticipated loading will come from heavy farm machinery and trucks, which can impose high demands.

All three bridges are 44.5 meters (146 ft) long and 9.1 meters (29.8 ft) wide. The superstructure consists of three spans, as shown in Figure 5. The stringers that support the deck are standard, Type-I prestressed concrete I-beams spaced at 2.4 meters (7.9 ft) on center, as shown in Figure 6. The thickness of each deck is 210 mm (8.3 in). Design specifications for the Conventional and Empirical decks required 21 MPa (3046 psi) strength concrete, while the HPC deck design specified 28 MPa (4061 psi) strength concrete.

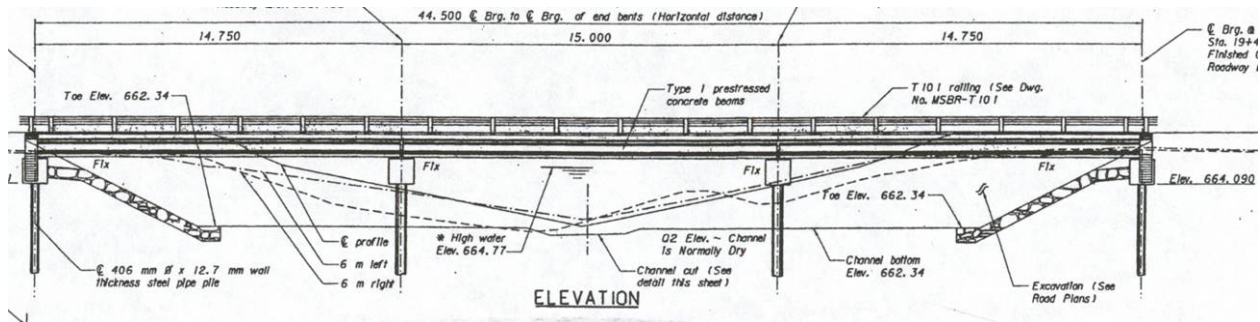


Figure 5: Elevation View of One of the Bridges

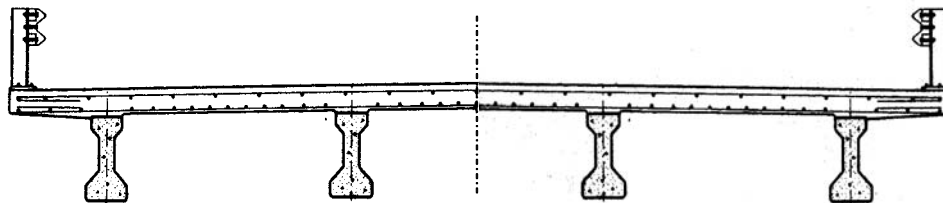


Figure 6: End View of Conventional Bridge Deck

While all three decks use epoxy coated reinforcing steel, the layout of the reinforcing steel varies between the three decks. The conventional and HPC decks are designed using the traditional strength approach described in the American Association of State Highway Transportation Officials (AASHTO) specifications (AASHTO, 2000). The traditional strength design method treats the deck as if it were a beam in flexure spanning the stringers. This design results in the primary reinforcement oriented transversely to the length of the bridge.

The empirical design approach, which requires no formal analysis, is permitted by the AASHTO specifications for monolithic concrete bridge decks that satisfy specific conditions. Using this design method, reinforcement ratios for the top and bottom mat in both the longitudinal and transverse directions are simply functions of the depth of concrete and length of span. AASHTO specifies a minimum reinforcement ratio equal to $3.8 \text{ cm}^2/\text{meter}$ ($0.18 \text{ in}^2/\text{ft}$) in

each direction in the top mat, and $5.7 \text{ cm}^2/\text{meter}$ ($0.27 \text{ in}^2/\text{ft}$) in each direction in the bottom mat. The reason for the increased amount of steel in the bottom mat is for better crack control in the positive bending regions of the slab. Comparatively, in the construction drawings for the decks constructed as part of this research project, the Conventional and HPC decks require 3679 kg more steel than the empirical deck. Figure 7 demonstrates the difference in the density of the reinforcement between the two deck designs, taken at the same place in the deck. Reducing the amount of steel in the empirical deck, especially in the top layer, decreases the opportunity for, and the affects of reinforcement deterioration.

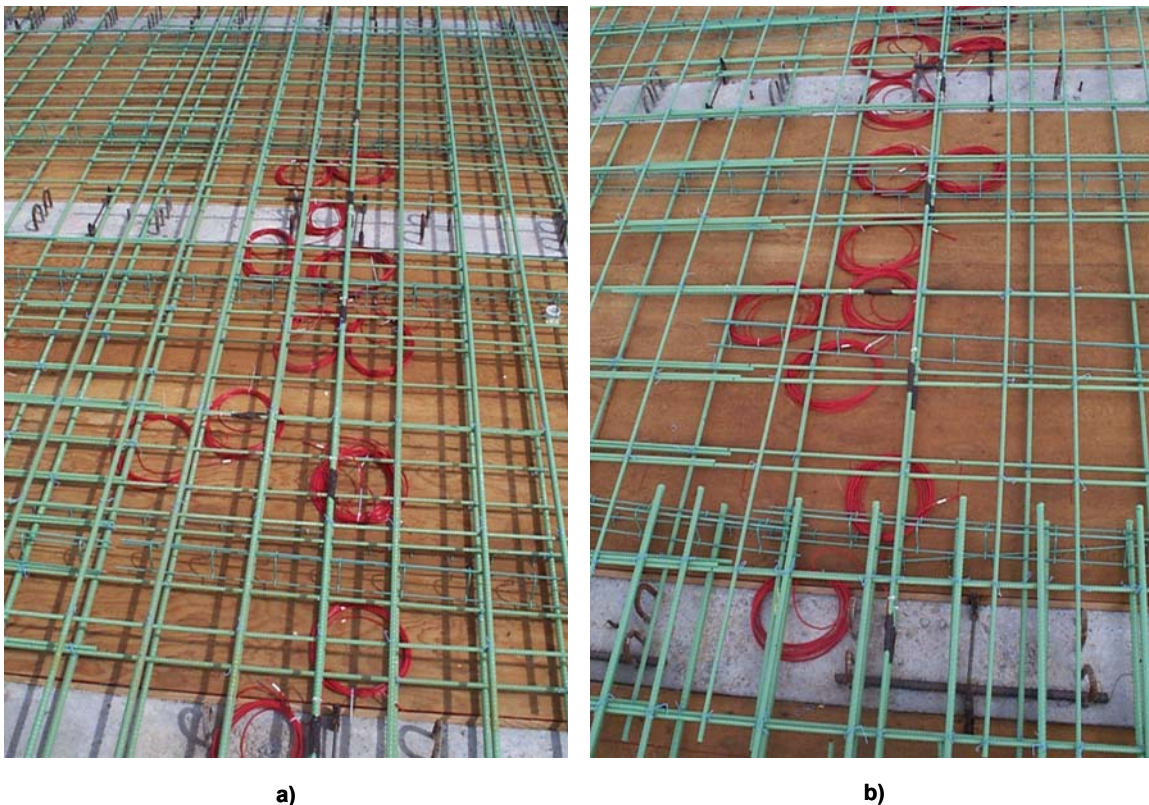


Figure 7: Example Reinforcement Densities of the Conventional and HPC Decks (a), and the Empirical Deck (b)

3.1 Concrete Bridge Deck

Concrete was poured into the decks using a two-yard bucket and a crane, and was leveled using an automatic screed (Figure 8). During construction of the bridge decks, MDT performed air content tests, slump tests, and collected test specimens from selected trucks on each bridge to make concrete test cylinders. Average results from slump and air content tests are provided in Table 1, and the detailed results from all tests are summarized in Appendix A. In addition, the Western Transportation Institute (WTI) collected concrete test specimens from a representative portion of the concrete used to cast the instrumented section of each deck. Sufficient samples

were collected to be tested at three distinct time intervals: 28-days, at the first live load test, and at the second live load test. All material sampling and testing was conducting in substantial compliance of ASTM specifications listed in Appendix B.

Table 1: Average Slump and Air Content from Bridge Deck Concrete

Bridge Deck	Average Slump (mm)	Average Air Content (%)
Conventional	79.4	6.3
Empirical	92.1	6.5
HPC	168.3	5.1

Sixteen to eighteen truckloads of concrete (approximately 125 cubic yards) were used to cast each bridge. In general, the instrumented areas of each bridge were cast with concrete from the fourth truck through the eighth truck. Rather than sampling from a single truck in the instrumented region of the decks, as was originally proposed, the decision was made at the time of the deck pours to collect samples from three of the trucks from the instrumented region of each deck (samples were actually collected from four trucks for the Conventional deck). For the most part, one truck from each bridge was more heavily sampled than the remaining trucks. Table 2 summarizes the number of each type of sample collected from each bridge.



Figure 8: Placing the Deck Concrete

Table 2: Concrete Samples Collected during Construction

Bridge	6 x 12 Cylinders	Rupture Beams	Shrinkage Beams
Conventional	35	9	3
Empirical	26	9	3
HPC	18	9	3

Concrete test cylinders 152 mm (6 in) diameter by 305 mm (12 in) long were used to determine uniaxial compressive strength, elastic modulus, and splitting tensile strength. Rectangular beams 152 mm (6 in) wide by 152 mm (6 in) deep by 508 mm (20 in) long were used to determine modulus of rupture. Shrinkage properties were determined using rectangular beams 76 mm (3 in) wide by 76 mm (3 in) deep by 406 mm (16 in) long. Selected concrete specimens were cured in a moist cure room at Montana State University (for 28-day testing) while the remaining samples were cured near the bridge decks. A complete summary of the samples collected from each bridge, the conditions under which these samples will be cured, and the tests to which these samples will be subjected is presented in Tables 3, 4, and 5.

Table 3: Concrete Sampling and Testing Matrix – Conventional Deck, Cast 6/05/03.

Truck No.	Type of Specimen ^a	Number of Specimens	Curing	Time to be tested	Type of test
C-4	cylinder	3	moist	28 days	compression
	cylinder	3	with deck	1 st live load	compression
	cylinder	3	with deck	2 nd live load	compression
	beam	2	with deck	1 st live load	bending
C-5	cylinder	2	with deck	1 st live load	compression
	cylinder	2	with deck	2 nd live load	compression
C-6	cylinder	3	moist	28 days	compression
	cylinder	3	with deck	1 st live load	compression
	cylinder	3	with deck	1 st live load	split cylinder
	cylinder	3	with deck	2 nd live load	compression
	cylinder	3	with deck	2 nd live load	split cylinder
	beam	2	with deck	1 st live load	bending
	beam	2	with deck	2 nd live load	bending
	shrink	3	with deck	periodically	shrinkage
	shrink	3	moist	periodically	shrinkage
C-7	cylinder	3	moist	28 days	compression
	cylinder	3	with deck	1 st live load	split cylinder
	cylinder	3	with deck	2 nd live load	compression
	beam	2	with deck	2 nd live load	bending

^a cylinder – 152 mm (6 in) diameter by 305 mm (12 in) long cylinder

beam – 152 mm (6 in) wide by 152 mm (6 in) deep by 508 mm (20 in) long beam

shrink – 76 mm (3 in) wide by 76 mm (3 in) deep by 406 mm (16 in) long beam

Table 4: Concrete Sampling and Testing Matrix – Empirical Deck, Cast 6/02/03.

Truck No.	Type of Specimen ^a	Number of Specimens	Curing	Time to be Tested	Type of test
E-5	cylinder	3	moist	28 days	compression
	cylinder	3	with deck	1 st live load	compression
	cylinder	3	with deck	2 nd live load	compression
	Beam	2	with deck	1 st live load	bending
E-7	cylinder	3	moist	28 days	compression
	cylinder	3	with deck	1 st live load	compression
	cylinder	3	with deck	1 st live load	split cylinder
	cylinder	3	with deck	2 nd live load	compression
	cylinder	3	with deck	2 nd live load	split cylinder
	Beam	2	with deck	1 st live load	bending
	Beam	2	with deck	2 nd live load	bending
	Shrink	3	with deck	periodically	shrinkage
	Shrink	3	moist	periodically	shrinkage
E-9	cylinder	3	moist	28 days	compression
	cylinder	3	with deck	1 st live load	compression
	cylinder	3	with deck	2 nd live load	compression
	Beam	2	with deck	2 nd live load	bending

^a cylinder – 152 mm (6 in) diameter by 305 mm (12 in) long cylinder
 beam – 152 mm (6 in) wide by 152 mm (6 in) deep by 508 mm (20 in) long beam
 shrink – 76 mm (3 in) wide by 76 mm (3 in) deep by 406 mm (16 in) long beam

Table 5: Concrete Sampling and Testing Matrix – HPC Deck, Cast 5/28/03.

Truck No.	Type of Specimen ^a	Number of Specimens	Curing	Time to be tested	Type of test
H-4	cylinder	1	moist	28 days	compression
	cylinder	2	with deck	1 st live load	compression
	cylinder	2	with deck	1 st live load	split-cylinder
	cylinder	2	with deck	2 nd live load	compression
	Beam	2	with deck	1 st live load	bending
	Beam	1	with deck	2 nd live load	bending
	Shrink	3	with deck	periodically	shrinkage
	Shrink	3	moist	periodically	shrinkage
H-6	cylinder	2	moist	28 days	compression
	cylinder	2	with deck	1 st live load	compression
	cylinder	2	with deck	2 nd live load	compression
	Beam	2	with deck	1 st live load	bending
	Beam	1	with deck	2 nd live load	bending
H-8	cylinder	1	moist	28 days	compression
	cylinder	2	with deck	1 st live load	compression
	cylinder	2	with deck	2 nd live load	compression
	Beam	1	with deck	1 st live load	bending
	Beam	2	with deck	2 nd live load	bending

^a cylinder – 152 mm (6 in) diameter by 305 mm (12 in) long cylinder

beam – 152 mm (6 in) wide by 152 mm (6 in) deep by 508 mm (20 in) long beam

shrink – 76 mm (3 in) wide by 76 mm (3 in) deep by 406 mm (16 in) long beam

The Western Transportation Institute (WTI) conducted 28-day compression tests on all moist cured test cylinders from all the bridges. Load and displacement data was collected from most of the specimens, and the stress-strain behavior of the concrete was determined. Average strength values from the 28-day compression tests conducted by WTI and MDT are provided in Table 6. Conflicting values between MDT and WTI may be associated with different curing and end cap conditions. Table 7 lists the moduli of elasticity from tests conducted at 28 days and during first live load tests. Results from all unconfined compression tests are shown in Appendix A.

Table 6: Average 28-Day Concrete Strengths

Testing Entity	Conventional (MPa)	Empirical (MPa)	HPC (MPa)
MDT	37.8	33.0	54.0
WTI	28.0	27.4	46.0

Table 7: Modulus of Elasticity of Deck Concrete

Bridge	28-day (GPa)	1st Live Load (GPa)
Conventional	29.3	29.9
Empirical	27.8	24.8
HPC	31.5	30.8

3.2 Steel Reinforcement

Epoxy-coated, Grade 60 steel rebar was specified for each of the bridge decks. Mill test reports were obtained from MDT for the rebar used in the project. The average yield strength is 478.5 MPa, the average tensile strength is 740.1 MPa and the elongation at failure is 14.5 %. Tests to evaluate the epoxy coating yielded acceptable results. Raw data is provided in Appendix C.

3.3 Prestressed Girders

Type I prestressed concrete beams were used to support the bridge deck. The dimensions and sectional properties of these beams are shown in Figure 9. The results of the concrete compressive strength tests for the prestressed girders (obtained from MDT) were averaged and are summarized in Table 8. The raw data is provided in Appendix D.

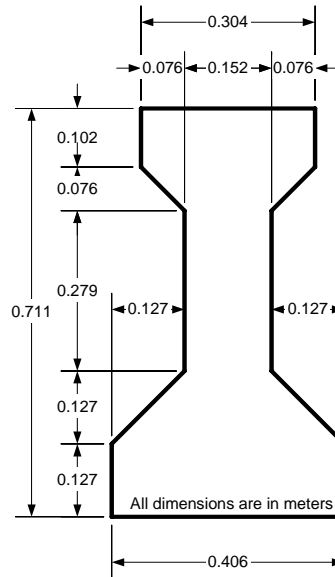


Figure 9: Dimensioned Cross-Sectional View of Saco Bridge Girders

Table 8: Average 28-day Prestressed Girder Concrete Compressive Strengths

Bridge	Prestressed Girder (MPa)
Conventional	63.0
Empirical	61.0
HPC	64.2

4 DEVELOPMENT AND IMPLEMENTATION OF THE INSTRUMENTATION PLAN

The instrumentation in the Saco Bridge Project was configured to fulfill multiple project goals. The two primary objectives were to observe long-term environmental and short-term live load deck responses. It was also desirable to separately monitor strain in the concrete and in the reinforcement, especially in areas prone to cracking. To meet these objectives, a detailed instrumentation plan was produced to determine general and specific gage locations. The instrumentation and data acquisition system were chosen based on durability, reliability and flexibility. Redundancy was necessary to ensure critical measurements were not missed. The following subsections detail 1) how gage locations were selected, 2) the various instrumentation used, 3) the data acquisition system capabilities and setup, and 4) how each of these components were installed and assembled.

4.1 Gage Locations

A three-dimensional analytical model of the bridges was used to help select critical instrumentation locations. The model was created using Visual Analysis, a multipurpose finite element program. The model was constructed using four-node plate elements to represent the bridge deck and beam elements to represent the stringers. All elements were linked together using stiff beam elements to simulate the composite action of the deck-girder superstructure system. Further care was exercised in developing the model so that the details of the deck and stringer configurations were accurately portrayed at the interior supports. The model was loaded with a three-axle truck placed at predetermined longitudinal and transverse positions of the bridge deck using point loads. Stress contour plots of the deck were generated for each truck position. These plots were then used to verify locations of high and low stress, and to identify any unexpected locations with high stresses, where instrumentation should be placed. Gage locations were selected to 1) capture the extreme response, 2) characterize the response in general, and 3) characterize the response at specific features/locations of interest. Gage locations were also selected to study the interaction between the deck and the supporting structure. For added verification, candidate instrumentation locations were compared with locations chosen by other researchers in similar bridge test programs.

To identify precise locations for instrumentation, envelopes of extreme fiber stresses were generated for the bridge deck in both the longitudinal and transverse directions. Using this information, specific reinforcing bars within these areas were chosen to be instrumented. When appropriate, instrumentation was embedded in the concrete near these instrumented bars to duplicate or augment strain information from the instrumented rebar. From this work, a formal instrumentation plan that detailed gage type, location, and expected level of response was generated (Appendix E).

The final instrumentation suite used three types of instrumentation to monitor strains in the bridge decks. Each bridge deck contained 35 strain gages bonded directly to the reinforcement, 9 strain gages embedded in the concrete, and 20 vibrating wire gages embedded in the concrete. During live-load testing, four external strain gages were attached to the underside of the stringers.

General locations selected for instrumentation are between the south abutment and Bent #2 (southernmost interior bent). The approximate positions of the deck gages oriented in the longitudinal and transverse directions are shown in Figures 10 and 11, respectively. The positions of the external strain gages, oriented in the longitudinal direction and attached to the bottom of the stringers, are shown in Figure 12. In the longitudinal direction, gage locations were primarily concentrated near the bents and diaphragms, while the transverse gages were focused in the area between the diaphragm and the bent. Most locations have gages placed at the top and bottom of the cross-section. Overall, these locations were chosen to study:

- stringer-bent interaction,
- bending across the bent,
- effects of the diaphragm,
- continuity effects,
- global bending,
- effect of saw cut,
- stringer effects,
- bent effects, and
- local deck behavior.

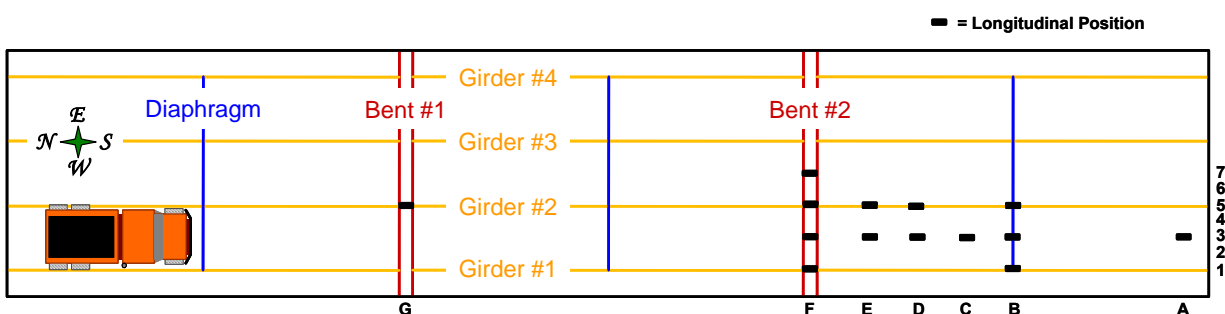


Figure 10: General Location of Strain Gages Oriented in the Longitudinal Direction (plan view)

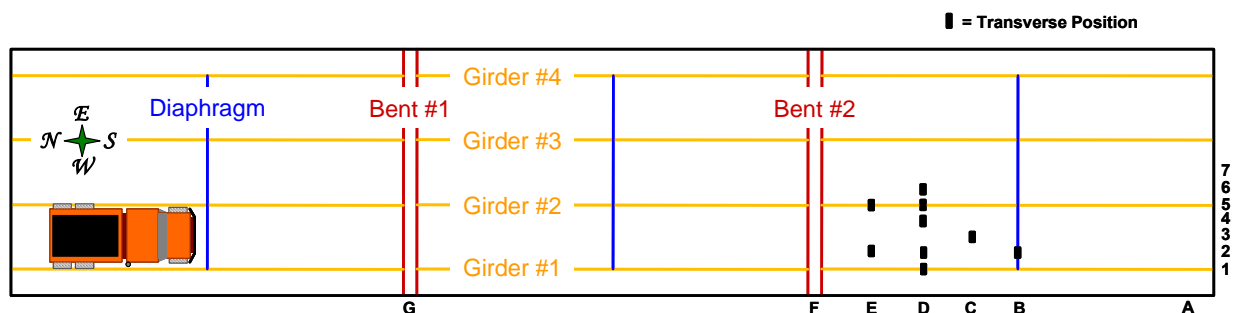


Figure 11: General Location of Strain Gages Oriented in the Transverse Direction (plan view)

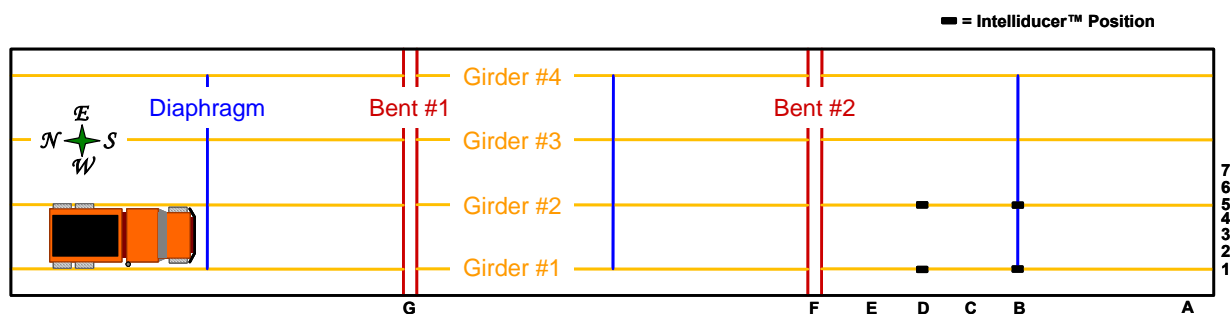


Figure 12: General Location of Intelliducer™ Gages Oriented in the Longitudinal Direction (plan view)

4.2 Position Referencing Nomenclature

A reference numbering system was created to help organize and distinguish each gage based on its location, orientation, type, and relative position. Altogether, the gage numbering system consists of six characters, as illustrated in Figure 13. The global location indicates which bridge the sensor is embedded in: Conventional (C), Empirical (E), and HPC (H). Gages are oriented either longitudinally (L) or transversely (T) with respect to the direction of traffic. Gage types are either strain gages bonded to the reinforcement (R), vibrating wire gages (V), or embedded concrete gages (E). Positions of the gages are referenced from the southwest corner of the bridge. Longitudinal distances from the south end of the bridge are denoted by the letters A through G. Transverse positions of the gages from the west side of the bridge are denoted by the numbers 1 through 7. Finally, the vertical position of each gage within the deck is described as bottom (B), middle (M), or top (T). The example in Figure 13 (C-LV-F-3-B) corresponds to a Longitudinally oriented Vibrating wire gage in the Conventional bridge deck, located at Gage Line F (approximately 14.625 meters from the south end of the bridge), transverse position 3 (approximately 2.15 meters from the west side of the bridge), and in the plane of the Bottom mat of reinforcement. These unique reference numbers are used throughout the remainder of the report.

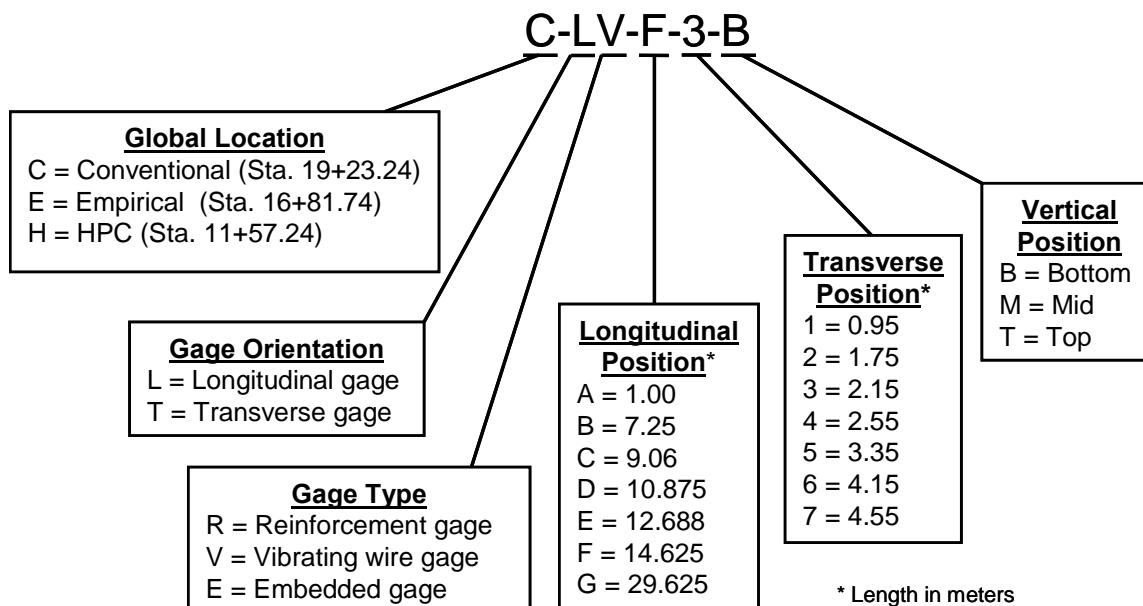


Figure 13: Gage Reference Numbering System

4.3 Instrumentation

Three types of strain gages were used to internally instrument the bridge decks and one type was used to instrument the bottom of the stringers. Resistance strain gages (a.k.a. foil gages) were used to measure strain in the reinforcement, vibrating wire gages were used to measure long term strains in the concrete, and pre-manufactured resistance gages encased in a rigid polymeric housing were used to measure strain in the concrete. Specially made Intelliducers™ manufactured by Bridge Diagnostics, Inc. (Boulder, Colorado) were used to measure strains at the bottom of the bridge stringers during live load testing only.

4.3.1 Resistance Strain Gages

Direct measurements of local strain in the reinforcement were made using resistance strain gages. These strain gages were bonded directly to the top and bottom surface of the reinforcement using a special epoxy. Bonding them to the top and bottom surface reduces the effects of local bending, so that only axial forces are recorded. Gage installation was conducted in College of Engineering laboratories at Montana State University (MSU). Each bridge deck contained 35 resistance strain gage locations.

Resistance strain gages are composed of a thin layer of metal foil bonded atop a thin polymer backing. The foil acts as an electrical resistor, and when attached to a material's surface, changes in the length of the material will result in a nearly identical change of length of the foil. These length changes result in a change in the gage's electrical resistance. Such

changes are quite small and are generally detected using a special circuit arrangement called a Wheatstone bridge, as discussed below.

The strain gages purchased from Micro-Measurements Group, Inc. are designated as type CEA-06-250UN-350 (using their nomenclature). Figure 14 shows a resistance strain gage prior to installation. CEA gages are general-purpose gages made of a constantan foil that are widely used in experimental stress analysis. The foil grid is fully encapsulated and includes exposed copper-coated integral solder tabs. The temperature range at which these gages will self-temperature-compensate is -75° to $+175^{\circ}$ C (-100° to $+350^{\circ}$ F) for static measurements on steel. The active gage length of these gages is 0.250 inches and their resistance in ohms is $350 \pm 0.3\%$. Strain in these gages should not exceed approximately ± 5000 microstrain ($\mu\epsilon$) and fatigue life will be approximately 10^5 cycles at $\pm 1500 \mu\epsilon$.

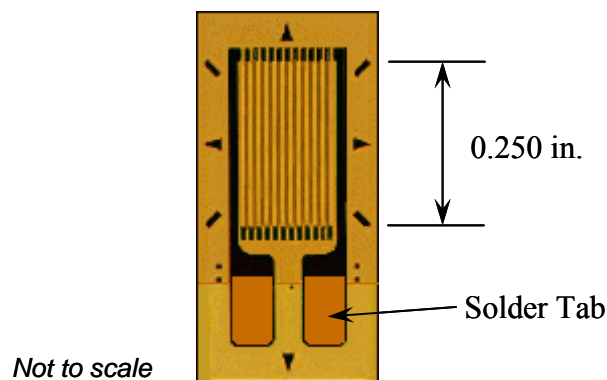


Figure 14: Resistance Strain Gage from Micro-Measurements Group, Inc. (CEA-06-250UN-350)

Bonding resistance strain gages to the epoxy-coated reinforcement followed several steps. This process included:

1. locating and marking the desired location,
2. grinding away the epoxy coating and steel ribs to make a smooth bonding surface,
3. cleaning and neutralizing the area,
4. gluing the gage onto the bar,
5. soldering the lead wires to the gage,
6. cleaning the area of any contaminants, and
7. covering the area with a coating to provide environmental and mechanical protection.

A two-part, medium viscosity epoxy (M-Bond AE-10) was used to attach the gages to the reinforcing steel. This epoxy system is highly resistant to moisture and chemicals and is used for general-purpose stress analysis, having improved longevity over other epoxies. Cure time was about six hours at 24° C (75° F).

A two-part polysulfide liquid polymer compound (Micro-Measurements M-COAT J) was used to environmentally protect the strain gages from damage during and after construction. This tough, flexible, black coating was mixed and applied over the strain gaged area in the lab and allowed to dry overnight before moving. M-COAT J provides good protection against oil, grease, most acids and alkalis, and most solvents. Figure 15 shows a strain gage bonded to the reinforcement before and after the environmental protection was installed.

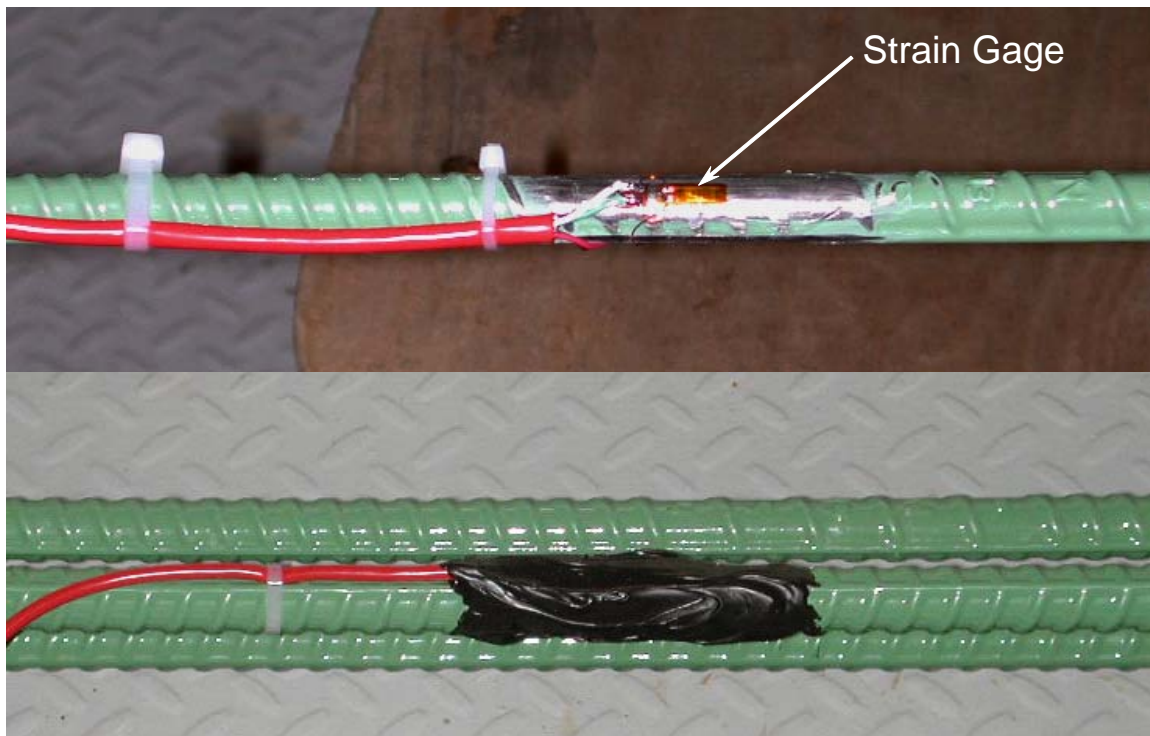


Figure 15: Strain Gage Bonded to the Reinforcement before (Top) and after (Bottom) Environmental Protection

Reinforcing bars scheduled for use during construction of the bridge decks were ordered directly from the manufacturer and shipped to MSU so that the resistance strain gages could be installed under controlled laboratory conditions rather than in the field. The instrumented rebar was installed in the bridges by Sletten Construction (the prime contractor on the job) under the Western Transportation Institute's (WTI's) supervision.

The resistance strain gages were quite durable, having a survival rate of 85%. Similar to the embedment gages, the gage locations that experienced the greatest losses were over the bents. Losses in this area were more frequent due to cracks that had developed over the bent. The crack allows larger daily strain shifts due to temperature swings and higher strains during vehicle loads. Losses were sustained at a few other gage locations, which could have occurred during installation or due to wire breaks.

4.3.2 Vibrating Wire Strain Gages

The 20 vibrating wire strain gages that were embedded in the bridge deck concrete for long term monitoring were purchased from Geokon (Model VCE-4200). This standard model, shown in Figure 16, has a 153 mm (6 in.) gage length, 3000 microstrain range, and 1 microstrain sensitivity. They are designed to be embedded directly in concrete and are typically used to monitor long-term strain and temperature in structures such as foundations, piles, bridges, dams, containment vessels, and tunnel liners.

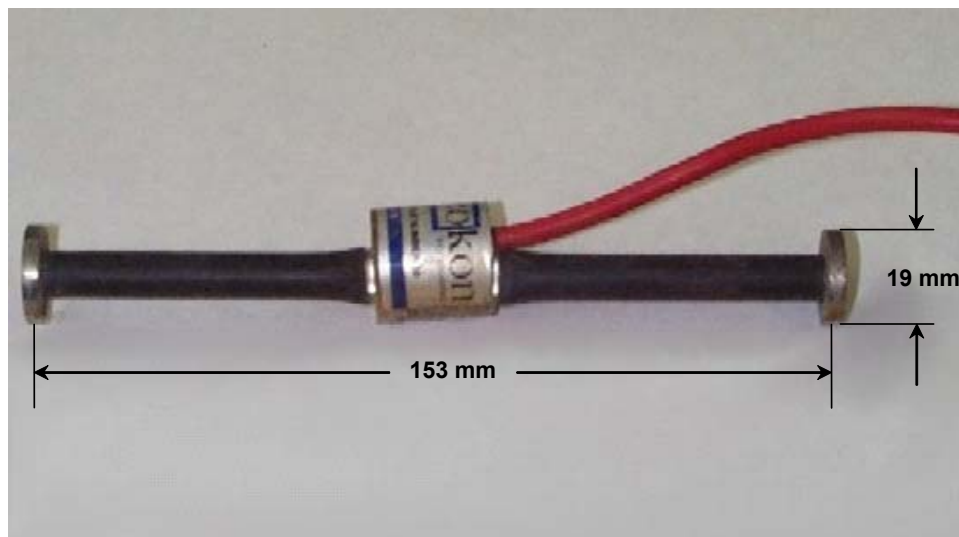


Figure 16: Vibrating Wire Strain Gage (VCE-4200)

The gages use a steel wire in tension between two circular end plates, to measure length changes in the concrete. As the concrete contracts or expands, the wire responds accordingly, thereby changing its resonant frequency of vibration. The wires are excited by electromagnetic coils, which also detect their resonant frequencies of vibration. Frequencies detected by the coil are converted to a DC voltage (using a Campbell Scientific, Inc. AVW1 unit) and recorded by the data logger. The AVW1 unit will accommodate a single vibrating wire gage or, if a multiplexer is used, up to 16 vibrating wire gages may be sequentially converted and recorded. The time required for the frequency sweep and the slow speed of the multiplexer makes it impractical to log data from the vibrating wire gages during live load testing with a moving vehicle (hence their focus on capturing long term environmental effects). Each vibrating wire gage is also equipped with a thermistor to record temperature. Temperature measurements are used to apply temperature corrections to measured strains. Differences between the thermal expansion coefficients of steel and concrete necessitate these temperature corrections.

Using plastic coated steel wire, each vibrating wire strain gage was suspended in the concrete between the reinforcing bars (Figure 17). As suggested by Geokon, a thin rubber pad was placed between the gage body and the tying wire to damp resonant vibrations in the steel wire and rebar cage.

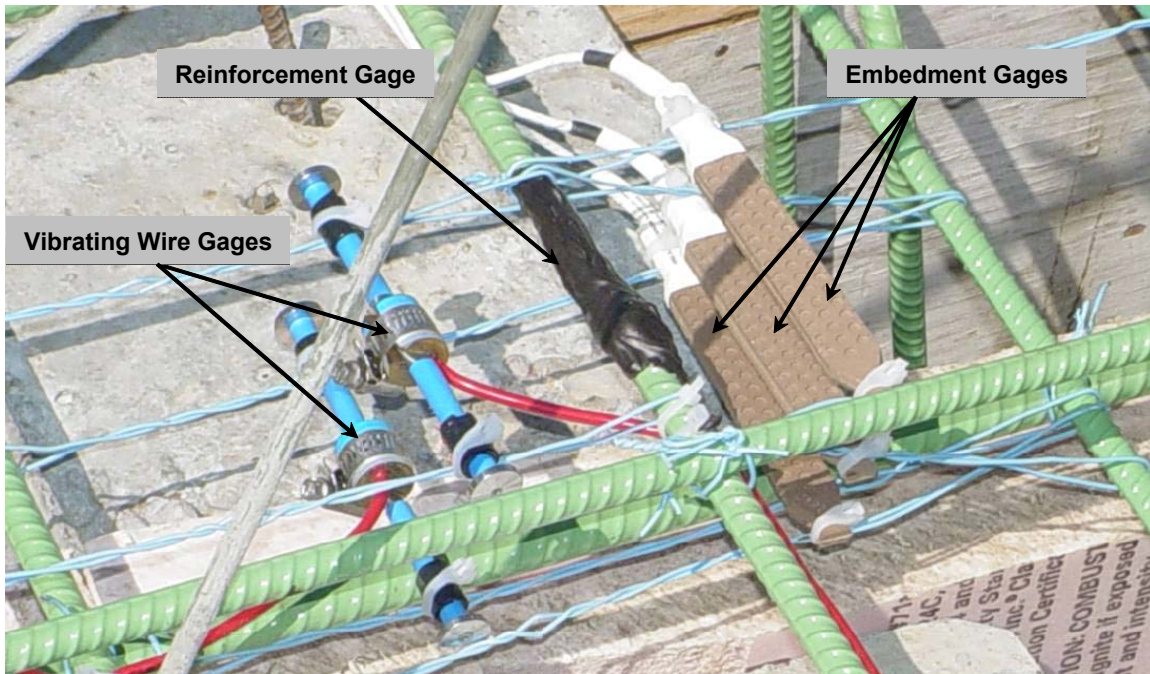


Figure 17: Illustration of Finished Gage Location Showing All Three Embedded Gages

4.3.3 Concrete Embedment Strain Gages

Nine concrete embedment gages, specially made to measure strains inside concrete structures, were used in each of the bridge decks. These gages (EGP-5-350), shown in Figure 18, were purchased from Micro-Measurements Group, Inc. Each embedment gage contains a single 350 ohm bonded-foil resistance strain gage (functionally similar to the ones described earlier). The sensing grid has an active gage length of 100 mm (4 in.) and is self-temperature-compensated to minimize thermal output when installed in concrete structures. The gage is set in a proprietary polymer body to protect them from corrosion, moisture and mechanical damage during construction and use. The outer body has a length of 130 mm (5 in.) and is dimpled to ensure proper adherence to the surrounding concrete. Embedment strain gages utilize a $\frac{1}{4}$ Wheatstone bridge (described later), since there is only a single resistance strain gage housed in the polymer body.

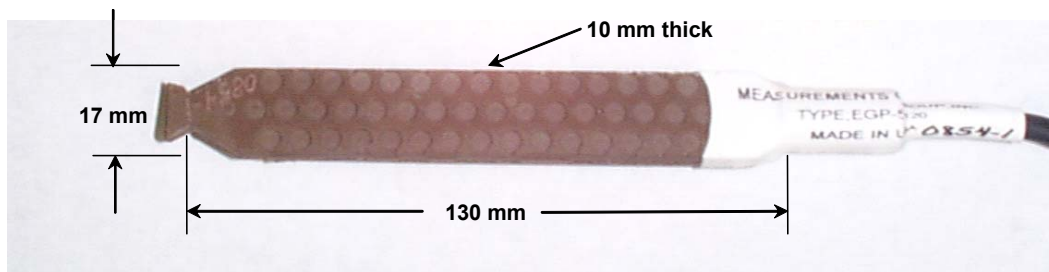


Figure 18: Concrete Embedment Strain Gage (EGP-5-350)

The concrete embedment gages were installed similar to the vibrating wire gages by suspending them from the reinforcing cage using plastic-coated tie wire, as shown in Figure 17. The embedment strain gages suffered the worst mortality, having only a 56% survival rate. Many of the embedment gages were located in the continuous deck over the bent, which cracked in all three decks several days after the deck concrete was poured. The cracking likely occurred due to flexural bending and axial stresses in response to diurnal temperature changes. At the crack, strains exceeded the maximum strain threshold of the embedment gage, causing them to fail.

4.3.4 Intelliducers™

During the live-load experiment only, Intelliducers™ manufactured and sold by Bridge Diagnostics, Inc. (BDI) of Boulder, Colorado were temporarily mounted to the bottom of the stringers of the bridges. Intelliducers™ are used to measure strain at the surface of structural elements. They are made of aluminum and have a 76.2 mm (3 in.) effective gage length, however, extensions are available for averaging strain over a longer gage length. In this application, a 228.6 mm gage length was used. Figure 19 shows an Intelliducer™, and Figure 20 shows an Intelliducer™ mounted to the bottom of a girder with the extensions used in this test program. The circuitry for monitoring the response of these gages consists of a full Wheatstone bridge with four active 350 Ω resistance gages. BDI states that the gages have an accuracy of $\pm 2\%$, a range of $\pm 4000 \mu\epsilon$, and should not be used below 30 $\mu\epsilon$. The Intelliducer™ gages suffered no mortality during the live load tests.

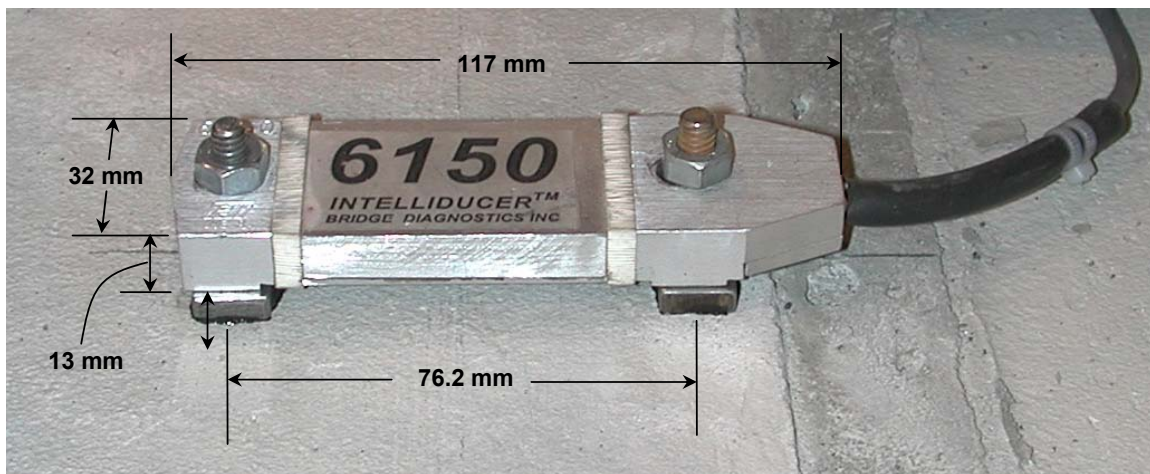


Figure 19: Intelliducer™ Mounted on Concrete Surface

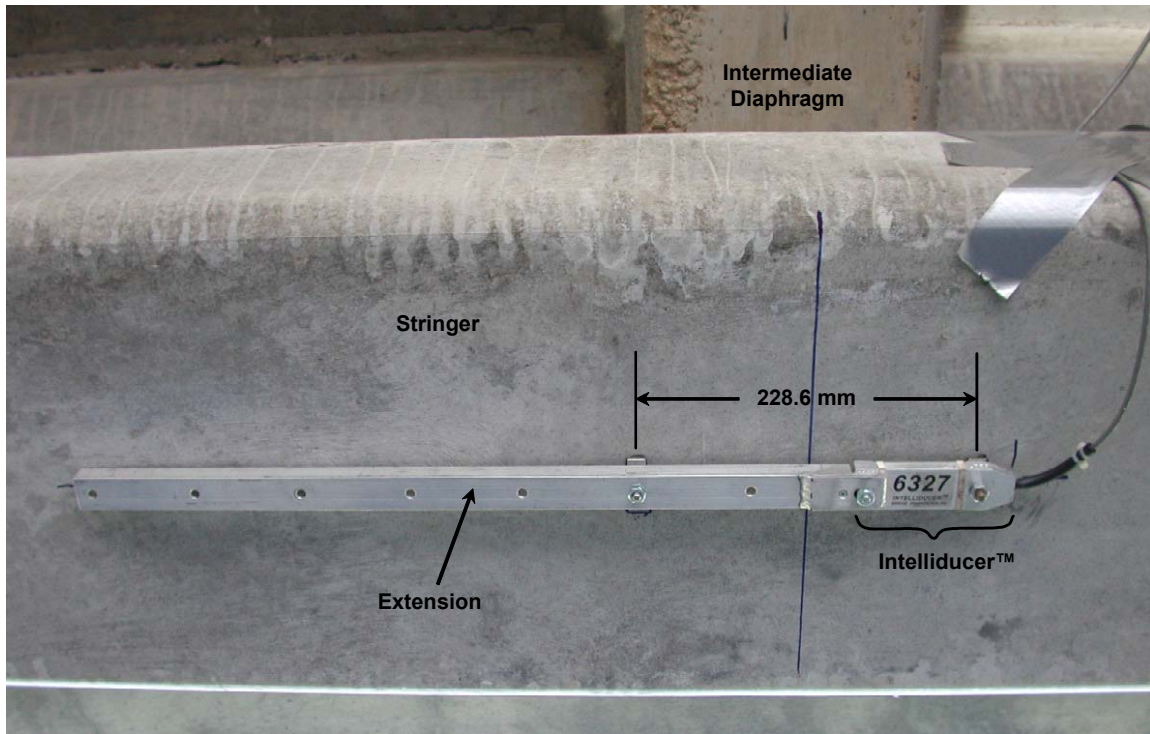


Figure 20: Intelliducer™ Mounted to Bottom of Concrete Girder with Extensions

4.4 Data Acquisition System

Each bridge site required an independent data acquisition system to store and transfer data. Each system consisted of a single data acquisition computer, two multiplexers, supporting circuitry, a 12-volt battery connected to a solar panel through a regulator, and a radio unit connected to an antenna. The CR5000 data acquisition computer, AM16/32 multiplexers, AVW1 vibrating wire conversion unit, and RF400 spread spectrum radios were purchased from Campbell Scientific, Inc. Solar panels, batteries, radio antennas and regulators were purchased from other sources. A weather-resistant steel enclosure was used to house the data acquisition computer, radios, multiplexers, and other peripheral circuitry. The various components contained within each data acquisition enclosure at each bridge are illustrated in Figure 21, and are discussed in more detail below.

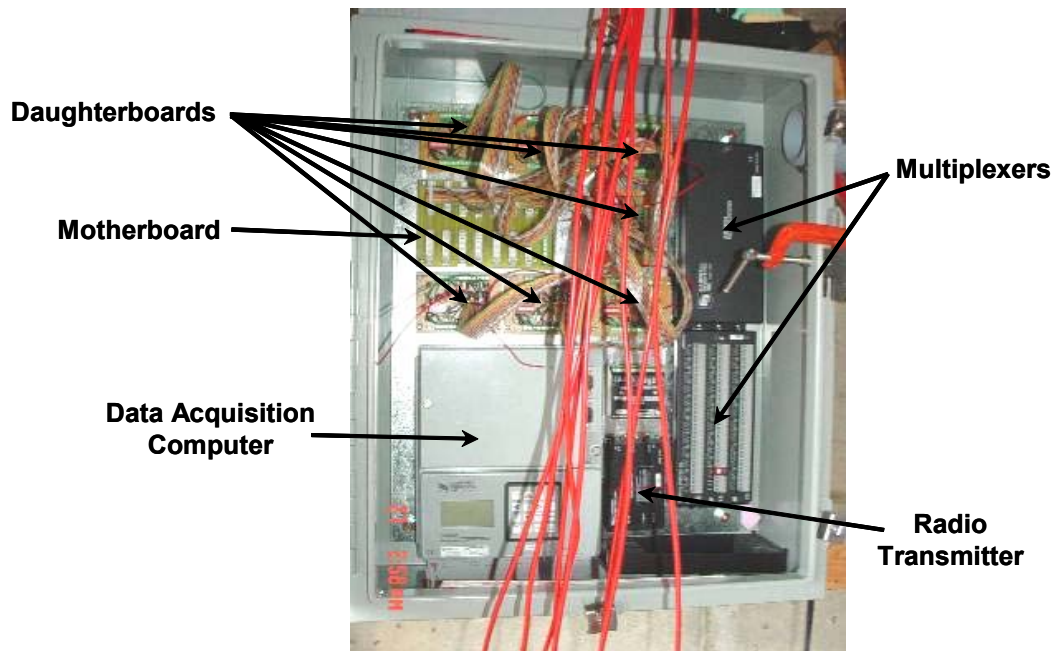


Figure 21: Various Components within a Data Acquisition Box

4.4.1 Data Acquisition Computer

The CR5000 measurements and control system from Campbell Scientific, Inc. is a rugged, high-performance data acquisition system. This system was selected for its durability, wide range of temperature operation, and internal computing and storage capabilities. Some of its other features include:

- a graphical display,
- low power draw,
- twenty differential (40 single-ended) input channels,
- 16 bit measurement resolution,
- 5-volt and 12-volt terminals to power sensors,
- 1,000,000 data point storage capacity,
- a maximum throughput of 2000 to 5000 measurements per second (depending on configuration), and
- an operable temperature of -40° to $+85^{\circ}$ C (-40° C to $+185^{\circ}$ F).

The data acquisition system uses a proprietary computer code to operate. A computer program was written to control data collection activities at the bridge site. Prior to installing the final program on the data acquisition computers, the program was tested at MSU to ensure that it was working properly. In general, the long term monitoring program was written to deliver excitation voltage to each of the sensors at predetermined times (i.e., each hour), capture each sensor's response and store that information in memory. Collected and stored data is transferred on command to MSU using a dedicated Internet connection via the RF400 radios and a series of

900 MHz antennas. For live load testing, a different computer program was required. This program was designed to record only the bonded-foil and embedded gages at a higher rate of speed (~50 Hz) during each test. Data sets collected during testing were transferred and stored on-site to a laptop computer.

4.4.2 Multiplexers

Multiplexers are used to increase the number of sensors that can be monitored by a single data acquisition computer. The CR5000 dataloggers can only directly accommodate 20 differential inputs. The AM16/32 multiplexer can accommodate up to 32 differential measurement channels. It acquires data at a slow rate (approximately 1 Hz) by switching through its channels and simultaneously transferring and storing the data through a single port on the face of the datalogger.

Two multiplexers are required at each bridge site to accommodate 16 vibrating wire gages, 16 temperature measurements, and 30 resistance strain gages during long term monitoring. The remaining resistance gage measurements are connected directly to the front face of the data logger. In this case, the advantage of using multiplexers is the increase in the number of available data ports without the expense of purchasing a second datalogger; the disadvantage is the relatively slower acquisition speed compared to a datalogger alone. Multiplexers were not used during the live load experiments because of their slow data acquisition rate.

4.4.3 Communication and Power

A spread spectrum radio (RF400) is used to transfer data to and from each of the bridges during the long term monitoring. Antennas connected to these radios communicate at 900 MHz to a single receiving antenna collocated with the weather station at the Saco Public School. Information is transferred from the school to WTI via the Internet. This communication path is illustrated in Figure 22. The antennas near the bridges are attached to a wooden pole along with the solar panel.

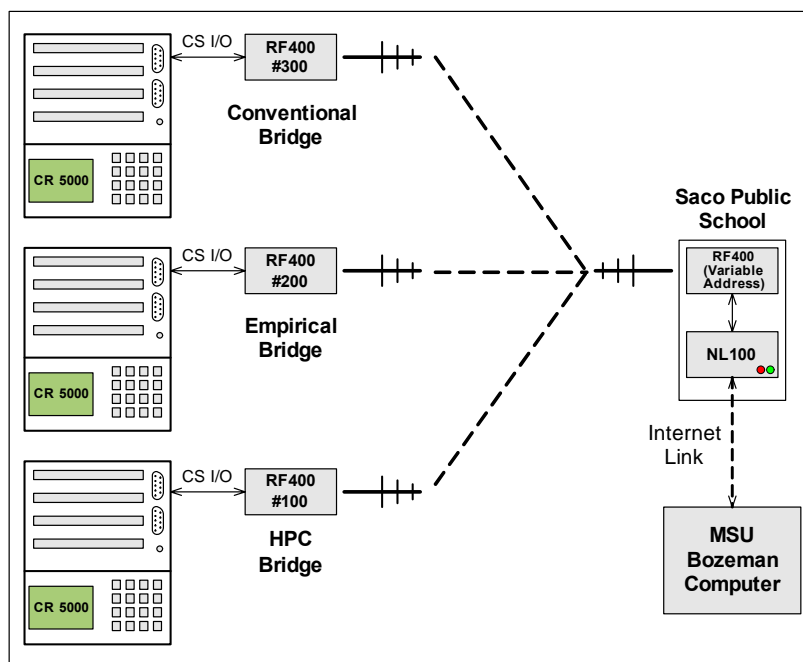


Figure 22: Communication Path for Long Term Monitoring

Power components consist of a 12 volt battery and a 60 Watt solar panel connected through a regulator to maintain a specific battery voltage over time. Each solar panel measures approximately 1.1 m by 0.5 m and is rigidly connected to a wooden pole near the southeast corner of each bridge. Deep-cell 12-volt batteries are being used because they are able to resist voltage decay during cold weather. A single battery at each bridge is housed under the bridge on top of the pile cap near the data acquisition cabinet. Each battery has approximately two weeks of life in the event the solar panel malfunctions or is damaged. Wiring for the communications and power were run through conduit and buried in soil to protect them from varmints and the environment. In addition, a lightning rod was connected to this pole to provide lightning protection.

4.4.4 Supporting Circuitry

Each bridge deck contains 35 resistance gages bonded to the reinforcement, 9 embedment gages, and 20 vibrating wire strain gages. The components used to support operations of the vibrating wires were discussed above. The circuitry that supports the resistance and embedded strain gages utilizes a Wheatstone bridge circuit. Seven identical circuit boards containing six Wheatstone bridge circuits were designed and built to service five resistance strain gages and one embedment strain gage. These seven boards are referred to as “daughterboards,” since they complete the necessary circuitry for the strain gages and relay the final output to the datalogger through the “motherboard.” This connection scheme facilitated rapid and accurate reconfiguration of the system, notably for the short turnaround time between live load tests on the three bridges. Due to limitations on the available number of connection points on the face of

the datalogger, two different arrangements were required based on the unique data acquisition needs of the long-term and the live load testing arrangements. These two arrangements will be discussed in further detail below.

4.4.4.1 Wheatstone Bridge Circuitry

The Wheatstone bridge arrangement is useful for detecting small changes in resistance elements, such as strain gages. Two of the four gage types employed in the instrumentation system for this project operate using a Wheatstone bridge arrangement: the bonded resistance strain gages and the embedment gages.

In its simplest form, the Wheatstone bridge is composed of four resistors, as depicted in Figure 23. A voltage E_{in} is applied to the circuit; for this project, +5V was used. If the resistances in the upper arms of the bridge are identical (i.e., $R_1 = R_2$), the voltage-divider theory dictates that the voltage at point A will be exactly half of the input voltage (i.e., +2.5V). The same relationship holds true for the lower arm. Therefore, if $R_1 = R_2$ and $R_3 = R_4$, points A and B have equal voltages. Thus, the bridge is perfectly balanced, and E_{out} equals zero volts. However, a change in resistance in any one of the four arms of the bridge (i.e., if one of the arms is a strain gage) results in a voltage difference between points A and B. The resulting imbalance is detectable using sensitive voltage-reading equipment. Using theoretical calculations, the resistance change may be calculated using E_{out} . The resistance change is proportional to the strain experienced by the gages and may be converted to a real strain using the manufacturer's published gage factor.

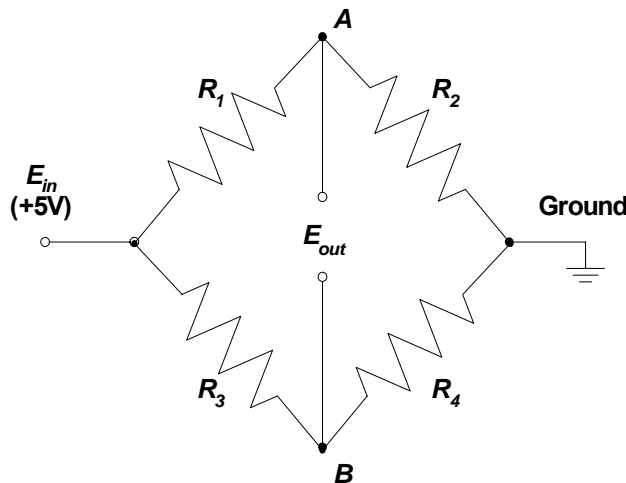


Figure 23: Ideal Wheatstone Bridge Circuit Arrangement

For this project, only axial strain is desired from the rebar strain gages. Thus, it is important that any effects due to local bending in the gaged portion of the bar be negated. This is electrically possible by using the arrangement shown in Figure 24(a) for all the strain gages bonded to the reinforcement. Notice that the two strain gages bonded to the rebar are connected

in series, and occupy a single arm of the bridge. If local bending does exist, bending strains of opposite sign occur at the top and bottom of the bar. Due to the symmetrical location of the gages about the neutral axis of the bar, these strains have an equal magnitude, but opposite sign. The tensile strain due to bending in one gage cancels out the equal bending compressive strain in the other gage. For that arm of the bridge, the net result yields only the amount of axial strain in the bar.

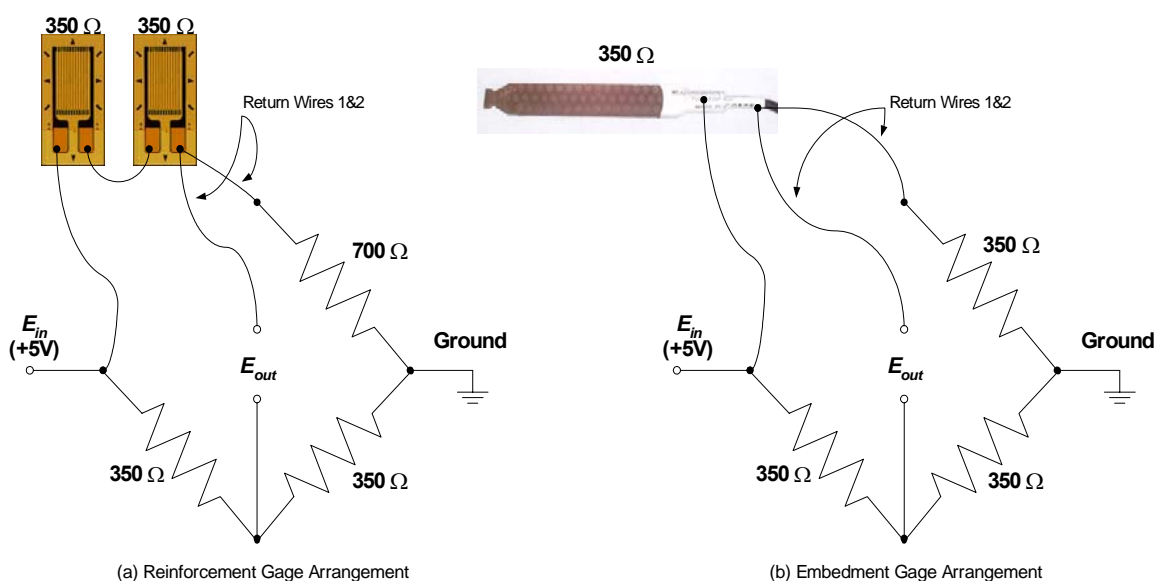


Figure 24: Wheatstone Bridge Arrangements Used on Saco Bridges

Practically, this arrangement is termed a “quarter bridge”: only one arm of the bridge is occupied by strain gages, while the other three arms are occupied by stable resistors. The arm with the strain gages is balanced by the 700 Ω resistance arm. Although other arrangements of the Wheatstone bridge also negate bending effects, this particular arrangement experiences the least sensitivity to changes in temperature – an important consideration for long-term monitoring. The two resistors comprising the 700 Ω resistance arm were unmatched precision resistors, having a tolerance of $\pm 0.01\%$, manufactured by Micro-Measurements Group. The two 350 Ω resistors used in the two lower arms of the Wheatstone bridge were a matched pair, having a tolerance of $\pm 0.005\%$.

A second notable feature of this Wheatstone bridge arrangement is the use of the three-wire system. This technique was employed to compensate for the resistive imbalance in the circuit due to the long lengths of the gage lead wires. If only a single wire was used, that wire would be susceptible to an unknown change in resistance under temperature changes, affecting the resistance of the gaged arm of the bridge. By adding a second wire of identical length to the other 700 Ω resistor arm, any temperature effects in the wire are present in both arms and the bridge remains balanced.

The quarter bridge Wheatstone bridge circuit was also used with the embedded gages (Figure 24(b)). The fundamental theory and operation are the same in this case, except all arms of the bridge are $350\ \Omega$. The three-wire system was also used for these gages.

Prior to recording strains in the bridge decks, baseline voltage measurements were recorded and subtracted from all readings to set the initial strain to zero. A process called “shunt calibration” was used to calibrate the relationship between the voltage output from the Wheatstone bridge and the strain sensed by the gage. By applying a very large resistance ($176\ \text{k}\Omega$) in parallel with the $700\ \Omega$ arm of the Wheatstone bridge, it simulates a particular strain value – approximately $1900\ \mu\epsilon$ in this case. The output voltage at this point is then the upper bound of the linear ratio measurement.

The Wheatstone bridge circuitry was assembled on each daughterboard to accommodate six gage locations: five resistance strain gage locations and one embedment gage location, in the configuration shown in Figure 25. Thus, seven daughterboards were required to accommodate 35 bonded and 7 embedment gages. A single $+5\text{V}$ voltage regulator (LM78L05) was used to ensure that a low-noise, constant supply voltage was provided to the six Wheatstone bridges on each board.

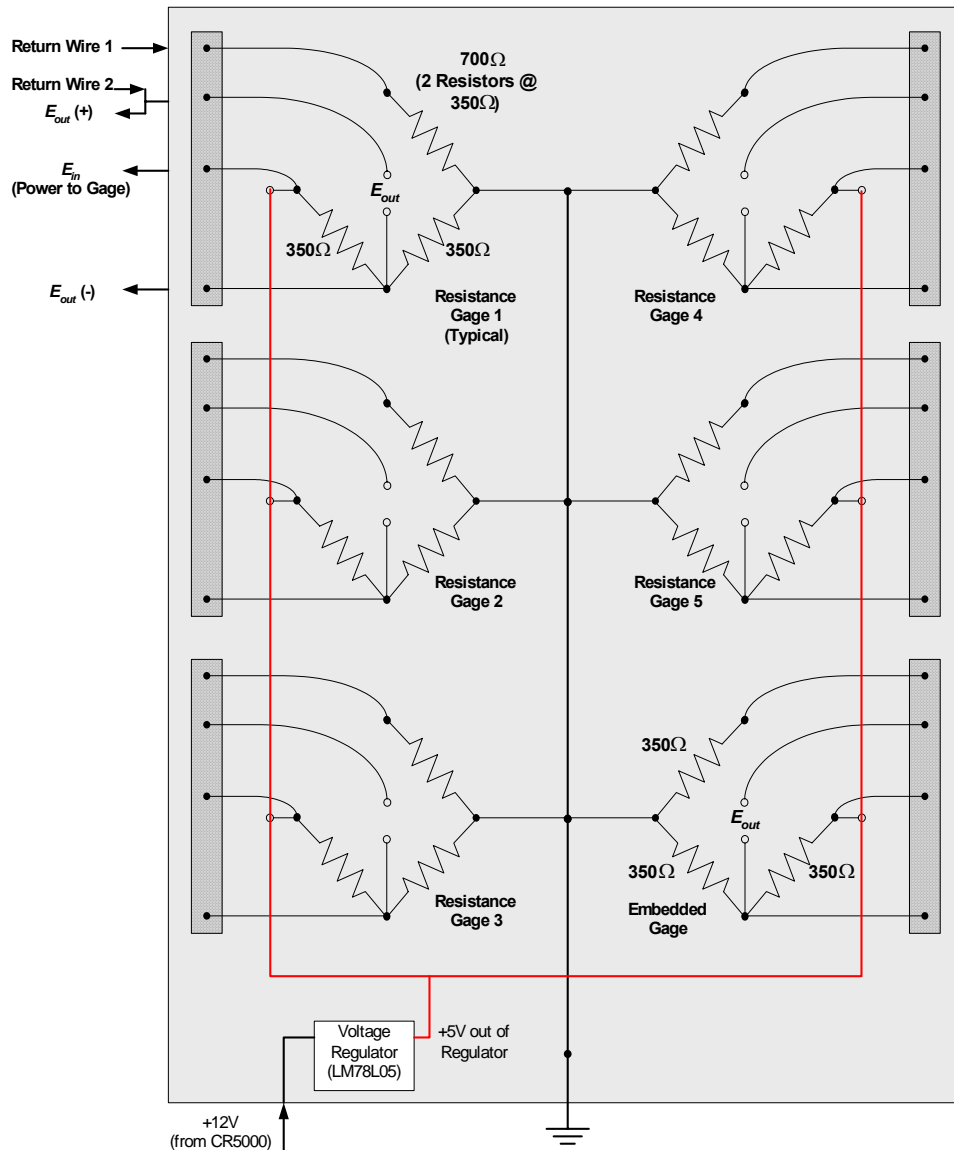


Figure 25: Diagram of Daughterboard Circuitry

4.4.4.2 Circuit Alternatives and Testing

All of the Wheatstone bridge arrangements require that a differential (two-wire) measurement be made to determine E_{out} . The CR5000 data acquisition unit used for this project is limited to 20 direct differential measurements. To accommodate more sensors, a multiplexer is generally used, however, multiplexers require additional cost, are relatively slow, and create one more connection through which noise may be introduced to the signal. Therefore, in the early stages of the project, several alternatives were investigated to increase the capacity of the datalogger without sacrificing accuracy and precision of the strain gages. One alternative was to use an instrumentation amplifier to convert differential analog outputs (a two-wire system) to single analog outputs (a one-wire system), as illustrated in Figure 26. By regulating one output

arm of the instrumentation amplifier at zero volts (i.e., ground), the other terminal can be read as a single-ended signal. This setup was attractive because the datalogger is able to accommodate 40 single-ended measurements, thereby doubling its capacity. However, based on the preliminary testing described below, this arrangement was not used in the final design.

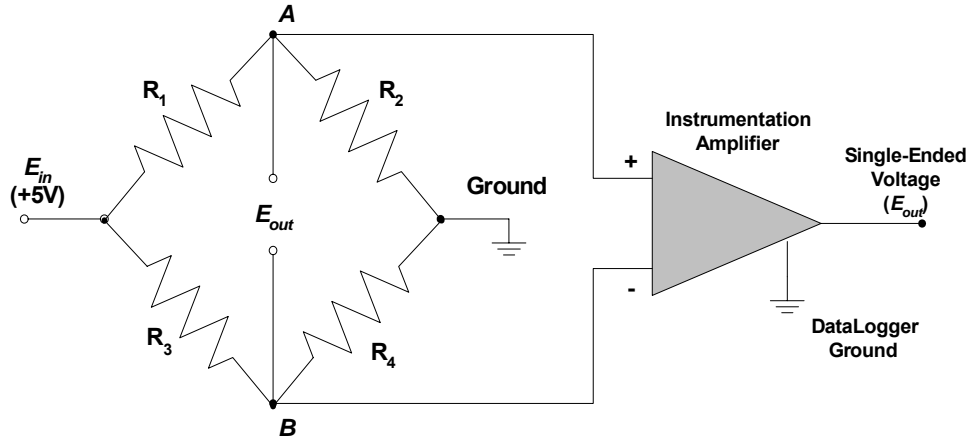


Figure 26: Alternative Circuit Design for Single-Ended Measurements

Items of concern regarding both types of circuitry (differential and single-ended) included: accuracy of outputs compared to theoretical calculations, electronic stability over time and temperature variation, and noise abatement. Initial tests found that the gage output from both circuit arrangements matched the theoretical predictions reasonably well, and that noise was generally controllable using various modifications to the circuits and datalogger programming.

To further investigate the relative performance of the two wiring configurations, a small-scale, reinforced concrete test beam (.25 m deep by .15 m wide by 1.52 m long) was designed and fabricated at MSU. In addition to testing the strain gage circuitry in a more realistic setting, this beam also afforded researchers an opportunity to evaluate the durability of the gage installations on the reinforcing steel. Other issues tested with this beam included: gage survivability during construction, cabling issues, and durability of the gages under loading.

To test gage durability, the gages at one location in the beam were purposefully abused during the construction process. All of the strain gages survived construction, confirming the durability of the installation procedure. Initial testing of the relative gage response found that the output matched the theoretical predictions reasonably well, and that noise was generally controllable using various circuits and programming modifications. However, it was difficult to assess electronic stability for long periods of time and at various temperatures due to the cumbersome nature of the concrete beam. Consequently, a small segment of rebar was instrumented at two locations along its length to further study the electrical stability, accuracy and reliability of the strain gage circuitry for longer periods of time and under more controlled conditions. One gage location was connected to a differential circuit and the other to a single-

ended circuit. Over a period of several days, a constant weight was suspended from the bar and the stability of the constant measurements evaluated against one another.

The single-ended circuit arrangement offered a significantly refined signal, with a low electrical noise band. This performance was attributed to the filtering characteristics of the instrumentation amplifier. However, performance of the single-ended voltage was too erratic over time for the long-term monitoring purposes of this project. The likely reason for this behavior was minor fluctuations in the electric potential of the ground. Small changes in the electric potential would create significant changes in the gage output since the magnitudes of the recorded signal were typically very small.

Overall, it was concluded from these laboratory experiments that the differential analog circuitry offered better stability and accuracy than the single-ended circuitry. Furthermore, this circuitry offered adequate noise abatement for the purposes of this project, although the single-ended circuit did have a better signal-to-noise ratio. Note also that additional time and cost would have been required to convert to single-ended measurements. Therefore, the final circuit design employed the differential outputs with a multiplexer.

4.4.5 Long-Term Monitoring Circuit Arrangement

For long-term monitoring, the available ports on the datalogger were inadequate to service all the necessary gages. As mentioned previously, multiplexers (Mux) were employed to expand the number of gages that could be monitored at hourly intervals. Using the daughterboard-motherboard arrangement seen in Figure 27, the voltage signals for the reinforcement and embedded gage readings were transmitted to the CR5000 directly or via the multiplexer. All of the vibrating wire readings were accommodated using a second multiplexer in conjunction with the AVW1 vibrating wire conversion unit. This daughterboard-motherboard arrangement offered flexibility for performing zeroing/calibration activities without the need for rewiring. Five of the daughterboards are used to monitor long-term strains only, as they are routed through the multiplexer. The remaining two daughterboards are connected directly to the face of the datalogger, allowing the gages wired into these boards to be logged at a relatively rapid rate. Events involving the passage of large vehicles are being recorded on each of the bridges using the 12 gages wired through these two boards.

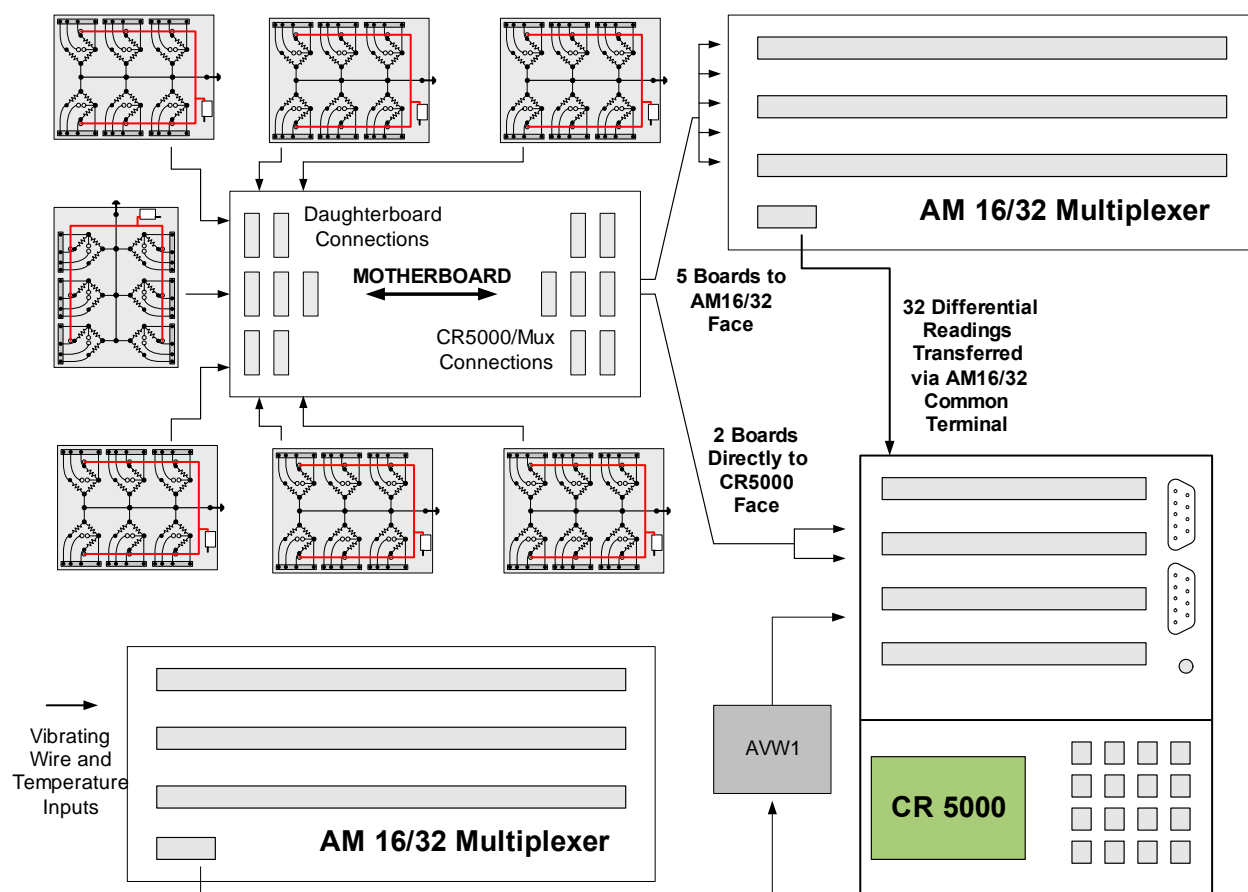


Figure 27: Data Acquisition Layout during Long-Term Monitoring

4.4.6 Live Load Testing Arrangement

During the live load testing, the instrumentation system was temporarily reorganized to accommodate a large number of sensors at the higher data acquisition speeds. As previously mentioned, the multiplexers could not be used during these tests since they were too slow. Consequently, all resistance gage measurements were connected directly to the loggers. All three CR5000 dataloggers were used together on a single bridge to simultaneously monitor and record 53 differential channels during live load testing, as shown in Figure 28.

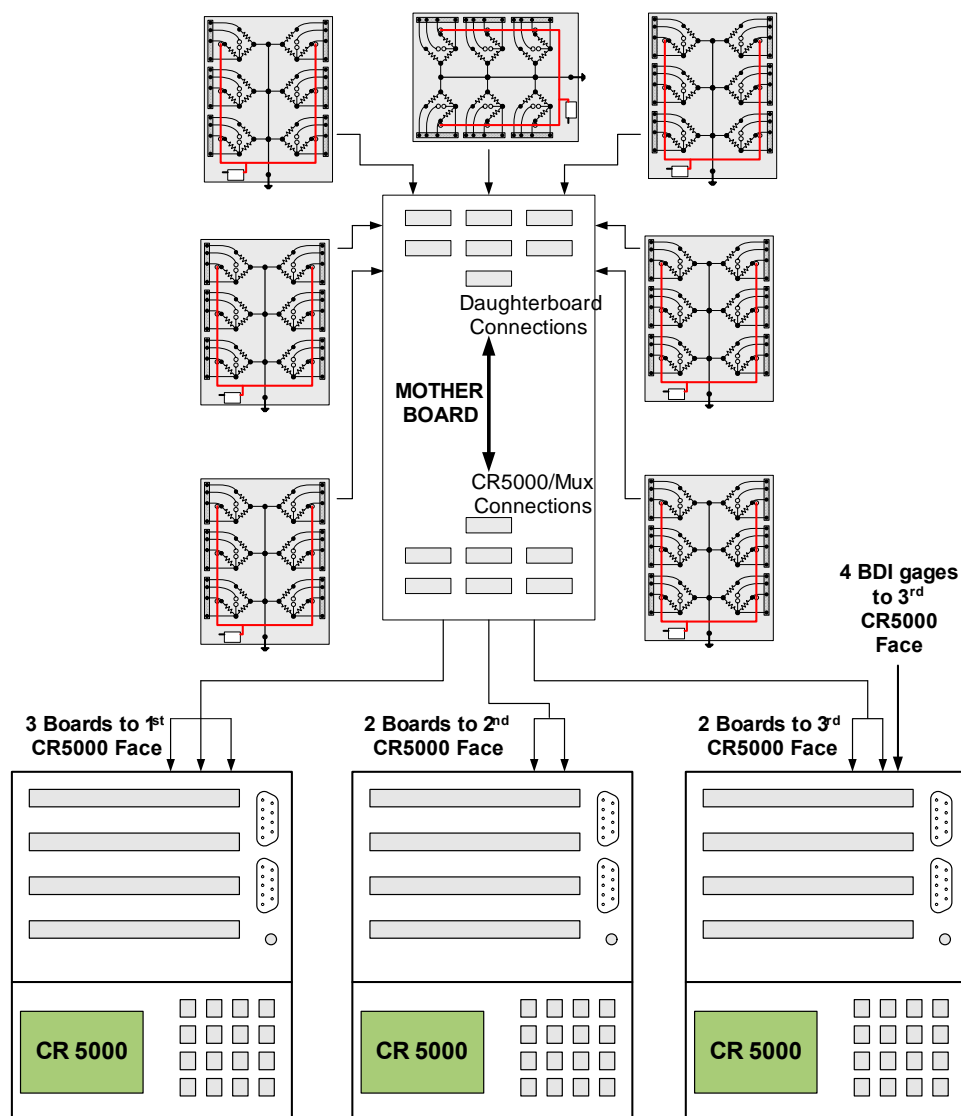


Figure 28: Data Acquisition Layout during Live Load Testing

For the live load tests only, Intelliducers™ were used to monitor strains at the bottom of the girders under the gaged section of each bridge; these gages were directly connected to the face of the third datalogger. Vibrating wire strain gages were not monitored during live load because they are only able to accurately monitor strain at approximately 0.5 Hz (100 times slower than what is necessary during live load testing). Once again, the daughterboard-motherboard interface allowed speedy transitions during live load testing by reducing the amount of physical rewiring required to modify the system to acquire data without multiplexers.

4.5 Installation and Assemblage

The instrumented reinforcing bars were bundled securely together and shipped to the construction site. The bars were then installed as the reinforcing cages were assembled in-place for each deck (in April 2003). The embedded resistance strain gages and the vibrating wire

strain gages were installed once the reinforcing cage for each bridge was complete. Lead wires were routed out through the bottom of the decks through predrilled exit ports. Cabling was bundled together and tied to the underside of reinforcing bars or to the chairs used to space the top mat of reinforcement from the bottom mat, as shown in Figure 29.



Figure 29: Example of Cable Run

Precise coordinates of each instrument location were documented after they were installed and prior to the deck concrete being placed. Once all sensors were in place, small plastic inserts were attached to the sides of the longitudinal formwork to indicate the approximate location of the transverse gage lines. The plastic inserts left a permanent indentation in the concrete when the forms were removed. These indentations will help to locate the gage lines in the future. In addition, longitudinal and transverse measurements were made to document the locations of all the gages. Photographs were also taken to record the orientation and layout of each gage.

When the decks were cast, all gage installations were flagged so that the construction workers would know where to exhibit greater care during concrete placement. The flags were constructed using thin dowels tied in the shape of a teepee. They were connected to the reinforcing cage near each gage location using plastic zip ties. Once the concrete was placed and vibrated, the flags were simply pulled free from the reinforcing cage.

The data acquisition box for each deck was temporarily installed under the bridge near the south bent prior to placing the bridge deck concrete. The lead wires from the gages were connected to the data acquisition system after being routed through the exit ports in the deck forms. After the pour, the bottoms of the bridge decks were deformed, and the data acquisition and power enclosures were permanently mounted to the diaphragm and pile cap, respectively. All lead wires were then trimmed and permanently plumbed in PVC conduit between the exit

ports and the data acquisition boxes. The final arrangement of the data acquisition system and power enclosures with the plumbing in place is shown in Figure 30.



Figure 30: Data Acquisition and Power Enclosure Arrangement under the Bridge Decks

5 WEATHER STATION

A weather station with a data acquisition system was installed at the Saco Public School in August of 2002. Weather sensors were mounted to an existing communications tower located on the roof of the school. Weather sensors include a combination temperature/relative humidity probe, a wind speed and direction sensor, and a barometric pressure sensor. Power and Internet connections are being supplied by the school in return for allowing them free access to the data. Weather data will be considered in conjunction with strain data collected from the bridges to help understand the effect of environmental factors on the behavior of the structures.

Remote communication with the data acquisition system was established using a dedicated, on-site, Internet connection. Automatic storage and downloading capabilities have allowed the data to be retrieved and analyzed via the Internet. A rudimentary website was created to allow remote monitoring and retrieval of the weather data. This website has been integrated into an existing website maintained by the Western Transportation Institute. Additionally, a database was developed to store and organize data collected from the weather station.

The active Internet link to view current and historical weather conditions at Saco, Montana is http://wtigis.coe.montana.edu/saco/Saco_Current.htm. Figure 31 shows a screenshot of the weather website. Specific features of this website include:

- 15 minute updates of temperature, wind speed and direction, relative humidity, dew point, and barometric pressure;
- a collection of the past 24 hours of data updated every 15 minutes;
- 1 month of daily averages;
- 1 month of daily maximums;
- 1 month of daily minimums;
- various pictures associated with the project; and
- links to the other project related information.

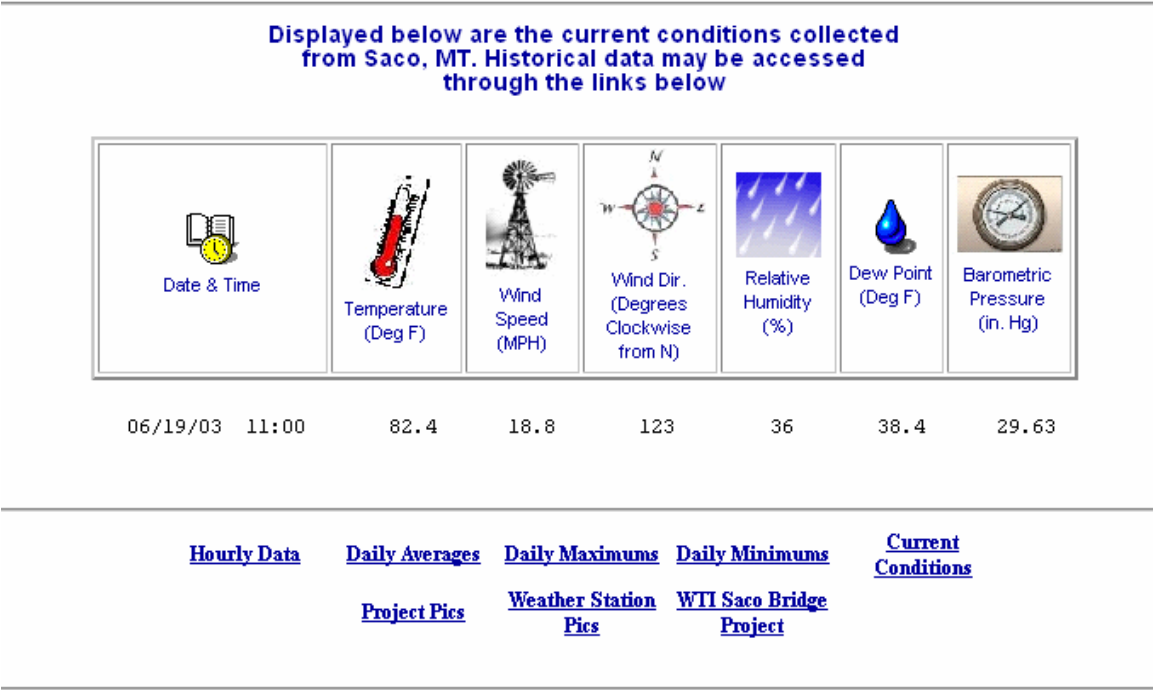


Figure 31: Internet Screenshot of Real-Time Weather Data from the Saco Weather Station

6 LIVE LOAD TESTING

The objective of the live load testing of the Saco bridge decks is to determine how each type of deck structurally transfers wheel loads from their point of application into the supports and to determine the magnitudes of the stresses and strains that develop in the decks as they perform this function. This information is used to understand whether the current approaches used for deck design reasonably represent actual structural behavior (with respect to the both the manner in which the load is carried and the levels of stress generated in the system) and to assess the likelihood of immediate and/or long-term crack development in the decks from vehicle loads. The primary focus of the live load tests is the manner in which wheel loads are locally transmitted from the deck transversely into the bridge stringers.

Live load tests were conducted on the three bridges the week of July 28, 2003 (approximately one month after placing the bridge deck concrete). These tests were conducted after the decks were grooved and sealed and shortly after the bridge approaches were paved, but prior to being opened to traffic. The vehicles used in these tests were 3-axle dump trucks provided by MDT Maintenance in Malta, Montana. Most test runs were conducted with a single truck, at slow and high speeds. Additional tests were conducted using two adjacent trucks traveling at slow speed.

6.1 Test Vehicles

Calculations were performed prior to live load testing to determine a desirable truck weight and configuration. The design moments for the deck were determined using an AASHTO standard HL-93 truck configuration (3-axle truck) with a 145 kN single axle, positioned to generate the highest possible transverse moment in the deck. Several vehicle configurations were investigated to generate demands in the bridges during the live load tests on the same order of magnitude as the design moments. These configurations included grain trucks, farm tractors, and tractor semi-trailers. These configurations were found to offer little advantage over a three-axle dump truck with respect to maximizing demands on the deck. A three-axle dump truck operating at a gross vehicle weight of 300 kN with 112 kN per axle on the back tandems was calculated to generate transverse moments in the deck equal to 90 percent of the design moments. At this load, the maximum longitudinal moment in the deck was estimated to be 104 percent of the longitudinal design moment generated by the HL-93 design vehicle. As this load was estimated to be approximately the maximum load a three-axle dump truck can physically carry, it was selected for test purposes.

Using a heavier vehicle for the live load tests pushes the decks closer to their design demands and may better reveal differences in deck behavior between the empirical and conventional reinforcement designs. A review of prior research found that other researchers have utilized heavy three-axle dump trucks with wheel loads on the same order of magnitude as

the proposed heavier load set (Yang and Myers, 2003; Stallings and Porter, 2003; Nassif et al., 2003). The weights and dimensions of the actual trucks used in the live-load experiments (a Sterling and a Volvo truck) are summarized in Figures 32 and 33, respectively. Figure 34 shows the Sterling truck which was used for all the single truck tests.

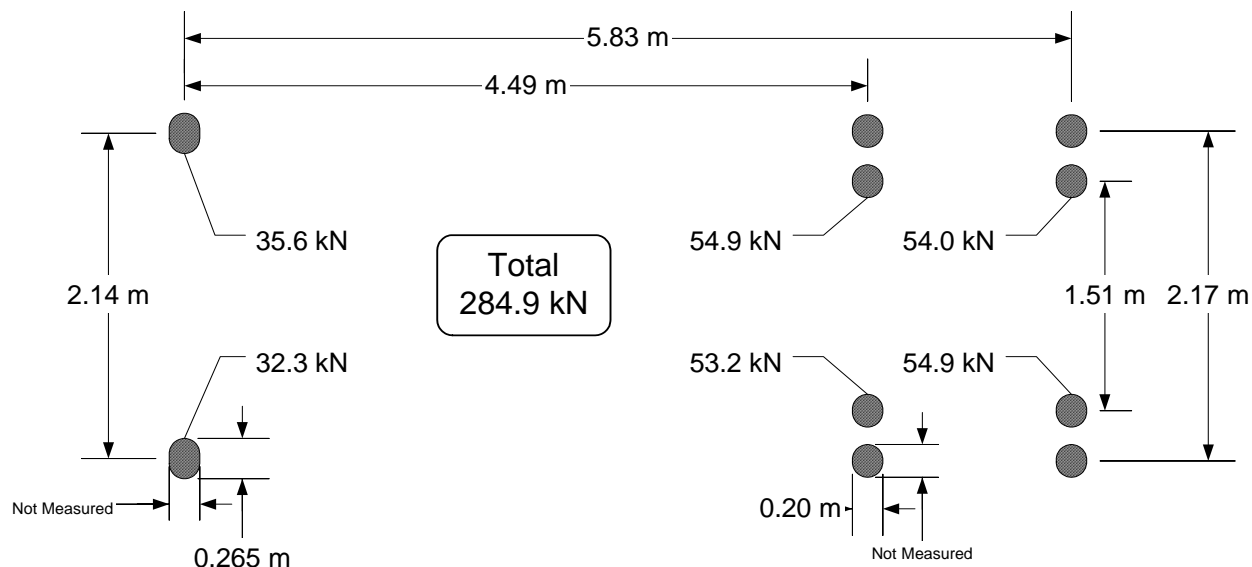


Figure 32: Dimension and Weight of the Sterling 3-Axle Dump Truck Used during Live Load Tests

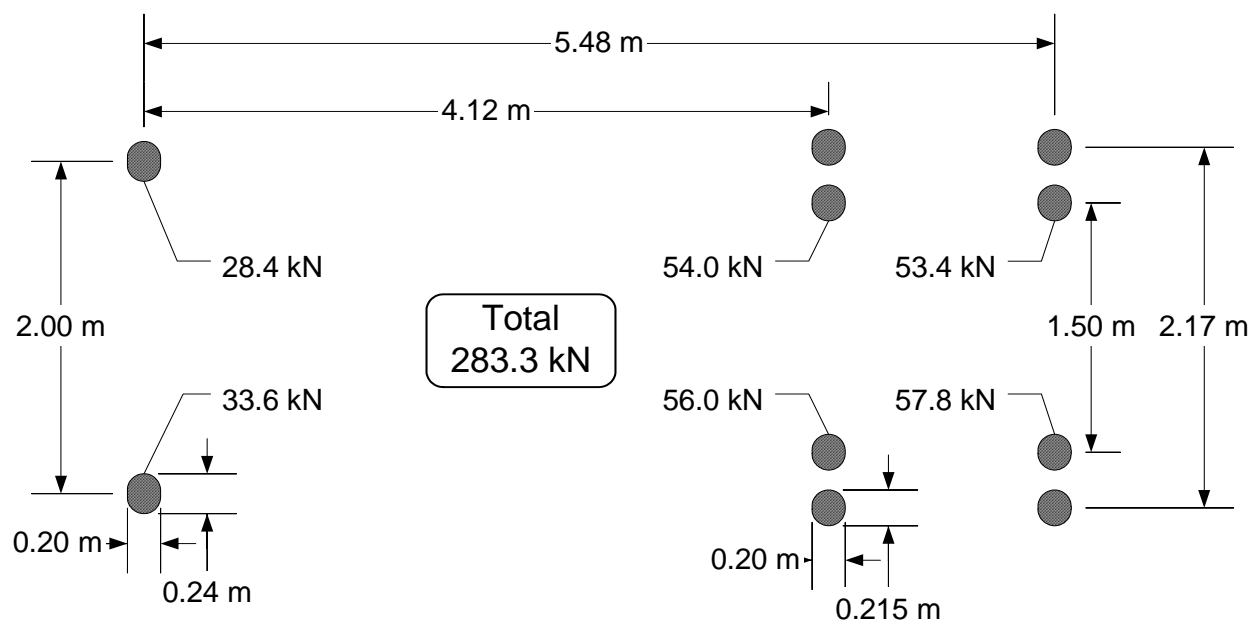


Figure 33: Dimension and Weight of the Volvo 3-Axle Dump Truck Used during Live Load Tests



Figure 34: Sterling 3-Axle Dump Truck

6.2 Testing Procedure

An identical regimen of live load tests was performed on each of the three Saco bridges. Each bridge was subjected to 15 test runs: 8 low speed single-truck tests, 5 high speed single-truck tests, and 2 low speed two-truck tests. Throughout the remainder of this document, low speed single-truck tests will be referred to simply as ‘Single Truck’ (ST) tests; high speed single-truck tests will simply be referred to as ‘High Speed’ (HS) tests; low speed two-truck tests will simply be referred to as ‘Two Truck’ (TT) tests.

Nine longitudinal truck paths were used in the live load tests. The positions, labeled R, S, T, U, V, W, X, Y, and Z, indicate the path of the front tire on the driver’s side of the truck as it traverses the bridge in each test (see Figure 35). To record the longitudinal position of the truck as it crossed the bridge, transverse lines were painted on the deck at two-meter intervals. As the truck traversed the bridge during the slow-speed tests (ST and TT), a hand-held button was depressed to electronically record each time the front axle of the truck reached each successive two-meter mark.

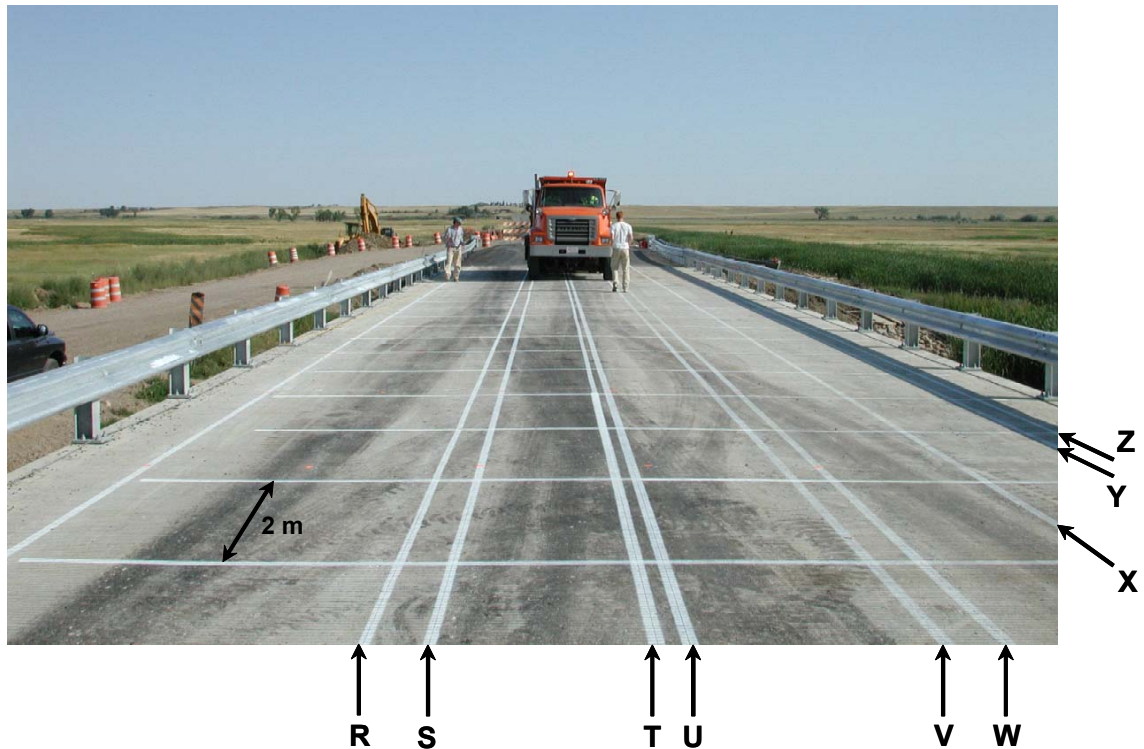


Figure 35: Photograph of Longitudinal Lines Used for Truck Positioning during Live Load Testing

The nine truck paths were selected to characterize deck response under the most critical load positions. Generally, tire loads were positioned to either be directly over a girder or at the midspan between girders, as shown in the cross-section views of Figure 36. Truck paths U and X position the center of the truck directly over a girder, such that the tires symmetrically straddle the girder. In Figure 36(a), the ‘Single Truck’ (ST) tests are followed by the letter of the appropriate truck path – R through Z. For example, ST-V represents a low speed single-truck test along the V truck line, as pictured in Figure 35. Likewise, positions in the two-truck and high-speed tests are shown in Figures 36(b) and 36(c), respectively.

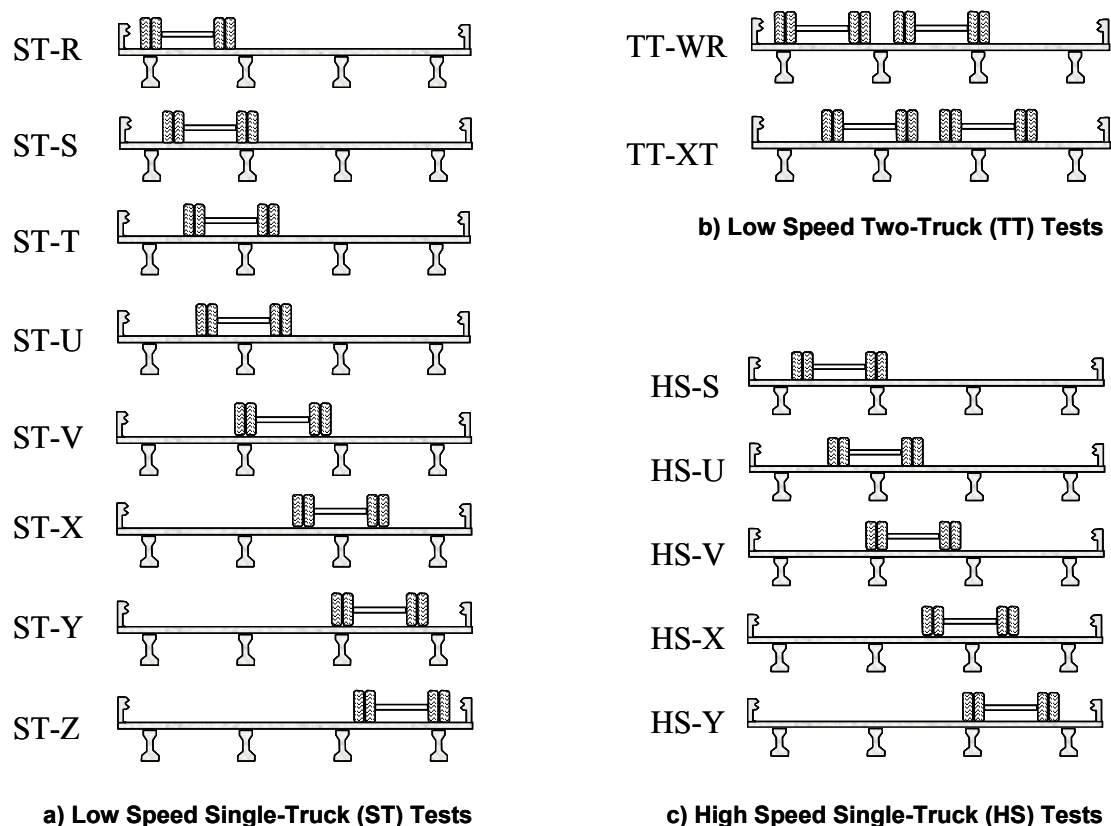


Figure 36: Truck Positions for Live Load Tests

Low-speed or “crawl” test were used in this investigation rather than statically stopping the truck at various locations and logging the data, as has been done in several bridge investigations. The information collected during such tests consists of a continuous stream of strain data as a function of longitudinal truck position. This approach is more efficient and provides more complete live load response information than static placement at discrete locations. Dynamic effects are negligible at the slow speeds used for these tests. The disadvantages of using a crawl test are the potential for minor deviations in the truck position and the inability to use certain types of gages (in this case the vibrating wire strain gages).

During the low-speed single-truck (ST) tests, the Sterling dump truck was driven along each of the eight selected longitudinal truck paths shown in Figure 36(a). One person marked the position of the front wheels using the hand-held button while the other guided the truck along the proper longitudinal path. Slow-speed tests were performed at a speed of approximately 3 miles per hour. For the low speed, two-truck (TT) tests, both the Sterling and Volvo dump trucks were driven across the bridges side-by-side at two sets of longitudinal truck paths: truck lines W and R, and X and T, as shown in Figure 36(b).

Five high speed single-truck (HS) tests were conducted using the Sterling truck. The truck was driven across the bridge at a speed of approximately 60 miles per hour along each of the five

selected longitudinal lines shown in Figure 36(c). Due to the relatively short duration of these tests and the high speeds involved, no correlation between strain response and truck position was electronically recorded. Truck lines R, Y and Z place the truck very close to the guardrail and thus were not used in the high speed tests due to safety concerns. The actual positioning of the truck in the high speed tests was not as precise as during the slow tests, but was within approximately 30 cm from the longitudinal lines. Lines that were close together, such as T and W, were omitted because of their close proximity to test lines U and V.

6.3 Data Processing

To facilitate analyses of the live load data, it was manipulated to output deck response as a function of vehicle position, rather than a function of the elapsed time (which was how the data was recorded). Notably, due to differences in the travel speeds of the vehicle during the various tests, the data arrays from all the tests were difficult to correlate. Utilizing the position stamps created by the hand-held push button, a routine was written to estimate, from the time histories, the strain data at specific longitudinal truck positions. In this way, all data sets consisted of strain response information at identical spatial positions of the truck. Additionally, it was determined that minimal changes occurred over the short duration of each test (less than 2 minutes) due to changes in ambient conditions (i.e., temperature variation). As such, all strain histories were shifted as necessary so that initial strains were zero for each experiment.

7 RESULTS AND ANALYSIS OF LIVE LOAD TEST DATA

The primary goal of this project is to compare the relative performance of the three bridge decks. However, because the bridges are relatively young, only subtle behavioral differences have emerged to date from data collected during the live load tests. Therefore, it is too early to assess what these differences indicate with regard to the overall durability and structural efficiency of each deck type. The significance of these differences in behavior on performance may become clearer as additional data is collected over the remainder of the project.

The live load test data can be used to develop a fundamental understanding of how each bridge deck responds to test vehicle loads. Simple observations in this regard allow useful comparisons to be drawn between the performance of the three decks when more complex behaviors arise. Comparisons between the reported data and expected responses derived from basic strength of materials concepts are also useful in this analysis. To analyze the live load test results, an attempt was made to isolate the bridge deck's behavior from the contributions of other structural elements in the bridges. Consequently, this analysis focused specifically upon the transverse deck response, since it was believed to be most significantly affected by the configuration of each bridge deck. Thus, the following analysis of the live load data focuses on strains recorded by transverse gages bonded to the reinforcement.

The following sections present an analysis of several fundamental behaviors that have been observed in the three bridge decks based on the live load data. Aspects of bridge deck behavior that are discussed include:

- longitudinal cracks,
- in-plane stresses,
- how each bridge carries load,
- transverse deck integrity over the girders, and
- general non-linear behavior.

Each of these behaviors is examined using data from the strain gages bonded to the reinforcement in the transverse direction. It also can be used to determine the height of the neutral axis within the deck, the relative magnitude of the bending moments experienced by the decks, and the validity of superposition for calculating deck demands under multiple vehicle events. These various items are indicative of deck condition relative to stiffness, cracking, and non-linear behavior.

7.1 General Behaviors

Before proceeding with detailed analyses of the data, it is critical to validate that behavioral responses reported in the data match the direction and relative magnitude of the expected response. One unique aspect of this project is the availability of several live load tests on three

different bridges. Certainly, some behavioral differences are expected between the three decks, which will be examined later in this chapter. Nonetheless, general behaviors are expected to be similar. These similarities build confidence in the data and what it can reveal. The response patterns and magnitudes can also be compared with published data from other bridge live load tests to validate that it is “reasonable.”

Presumably, the longitudinal bridge response is best understood conceptually. As a loaded truck passes over the center span, the deck deflects downward generating positive moments (compression top, tension bottom) in the loaded span, as illustrated in Figure 37. Under the same load, the curvature reverses over the interior bents, creating negative moments (tension top, compression bottom) over the bent and in adjacent spans, eventually transitioning to positive bending moment furthest from the load at the integral (quasi-fixed) supports.

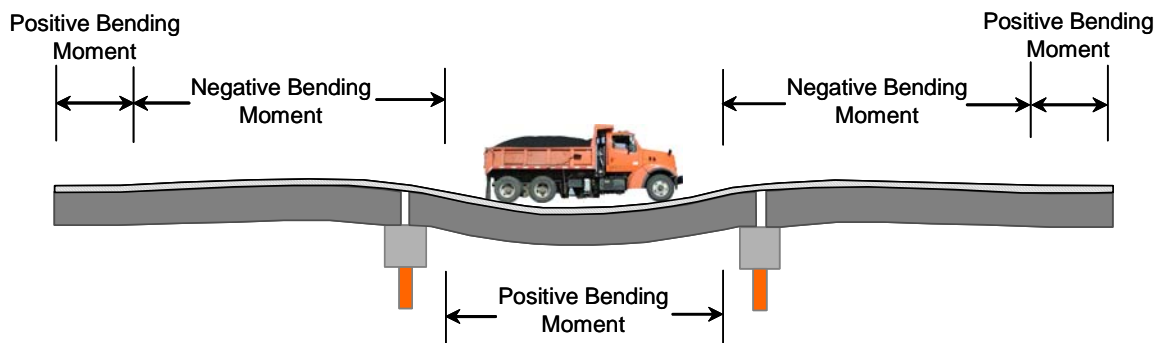


Figure 37: Illustration of Global Longitudinal Behavior

The longitudinal strain history at the longitudinal quarter-span (Gage Location D-3) is shown in Figure 38. For this style of plot, the positions denoted along the horizontal axis refer to the position of the test truck’s front tire as it traverses the bridge. The strain trace is the record of the strain at a single, stationary gage location when the truck is at the various longitudinal positions along the deck. Thus, for example, the peaks corresponding to the tandem axles are later in the strain history than the front axle (i.e., the front axle passes over the fixed gage location first, followed by the tandem axles – about 5m later). The beginning and end of the decks are denoted by dashed lines in conjunction with the illustration of the elevation view of the bridge, above the graph. The strain response continues even after the front axle of the truck leaves the south end of the deck, since the rear tandem axles are still on the deck for approximately five more meters.

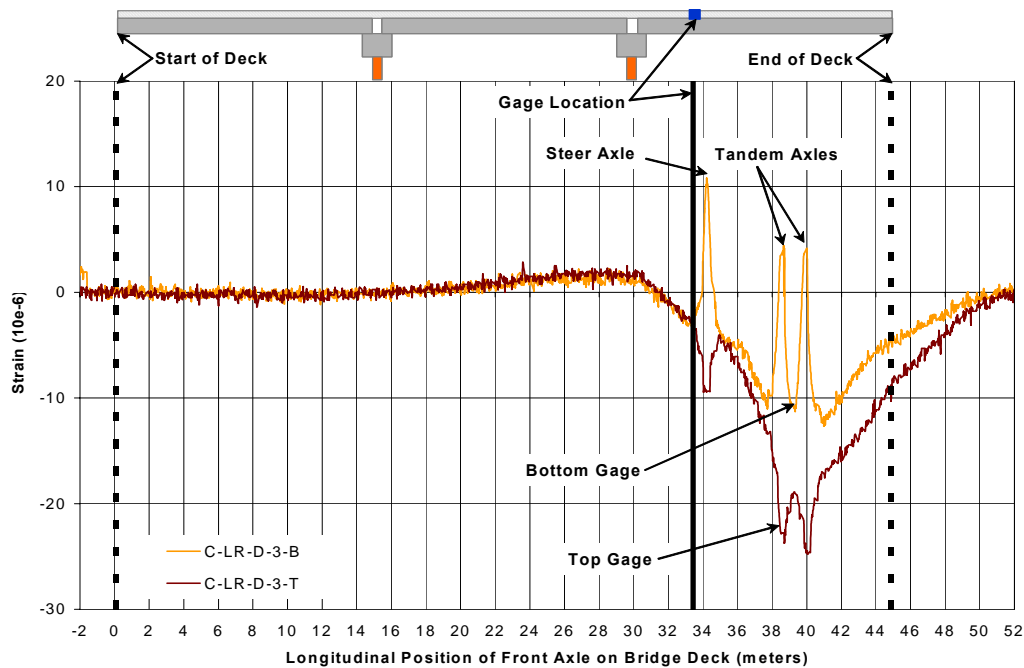


Figure 38: Strain History - Conventional Deck longitudinal Gage Location D-3 (ST-T Test)

Returning to Figure 38, when the truck loads the center span of the bridge (longitudinal positions 15m-30m), negative moments are induced in the adjacent instrumented span, as shown by the nominal tensile strains at Gage Location D-3. Note that in longitudinal bending behavior, the deck acts like the flange of a T-beam in concert with the stringers which act as the stem. As such, positive (tensile) strains in the deck indicate negative moment, while negative (compressive) strains in the deck indicate positive moment. As the truck tires enter the instrumented span, the response quickly changes to the expected positive bending moment response. Under positive moment, the top and bottom gages are both in compression. Also notable is the sharp positive moment peak in the gage response when each axle passes over the gage line. This characteristic response is caused by the local positive moment in the deck in the immediate vicinity of each tire footprint (i.e., a small ‘dish’ is formed around each tire load). These behaviors are not unexpected, since Gage Location D-3 is not directly supported by a girder; therefore, the deck experiences local deformation superimposed on the global response when the applied load is in the immediate vicinity of the gage. The shape and magnitude of this phenomenon is similar to longitudinal deck strains observations by Stallings and Porter (2002) (see Figure 2). The longitudinal response at Gage Location (D-3) for all three bridges is shown in Figure 39. Notably, all three bridges exhibit similar shapes and magnitudes of response, thereby building confidence in the data.

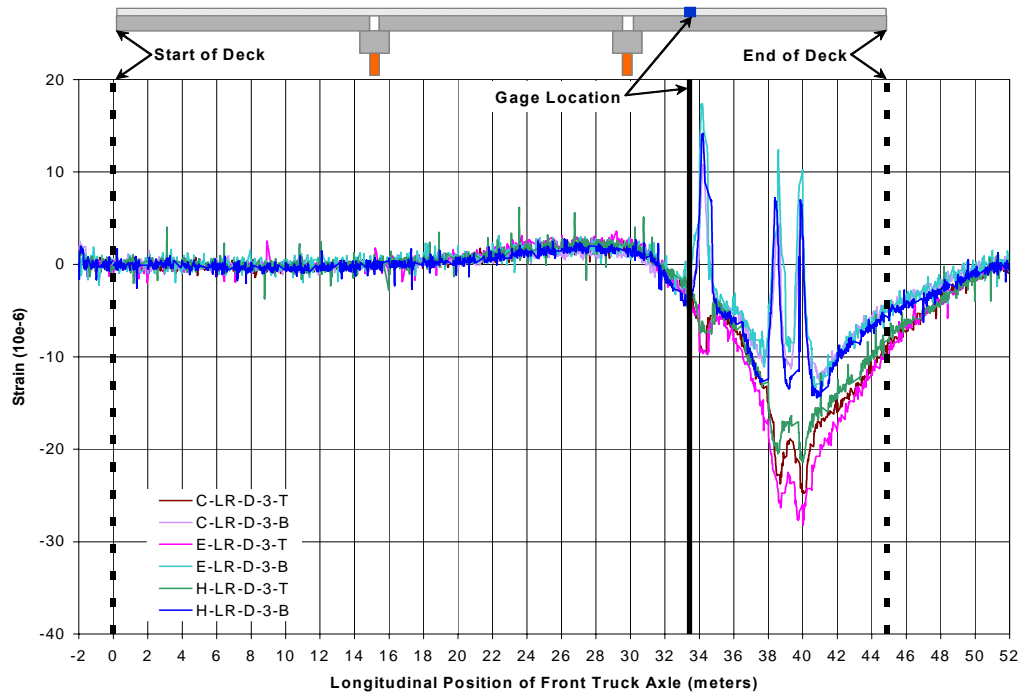


Figure 39: Strain History - All Three Decks Longitudinal Gage Location D-3 (ST-T Test)

Due to global bending behaviors, a negative moment in the longitudinal direction is expected over the bents for a truck positioned on the center span of the bridge. The longitudinal deck strain response over the bent is shown in Figure 40. The strain history in Figure 40 is recorded from the Empirical deck, longitudinal Gage Location F-1, immediately over Bent 2 (the interior bent containing the instrumentation). In contrast to the longitudinal strain histories at Gage Location D-3 (Figures 38 and 39), a negative bending moment (tension top, compression bottom) dominates the response of Gage Line F. It should be noted that the deck is continuous across the bent, but the girders are not. Therefore, unlike gage line D, the depth of the cross-section is simply that of the deck, not the composite deck and girder section. The reduction of the moment output when the tandem axles of the truck are directly over Gage Line F (front axle at approximately 35 to 36m) is because, at this truck position, only the front axle is loading the deck away from the bent, thereby reducing the negative moment over the bent.

Strain histories for all three bridges at Gage Location F-1 are shown in Figure 41. Negative moments are evident in all three decks under the same load at this location. The strains recorded in the top mat of reinforcement are all more tensile than the strains in the corresponding bottom mat, and the magnitude of the bending moment is similar for each deck (i.e., the difference between the top and bottom strains). The primary difference between the three bridges arises from the magnitude and direction of in-plane axial forces at this point in the deck. The Empirical deck response shows much less axial strain, and most obviously reveals the negative bending moment. Although the Conventional deck traces reveal a net tension in the continuous deck over

the bent, the negative moment is also evident here. Similarly, the HPC deck also reveals the negative moment, despite having a net compression across the cross-section at this point.

The accuracy of these differing responses was verified using co-located embedment gages. It is suggested that these differences in response are indicative of variations in the presence and restraint of longitudinal forces in each bridge. Despite the uniqueness of the specific response over the bent in each bridge, the recorded responses still verify that the expected behavior (i.e., negative bending moment) is present in each of the decks at magnitudes that are ‘reasonable’. All of the remaining longitudinal gages also show similar behavior among the three decks. This consistency in response further builds confidence in the accuracy of the data.

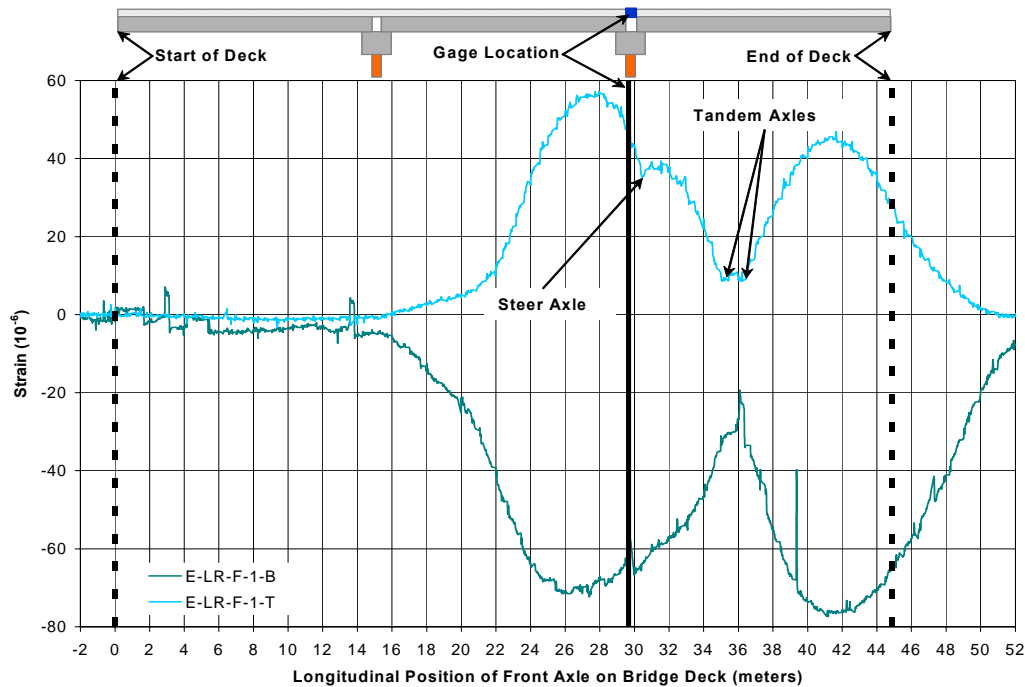


Figure 40: Strain History - Empirical Deck Longitudinal Gage Location F-1 (ST-T Test)

Strain histories in the transverse direction are the focus of the remainder of this analysis. The transverse gages were installed, conditioned, and recorded in the same manner as the longitudinal gages; thus, the corresponding strain histories should be valid. As observed for the longitudinal strains above, the measured transverse responses in all three bridges were generally similar in shape and magnitude under corresponding vehicle tests (several of these traces are presented and discussed in detail in the following sections of this report). These observations validate that it is reasonable to proceed with more complex analyses and begin drawing conclusions about deck behaviors from the data.

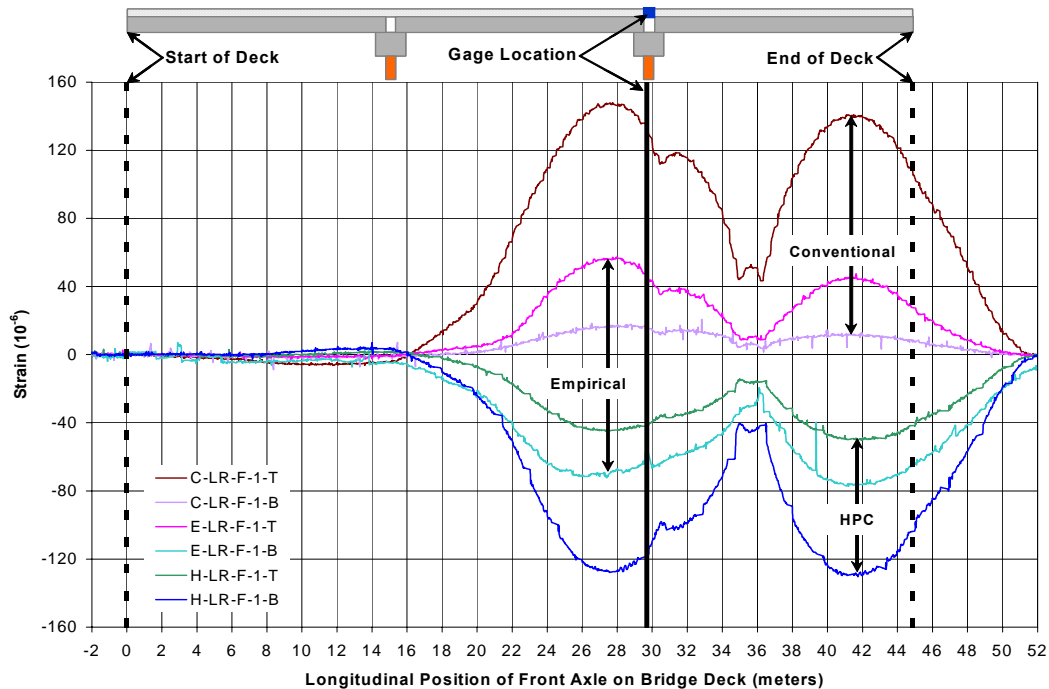


Figure 41: Strain history - all three decks longitudinal Gage Location F-1 (ST-T test)

7.2 Deck Cracking and Axial Strain Analysis

A brief review of the standard theories for bridge deck behavior is presented here to establish a foundation for interpreting the live load data. Recall that AASHTO (2000) traditionally represents a bridge deck as a continuous beam in the transverse direction, supported by rigid girders below. According to this model, the deck transmits applied tire loads transversely to the girders and hence into the remaining substructure. This approach is reportedly based upon the work of Westergaard, which was conducted in 1930 (Csagoly and Lybas, 1989; Cao, 1996). Westergaard's treatment of the bridge deck as a continuous beam over rigid girders is simple in nature, and is supported by several behavioral observations presented later in this report. Actual load carrying mechanisms, however, are more complex in nature and require a more sophisticated representation of the deck-girder system to identify subtle differences in behavior between the three decks. The assumption Cao (1996) made is that the girders act as springs rather than fixed supports. This behavior is also evident in the live load responses observed in these tests.

Admittedly, AASHTO (2000) has recognized that the primary load supporting mechanism in the transverse direction of bridge decks is internal arching action combined with a small flexural component, providing justification for the empirical design method. This load-carrying mechanism occurs in scenarios of high stresses. However, this load-carrying mechanism manifests itself only after the bottom of the deck has cracked (AASHTO 2000; Csagoly and Lybas 1989; Fang, et al. 1990; Fenwick and Dickson 1989). The competency of the cracked

region is then dependent upon the restraint provided by surrounding regions of concrete and other supporting elements, such as girders or diaphragms. As discussed in the literature review, the deck concrete surrounding the area of loading experience compressive membrane forces. However, Fang et al. (1990) performed testing on Texas bridge decks with Ontario design and observed that the deck remained in the linear elastic region under service loads and overloading (three times the AASHTO design load). Additionally, tensile membrane forces were observed in the deck up to the point of cracking in the positive moment regions; compressive membrane forces were only apparent after the occurrence of cracking. Thus, it will be useful to determine if any of the Saco bridge decks shows evidence of tensile cracking, membrane forces, or internal arching behavior.

Longitudinal cracking is not expected to occur at the strain levels observed in the Saco bridge decks during the live load tests. The maximum transverse tensile strain recorded in any of the bridges during live load testing was approximately $50\ \mu\epsilon$ at Gage D-4-Bottom during the ST-U test. A strain of $50\ \mu\epsilon$ in the lower mat of reinforcing steel corresponds to a strain of $75\ \mu\epsilon$ at the lowest extreme fiber of the concrete. Therefore, transverse deck strains are below the magnitude that would suggest concrete cracking. While there is no consensus on how the cracking strain of a particular concrete can be determined, it generally is expected to be in the range of 78 to $136\ \mu\epsilon$ (Annex, 1997). In the case of the Saco decks, expected cracking strains on the order of magnitude of $100\ \mu\epsilon$ were calculated, based on the elastic modulus and the peak tensile strength for the concrete in each deck at the time of the first live load test.

It is commonly accepted that strain development in bridge decks is dominated by environmental temperature changes (Hughes et al., 2000; Boothby and Laman, 1999). Strain levels of this magnitude are able to induce longitudinal cracks in the bridge deck. If cracking of the deck had occurred due to changes in ambient conditions, it should be evident in some aspects of the deck response under live load demands. No visible longitudinal cracking was evident during the live load tests. This observation certainly does not preclude the possibility of micro-cracking, which could have similar effects on deck behavior as macro-cracking, although not to the same extent.

The initial investigation of axial strains within the deck was primarily focused upon determining the possible presence of internal arching behaviors. However, in later stages of the analysis, it became apparent that the investigation of axial strains could provide additional insight into deck behaviors, independent of the presence of arching action. Furthermore, in light of Fang's observation, it was unlikely that load levels in the Saco tests were high enough to create this behavior (Fang et al., 1990). This portion of the analysis will serve as a baseline for evaluating future live load testing results, to determine if the internal arching mechanism has become more or less pronounced.

Five transverse gages bonded to the reinforcement along Gage Line D were used to study transverse deck behaviors (Figure 42(a)). The cross section of the superstructure shown in Figure 42(b) indicates the position of each gage with respect to features of the deck. These five gages are used throughout the analysis to characterize transverse deck behaviors.

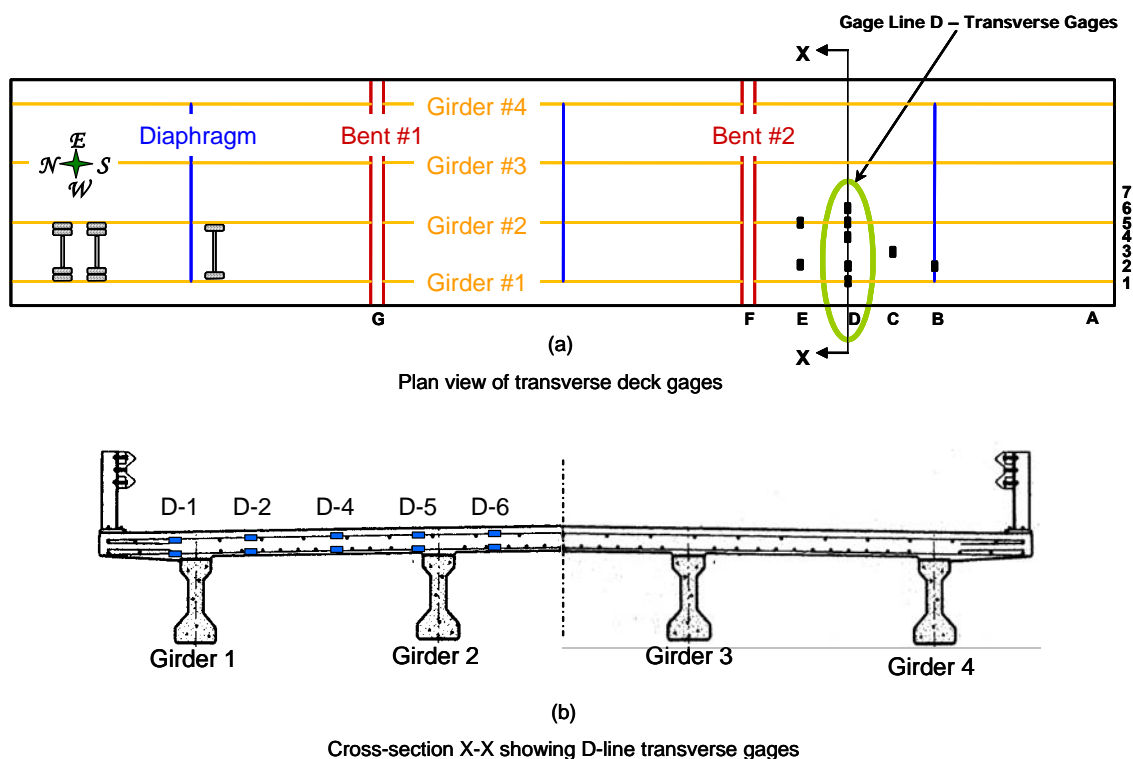


Figure 42: Transverse Gages of Interest (Gage Line D)

7.2.1 Position of Neutral Axis in Bridge Decks

One feature of a reinforced concrete cross-section, indicative of both its possible condition (i.e., cracked or uncracked) as well as the source of the normal stresses it may be experiencing (i.e., bending or in-plane forces), is the location of the neutral axis. This location is easily determined from the strain data collected in the Saco bridge decks, so this analysis begins with an investigation of the location of the neutral axis in the deck cross-sections under the various live load events. This analysis is prefaced by a brief review of the concept of the neutral axis.

The neutral axis of a beam is simply the height within its cross-section at which it experiences zero normal stress when loaded in bending. The **bending neutral axis** is the height of the beam's neutral axis under pure bending (i.e., no axial forces present). For beams composed of homogeneous materials, the height of the bending neutral axis can be determined from the geometry of the cross section, by using the first moments of areas. For example, the bending neutral axis of a rectangular homogeneous cross-section lies exactly at mid-depth, through the centroid, as shown in Figure 43.

For composite materials such as reinforced concrete, the relative amount, location, and stiffness of the two materials each factor into the position of the bending neutral axis. The standard procedure used to locate the bending neutral axis is called the Method of Transformed Areas. This method converts the actual area of steel to a theoretical area of concrete that would provide equivalent flexural resistance. Thus, the ‘transformed’ cross-section is composed of a homogeneous material; and the location of the bending neutral axis can be determined by taking the first moments of area (Wang and Salmon, 1985).

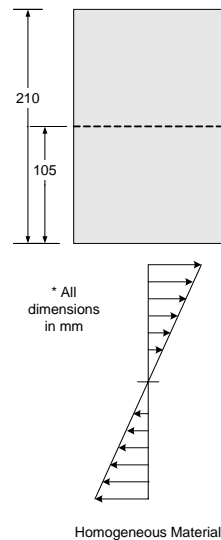


Figure 43: Homogeneous Deck Cross-Section Geometry with Calculated Bending Neutral Axis and Expected Bending Strain Profile (uncracked)

In typical design practice, it is common to neglect the area of concrete in tension when determining the position of the bending neutral axis, since its tensile load carrying capacity is minimal when compared to the compressive region. However, the material research of Gopalaratnam and Shah (1985) and Fenwick and Dickson (1989) indicate that concrete does, in fact, provide a substantial contribution in the tensile regions of the cross-section. Specifically for bridge decks, Fang et al. (1990) observed that under typical service loads, the tensile regions of the bridge deck remained uncracked. Thus, in the following analyses, the tensile contribution of the concrete will be included as part of the cross-section when calculating the bending neutral axis. However, it is important to realize that the integrity of the concrete could greatly affect the position of the bending neutral axis, and if for any reason significant cracking is expected to have occurred, this assumption should be revisited.

Assuming that the concrete is uncracked, the expected location of the bending neutral axis was calculated for the Saco bridge decks using the Method of Transformed Areas (described above). All three decks had a specified thickness of 210 mm. For both the Conventional and HPC decks, the size (19 mm diameter) and distribution (230 mm on center) of the transverse

steel is identical in the top and bottom reinforcing mats. However, the mats are not symmetrically located in the depth of the cross-section; the clear cover on the top surface (60 mm) is larger than at the bottom (25 mm).

Taking into consideration the different concrete strengths in the two decks, the bending neutral axes for the Conventional and HPC decks were calculated to be 104.2 mm and 104.4 mm above the bottom fiber of the deck, (Figure 44(a) and 44(b), respectively) – nearly the same height, lying just below mid-depth. As the reinforcing steel was laid out identically in these two decks, the ratio of strains in the bottom steel versus strains in the top steel were also predicted to be similar: 1.92 for the Conventional deck and 1.94 for the HPC deck. Although strains recorded in the rebar will have different magnitudes, strains in the concrete at the extreme fibers of the deck should have approximately equal magnitudes under pure bending, but be opposite in sign.

The Empirical deck cross-section has a slightly different geometry from the Conventional and HPC decks. The transverse steel in this deck is not identical in the upper and lower mats, as shown in Figure 44(c). Although the specified clear covers are the same as the other two decks, the bottom mat of transverse rebar is made up of 16 mm diameter bars spaced 345 mm on center and the top mat of transverse rebar is made up of 13 mm diameter bars spaced 330 mm on center. Despite this difference, the bending neutral axis for the uncracked Empirical deck was also predicted to lie relatively close to mid-depth, at 104.4 mm. Although the bending neutral axis was nearly identical to those of the Conventional and HPC decks, the predicted ratio of bottom rebar strains to top rebar strains is 1.82. This difference stems from the smaller bar sizes in the Empirical deck – given the same clear cover; the smaller bars place the mid-plane of each bar farther from the neutral axis. Again, the concrete strains at the extreme fibers will have approximately the same magnitude, with opposite sign.

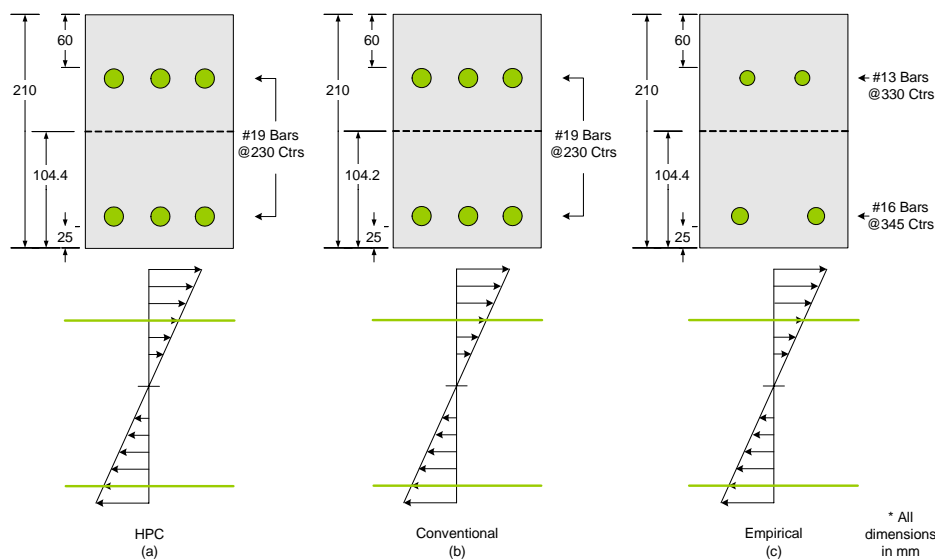


Figure 44: Saco Bridge Deck Cross-Section Geometries with Calculated Bending Neutral Axes and Expected Bending Strain Profiles (uncracked)

7.2.1.1 Actual Neutral Axis Determination

The location of the bending neutral axis in the bridge decks was determined using strain data recorded during live load testing. This neutral axis will be referred to as the **actual neutral axis** throughout the remainder of this report. Differences between the actual neutral axis and the predicted bending neutral axis are subsequently used in explaining deck behaviors observed under the live load events. Before looking at the specific neutral axis position, it is informative to review what these gages indicate relative to general behavior of the deck at this location during test ST-S. Loading from the ST-S live load test near the strain gages located at position D-4 produces a positive moment (top compression, bottom tension) in the deck, as expected. Strain histories generated from Gage Location D-4 during the ST-S test are shown in Figure 45 for all three bridge decks. Gages located in the bottom mat show tensile strains approximately twice as large in magnitude as the compressive strains in corresponding top gages, which is generally consistent with bottom-to-top strain ratios predicted above for pure bending in the decks (1.92:1, 1.94:1 and 1.82:1 for the and Conventional, HPC and Empirical decks, respectively). This general behavior is evident in all of the free-span areas under the influence of positive moments (i.e., it is not unique to Gage Location D-4). In addition, this behavior is also verified by strains reported from co-located concrete embedment gages at mid-depth and in the plane of the upper mat of reinforcing steel (not shown in Figure 45). Namely, in situations where positive moments are imparted by the test truck, tensile strains are recorded by gages located at mid-depth, which qualitatively supports the assertion that the actual neutral axis is nearer to the top mat of steel than to the bottom.

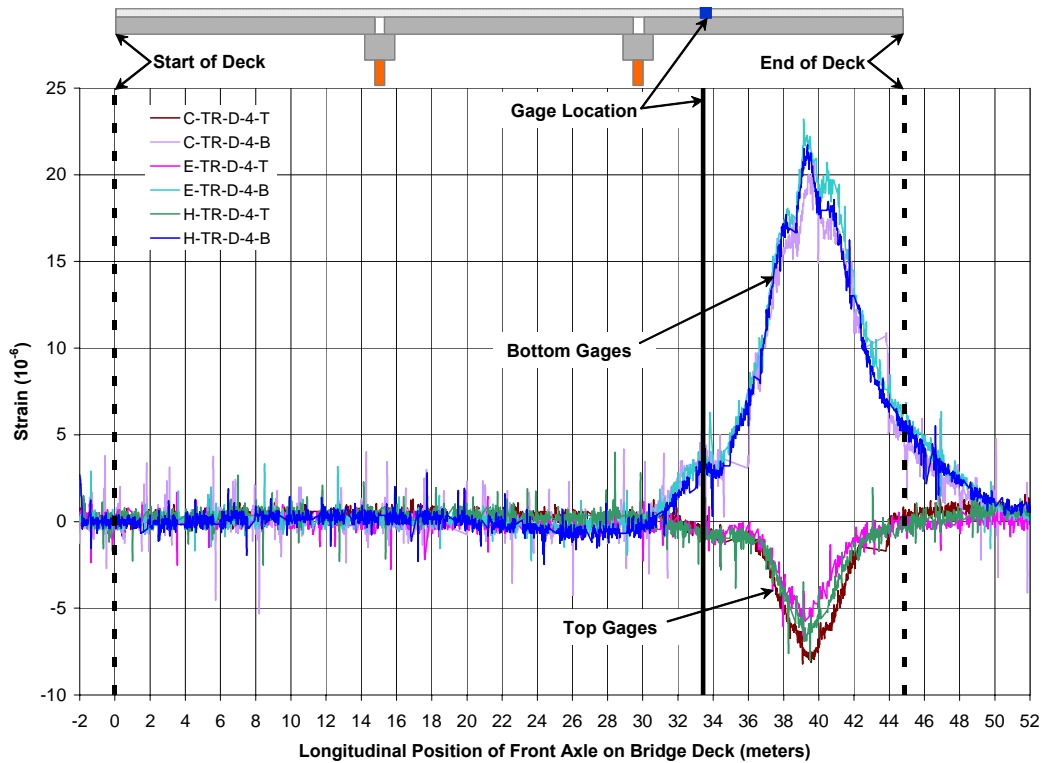


Figure 45: Typical Positive Moment Response from Bonded Strain Gages (Gage Location D-4, ST-S Test)

Recorded strains from each truck test were used to calculate the position of the actual neutral axis at each gage location, assuming a linear strain distribution across the depth of the deck (as illustrated in Figure 46). The point of intersection of the linear profile with the zero-strain-axis defines the actual neutral axis position, as indicated by point AA in Figure 46. The angle ϕ is the interior angle formed between the internal linear strain profile and the vertical zero-strain-axis. Coincidentally, the value of ϕ is directly related to the strength-of-materials value of curvature, κ , and is also proportional to the bending moment. Larger values of ϕ indicate larger magnitude moment, assuming the stiffness remains unchanged, and positive values of ϕ are counter-clockwise and indicate positive moment, while negative values of ϕ indicate negative moment.

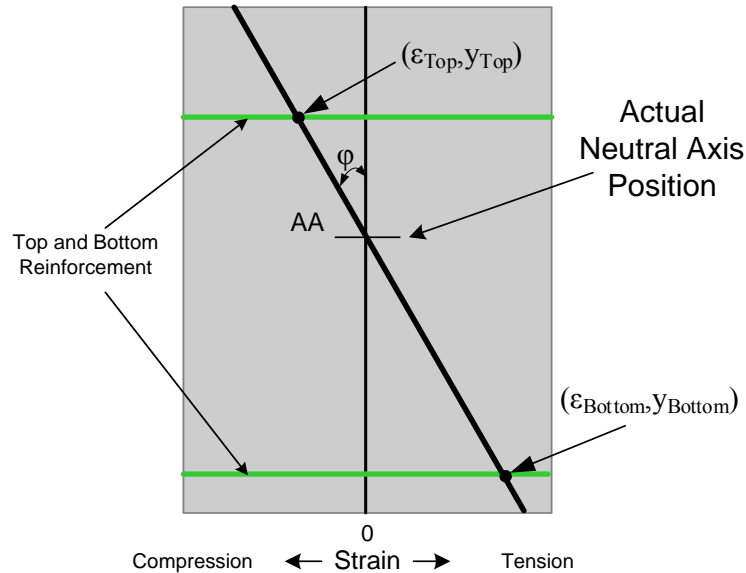


Figure 46: Illustration of How Actual Neutral Axis Height is Determined

Using the methodology described above, actual neutral axis positions were determined for the Conventional, Empirical, and HPC decks, as reported in Tables 9, 10, and 11. All values are height (in mm) of the actual neutral axis above the bottom fiber of the deck concrete. The actual neutral axis positions were determined for a single truck tests at two separate positions of the test vehicle along the bridge deck. In the first position, the front axle is at 40 m and the back tandem axle is directly over Gage Line D. In the second position the front axle is at 42 m, and the back tandem axle is two meters south of Gage Line D. Hereafter, these two positions are simply referred to as the 40 m and 42 m truck positions, as shown in Figure 47. As might be expected, distinct behaviors were sometimes observed in the immediate vicinity of the concentrated wheel loads (evident in the 40 m response), relative to the global effects observed away from the vicinity of the wheel loads (observed in the 42 m response). Tables 9, 10, and 11 contain the actual neutral axis positions for the Conventional, Empirical and HPC bridge decks, respectively, for the 40 m and 42 m truck positions.

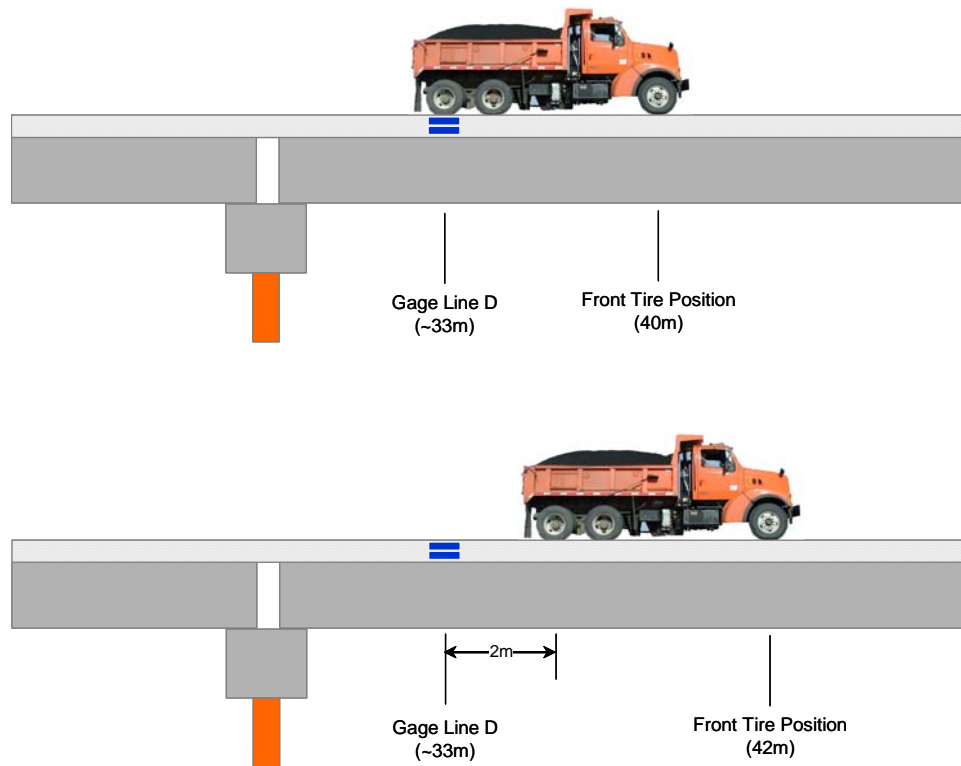


Figure 47: 40 m and 42 m Truck Positions, Relative to Gage Line D

Table 9: Actual Neutral Axis Positions for the Conventional Bridge Deck

Truck Position	Strain Gage Location	Single-Truck Tests * (mm)								Two-Truck Tests * (mm)	
		ST-R	ST-S	ST-T	ST-U	ST-V	ST-X	ST-Y	ST-Z	TT-XT	TT-WR
40 m	D-1	-299	-3	48	35	30	56	103	18	50	-22
	D-2	117	109	120	123	71	90	99	129	118	159
	D-4	111	111	102	104	132	91	101	105	107	115
	D-5	204	144	39	28	125	88	99	100	73	830
	D-6	79	169	122	118	120	118	111	114	120	120
42 m	D-1	252	†	-178	-178	-72	49	100	16	-121	-150
	D-2	142	141	141	139	-49	86	94	141	166	177
	D-4	137	126	114	115	118	56	93	97	120	129
	D-5	132	120	110	112	110	†	93	97	116	121
	D-6	202	136	130	122	120	127	102	109	125	126

† values are very large due to small strains

* shading indicates negative moment

Table 10: Actual Neutral Axis Positions for the Empirical Bridge Deck

Truck Position	Strain Gage Location	Single-Truck Tests * (mm)								Two-Truck Tests * (mm)	
		ST-R	ST-S	ST-T	ST-U	ST-V	ST-X	ST-Y	ST-Z	TT-XT	TT-WR
40 m	D-1	-237	-19	36	46	56	66	112	130	29	-50
	D-2	126	118	121	125	94	102	108	116	131	190
	D-4	120	121	117	118	141	105	113	113	122	126
	D-5	775	172	82	78	159	101	113	101	91	39
	D-6	86	207	126	122	123	65	120	119	123	125
42 m	D-1	337	322	-283	-299	40	33	102	130	-280	-704
	D-2	144	138	134	150	33	95	112	110	283	187
	D-4	141	135	130	130	130	84	107	103	143	140
	D-5	162	142	129	128	126	†	104	88	136	144
	D-6	270	144	131	133	128	137	114	113	133	139

† values are very large due to small strains

* shading indicates negative moment

Table 11: Actual Neutral Axis Positions for the HPC Bridge Deck

Truck Position	Strain Gage Location	Single-Truck Tests * (mm)								Two-Truck Tests * (mm)	
		ST-R	ST-S	ST-T	ST-U	ST-V	ST-X	ST-Y	ST-Z	TT-XT	TT-WR
40 m	D-1	-225	-20	25	19	35	129	282	406	36	-77
	D-2	113	107	114	117	80	97	104	111	107	167
	D-4	109	115	111	112	141	106	117	118	112	118
	D-5	247	155	73	69	148	98	107	105	90	41
	D-6	96	227	124	123	122	130	116	117	121	125
42 m	D-1	312	277	441	-1979	-178	88	141	406	847	794
	D-2	131	128	131	129	-1344	81	96	107	141	176
	D-4	114	128	124	126	126	85	117	111	128	136
	D-5	139	126	117	118	117	35	99	100	123	127
	D-6	353	145	121	130	128	173	109	110	129	133

† values are very large due to small strains

* shading indicates negative moment

In many cases, the actual neutral axis locations reported in Tables 9, 10, and 11 are quite different from the predicted bending neutral axis position of approximately 104 mm. In general, the actual neutral axis is higher than the bending neutral axis, under positive bending moments. This observation is statistically supported by a one-sided t-test, with 104 mm as the null hypothesis and using the mean of all positive moment neutral axis heights as the test statistic. A statistical t-test was also used to investigate differences between mean neutral axis heights of different decks. The mean neutral axis height of the Empirical deck under positive moment was found to be significantly higher than the mean neutral axis height of the Conventional deck under

positive moment ($\alpha = 0.05$). The mean neutral axis height for the HPC deck under positive moment rests somewhere between the means of the other two decks, but it is not statistically different from either of them. Excluding the Two Truck tests values, a second comparison between mean neutral axis heights under positive moment found that the means for both the Empirical and HPC decks were significantly higher than the mean neutral axis height of the Conventional deck, at an $\alpha = 0.025$ significance level.

The neutral axis positions reported under negative moment were scattered, having many values higher and lower than the predicted bending neutral axis (see Tables 9, 10, and 11). These outliers made it difficult to assess trends in these values with any confidence. In general, however, most of the negative moment neutral axis heights for the Conventional deck were below the predicted value of 104 mm; most of the Empirical and HPC values were above 104 mm. Nonetheless, in the presence of negative bending moment, the actual neutral axis heights appear generally lower than for the positive moment.

Comparing the localized effects and the more generalized global effects, the 42 m neutral axis heights seem generally higher than those at 40m, although this observation is not consistently supported with statistical significance. In most cases, the neutral axes obtained during Two-Truck tests appear about the same or nominally higher than the Single-Truck experiments.

Perhaps the most important conclusion that can be drawn is that the actual height of the neutral axis differs from the predicted height of the bending neutral axis. This difference in the neutral axis location could be the result of either of two distinct phenomena (or a combination of both): 1) a geometric shift of the bending neutral axis due to cracking or other irregularities in the cross-section, or 2) the presence of in-plane axial tension or compression forces. Two separate analyses were conducted to investigate which of these phenomena is most dominant. Due to the different transverse locations of the gages across the deck, they are difficult to compare directly. Therefore, each gage location is considered separately, based on the surrounding geometry and presumed behaviors at that position in the bridge deck. The most conclusive evidence used to evaluate each bridge deck for cracking and axial effects was found in the data from Gage Locations D-4 and D-1, respectively. Specific evidence from these two gage locations is presented in the two subsections below. Data obtained from the remaining three gage locations (D-2, D-5, and D-6) corroborate and support the evidence from the other two gages locations, but do not offer any unique insights.

7.2.1.2 Deck Cracking Analysis

The presence of cracks throughout the deck cross section will cause an apparent shift in the neutral axis. Cracks located in the underside of the bridge deck will cause the bending neutral axis to shift upward under positive moments. The amount of this shift depends on the height of the crack. Three theoretical cracking scenarios are presented in Figure 48; uncracked, cracking

up to the lower mat of reinforcement, and all tensile concrete cracked. When the concrete cracks in the bottom fibers due to a positive moment, the cross-section geometry changes and the neutral axis is expected to shift upward in the cross-section. The heights of bending neutral axes for these three theoretical conditions in each of the bridge decks are provided in Table 12.

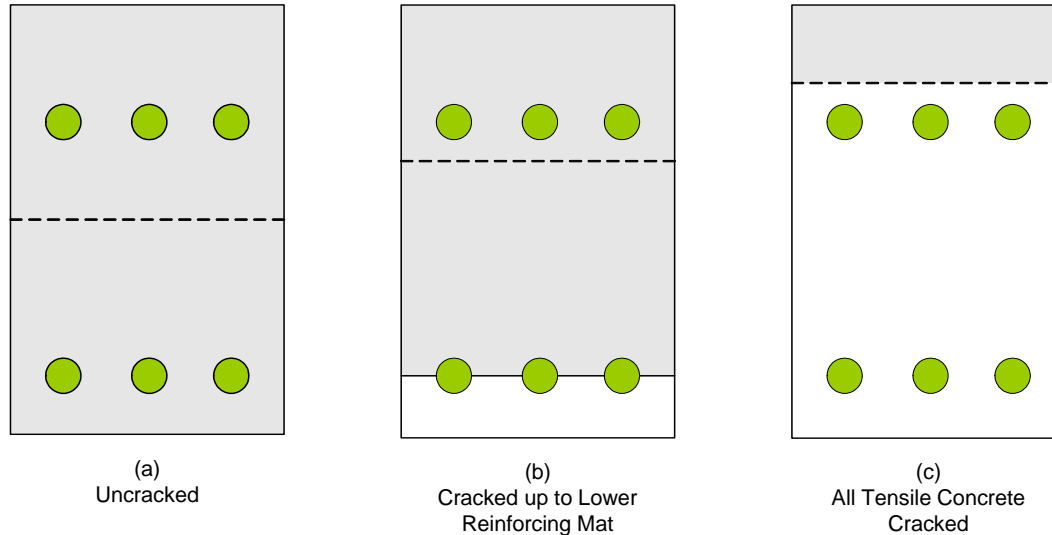


Figure 48: Theoretical Cracking Scenarios

Table 12: Bending Neutral Axis Heights at Various Cracking Levels under Positive Moment

Bridge Deck	Height of Bending Neutral Axis (mm)		
	Uncracked	Cracking up to Lower Reinforcing Mat	All Tensile Concrete Cracked
Conventional	104.2	120.0	166.2
Empirical	104.4	120.0	175.7
HPC	104.4	120.5	170.1

Many of the actual neutral axis heights calculated from strain data are similar to the height of the bending neutral axis for cracking up to the lower reinforcing mat (~120 mm), suggesting that the decks might be cracked. Such cracking might not be visually pronounced and were not noticed during the live load tests (i.e., the cracks might close in the unloaded condition). Conversely, cracking of all tensile concrete (approximately 85% of the cross-section height) would certainly have been noticed.

If a crack exists near the bottom of the bridge deck, the height of the bending neutral axis is expected to increase when compared to an uncracked section, under increasing positive moments. Increasing positive moments in the deck will increase the height of the bending neutral axis if the crack is unstable (i.e., the crack propagates upward under increasing positive

moment), or the height of the bending neutral axis will remain constant if the crack is stable (i.e., the crack does not propagate upward under increasing positive moment). In the presence of a crack in the bottom fibers, it is not expected that the height of the bending neutral axis will reduce under higher positive moments.

Recall that ϕ (interior angle formed between the internal linear strain profile and the vertical zero-strain-axis – illustrated in Figure 46) is an indicator of the magnitude of moments in the deck cross section. To compare magnitude of positive moments within each bridge deck, several values of ϕ determined from strain data at Gage Location D-4 are shown in Table 13 for truck tests ST-R, ST-S, ST-T, and ST-U. Gage Location D-4 offers the best location to investigate deck cracking, since it is positioned relatively close to the midspan between Girder 1 and Girder 2. At this location, the expected behaviors are presumably the best understood, with the deck behaving most like a beam spanning between the adjacent girders. Values of ϕ are also provided for the 40 m and 42 m longitudinal positions (refer to Figure 47) to illustrate that ϕ decreases as the load moves away from the gage location, as expected.

Table 13: Values of ϕ at Gage Location D-4

Longitudinal Position	Deck	ϕ (degrees)			
		ST-R	ST-S	ST-T	ST-U
40 m	Conventional	15.9	15.0	31.2	30.6
	Empirical	15.2	14.0	29.5	29.5
	HPC	16.6	14.5	30.3	31.4
42 m	Conventional	5.6	7.6	11.8	11.3
	Empirical	6.0	7.3	10.2	10.9
	HPC	7.2	7.5	10.4	12.7

Based on these ϕ angles, the positive moments induced at Gage Location D-4 are higher during the ST-T and ST-U tests than the ST-R and ST-S tests (assuming stiffness remains constant). In fact, the positive moments observed at Gage Location D-4 during ST-T and ST-U, are the largest of all the live load tests. Therefore, if cracking had occurred, it would be most pronounced in these live load tests. However, the actual neutral axis heights in these tests do not show that cracking occurred, since they are generally lower under greater positive moment. The actual neutral axis heights determined using strain data from Gage Location D-4 in all the decks during tests ST-R, ST-S, ST-T, and ST-U, are presented in Table 14. The reported neutral axis heights are lower for tests ST-T and ST-U than for the corresponding ST-R and ST-S tests, with the exception for the HPC deck, notably for the ST-R truck test. This relative anomaly in the results for the HPC, ST-R test is under investigation, and could result from the manner in which this test was conducted or an actual difference in structural behavior. Nevertheless, in the Saco

decks, higher positive moments generally are associated with lower neutral axis heights. Additionally, neutral axis heights are reportedly higher at the 42 m truck position than at the 40m truck position, which is counterintuitive. For a partially cracked cross-section, recall that lower neutral axis positions are not expected under higher positive moments. This expected behavior is not supported by the data presented here. Thus, it is unlikely the bottom of any of the decks has cracked.

Table 14: Actual Neutral Axis Heights (Gage Location D-4)

Longitudinal Position	Deck	Actual Neutral Axis Height (mm)			
		ST-R	ST-S	ST-T	ST-U
40m	Conventional	111	111	102	104
	Empirical	120	121	117	118
	HPC	109	115	111	112
42m	Conventional	137	126	114	115
	Empirical	141	135	130	130
	HPC	114	128	124	126

In light of these two observations regarding the relationship between positive moment and the actual neutral axis, it is unlikely that cracking occurred in the bottom fibers of the free span regions of any of the three decks during live load testing. It is important to qualify that this conclusion can only be definitively drawn in the region near the strain gages. However, it is assumed that the gages, which are located at critical response points, adequately represent other positive moment regions of the deck (note that negative moment effects over the girders are discussed later in this report in section 7.2.2). While the actual neutral axis has shifted in the decks relative to the theoretical bending neutral axis, cracking does not appear to be responsible.

7.2.1.3 Axial Force Analysis

In the preceding discussion, a logical analysis of the strain data from the decks indicated that none of the decks had cracked. In the following discussion, a similar approach is used to investigate the possibility that changes in neutral axis height are caused by the presence of in-plane axial forces and associated strains.

With or without the presence of cracks, axial forces within the plane of the bridge deck will result in an apparent neutral axis shift. When a member is loaded in pure bending, no net axial stress exists, and the strain profile for each deck will resemble those presented in Figure 44. Because the bridge deck and stringers act compositely, a more complicated distribution of moment and stress within the plane of the bridge decks is likely. Therefore, it is possible that in-plane axial stresses are being transferred throughout the deck. These stresses are superimposed

on top of the stresses throughout the cross section from bending. This results in a strain profile that is parallel to the predicted profile, but is shifted horizontally along the strain-axis, as shown in the two cases of Figure 49.

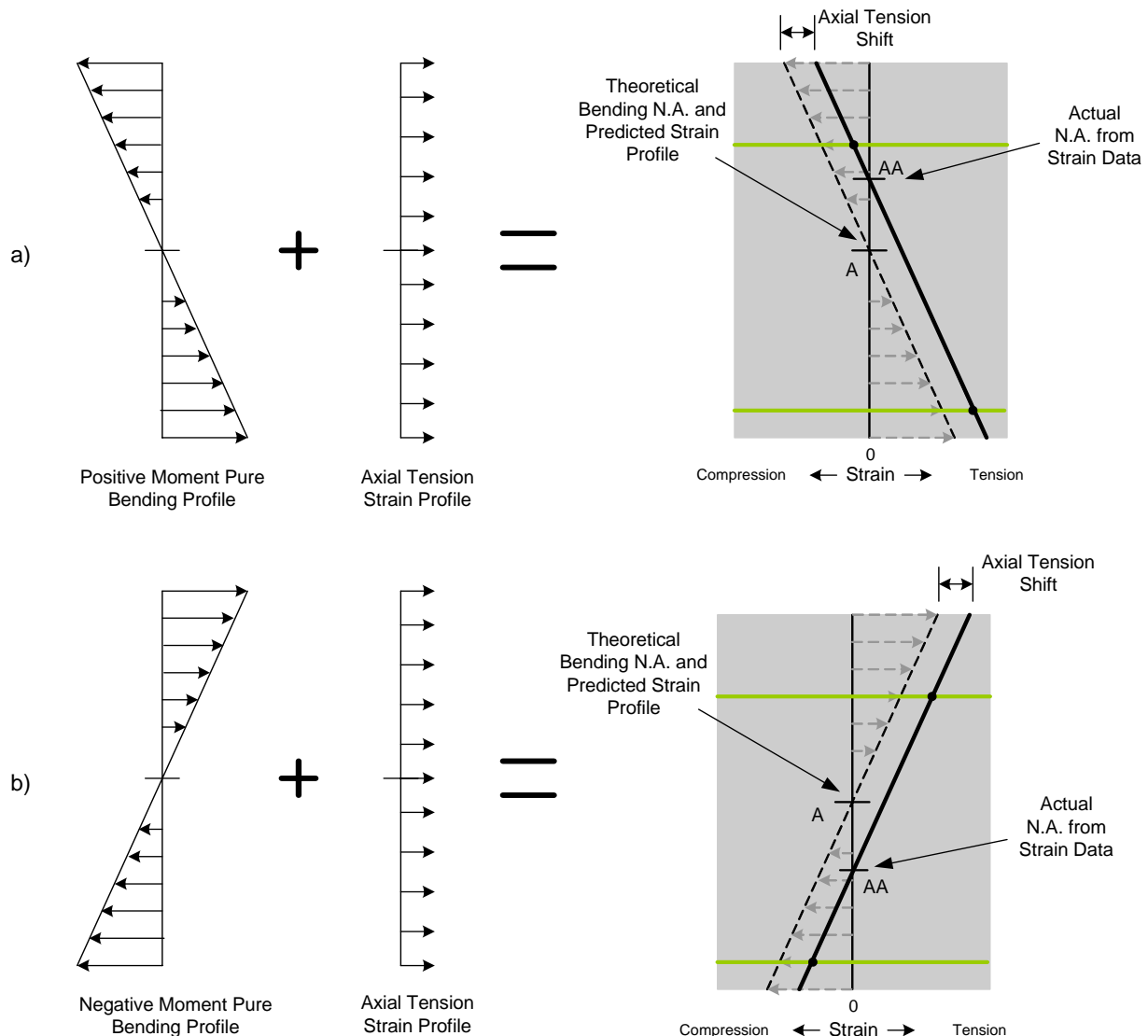


Figure 49: Illustration of Neutral Axis Shift Due to In-Plane Axial Strains under a) Positive Moment and b) Negative Moment

The addition of a uniform axial force effectively changes the height of the actual neutral axis from Point A (the height of bending neutral axis) to Point AA (the height of the actual neutral axis). In the presence of positive moments, the neutral axis shifts upward under axial tension (Figure 49(a)); correspondingly, it shifts downward in the presence of negative moments (Figure 49(b)). The neutral axis would shift in the opposite direction in a uniform axial compression field (not shown).

The uniform axial strains necessary to cause the actual neutral axis to shift from the bending were determined for all truck runs on each bridge. These strains are presented in Tables 15, 16, and 17 for the Conventional, Empirical, and HPC decks, respectively. To calculate this axial strain shift, strain data from the live load tests were used to determine the slope of the linear strain profile at each gage location. Rebar strains for pure bending were then predicted by drawing a parallel profile through the theoretical uncracked bending neutral axis (the dashed profile shown in Figure 49). The amount of superimposed axial strain necessary to shift the strain profile to the actual neutral axis was simply the strain difference between the pure bending profile and the actual profile. In Tables 15, 16, and 17, a positive sign indicates a tensile axial strain, while a negative sign indicates a compressive axial strain. Shaded cells indicate negative moment.

Table 15: Back-Calculated Axial Strains for the Conventional Deck

Truck Position	Strain Gage Location	Single-Truck Tests * ($\mu\epsilon$)								Two-Truck Tests * ($\mu\epsilon$)	
		ST-R	ST-S	ST-T	ST-U	ST-V	ST-X	ST-Y	ST-Z	TT-XT	TT-WR
40 m	D-1	5.3	7.2	4.0	4.3	1.6	0.9	0.0	-3.6	4.7	7.8
	D-2	2.4	2.0	1.5	1.2	1.5	0.9	0.3	-0.9	1.9	4.4
	D-4	1.9	1.8	-1.1	-0.2	1.4	0.9	0.2	-0.1	1.2	3.2
	D-5	4.7	5.1	4.8	4.9	2.8	1.7	0.4	0.4	6.0	6.8
	D-6	1.2	2.5	7.3	4.8	5.2	0.8	-0.7	-1.3	7.6	7.2
42 m	D-1	2.8	3.9	2.7	2.9	1.7	1.1	0.1	-3.4	3.2	5.5
	D-2	3.0	3.6	2.6	1.9	2.0	1.0	0.5	-1.0	3.4	4.6
	D-4	3.2	3.0	2.0	2.1	1.3	0.9	0.6	0.4	3.2	4.4
	D-5	2.5	2.3	1.5	1.8	1.1	1.0	0.6	0.5	2.6	3.9
	D-6	1.8	2.3	5.5	3.7	3.8	1.9	0.1	-0.5	6.2	4.7

* shading indicates negative moment; positive values = axial tension; negative values = axial compression

Table 16: Back-Calculated Axial Strains for the Empirical Deck

Truck Position	Strain Gage Location	Single-Truck Tests * ($\mu\epsilon$)								Two-Truck Tests * ($\mu\epsilon$)	
		ST-R	ST-S	ST-T	ST-U	ST-V	ST-X	ST-Y	ST-Z	TT-XT	TT-WR
40 m	D-1	5.6	5.9	3.9	3.2	1.1	0.3	0.0	-0.2	5.6	7.3
	D-2	3.7	4.8	0.9	0.6	0.4	0.1	-0.2	-0.5	2.4	4.6
	D-4	4.4	4.2	7.1	7.7	1.4	-0.1	-0.5	-0.4	7.6	6.3
	D-5	4.2	4.8	2.7	3.0	4.2	0.2	-0.5	0.2	2.7	5.5
	D-6	1.2	2.6	8.6	5.9	5.4	-0.8	-1.7	-1.7	8.2	8.1
42 m	D-1	2.5	2.6	2.5	1.8	0.9	0.6	0.0	-0.2	4.2	4.4
	D-2	3.0	3.4	2.0	2.2	0.9	0.4	-0.2	-0.2	4.4	4.8
	D-4	3.8	3.9	4.5	4.9	2.0	0.5	-0.1	0.1	6.1	5.9
	D-5	2.5	3.1	3.4	3.2	2.8	1.0	0.0	0.6	4.5	5.0
	D-6	2.1	2.7	5.0	5.3	4.7	1.0	-0.7	-0.7	6.4	5.7

* shading indicates negative moment; positive values = axial tension; negative values = axial compression

Table 17: Back-Calculated Axial Strains for the HPC Deck

Truck Position	Strain Gage Location	Single-Truck Tests * ($\mu\epsilon$)								Two-Truck Tests * ($\mu\epsilon$)	
		ST-R	ST-S	ST-T	ST-U	ST-V	ST-X	ST-Y	ST-Z	TT-XT	TT-WR
40 m	D-1	5.6	5.7	4.0	3.8	1.2	-0.2	-0.5	-0.6	4.3	7.0
	D-2	1.6	0.9	0.9	1.0	0.8	0.4	0.0	-0.2	0.4	3.5
	D-4	1.4	2.9	3.7	4.8	1.2	-0.1	-0.7	-0.6	3.4	4.0
	D-5	4.4	4.8	3.4	3.7	2.9	0.7	-0.2	0.0	3.5	5.3
	D-6	0.6	2.5	8.6	7.4	5.7	0.9	-1.2	-1.6	7.6	8.8
42 m	D-1	2.5	2.3	1.9	2.0	1.3	0.1	-0.1	-0.6	2.1	3.9
	D-2	1.9	2.6	1.8	1.5	1.4	0.7	0.3	-0.1	2.1	3.2
	D-4	1.2	3.1	3.6	4.9	1.7	0.4	-0.4	-0.3	3.6	4.0
	D-5	2.4	2.4	2.3	2.4	1.8	0.9	0.3	0.3	3.1	3.7
	D-6	1.2	2.5	3.1	5.0	4.4	1.9	-0.3	-0.5	5.4	4.8

* shading indicates negative moment; positive values = axial tension; negative values = axial compression

Notably, most of the axial strains calculated from the live load data were tensile. Recall that Fang et al. (1990) observed no deck cracking and observed in-plane tension membrane stresses in the decks up until cracks occurred at three times the AASHTO service load. With respect to their magnitudes, they are small but not insignificant. Many of the negative moment regions also reveal axial tension strains, which again are small but not insignificant in magnitude. With a minor exception in the Conventional deck, the only axial compressions noted were in regions experiencing negative moment, primarily during test runs ST-X, ST-Y, and ST-Z. All the decks reveal fairly similar magnitudes and directions of axial strains, although the Empirical deck appears to show generally higher strains than the other two decks. A statistical one-sided t-test was performed to compare the means of axial strains in the three decks under positive moment only. The mean of the axial tension strains in the HPC deck under positive moment are statistically higher than the mean of the Conventional deck ($\alpha = 0.05$). The Empirical deck has a statistically higher mean axial tension strain in positive moment regions than the Conventional and HPC decks ($\alpha = 0.025$).

One explanation of this tension is that, as the truck nears the region of the gages, the deck deforms like a plate in flexure, which tends to “draw in” toward the tire location. However, because the bridge deck is supported laterally by the girders, diaphragms, and surrounding deck concrete, the “drawing in” action is resisted and axial forces and strains are present in the deck section. This is similar to the behavior exhibited by a beam or plate, pinned at both ends and subjected to transverse load. Unlike a simply supported member which is allowed to deform along its axis under a load, the lateral restraint in a pinned-pinned member resists those deformations, thereby shifting the bending neutral axis due to in-plane axial stresses and corresponding axial strains. This behavior can occur in a linear-elastic fashion if the beam has already transversely deflected under the action of other loads (i.e., self-weight of the member).

For the Saco bridge decks, the data reported at Gage Location D-1 presents further evidence that axial forces are indeed present. Gage D-1 is located in the cantilevered portion of the bridge deck, just outside Girder 1 (refer to Figure 42). Many of the actual neutral axes calculated from strains at Gage Location D-1 fall outside of the geometric limitations of the cross-section (refer to Tables 9, 10, and 11). This phenomenon is physically impossible without the presence of axial forces. To illustrate this point, the diagram presented in Figure 50 shows a strain profile resulting from a positive bending moment coupled with a uniform axial tension field. In this case, the position of the neutral axis can be above the upper fiber of the cross-section.

The net tension in the deck at Gage Location D-1 is obvious in the transverse strain profile recorded from all three bridges at 40 m (truck tires in the vicinity of Gage Line D) for test ST-S, as shown in Figure 51. The moments induced at Gage Location D-1 are relatively small, as indicated by small ϕ angles. As such, bending and/or cracking effects are not expected to be very dramatic in this region. Therefore, it is reasonable to conclude that axial strains are predominantly governing the position of the actual neutral axis at Gage Location D-1.

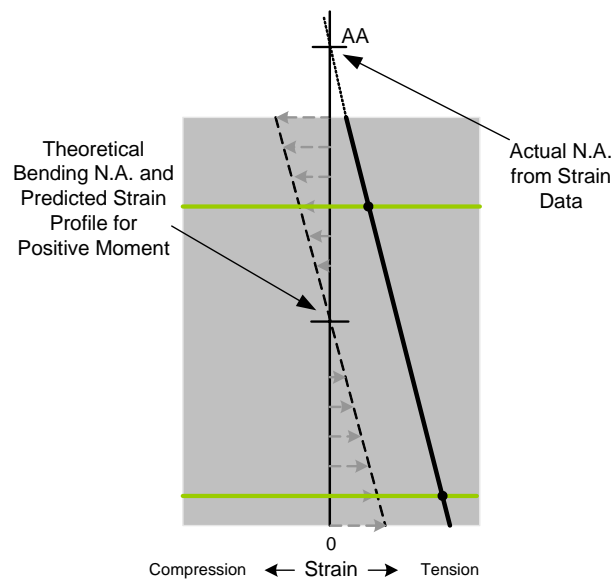


Figure 50: Illustration of Axial Tension Behavior at Gage Location D-1

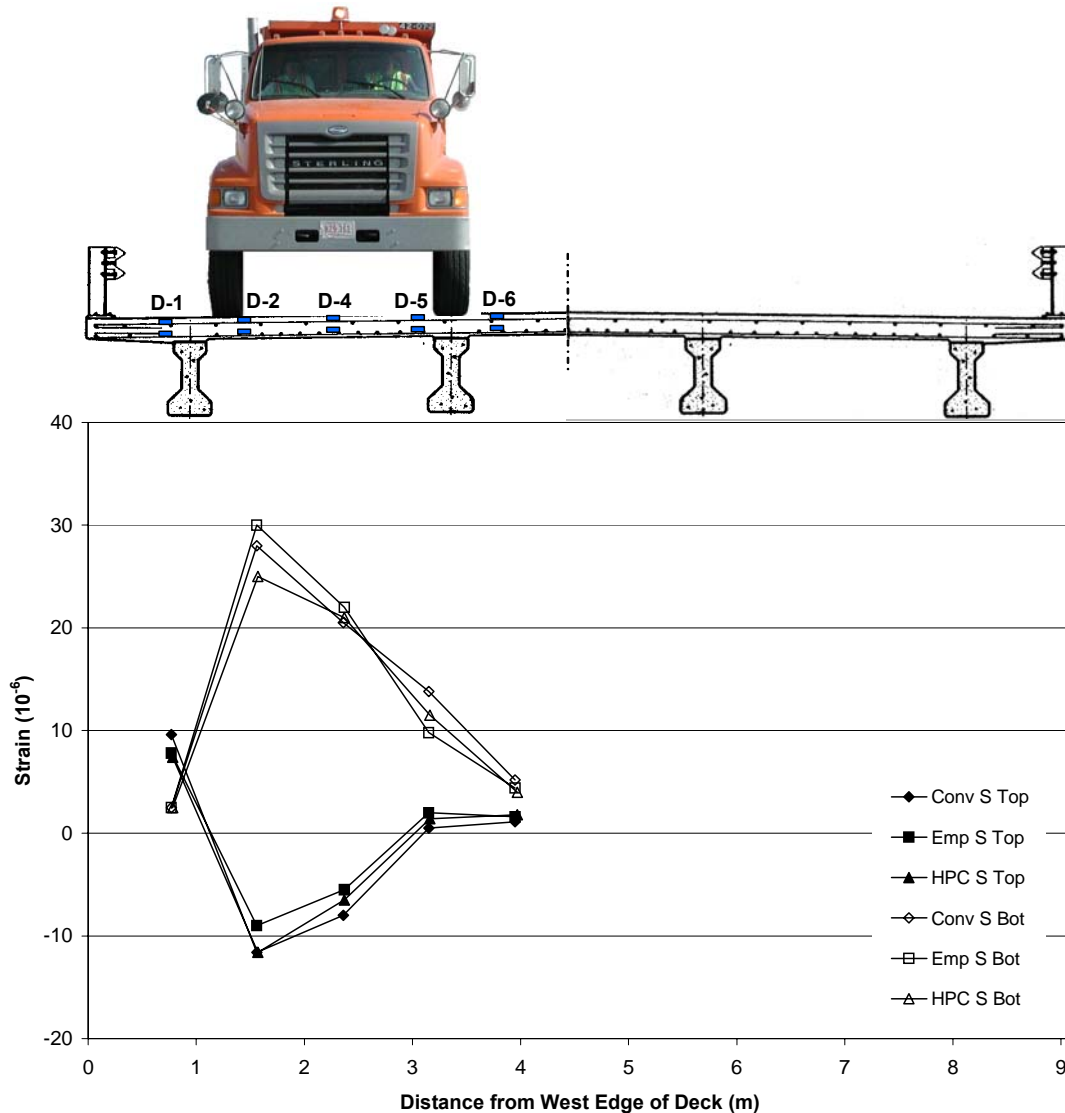


Figure 51: Transverse Strain Profile Revealing Axial Tension (ST-S Test at 40 m Truck Position)

Net tension is also evident at Gage Locations D-5 and D-6 in the transverse strain profile shown in Figure 51, further supporting the evidence of in-plane axial tension in the bridge decks. Although not as obvious from Figure 51, net axial tension is present in Gage Locations D-2 and D-4 as shown in Tables 15, 16, and 17. Similar results were found from all the bridge decks, that is, in-plane axial forces are present in all of the bridge decks, and that these axial forces are likely responsible for shifting the neutral axis.

7.2.1.4 Conclusions

A shift in the height of the bending neutral axis is most likely due to in-plane axial forces rather than deck cracking. Evidence presented using Gage Location D-4 (and supported by the other locations) consistently shows that cracking has not occurred in any depth of the deck.

Convincing evidence was found to support this conclusion in the data of Gage Location D-1 and others. Undeniably, certain anomalies exist in the data, which limit the development of patterns or predictive models regarding these axial effects. Nevertheless, in light of the analysis using strain data collected from the Saco bridge decks, it is reasonable to conclude that cracking of the Saco bridge decks did not occur during the live load tests. Furthermore, instead of observing net axial compression strains indicative of the internal arching mechanism, axial tension was observed in a majority of the readings, indicating that internal arching is not the dominant behavior in any of the bridge decks at live load stress levels.

7.2.2 Deck Integrity over Girders

Integrity of the bridge deck in the vicinity of the girders is important since cracking may lead to corrosion of the reinforcement and direct freeze-thaw damage of the deck concrete. The integrity of the bridge deck in this region can be assessed by analyzing the strains, moments, and stiffness in the transverse direction of the bridge deck. When the tires of a truck straddle a girder, a negative moment is induced over the top of that girder, inducing tension in the upper fibers of the deck. If the strains are large enough, the deck surface may crack parallel to the girders, leading to premature damage of the bridge deck.

This particular live load distress is expected to be the most critical during truck tests that position the truck tires to straddle a girder, namely ST-T and ST-U, in which the truck tires straddle the second Girder (Figure 36). The transverse strains measured in ST-U for the Conventional deck at Gage Location D-5 at the face of the girder are presented in Figure 52. While negative moments were expected at this location, the response begins in positive moment when the front axle of the test truck moves onto the third span (at a position of approximately 30 m), as evidenced by the compression strains in the top gages and tension strains in the bottom gages of the deck. When the front axle reaches Gage D-5 (at 34 m), the moment reverses and becomes negative. When the first rear axle begins to enter the third span (front axle at approximately 35 m), the moment again becomes positive, until the first rear axle is directly over the gages (front axle at approximately 38.5 m), where the moment reverses and becomes negative. Once the second rear axle has passed over the gage line (front axle at approximately 40.5 m), the moment again reverses and becomes positive.

The moment response described above was observed in all three decks, as shown in Figure 53, and it may be simply explained as the superposition of local axle and more global truck effects, as these loads flow through the deck and girder system. Referring to Figure 54, the bridge responds globally to the truck live load by deforming in to a large dish shape, indicative of positive bending moment. This behavior is most obvious when the truck is at the 42 m position, as illustrated in Figure 54(b). When the truck is positioned so that either the steer axle or the rear tandem axle is directly over Gage Location D-5 (at the 40 m location), the local response of the bridge to the individual point loads of the tires is evident, as the bridge locally

deforms in to smaller dish shapes within the immediate vicinity of the tires, as illustrated in Figure 54(c). Depending on the position of the test truck, these two effects may act independently or be superimposed.

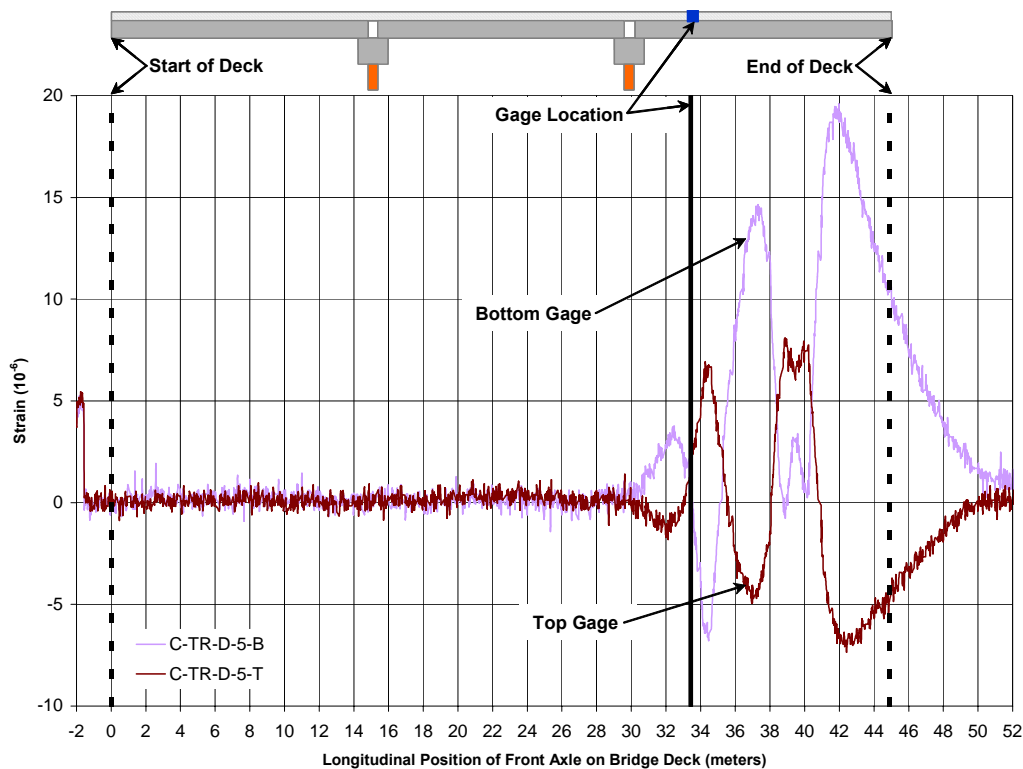


Figure 52: Strain History at Gage Location D-5 during ST-U Test (Conventional Deck)

Nevertheless, referring to Figure 53, the maximum tensile strains in the top reinforcing steel in the decks during the negative moment response are less than $10 \mu\epsilon$. The corresponding tensile strains on the surface of the decks would be on the order of magnitude of approximately $30 \mu\epsilon$. This level of strain would not be expected to crack the decks, and there was no physical evidence of longitudinal cracks in the decks at this location immediately following the live load tests. Thus, this form of live load distress has not been as critical to deck performance as originally expected. This conclusion is not inconsistent with Cao's (1996) observation that negative moment effects are overstated in traditional design procedures because of the assumption that the girders act as rigid supports for the deck.

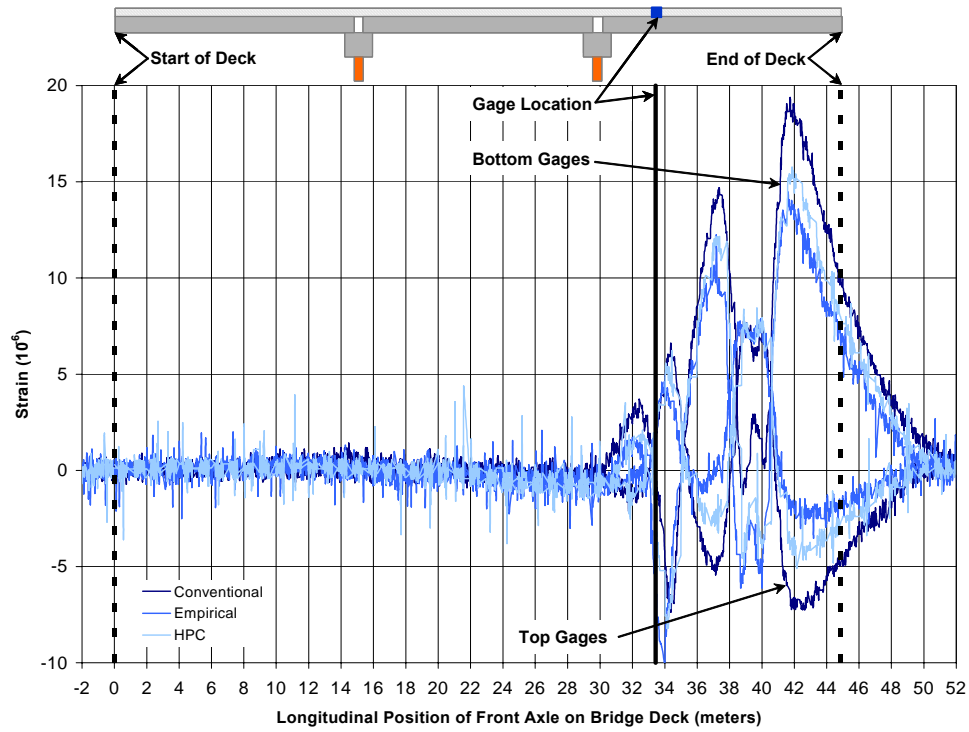


Figure 53: Strain History at Gage Location D-5 during ST-U test (All Three Decks)

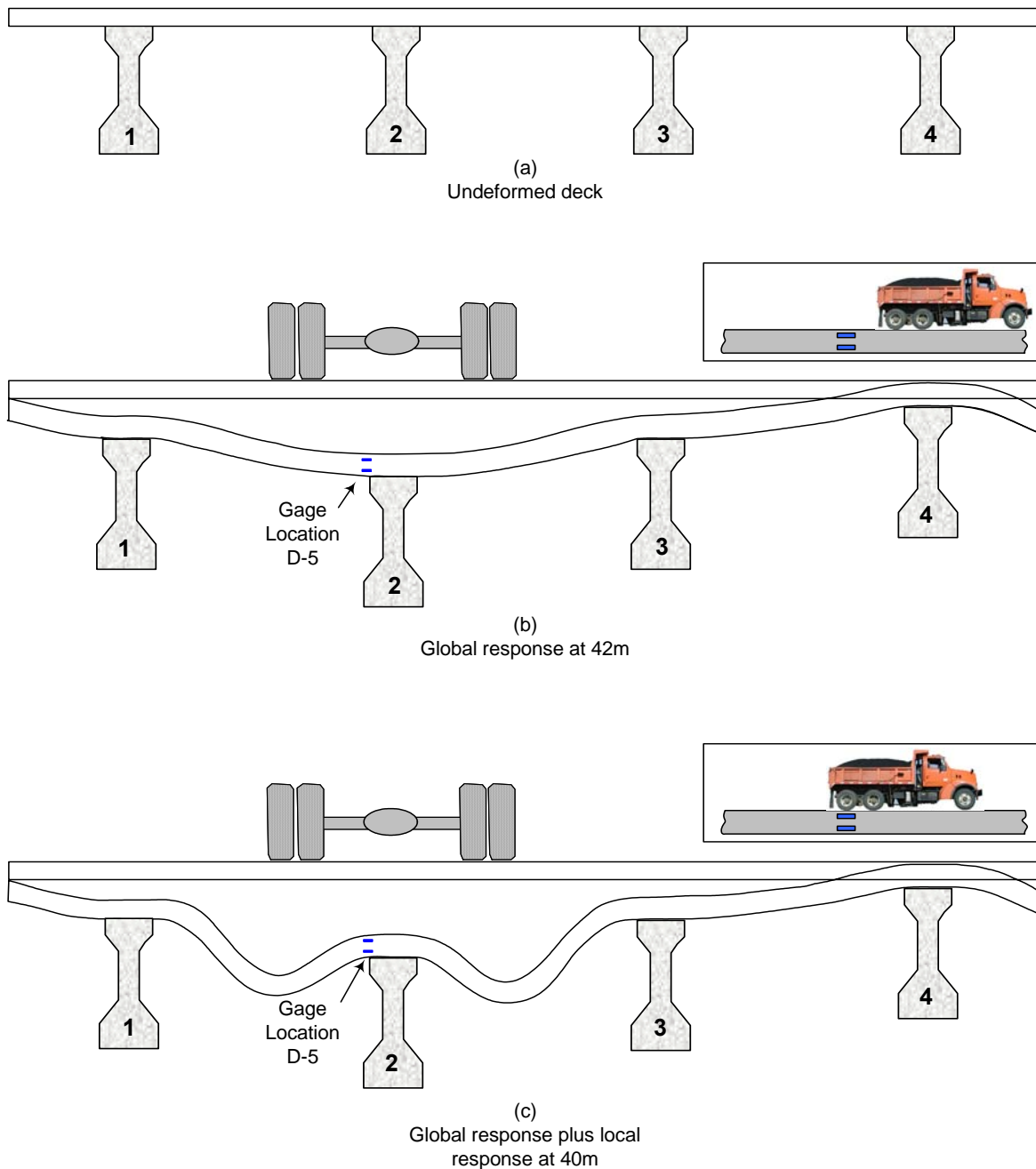


Figure 54: Illustration of Global and Local Bridge Deck Behavior from Live Loads

Negative transverse moments are also generated in the deck remote from the location of the test truck. This loading situation was created when the test vehicle was driven down the opposite side of the deck from the instrumented regions in transverse truck positions ST-X, ST-Y, and ST-Z. In these tests, global negative moments (tension top, compression bottom) were generated in the gaged portion of the deck. The strain profiles for all three decks at 40 m during the ST-X test are shown in Figure 55. The shapes and magnitudes for the ST-X test are similar to those

from the ST-Y and ST-Z tests. The tensile strains reported in Figure 55 are all below $6 \mu\epsilon$, which is well below the cracking strain of the concrete.

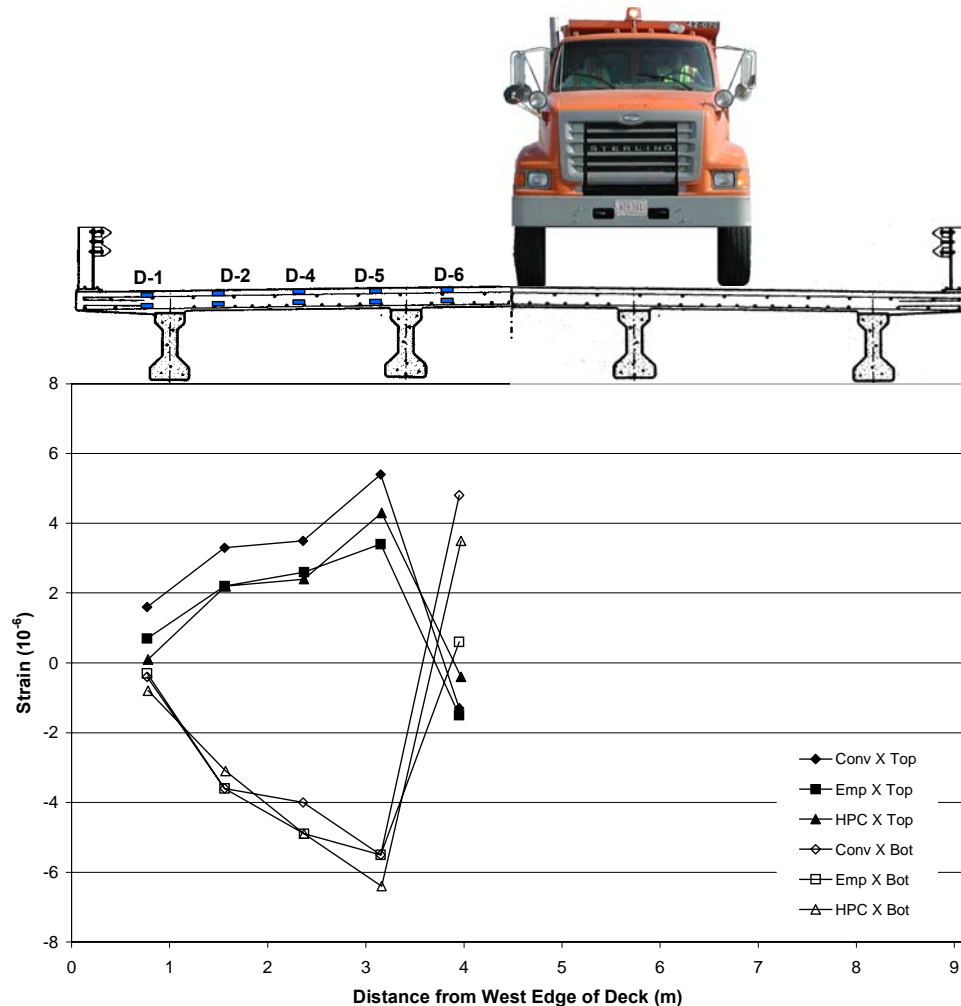


Figure 55: Transverse Strain Profile Showing Tensile Shift under Negative Moment (ST-X Test at 40 m)

The absence of cracking in the negative moment regions of the deck can also be inferred from an analysis of the location of the neutral axis in negative bending (similar to the analysis done for the positive moment case). From the bending neutral axis calculations for an uncracked cross-section, a negative moment is expected to impart compressive strains in the bottom reinforcing steel that are approximately twice as large as the tensile strains in the top mat. The transverse strain profile seen in Figure 55 is consistent with the actual neutral axis being *higher* than the uncracked bending neutral axis because the top strains and bottom strains are approximately equal in magnitude and opposite in sign. If the deck was partially cracked in the top tension zone, the bending neutral axis would have shifted downward, and not upward. Thus, it is unlikely that there are any longitudinal cracks in the upper fibers of the bridge deck near the girders. Rather, neutral axis shifts are likely the result of in-plane axial forces (and

corresponding axial strains), as discussed in detail earlier and previously reported in Tables 15, 16, and 17.

7.2.3 Deck Stiffness

Differences in the stiffnesses of the bridge decks could be responsible for some of the differences in the magnitudes of the strains experienced in each deck. The strain histories in Figure 53, for example, show that for the same test event, the strain responses have similar waveforms for all three bridges, but not the same magnitude. Referring to Figure 53, the behaviors of interest in this analysis occurred when the front axle of the test truck was positioned at 40 m, which placed the rear tandem axle directly on Gage Line D. With the truck in this position, the transverse section of the bridge deck was expected to act most closely to a continuous beam with applied point loads. The relative magnitudes of the strains at 40 m in Figure 53 suggest that a larger magnitude negative moment is present in the Empirical deck, relative to the other two decks. To further validate this observation, ϕ , which is related to the curvature (κ) for beams, was compared between the three decks for the ST-U test when the truck was at the 40 m position (Table 18). Curvature is indicative of both the bending moment (M) and flexural stiffness of the beam cross-section by the following relationship: $\kappa = M/EI$, where E is the elastic modulus of the material and I is the moment of inertia of the cross-section. Therefore, differences in ϕ can either indicate differences in moment, differences in stiffness, or a combination of these effects.

Table 18: Values of ϕ at 40 m during ST-U Test

Deck	ϕ at each gage position* (degrees)				
	D-1	D-2	D-4	D-5	D-6
Conventional	-3.51	3.83	30.57	-3.67	19.43
Empirical	-3.16	1.81	29.49	-6.40	19.07
HPC	-2.54	4.42	31.36	-5.87	21.33

* shading indicates negative moment

The cross-section moment of inertia (I) was calculated using an uncracked cross-section. Corresponding relative stiffnesses (EI) of the three decks in the transverse direction were calculated and are summarized in Table 19. The transverse flexural stiffness of the Empirical deck is noticeably lower than the other two decks, as might be expected based upon the reduction of reinforcing steel in that deck. Overall, the differences noted in the ϕ values of Table 18 correlate closely with the differences in stiffness shown in Table 19. These results indicate that the differences in the magnitudes of the strains in the three decks observed in Figure 53 result from differences in their stiffnesses rather than the moments they are carrying.

Table 19: Summary of Transverse Stiffnesses for Each Deck

Deck	Concrete Elastic Modulus, E (GPa)	Deck Cross-Section Moment of Inertia, I (cm⁴)	Stiffness, EI (10⁶ N*m²)
Conventional	39.2	18470	7.24
Empirical	32.1	18180	5.84
HPC	49.0	18290	8.96

7.2.3.1 Girder Distribution Factors

The stiffness of the decks in the transverse direction also has an effect on the manner in which the bridge carries load longitudinally. Bridge engineers and analysts characterize the stiffness of the bridge superstructure using a parameter called the Girder Distribution Factor (GDF). GDF is often expressed as a percentage, which indicates the quantity of the applied load carried by each girder in the superstructure. The specific manner in which the applied load is shared by the girders is dependent upon the transverse stiffness of the deck relative to the longitudinal stiffness of the girders. Because of the composite interaction between the girders and the deck in the longitudinal direction, load sharing is also influenced by the longitudinal rigidity of the deck. Conceptually, the stiffness of the deck may be correlated with the GDFs in the following manner. Lower longitudinal deck stiffness will result in an overall softer longitudinal response, and likewise, higher girder deflections near the truck. Additionally, as a particular girder deflects further downward, adjacent girders begin to carry more of the load. The degree to which the load is shared with adjacent girders is dependent (among other things) on the transverse stiffness of the deck. Therefore, as the transverse stiffness of the deck increases relative to the longitudinal stiffness of the girder-deck system, more uniform load sharing results. In other words, stiffer decks or softer girders results in more uniform load sharing in the bridge superstructure.

7.2.3.1.1 AASHTO LRFD Girder Distribution Factors

AASHTO LRFD Bridge Design Specifications provides an approximate method for determining the girder distribution factors for interior and exterior girders. These empirical equations were developed under the NCHRP Project 12-26 whose objective was to determine how various bridge parameters affected GDFs. The GDF values determined by these equations are expected to be greater than 5% of the actual values. The equations can only be applied to certain bridge geometries. Currently, Jay Puckett of Bridge Tech, Inc. is investigating the possibility of simplifying and expanding the range of applicability of these equations. This project (NCHRP Project 12-62) should be completed in late 2004.

The AASHTO LRFD Bridge Design Specifications (AASHTO, 2000 Interim) were used to calculate GDFs for the three bridges under investigation using LRFD Tables 4.6.2.2.2b-1 and

4.6.2.2d-1 in the Design Specifications. Girder distribution factors were calculated using the geometry and actual material properties for each bridge. The modulus of elasticity values determined by laboratory tests for each structure, are given in Table 20.

Table 20: Bridge Concrete Parameters

Bridge	Girder Elasticity (GPa)	Deck Elasticity (GPa)
Conventional	37.6	30.2
Empirical	37.0	24.8
HPC	37.9	30.8

The only distinctly different material parameter is the modulus of elasticity for the concrete in the Empirical deck, which is only around 80% of the stiffness of the concrete in the other two decks. This difference ultimately had little effect on the distribution factors calculated for the bridges, which are presented in Table 21. This result can be attributed to the insensitivity of the GDF equations to girder and beam stiffnesses. Distribution factors are primarily dependent on girder spacing.

Table 21: AASHTO LRFD Distribution Factors

Load Type	Bridge	Interior Girder	Exterior Girder
Single Truck	Conventional	49%	29%
	Empirical	49%	29%
	HPC	49%	29%
Double Truck	Conventional	65%	64%
	Empirical	66%	65%
	HPC	65%	64%

7.2.3.1.2 Measured Girder Distribution Factors

Strain data obtained during the live load tests was used to determine actual GDFs. The strain data used in this analysis was collected using the Intelliducer™ gages provided by Bridge Diagnostics Inc. (BDI). These gages were fixed to the bottom of the two western most girders one and two, see Figure 56. Bonded reinforcement gages located in the bridge deck were also used to validate the results from the BDI gages. This information was especially useful when evaluating the accuracy of the superpositioning of multiple truck paths.

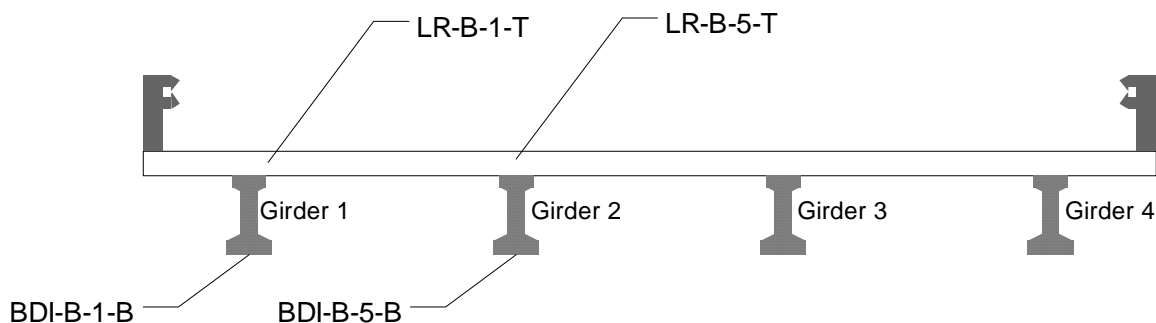


Figure 56: Bridge Profile at Center Span

In this analysis of GDFs, the bridges were assumed to respond elastically with small global deflections. This assumption allows for the superposition of results from different tests. In addition, distributed lane loads as specified in the LRFD were ignored and assumed to have minimal impact on the distribution factors due to their inherent nature.

Multiple presence factors from the AASHTO LRFD were used in this analysis (LRFD Table 3.6.1.1.2-1). In cases where two lanes were loaded, a multiple presence factor of 1.0 was used. In single lane loading a multiple presence factor of 1.2 was used.

Results for girders three and four were determined by enforcing symmetry on the structure. For example; the response of girders three and four for truck path R is equal to the response of girders one and two for truck path Z (refer to Figure 36). Similarly, girder responses can be found for longitudinal truck paths S and U which correspond to truck paths Y and X. In this fashion, the strain in each girder was determined for a given loading condition. The fraction of that load carried by each girder was then simply calculated as the strain in the girder divided by the sum of the strains across all the girders, as illustrated in Table 22. The strain values used in this calculation were the absolute maximum values observed during the test, which typically occurred within a meter of each other and when the tandem axle was centered in the bridge span. Girder distribution factors were determined for the following truck load paths (with some adjustments to the methodology for the two truck tests):

- Single Truck
 - ST-R + ST-Z (Superposition All Girders)
 - ST-S + ST-Y (Superposition All Girders)
 - ST-U + ST-X (Superposition All Girders)
- Two Trucks
 - TT-WR (Direct Measure Girders 1 & 2)
 - TT-XT (Direct Measure Girders 1 & 2)
 - ST-R + ST-V (Superposition Girders 1 & 2)

Any of the single truck tests can be combined to form their respective Two Truck tests.

The following load paths were inspected because of their unique loading characteristics.

- Single Truck
 - ST-R (Worst Case Exterior Girder)
 - ST-U (Worst Case Interior Girder)
- Two Trucks
 - TT-XR (Closely Resembles Recommended AASHTO LRFD Truck Spacing Specifications)
 - TT-WR (Worst Case Physically Achievable)
 - ST-R + ST-V (Closely Matches the W-R Two Truck Test using Superposition)

Table 22: Typical GDF Calculation, Single truck Test R (ST-R) on the Empirical Deck

Parameter	Girder 1 ^a	Girder 2 ^a	Girder 3 ^b	Girder 4 ^b	Sum
Girder Strains	76	46	21	8	151
Fraction of Total Strain	50%	30%	14%	5%	100%

a) directly measured in test R

b) inferred from test Z

From those calculations, a worst case scenario emerged that consisted of placing two trucks on the bridge as close as possible to each other and as close to the railing as possible. Figure 57 shows this truck placement. The GDFs for this scenario are given in Table 23, along with AASHTO-calculated GDFs.

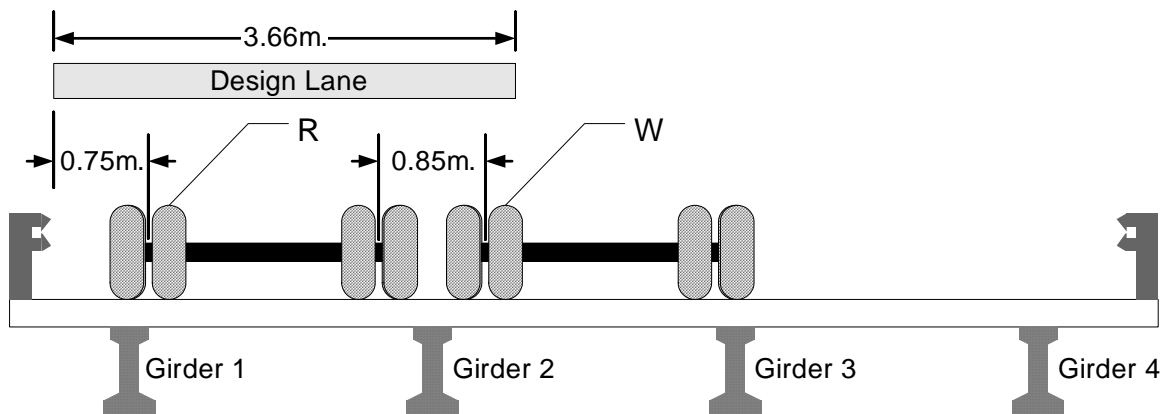


Figure 57: Worst Case – Two Design Lanes Using Truck Positions R and W

Table 23: Summary of Saco Bridge Girder Distribution Factors

Girder	Bridge	AASHTO GDF EQUATION	WORST CASE (R-W)
Interior Girder	Conventional	65%	61%
	Empirical	66%	59%
	HPC	65%	57%
Exterior Girder	Conventional	64%	65%
	Empirical	65%	59%
	HPC	64%	61%

7.2.3.1.3 Discussion

Referring to Table 23, the GDFs calculated from the test data are similar but lower in magnitudes than the AASHTO GDFs for all the bridges. The empirical bridge deck had the greatest load sharing capability (lowest GDFs) between the girders. Conversely, the conventional bridge deck highest GDFs.

This situation implies that the Empirical deck is stiffer in the transverse direction than the other two decks, since the longitudinal girders used in the bridges are identical. However, the calculated flexural stiffnesses (EI) listed in Table 24 indicate that the Empirical deck is the softest of the three decks in the transverse direction, as would be expected.

Table 24: Bridge Deck Stiffness Parameters

Bridge	E (GPa)	Longitudinal Direction		Transverse Direction	
		I (10^8 mm^4)	EI ($10^7 \text{ N}\cdot\text{m}^2$)	I (10^8 mm^4)	EI ($10^7 \text{ N}\cdot\text{m}^2$)
Conventional	30.2	7.847	2.366	8.145	2.546
Empirical	24.8	7.870	1.956	7.979	1.983
HPC	30.8	7.844	2.415	8.135	2.504

Note: longitudinal stiffness ignores the contribution of the girders

Relative to the other two decks, the Empirical deck has less longitudinal steel over the bents, in addition to the deck-wide reduction in the transverse steel. The removal of the steel over the bents greatly reduces the longitudinal stiffness of the whole deck. This softening was also confirmed by investigating several longitudinal gage responses. Due to the lower longitudinal stiffness, the GDF values make the Empirical deck appear stiffer in the transverse direction than the other two decks. Thus, the Empirical deck is softer both longitudinally and transversely than the other decks, which was expected from the reduction in steel volumes for this deck design.

7.2.4 Superposition

The Principle of Superposition was used to determine whether the Saco bridge decks behave in a linear elastic manner. This principle, which has been used in scientific and engineering applications ranging from heat transfer to simple beam theory, essentially states that in a linear system, the effects caused by combined loadings may be predicted by the summation of individual effects due to each load in the combination. Therefore, validation of superposition should verify that the bridge decks are behaving linear elastically.

During live load testing, the three Saco bridges were tested using two heavily loaded three-axle dump trucks, traveling side-by-side along the length of the bridge, namely two-truck tests TT-WR and TT-XT (refer to Figure 36-b). Using superposition, strains measured during individual single-truck tests (ST-X and ST-T) were added together and the results compared to the strains measured during two-truck test (TT-XT) for the Conventional bridge deck at two truck positions, 40 m and 42 m. (Single truck test ST-W was not run, so superposition could not be directly evaluated for two truck test TT-WR.) Figures 58 and 59 compare the summed response from the separate single truck tests to the measured two-truck test response along Gage Line D for the Conventional deck at the 40 m and 42 m truck positions, respectively. With regard to shape and magnitude, the two transverse profiles look very similar overall, indicating superposition is valid. The greatest differences in strain magnitudes are observed at Gage Location D-2, but even these differences are nominal. It is unclear why differences at this location are larger than the other gage locations. Gage Location D-2 may be near the point of curvature reversal in the deck, and therefore be more sensitive to minor variations in the specific locations of the tires and/or the presence of an additional truck.

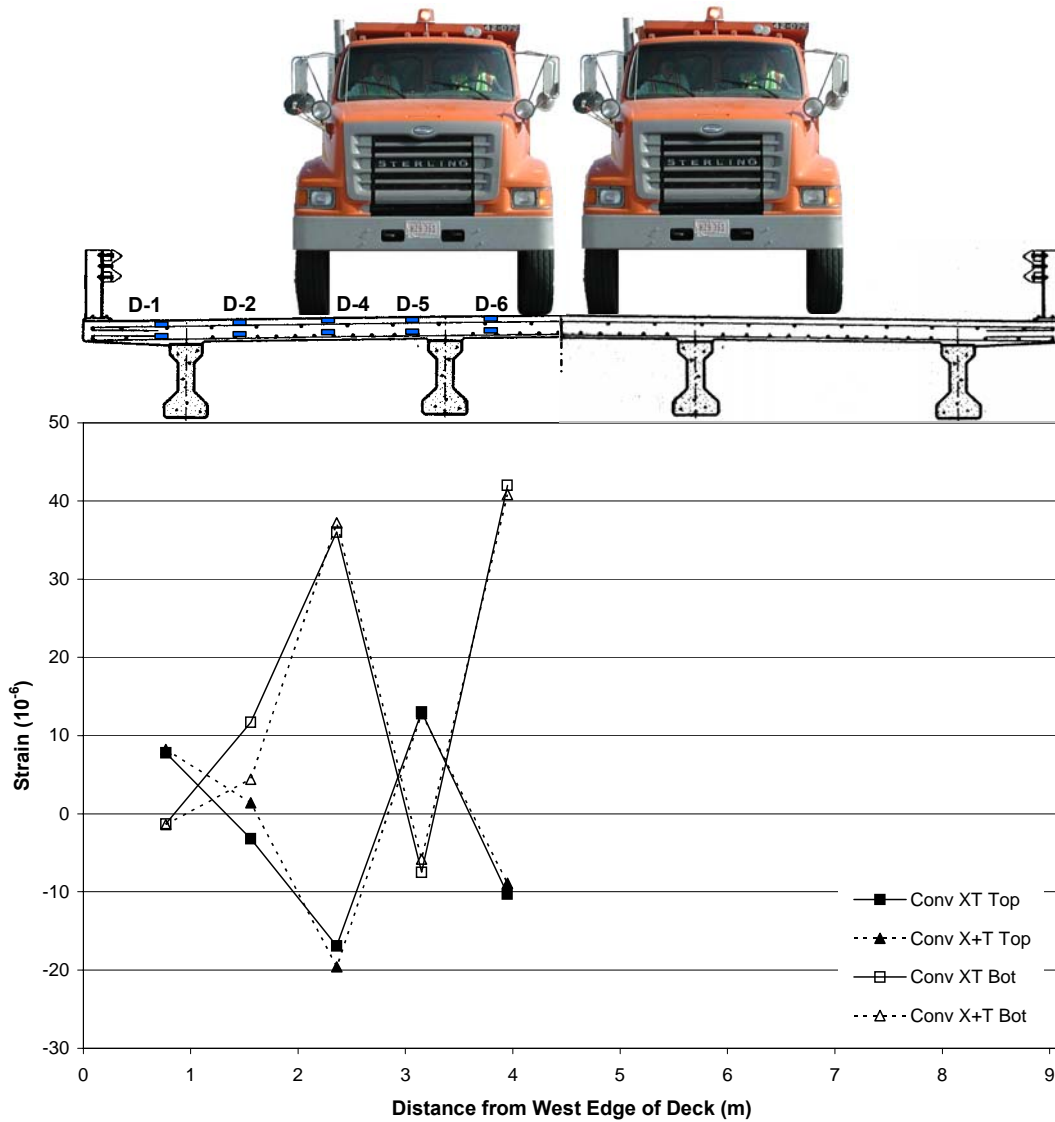


Figure 58: Transverse Strain Profile Showing Superposition in the Conventional Deck from Gage Line D at the 40 m Truck Position

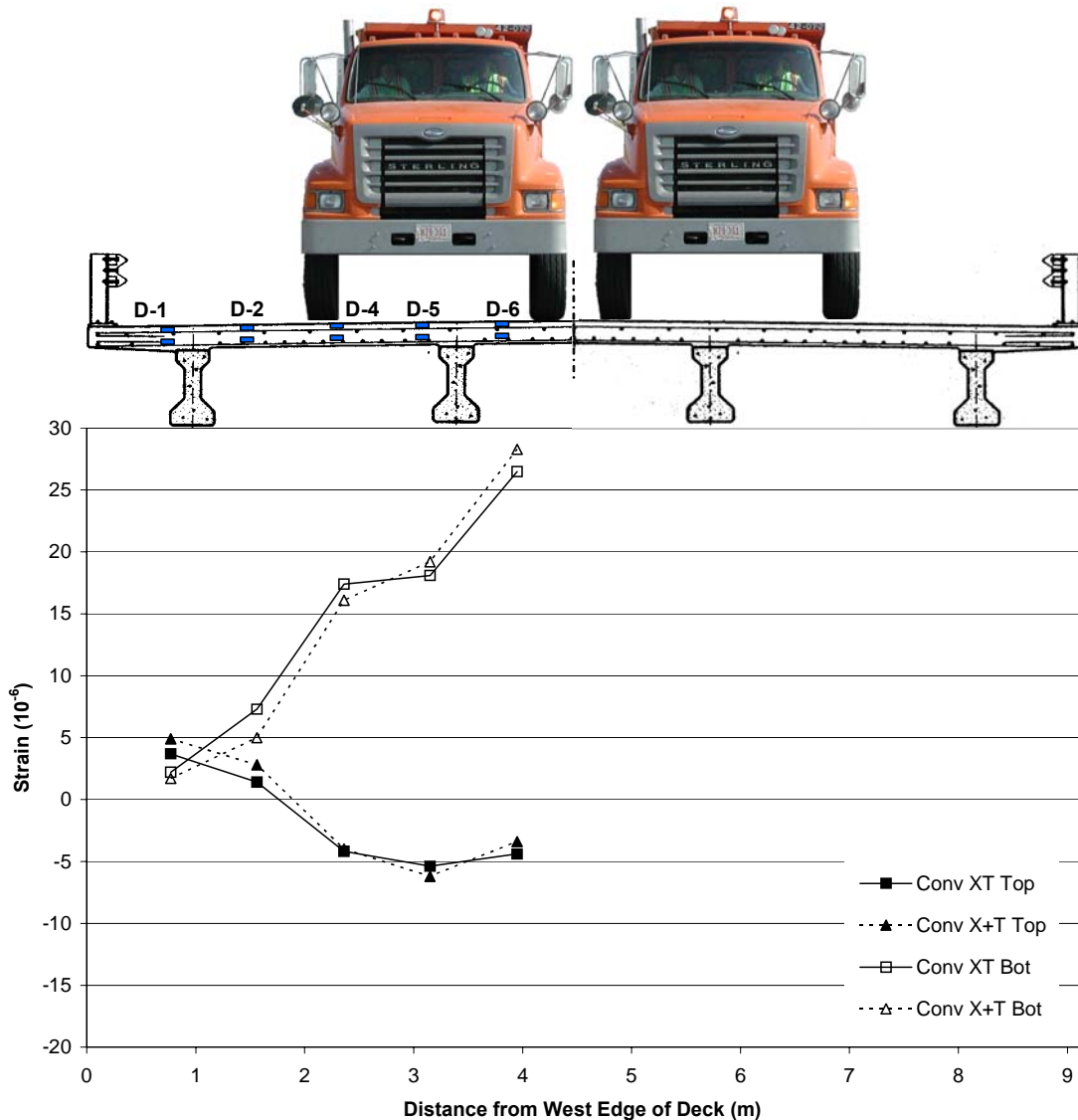


Figure 59: Transverse Strain Profile Showing Superposition in the Conventional Deck from Gage Line D at the 40 m Truck Position

Based on further analysis of live load test data, superposition works equally well for all three bridges, and there are no apparent differences in performance between the three bridges. Additionally, similar results were obtained when the TT-WR test was compared to response to the additive results of the ST-R and ST-V, even though ST-V was used to approximate position W. Overall, these results indicate that none of the decks is exhibiting non-linear behavior.

7.3 High Speed Live Load Tests

Typical longitudinal strains measured at the same location for the same test vehicle traveling at low and high speeds on the same longitudinal path are presented in Figure 60 (results for the conventional deck are shown). For this vehicle path and in this span, the maximum strain

reported in the high speed event was only 90 percent of the maximum strain reported in the low speed event. Generally, the dynamic load allowance used for design is greater than one (1.33). This allowance is significantly influenced by surface and approach roughness. With new, smooth bridge decks and approaches, a value for this factor approaching unity seems reasonable. In this case, the further apparent reduction in strain in the high speed test relative to the low speed test speed may possibly be explained by vehicle positioning error. Vehicle position was more difficult to control in the high speed tests relative to the low speed tests. Thus, the longitudinal path of the vehicle may not have been identical in the two tests. Therefore, until further review of the data is completed, care should be exercised in attaching too much significance to the difference in strain response observed above.

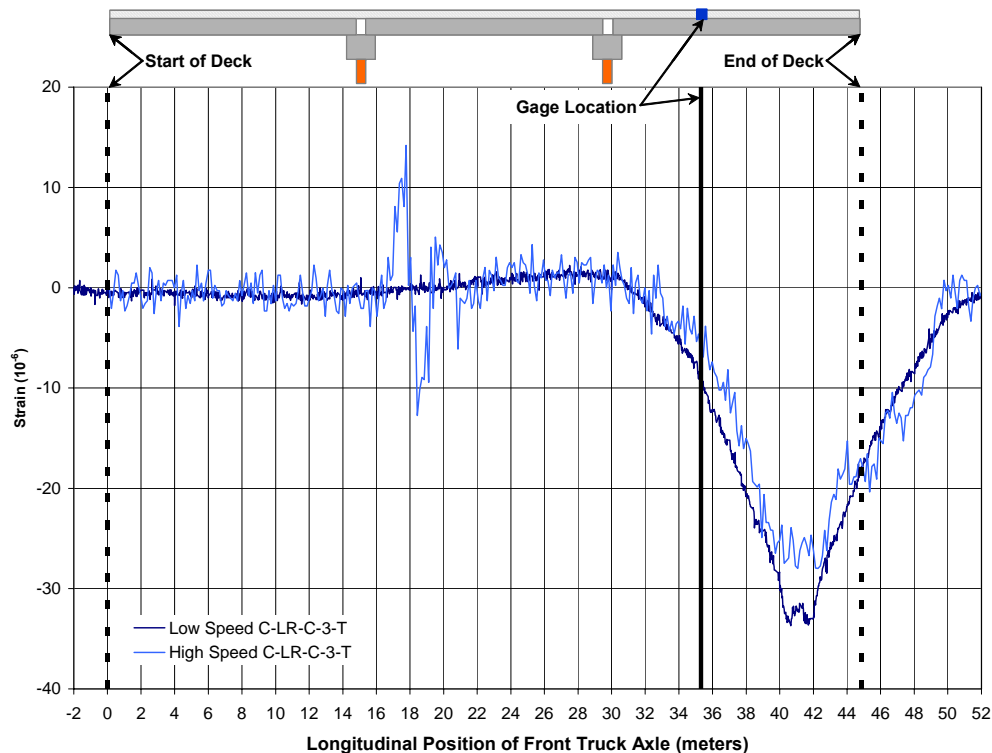


Figure 60: Comparison of the Longitudinal Strain Response in Low and High Speed Tests for the Conventional Deck

7.4 Review of Analysis Observations

Throughout the preceding analyses of the live load test data, several conclusions were reached, namely:

- All three decks exhibit similar global longitudinal behaviors, and these behaviors are in agreement with expected behaviors.
- No longitudinal cracking of the underside of the concrete decks is evident from strain data collected in the positive moment regions of any of the decks.

- The presence of in-plane axial forces is inferred from the strain data from each of the decks. Most of the reported axial strains are tensile and of relatively small magnitude (less than $10 \mu\epsilon$). Finite element analysis also confirmed the presence of axial tension in an uncracked deck.
- No internal arching is evident in any of the decks because none of the decks is cracked and little evidence of in-plane compression exists.
- No longitudinal cracking of the topside of the concrete is evident from the strain data in the negative moment regions over the top of the girders of any of the decks, nor is such cracking imminent.
- Negative bending over the girders is not critical under live load demands.
- The Empirical deck is softest, both longitudinally and transversely, despite classic computation of the Girder Distribution Factors (GDFs), which gives the appearance that the Empirical deck is stiffer in the transverse direction.
- Linear superposition works well for all three bridge decks, indicating that all three decks are behaving linear-elastically.
- For the parameters analyzed in this research, no difference in performance (i.e., occurrence of cracking, non-linear behavior, or possible indication of accumulating damage) was observed between the three bridge decks.

8 LONG TERM MONITORING

Long term monitoring at the bridges consists of measuring internal deck strains and temperatures, assessing corrosion potential, mapping cracks, and detecting global movement of the bridge structures from survey data. The data acquisition system is programmed to collect strain and temperature information from all of the embedded sensors on an hourly basis. All other effects are being monitored through periodic visits to the bridge site (three to six month intervals immediately following construction, transitioning to annual surveys thereafter).

8.1 Internal Strain Measurements

Approximately twelve months of long-term data has been collected from embedded sensors in each of the bridge decks. All the active long term sensors are currently set up to provide measurements once every hour. This data acquisition schedule has been interrupted on occasion due to maintenance and other activities. These interruptions are considered inconsequential in terms of the entire length of the project and are noticed as gaps in the graphs of the long term data.

The data available from the long term monitoring effort will be studied over the next several months with the goal of correlating changes in deck performance with the vehicle and environmental loads they experience, and then to further evaluate the relative performance of the three types of decks. Presented herein are some early (and preliminary) observations from this process. Notably, specific examples of long-term effects that clearly illustrate data trends, crack formation and shrinkage are considered. Several sensors were installed over the interior bents (mostly Bent #2 or Gage Line F) to capture the effects of anticipated cracking in that region. Physical cracks have been observed over all the interior bents, and the data collected from the vibrating wire strain gages spanning Gage Line F reflect the occurrence of these cracks. In general, cracking that intercepts the vibrating wire gage will increase cyclic strain levels due to daily and seasonal temperature fluctuations. The gage length of the vibrating wire strain gages is 153 mm, so prior to the formation of a crack anywhere along its length, measured strains would indicate tensile or compressive strains only in this region. After a crack forms, strains will also include differential movements of the separate concrete segments, made up of the three bridge deck panels. Figure 61 illustrates this phenomenon using strain data from vibrating wires on G Gage Line F for all three decks. Recall that the HPC bridge deck was poured on May 28, the Empirical deck on June 2 and the Conventional deck on June 5. Both the HPC and Conventional decks show small daily strain fluctuations ($\sim 10\text{-}20\ \mu\epsilon$) prior to cracking. Once the crack formed, daily fluctuations are greatly increased to approximately $250\ \mu\epsilon$. The empirical deck behaved slightly differently in that the data indicated the presence of a hairline crack in the deck shortly after the pour and a more fully developed crack occurring later. Notably, all cracks seem to have

either formed or fully formed near June 19th. Further investigation into this matter may reveal the reason for this concurrent behavior.

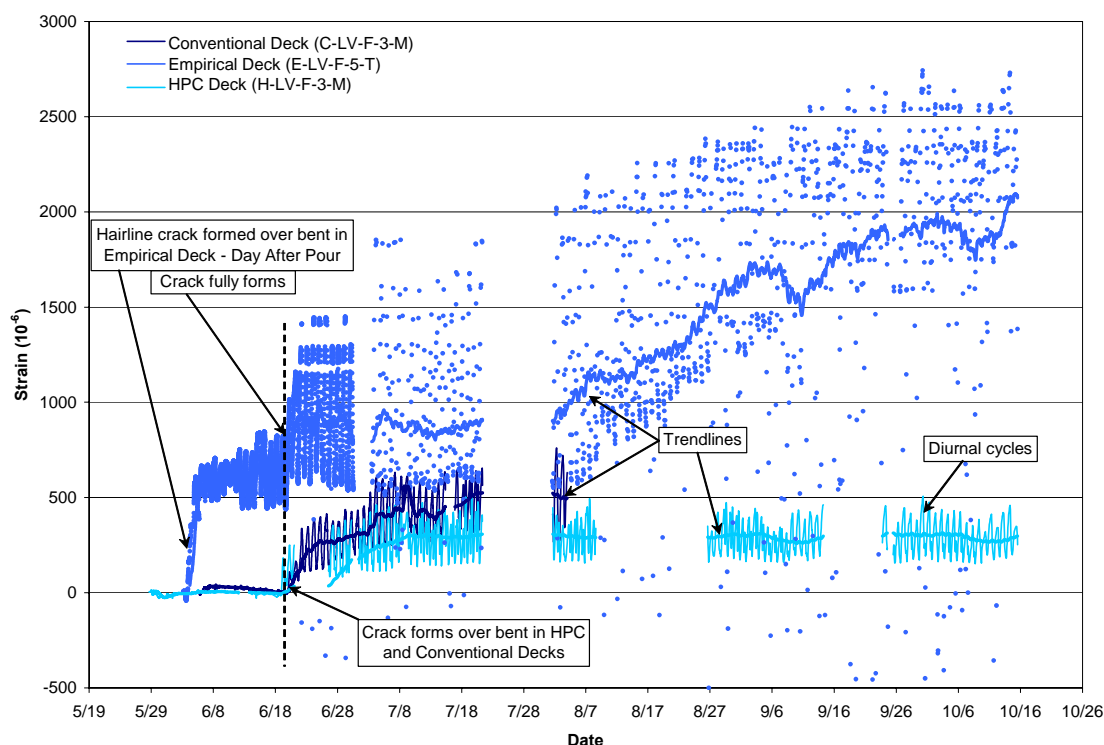


Figure 61: Long Term Data Showing the Formation of Cracks in All Three Decks.

Unlike sensors spanning the bents, longitudinal sensors installed away from the bents (i.e., position D-3, halfway between the bents and the diaphragms and halfway between two girders) did not show that cracking had occurred. Figure 62 shows the response from vibrating wire strain gages near the top of the deck in each of the decks at this position. Diurnal strain fluctuations are small (approximately 20 to 70 $\mu\epsilon$), indicating contraction due to temperature changes and not cracks in the concrete.

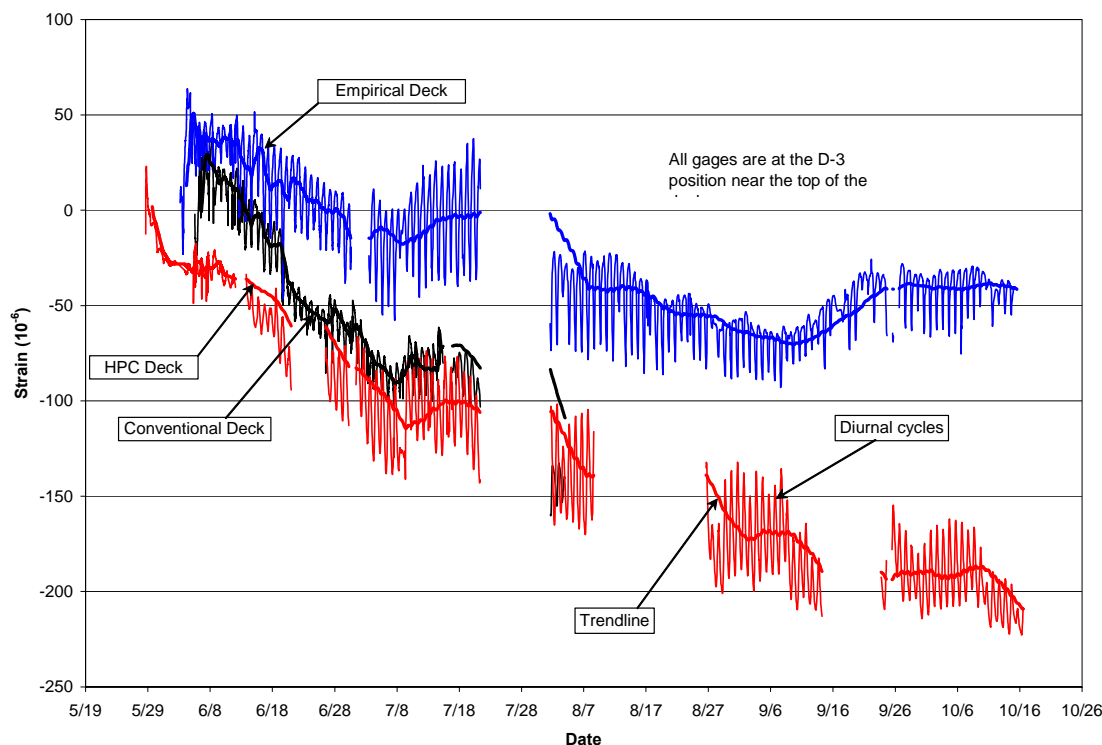


Figure 62: Long Term Data Illustrating Non-Cracked Portion of the Deck.

The formation and presence of a crack can clearly be seen in the data from the Conventional deck presented in Figure 63. In this case, longitudinal strains collected over the interior bent (Gage Location F-3) and over the intermediate diaphragm (Gage Location B-3) are compared. Prior to cracking, strains in these two locations are almost identical, simultaneously fluctuating based on daily temperature oscillations. Notably, prior to a crack formation, lower temperatures caused decreases in strain indicating thermal compression. Conversely, higher temperatures produced increases in strain (Line A, Figure 63).

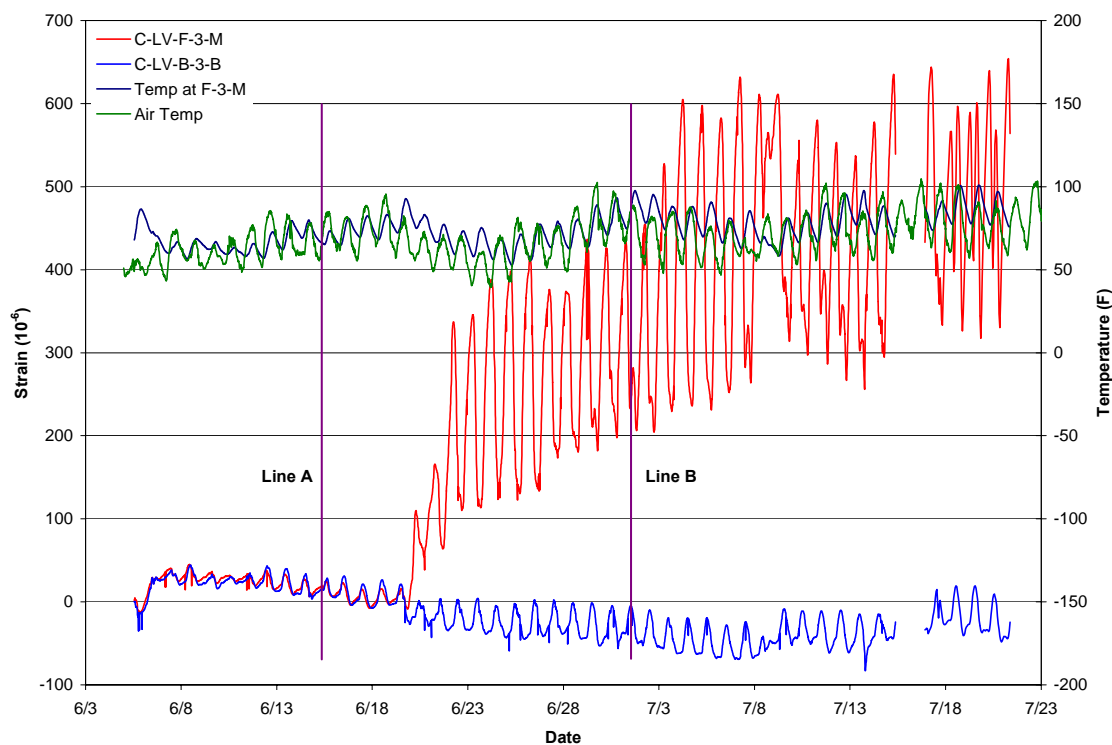


Figure 63: Comparison of Cracked and Non-cracked Position in the Conventional Deck.

On the evening of June 19th, strains over Bent #2 (Gage Location F-3) noticeably began to deviate from those at Gage Location B-3. This deviation is most certainly because a crack formed over the bent and intercepted the vibrating wire gage installed at that location. Following the formation of the crack at position F-3, two effects can be observed, 1) diurnal strain fluctuations increase in magnitude at the crack location, and 2) the mean level of strain at the crack location increases in magnitude and becomes tensile in nature due to deck concrete shrinkage on either side of the crack. First, daily changes in temperature produce higher strain values over the bent since the bridge deck concrete is essentially separated at that point. This separation causes contractive strains from each section of deck to be realized as increased strains across the crack. Therefore, what used to be decreasing strains over the bents before the crack occurred are now increasing strains. Moreover, the lowest temperatures during the day are now producing the highest strains over the bents (Line B, Figure 63). Strains at Gage Location B-3, however, have retained their original cyclic behavior.

Shrinkage of the deck concrete can also be observed using these same two locations. Average strain at both positions is decreasing slightly over time until the crack forms over the bent. At that time, the average strain at position B-3 continues to decrease, but average strain at position F-3 begins to increase. In the body of the deck (B-3), the concrete is shrinking, placing the gage in compression. Conversely, as the “slabs” on either side of the crack shrink, they draw away from the crack, placing the gage at the crack in tension. Possible reasons for the higher

rate of increase of the mean strains at the bents (F-3) relative to the body of the slab (B-3) are that 1) strains across the crack represent a concentration of the shrinkage strain effects that are distributed across the adjacent “slabs”, and/or 2) ratcheting of the crack is occurring as small concrete particles hold it increasing open after each cycle of expansion.

Hourly strain data continues to be collected and stored, and analysis of this data is still pending.

8.2 Internal Temperature Measurements

Each of the vibrating wires has an internal thermistor to measure temperature. Information from this thermistor is used to correct strain data collected by all the sensors. The resistance strain gages bonded to the reinforcement do not have temperature measurement capabilities, yet need to be corrected for changes in temperature. Analysis of internal temperature data collected from the vibrating wire sensors revealed that sensors near the top of the bridge deck were, on average, warmer than sensors located near the bottom. Therefore, temperatures from vibrating wire gages located in the top mat of reinforcement were averaged together to adjust strain outputs in the reinforcement gages in the top mat, and likewise for gages located in the bottom mat.

Early data collected from the bridges showed that internal temperatures were elevated during curing of the concrete. Cyclic behavior has been seen in most of the strain gages that obviously correlates with diurnal temperature fluctuations. Figure 64 shows the temperature near the bottom of the three bridge decks as a function of time since they were cast. Variations in the hydration temperatures between the decks are obvious at early times after their construction. Temperatures were measured at Gage Location F-3. Note that the peak temperature in the HPC deck occurred later than the peaks for the Empirical and Conventional decks. This behavior is most likely attributable to the retardant used in the HPC mix design. Also note that even though the Conventional and Empirical decks utilized the same concrete mix design, their peak temperatures are quite different. Ambient conditions for these two decks during the pour were similar. At this point, there is no certain explanation as to why these differences occurred or if they are truly significant. Temperatures measured at different locations in one deck have been seen to vary by up to ten degrees during curing. Cyclic behavior of the deck temperature is a result of diurnal temperature fluctuations. These affects are more noticeable once the curing cycle was complete. Straight-line portions of the graph correspond to intervals when the data logger was not operating.

Further analysis of the temperature data will be conducted in conjunction with long term strain data from embedded sensors. Specifically, data will be analyzed to determine the affect temperature has on the magnitude and direction of internal strains at various locations within the

three bridge decks. Moreover, the intent is to quantify any differences between the behavior of the three bridge decks during daily and seasonal temperature fluctuations.

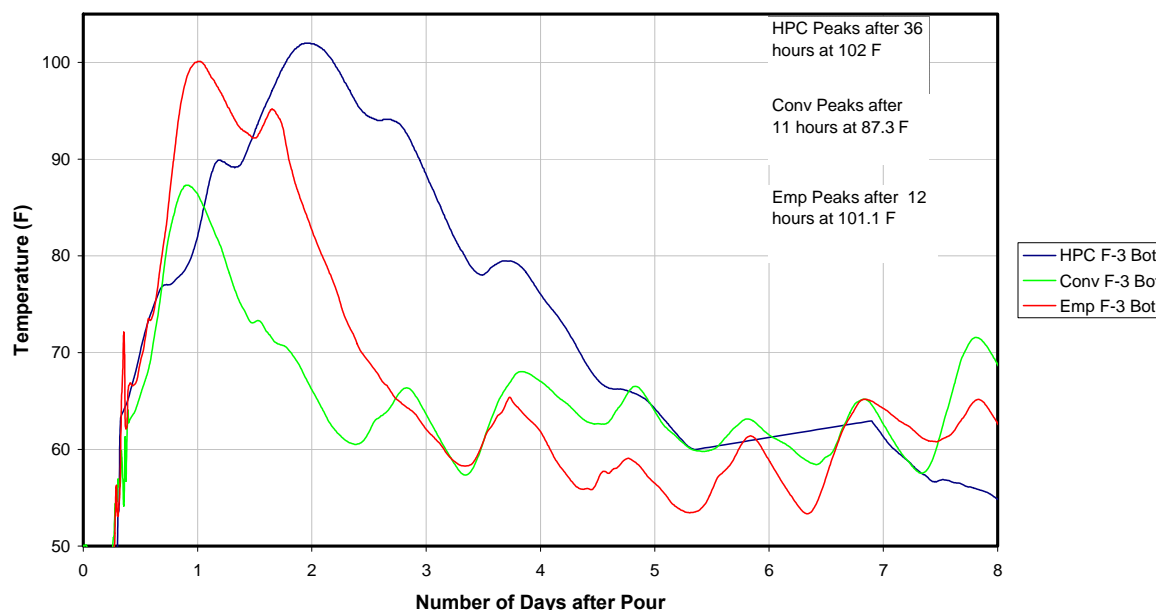


Figure 64: Comparison of Bottom Deck Temperatures during the Cure Cycle.

8.3 Large Event Monitoring

Using the information from the live load tests, specific sensors were chosen to be continuously monitored in order to capture strains associated with “large” vehicle events after the bridges were open to traffic. Selections were based on the quality and level of the output, which depended on their location and orientation. Accordingly, ten bonded strain gages and two embedded concrete strain gages were selected to capture deck response to large vehicle events. These gages were rewired to run through only two bridge completion boards to conserve battery power, and the long term data acquisition program was rewritten to include logging the data from these sensors when they are triggered by a large event. On each bridge, one of the 12 sensors is designated as a trigger gage to initiate the data storage process. The general magnitude of the response of these sensors was determined from the live load testing. Trigger values were set to be approximately 40% of the maximum response recorded for that sensor during the high speed live load tests. If the output from the trigger gage increases by more than 40% when a vehicle crosses the bridge, 1.5 seconds of data is captured before and after the event. Due to variations in the bridges’ response to environmental and traffic loading, the threshold values used on each bridge are not the same. The early vehicle event data collected from each bridge was scrutinized relative to setting the individual triggers so that each bridge records the same events. A maximum of 60 events can be stored on the data acquisition computer before it needs to be

downloaded and cleared. Information from these gages will be compared to data collected by the classifier (permanently installed on Route 243 near the Saco bridges) and portable WIM (temporarily set out annually in September). These comparisons should allow for correlations to be made between the deck response and the class and weight of the vehicles that cause this response.

The data loggers have been monitoring large vehicle events since mid-November 2003. Table 25 summarizes the number of events captured from each bridge between November 12 and December 31, 2003. While differences are apparent, the majority of the events being captured correlate well across all three bridges. Figure 65 shows the typical response during a large vehicle event. Large vehicle event data will be correlated to data obtained from the portable WIM and truck classifier in months to come.

Table 25: Example Summary of Large Event Data Collected on Saco Bridges

Date Range	# of Events Recorded		
	CONV	EMP	HPC
Nov 12-17	12	15	19
Nov 17-19	13	14	12
Nov 19-20	4	6	5
Nov 20-26	19	22	26
Nov 26 – Dec 2	4	5	7
Dec 2-8	7	11	24
Dec 8-17	6	5	17
Dec 17-23*	1	3	5
Dec 23-31	6	7	7
Nov 12 – Dec 31	72	83	122

* Conventional threshold lowered 12/23

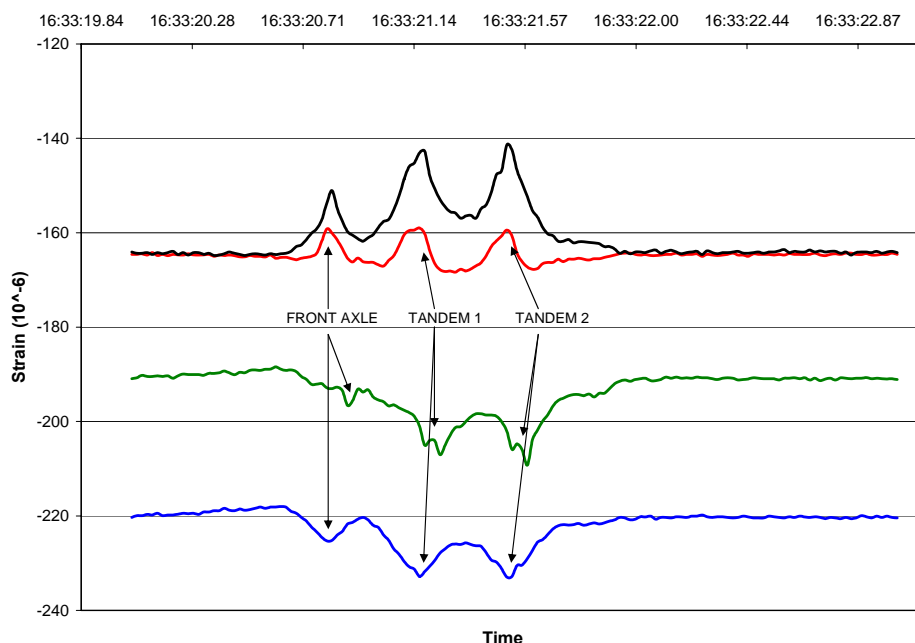


Figure 65: Typical Strain Response during a Large Vehicle Event

8.4 Corrosion Testing

Corrosion of reinforcing steel is a major concern with respect to the long-term durability of bridge decks. This corrosion is often associated with the migration of chloride ions from deicers into the deck concrete. However, the Saco bridge decks are expected to experience only nominal exposure to deicers over their service life. Chloride content and half-cell potential tests were conducted to provide benchmark data on these parameters. Half-cell potential tests were conducted on selected bars (and will only be valid for these bars, as epoxy coated reinforcement is being used in the bridges). Similar to the situation with corrosion of the reinforcing steel, carbonation is a possible deterioration mechanism of the concrete, but it is believed to be unlikely in this case. Nonetheless, benchmark carbonation tests were conducted at the beginning of the program, in the event that unusual deterioration of the concrete is observed over the life of the decks.

8.4.1 Half-Cell Potential Tests

Half-cell tests measure the potential for corrosion in the embedded reinforcement within the bridge decks. This test is used to estimate the likelihood of corrosion activity at the time of the measurement, but does not provide any information on the rate of corrosion of the reinforcement. Corrosion of steel is an electrochemical process involving anodic (corroding) and cathodic (passive) areas of the metal. By measuring the electrical potential between the surface of the concrete and a standard reference electrode (the reinforcement), the presence and location of corrosion and its probable future development may be assessed. Corrosion probability

determined from half-cell resistance measurements fall into one of three categories, as described in Table 26.

Table 26: Categories of Corrosion Probability for the Half-Cell Test

Category	Corrosion Probability
I	90% probability of no corrosion
II	an increasing probability of corrosion
III	90% probability of corrosion

ASTM C876 the “Standard Test Method for Half-Cell Potentials of Uncoated Reinforcing Steel in Concrete” is intended to be used for uncoated rebar only, however, prior to pouring the bridge deck concrete, copper wire leads were connected to two transverse and two longitudinal bars in each deck to facilitate a direct connection with the epoxy-coated reinforcement (see Figure 66). The lead wires exit the concrete on the west side of the bridge decks. Normally, one of the wire leads can be connected to the guardrail or other metal object that is in contact with the embedded reinforcing mat, however, the epoxy coating insulates the reinforcing bars from one another, making it necessary to connect individual leads to each bar.

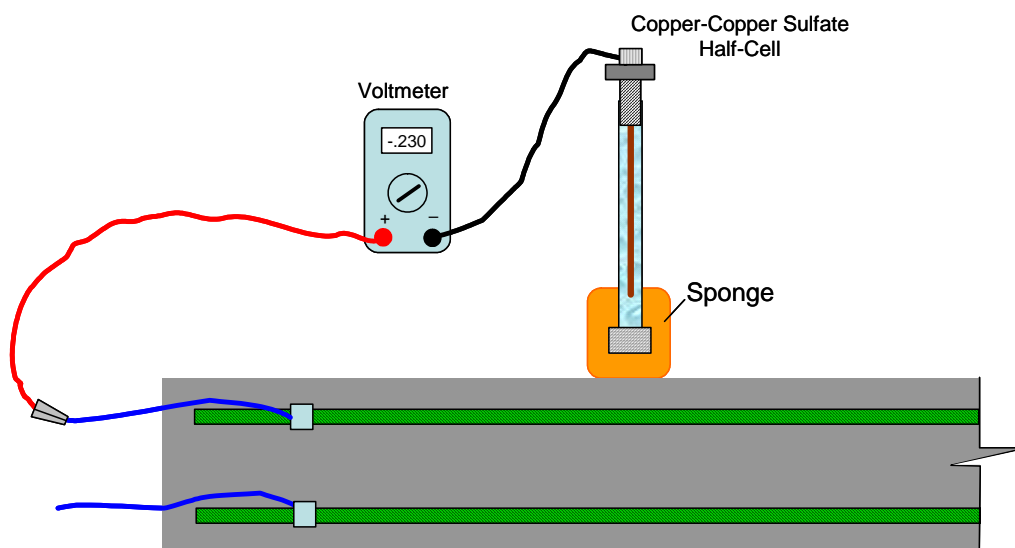


Figure 66: Illustration of Half-Cell Test on Saco Bridges

Initial half-cell potential readings were taken in July 2003. The results from these tests for each bridge are summarized in Table 27. Overall, very little potential for corrosion was measured using the half-cell test method.

Table 27: Results of First Series of Half-Cell Testing

Bridge	Reinforcement		Percent of Readings in Each Category		
	Orientation	Position	I	II	III
Con	Longitudinal	Top	100.0%	0.0%	0.0%
		Bottom	100.0%	0.0%	0.0%
	Transverse	Top	100.0%	0.0%	0.0%
		Bottom	100.0%	0.0%	0.0%
Emp	Longitudinal	Top	98.6%	1.3%	0.1%
		Bottom	99.4%	0.6%	0.0%
	Transverse	Top	97.1%	2.9%	0.0%
		Bottom	100.0%	0.0%	0.0%
HPC	Longitudinal	Top	92.9%	7.1%	0.0%
		Bottom	100.0%	0.0%	0.0%
	Transverse	Top	100.0%	0.0%	0.0%
		Bottom	100.0%	0.0%	0.0%

8.4.2 Carbonation Tests

A solution of phenolphthalein (a colorless acid/base indicator that turns purple when the pH is above 9) was used to detect the presence of carbonation – $\text{Ca}(\text{OH})_2$. When this solution is blotted on a sample of concrete and it turns purple (or a shade thereof), carbonation has not occurred. A concrete's resistance to carbonation is an indicator of its ability to protect embedded reinforcement from being penetrated by carbon dioxide which fuels corrosion. The pore microstructure of the concrete is how carbon dioxide penetration is facilitated.

Benchmark carbonation tests were conducted on the surface of all three bridge decks. To conduct these tests, two areas of the deck were first cleaned using an abrasive pad to remove the outer layer of applied sealer. On each deck, one test was done in the wheel path and one was done out of the wheel path. Once the area was blown free of dust, a dropper-full of phenolphthalein was blotted on the surface and allowed to absorb into the surface. In all cases, the phenolphthalein turned purple, which indicated that no carbonation had occurred at any of the locations on all three decks. Follow on tests will be repeated in the future to determine the extent of carbonation.

8.5 Crack Mapping

The development of cracks in the bridge decks are being monitored by periodically mapping the cracks. A schedule of the crack surveys conducted thus far in the project is provided in Table 28. Initial results showed that hairline cracks had formed over the bents on all the bridges with the exception of Bent #2 on the HPC deck. Bent #2 on each of the bridges was saw-cut to

control the position of the anticipated crack over the bent, which made it difficult to perceive the formation of the crack in this area. The Conventional and Empirical decks cracked at Bent #2 prior to the saw-cut, making the cracks easier to detect. It is believed that Bent #2 on the HPC deck cracked at approximately the same time as the other bridges but went unnoticed due to the saw-cut and crack sealant. The visible crack over the bent in the HPC was noticeably narrower than similar cracks in the other two decks. No new cracks were reportedly discovered during the visit in November 2003. During the visit in March the Empirical deck had formed a crack on the southeast corner of the deck in a diagonal direction. During the last site visit in July 2004, the cracks shown in Figures F-1, F-2, and F-3 in Appendix F were observed in the Conventional, Empirical and HPC decks, respectively. Cracks will continue to be mapped through the remainder of the project on a six-month schedule.

Table 28: Date of Crack Surveys

Date of Crack Map	Approximate Age of Bridge Decks
July 2003	2 mo.
November 2003	5 mo.
March 2004	9 mo.
June 2004	12 mo.
July 2004	13 mo.

Overall, cracking in the Empirical deck is more severe than the other two decks. Besides the full depth cracks over the bents in all three bridge decks, full depth cracks had also formed near the ends of the Conventional and Empirical bridge decks, but more so on the Empirical deck. White precipitate formed around these full depth cracks on the underside of the deck, highlighting them as shown in Figure 67. The Empirical bridge deck also showed signs of crazing on the surface. The HPC deck had periodic cracks along the overhang on both sides of the bridge deck that appeared to terminate at the outer edge of the stringers, as shown in Figure 68. These cracks may be related to shrinkage of the deck concrete. Additionally, very fine surface cracks were found on the underside of the HPC decks. All such visible cracks in one area were highlighted with a red marker, as shown in Figure 69.



Figure 67: Full-Depth Crack in Empirical Deck as Seen from Underside



Figure 68: Cracks in the Overhang of the HPC Deck



Figure 69: Surface Cracks on the Bottom of the HPC Deck

8.6 Surveying

Global bridge movements are being monitored by measuring relative changes in the elevation and the horizontal position of various points on the surface of each deck. Initial elevation and position measurements were made just prior to conducting the live load tests and were referenced from permanent points installed at the west side of the north abutments of each bridge during construction. Elevation measurements were made at 50 locations on each deck, namely, over the abutments, interior bents, and diaphragms of each bridge at the location of each stringer and between stringers in the instrumented areas of the decks. In the horizontal plane, 18 position measurements were made over the abutments, interior bents, and diaphragms of each bridge at the location of the exterior stringers. Elevation and position measurements also were made at the east and west ends of each abutment. Figure 70 shows where each of these measurements was made. Elevation measurements were shot with an accuracy of approximately 1 millimeter whereas the horizontal locations were measured with an accuracy of approximately 3 millimeters. This information has been input into a database for future reference. The bridge decks will be surveyed at one year and two years past casting of the bridge deck. Later surveys will be compared to earlier ones to determine whether the structure has moved globally.

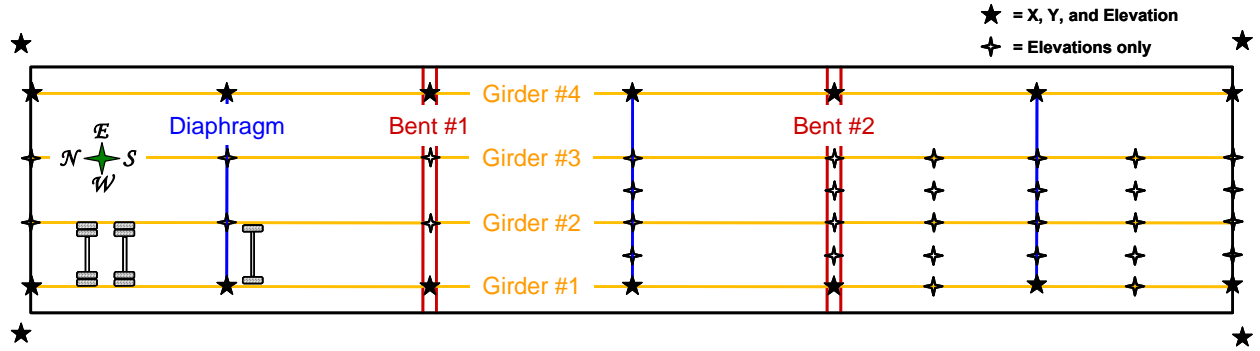


Figure 70: Survey Points Shown on Plan View of Bridge Deck

9 SUMMARY AND CONCLUSIONS

The deterioration of bridge decks in Montana prompted the Montana Department of Transportation (MDT) to investigate possible solutions to mitigate this problem. Specifically, MDT was interested in evaluating procedures that reduce concrete cracking and corresponding steel corrosion resulting from corrosive agents accessing the steel via those cracks. Three new bridges with identical geometries being constructed near Saco, Montana within one mile of each other along the same roadway afforded an excellent opportunity for such an investigation. The bridges were built by the same contractor and the decks were poured within two weeks of each other. The only difference between the three bridges was the composition of the reinforced concrete deck. One bridge was designed using a conventional deck design, which is the standard design used by MDT, using a standard concrete mix design and typical reinforcement layout. The second bridge deck was built using an empirical design methodology, designed according to AASHTO specifications, which allows the volume of the steel to be reduced throughout the deck, but utilizes a standard concrete mix design like the Conventional bridge deck. The third bridge deck was built using High Performance Concrete (HPC) coupled with the conventional reinforcement layout.

9.1 Summary

Prior to pouring the deck concrete on each bridge, a suite of strain and temperature sensors was installed in the decks. Concrete embedment strain gages and vibrating wire strain gages were used to monitor strains in the deck concrete, and resistance strain gages were bonded to the reinforcement to monitor strains in the reinforcing steel. Deck temperatures were recorded from thermistors built into the vibrating wire gages. During live-load testing only, four temporary strain transducers from Bridge Diagnostics, Inc. were mounted to the bottom surface of the concrete girders. A data acquisition system consisting of a datalogger, two multiplexers, supplemental Wheatstone Bridge circuitry, communication radios, and power components was assembled and located beneath each bridge to record, store, and transmit data from the sensors.

Prior to opening the bridges to regular traffic, live load tests were performed on each bridge. A series of eight low speed single-truck tests, five high speed single-truck tests, and two low speed two-truck tests was performed on each bridge.

Strains recorded during the live load testing were analyzed to evaluate structural behaviors for each deck. Strain data recorded from longitudinally-oriented gages during these tests was analyzed to establish the validity of the measured response relative to expected direction and magnitude. Strains from transversely-oriented reinforcement gages were subsequently used to investigate deck behaviors unique to each deck design. This analysis investigated several aspects of the deck behavior, including longitudinal cracking, in-plane axial forces, deck integrity, relative deck stiffness, and general non-linear behaviors.

9.2 Conclusions

The primary conclusion from the live load data analysis is that all three bridge decks are behaving similarly. The shape and magnitude of the strain response under vehicle loads matches expected behavior and is similar in the three decks. No evidence of concrete cracking in the deck was found from the analysis of the live load data. Particularly, there was no indication of cracking of the top of the decks over the girders, nor was there any indication that cracking will occur in the future over the girders due to vehicle loads. Neither was there any evidence that cracking had occurred in the bottom of the deck at the time of live load testing. Moreover, there was no evidence of non-linear behavior in any of the three decks, as determined by examining strains via superposition, implying that the decks are behaving linear-elastically.

During live load data analysis, the height of the actual neutral axis within the cross-section was determined from strain data and used as a tool to evaluate whether deck cracking had occurred. After determining that cracking had not occurred in any of the decks, further investigation into shifts of the actual neutral axis height revealed in-plane axial forces acting in all of the decks. In-plane axial tension forces were inferred from the strain data in all of the tests, implying that traditional deck models derived from flexural beam bending do not fully capture true behaviors. In the absence of both cracking and in-plane axial compression forces, it was determined that no internal arching had begun to occur in the decks at the time of the first live load tests, which was expected at these load levels, based on the results of other research.

Although the behavior of all three decks was similar in nearly all respects, a few nominal differences were observed between them. These differences are merely behavioral differences noted during the analysis, which do not necessarily reveal differences in the performance of each deck relative to long-term durability, cracking or corrosion. Longitudinal behavior over the bent was different between the three bridges, indicating differences between the three decks in the in-plane axial forces at this location. The stiffness of the three decks was also found to be different, both longitudinally and transversely. The Empirical deck was determined to be the least stiff in both directions, which was expected based upon the reduced steel volume throughout the deck.

The analysis presented herein serves as a baseline for the relative condition of the three bridges before any exposure to demands from traffic and the environment. Data obtained from long-term monitoring and the second live load test will provide a more complete body of evidence from which to make judgments about which deck design is “superior”.

10 REFERENCES

- AASHTO LRFD Bridge Design Specifications, 2nd ed. (2000 Interim). American Association of State Highway and Transportation Officials, Washington D.C.
- Amer, A., Arockiasamy, M., Shahawy, M. (1999). "Load Distribution of Existing solid Slab Bridges Based on Field Tests", *Journal of Bridge Engineering*, ASCE, Vol. 4, No. 3, August, 1999, pp. 189-193.
- Annex 1: Determination of Tensile Strain Capacity (1997). Publication number ETL 110-2-542, U.S. Army Corps of Engineering Internet Publishing Group, May 30, 1997. Retrieved April 24, 2004, from <http://www.usace.army.mil/publications/eng-tech-ltrs/etl110-2-542/annex1.pdf>
- Bakht, B., Al-Bazi, G., Banthia, N., Cheung, M., Erki, M., Faoro, M., et al. (2000). "Canadian Bridge Design code Provisions for Fiber-Reinforced Concrete Bridges", *Journal of Composites for Construction*, ASCE, Vol. 4, No. 1, February, 2000, pp. 3-15.
- Bakht, B. and Lam, C. (2000). "Behavior of Transverse confining Systems for Steel-Free Deck Slabs", *Journal of Bridge Engineering*, ASCE, Vol. 5, No. 2, May, 2000, pp. 139-147.
- Bakht, B. and Mufti, A. A. (1998). "Five Steel-Free Bridge Deck Slabs in Canada", *Structural Engineering International*, March 1998, pp. 196-200.
- Boothby, T. E. and Laman, J. A. (1999). "Cumulative Damage to Bridge Concrete Deck Slabs Due to Vehicle Loading", *Journal of Bridge Engineering*, ASCE, Vol. 4, No. 1, February, 1999, pp. 80-82.
- Buckler, J.; Barton, F.; Gomez, J.; Massarelli, P.; and McKeel Jr., W. "Effect of Girder Spacing on Bridge Deck Response," Virginia Transportation Research Council, 2001.
- Cao, L., Allen, J.H., Shing, P.B. and Woodham, D; "A Case Study of Concrete Deck Behavior in a Four-Span Prestressed Girder Bridge: Correlation of Field Tests and Numerical Results," Report No. CDOT-CU-R-94-8, Colorado Department of Transportation, April 1994.
- Cao, L. (1996). "Analysis and Design of Slab-on-Girder Highway Bridge Decks", PhD Dissertation. University of Colorado, August, 1996.
- Csagoly, P. F. and Lybas J. M. (1989). "Advanced Design Method for Concrete Bridge Deck Slabs", *Concrete International*, May, 1989, pp. 53-63.
- Fang, I. K., Worley, J., Burns, N. H., and Klingner, R. E. (1990). "Behavior of Isotropic R/C Bridge Decks on Steel Girders", *Journal of Structural Engineering*, ASCE, Vol. 116, No. 3, March 1990, pp. 659-678.
- Fenwick, R. C. and Dickson, A. R. (1989). "Slabs Subjected to Concentrated Loading", *ACI Structural Journal*, V. 86, No. 6, Nov-Dec 1989, pp. 673-678.
- Gopalaratnam, V. S. and Shah, S. P. (1985). "Softening Response of Plain Concrete in Direct Tension", *ACI Journal*, May-June, 1985, pp. 310-323.
- Hughes, G., Smith, J. S. C., and Kanagasundaram, S. (2000). "Remote Monitoring of Bridge Decks", *Concrete Engineering International*, May 2000, pp. 46-49.

- Lenett, M. S., Hunt, V. J., Helmicki, A. J., and Aktan, A. E. (2001). "Instrumentation, Testing, and Monitoring of a Newly Constructed Reinforced Concrete Deck-on-Steel Girder Bridge – Phase III", Report # UC-CII 01/1, Cincinnati Infrastructure Institute, May 2001.
- Mourad, S. and Tabsh, S. W. (1999). "Deck Slab Stresses in Integral Abutment Bridges", *Journal of Bridge Engineering*, ASCE, Vol. 4, No. 2, May, 1999, pp. 125-130.
- Nassif, H., Suksawang, N., Gindy, M., Abu-Amra, T., and Davis, J. (2003). "Instrumentation and Field Testing of the Doremus Avenue Bridge", Compendium of Papers CD-ROM of the 82nd Annual Meeting of the Transportation Research Board, January 12-18, 2003, Washington, D. C.
- Sargent, D. D., Ventura, C. E., Mufti, A. A., and Bakht, B. (1999). "Testing of Steel-Free Bridge Decks", *Concrete International*, August, 1999, pp. 55-61.
- Stallings, J. M. and Porter, P. (2002). "Live Load Tests of Alabama's HPC Bridge", TE-036 Report, ALDOT Research Project 930-373, Auburn University Highway Research Center, 2002.
- Tabsh, S. W. and Tabatabai, M. (2001). "Live Load Distribution in Girder Bridges Subject to Oversized Trucks", *Journal of Bridge Engineering*, ASCE, Vol. 6, No. 1, January/February, 2001, pp. 9-16.
- Wang, C. K. and Salmon, C. G. (1985). *Reinforced Concrete Design* (4th Ed.). New York: Harper and Row.
- Yang, Y. and Myers, J. J. (2003). "Live Load Test results of Missouri's First High Performance Concrete Superstructure Bridge", Paper No. 03-3717, Compendium of Papers CD-ROM of the 82nd Annual Meeting of the Transportation Research Board, January 12-18, 2003, Washington, D. C.

Appendix A – Deck Concrete Material Properties

Table A-1: Concrete Summary Data for All Deck from MDT

Sample #	Bridge Location	Sample Location	Date Cast	Cement Brand	Cement Type	Bin & Grind No.	Air Content (%)	Slump (in.)	Date Tested	Age (days)	Strength (psi)	Load (lbs)
1HPC11	11+57.24	11+44	5/28/2003	Holnam	HPC-GU	T-476	5.0	5.5	6/5/2003	8	5947	168,147
2HPC11	11+57.24	11+44	5/28/2003	Holnam	HPC-GU	T-476	5.0	5.5	6/25/2003	28	8267	233,744
3HPC11	11+57.24	11+44	5/28/2003	Holnam	HPC-GU	T-476	5.0	5.5	6/25/2003	28	8267	233,744
4HPC11	11+57.24	11+72	5/28/2003	Holnam	HPC-GU	T-476	5.2	7.75	6/5/2003	8	5221	147,620
5HPC11	11+57.24	11+72	5/28/2003	Holnam	HPC-GU	T-476	5.2	7.75	6/25/2003	28	7542	213,245
6HPC11	11+57.24	11+72	5/28/2003	Holnam	HPC-GU	T-476	5.2	7.75	6/25/2003	28	7252	205,045
1SD16	16+81.74	16+72	6/2/2003	Holnam	1-2	T-524	6.5	3.25	6/11/2003	9	3481	98,423
2SD16	16+81.74	16+72	6/2/2003	Holnam	1-2	T-524	6.5	3.25	6/30/2003	28	4641	131,221
3SD16	16+81.74	16+72	6/2/2003	Holnam	1-2	T-524	6.5	3.25	6/30/2003	28	4641	131,221
4SD16	16+81.74	16+95	6/2/2003	Holnam	1-2	T-524	6.5	4.0	6/11/2003	9	3626	102,523
5SD16	16+81.74	16+95	6/2/2003	Holnam	1-2	T-524	6.5	4.0	6/30/2003	28	4931	139,421
6SD16	16+81.74	16+95	6/2/2003	Holnam	1-2	T-524	6.5	4.0	6/30/2003	28	4931	139,421
7SD19	19+23.24	19+19	6/5/2003	Holnam	1-2	T-524	6.4	3.0	6/12/2003	7	3626	102,523
8SD19	19+23.24	19+19	6/5/2003	Holnam	1-2	T-524	6.4	3.0	7/3/2003	28	5221	147,620
9SD19	19+23.24	19+19	6/5/2003	Holnam	1-2	T-524	6.4	3.0	7/3/2003	28	5076	143,521
10SD10	19+23.24	19+39	6/5/2003	Holnam	1-2	T-524	6.1	3.25	6/12/2003	7	4351	123,022
11SD19	19+23.24	19+39	6/5/2003	Holnam	1-2	T-524	6.1	3.25	7/3/2003	28	5802	164,048
12SD19	19+23.24	19+39	6/5/2003	Holnam	1-2	T-524	6.1	3.25	7/3/2003	28	5802	164,048

Table A-2: Concrete Cylinder Summary Data for Conventional Deck from WTI

Truck	Specimen Number	Specimen Type	Size (in)	Curing	Test Type	Time to Test	Age (days)	Stress (psi)	Stress (Mpa)	Notes:
C-4	1C	cylinder	6x12	moist	compression	28 days	28	4,910	33.9	
	2C	cylinder	6x12	moist	compression	28 days	28	4,853	33.5	See Figure 1
	3C	cylinder	6x12	moist	compression	28 days	28	4,743	32.7	See Figure 1
	4C	cylinder	6x12	with deck	compression	live load 1	61	5,711	39.4	
	5C	cylinder	6x12	with deck	compression	live load 1	61	5,929	40.9	See Figure 2
	6C	cylinder	6x12	with deck	compression	live load 1	61	6,210	42.8	See Figure 2
	7C	cylinder	6x12	with deck	compression	live load 2				
	8C	cylinder	6x12	with deck	compression	live load 2				
C-5	9C	cylinder	6x12	with deck	compression	live load 2				
	1C	cylinder	6x12	with deck	compression	live load 1	61	4,750	32.8	
	2C	cylinder	6x12	with deck	compression	live load 1	61	5,293	36.5	See Figure 2
	3C	cylinder	6x12	with deck	compression	live load 2				
C-6	4C	cylinder	6x12	with deck	compression	live load 2				
	1C	cylinder	6x12	moist	compression	28 days	28	4,757	32.8	
	2C	cylinder	6x12	moist	compression	28 days	28	4,661	32.1	See Figure 1
	3C	cylinder	6x12	moist	compression	28 days	28	4,569	31.5	See Figure 1
	4C	cylinder	6x12	with deck	compression	live load 1	61	5,332	36.8	
	5C	cylinder	6x12	with deck	compression	live load 1	61	5,622	38.8	See Figure 2
	6C	cylinder	6x12	with deck	compression	live load 1	61	5,362	37.0	See Figure 2
	7C	cylinder	6x12	with deck	split cylinder	live load 1	61	796	5.5	
	8C	cylinder	6x12	with deck	split cylinder	live load 1	61	817	5.6	See Figure 2
	9C	cylinder	6x12	with deck	split cylinder	live load 1	61	882	6.1	See Figure 2
	10C	cylinder	6x12	with deck	compression	live load 2				
	11C	cylinder	6x12	with deck	compression	live load 2				
	12C	cylinder	6x12	with deck	compression	live load 2				
	13C	cylinder	6x12	with deck	split cylinder	live load 2				
	14C	cylinder	6x12	with deck	split cylinder	live load 2				
	15C	cylinder	6x12	with deck	split cylinder	live load 2				
C-7	1C	cylinder	6x12	moist	compression	28 days	28	4,655	32.1	
	2C	cylinder	6x12	moist	compression	28 days	28	3,967	27.4	See Figure 1
	3C	cylinder	6x12	moist	compression	28 days	28	4,184	28.8	See Figure 1
	4C	cylinder	6x12	with deck	split cylinder	live load 1	61	706	4.9	
	5C	cylinder	6x12	with deck	split cylinder	live load 1	61	845	5.8	
	6C	cylinder	6x12	with deck	split cylinder	live load 1	61	868	6.0	
	7C	cylinder	6x12	with deck	compression	live load 2				
	8C	cylinder	6x12	with deck	compression	live load 2				
	9C	cylinder	6x12	with deck	compression	live load 2				

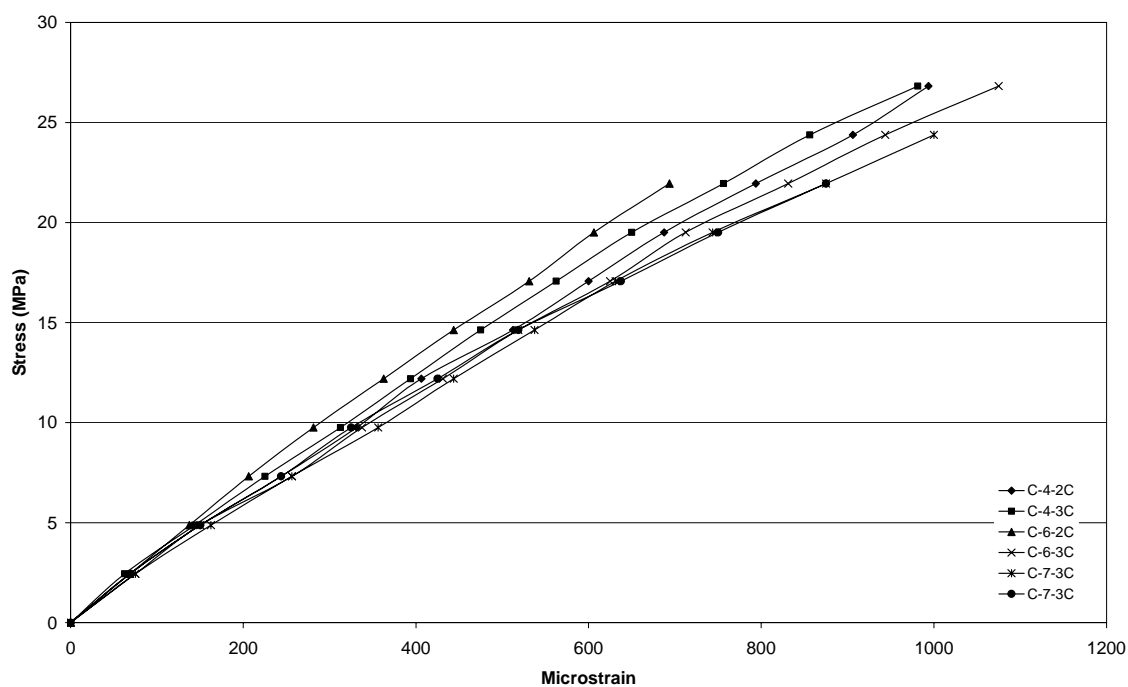


Figure A-1: Concrete Stress/Strain Plots for the Conventional Bridge Deck (28-Day)

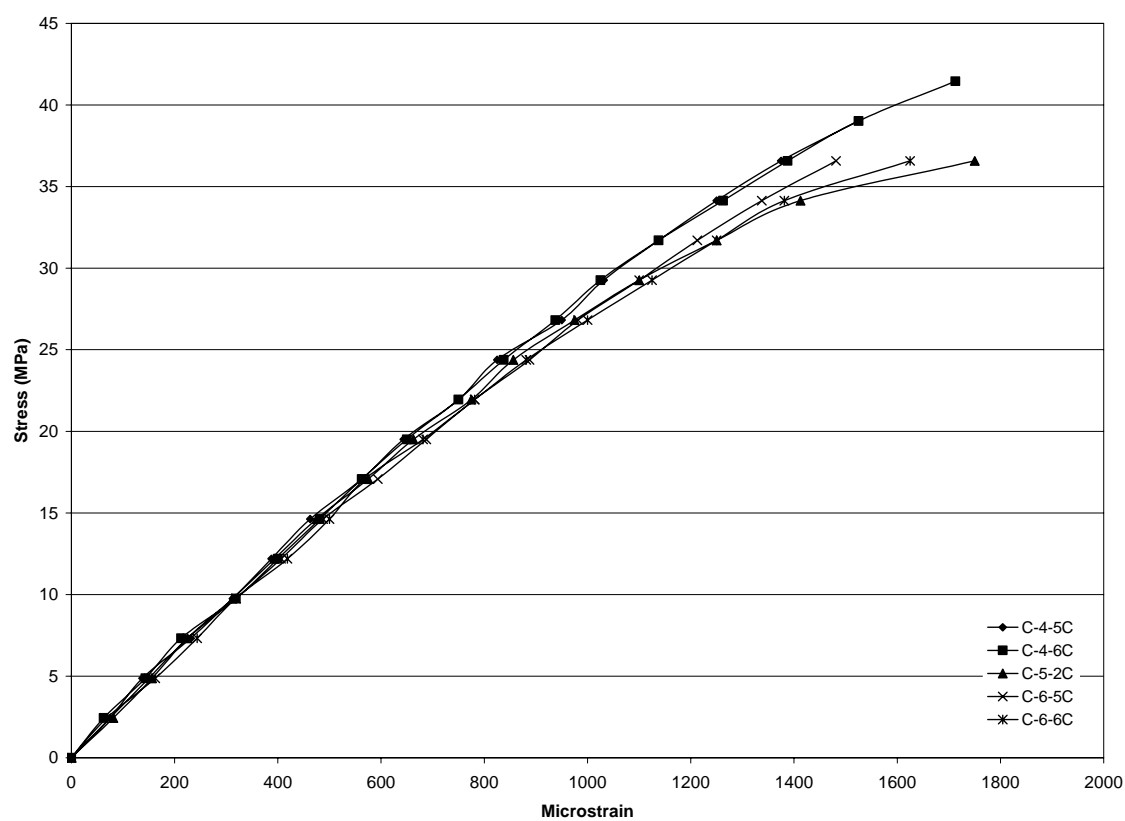


Figure A-2: Concrete Stress/Strain Plots for the Conventional Bridge Deck (Live-Load 1)

Table A-3: Concrete Rupture Beam Summary Data for the Conventional Deck from WTI

Truck	Specimen Number	Specimen Type	Size (in)	Curing	Test Type	Time to Test	Age (days)	Stress (psi)	Stress (Mpa)
C-4	1R	rupture beam	6x6x20	with deck	bending	live load 1	60	522	3.6
	2R	rupture beam	6x6x20	with deck	bending	live load 1	60	439	3.0
C-6	1R	rupture beam	6x6x20	with deck	bending	live load 1	60	540	3.7
	2R	rupture beam	6x6x20	with deck	bending	live load 1	60	546	3.8
	3R	rupture beam	6x6x20	with deck	bending	live load 2			
	4R	rupture beam	6x6x20	with deck	bending	live load 2			
	5R	rupture beam	6x6x20	with deck	bending	extra			
C-7	1R	rupture beam	6x6x20	with deck	bending	live load 2			
	2R	rupture beam	6x6x20	with deck	bending	live load 2			

Table A-4: Concrete Cylinder Summary Data for the Empirical Deck from WTI

Truck	Specimen Number	Specimen Type	Size (in)	Curing	Test Type	Time to Test	Age (days)	Stress (psi)	Stress (Mpa)	Notes:
E-5	1C	cylinder	6x12	moist	compression	28 days	28	4,089	28.2	
	2C	cylinder	6x12	moist	compression	28 days	28	4,055	28.0	See Figure 3
	3C	cylinder	6x12	moist	compression	28 days	28	3,926	27.1	See Figure 3
	4C	cylinder	6x12	with deck	compression	live load 1	63	5,021	34.6	
	5C	cylinder	6x12	with deck	compression	live load 1	63	4,677	32.2	See Figure 4
	6C	cylinder	6x12	with deck	compression	live load 1	63	4,496	31.0	See Figure 4
	7C	cylinder	6x12	with deck	compression	live load 2				
	8C	cylinder	6x12	with deck	compression	live load 2				
	9C	cylinder	6x12	with deck	compression	live load 2				
E-7	1C	cylinder	6x12	moist	compression	28 days	28	3,728	25.7	
	2C	cylinder	6x12	moist	compression	28 days	28	4,103	28.3	See Figure 3
	3C	cylinder	6x12	moist	compression	28 days	28	4,154	28.6	See Figure 3
	4C	cylinder	6x12	with deck	compression	live load 1	63	4,736	32.7	
	5C	cylinder	6x12	with deck	compression	live load 1	63	4,823	33.3	
	6C	cylinder	6x12	with deck	compression	live load 1	63	4,330	29.9	See Figure 4
	7C	cylinder	6x12	with deck	split cylinder	live load 1	64	415	2.9	
	8C	cylinder	6x12	with deck	split cylinder	live load 1	64	415	2.9	
	9C	cylinder	6x12	with deck	split cylinder	live load 1	64	484	3.3	
	10C	cylinder	6x12	with deck	compression	live load 2				
	11C	cylinder	6x12	with deck	compression	live load 2				
	12C	cylinder	6x12	with deck	compression	live load 2				
	13C	cylinder	6x12	with deck	split cylinder	live load 2				
	14C	cylinder	6x12	with deck	split cylinder	live load 2				
	15C	cylinder	6x12	with deck	split cylinder	live load 2				
E-9	1C	cylinder	6x12	moist	compression	28 days	28	4,276	29.5	
	2C	cylinder	6x12	moist	compression	28 days	28	3,583	24.7	See Figure 3
	3C	cylinder	6x12	moist	compression	28 days	28	3,872	26.7	See Figure 3
	4C	cylinder	6x12	with deck	compression	live load 1	63	5,054	34.8	
	5C	cylinder	6x12	with deck	compression	live load 1	63	5,119	35.3	See Figure 4
	6C	cylinder	6x12	with deck	compression	live load 1	63	4,658	32.1	See Figure 4
	7C	cylinder	6x12	with deck	compression	live load 2				
	8C	cylinder	6x12	with deck	compression	live load 2				
	9C	cylinder	6x12	with deck	compression	live load 2				

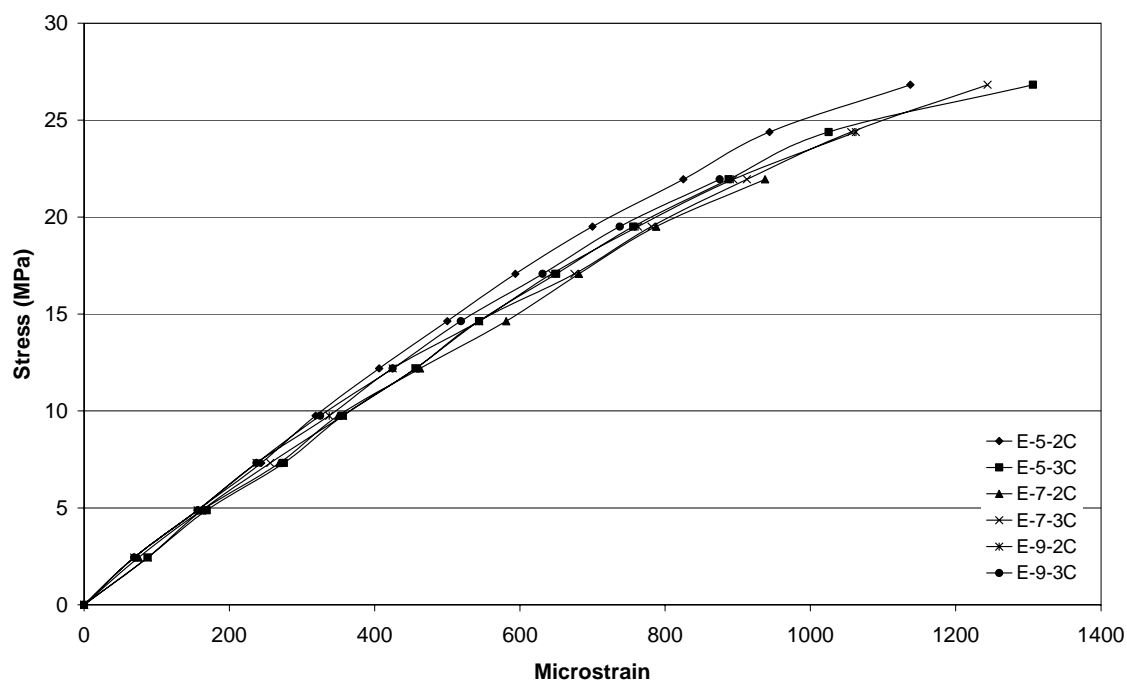


Figure A-3: Concrete Stress/Strain Plots for the Empirical Bridge Deck (28-Day)

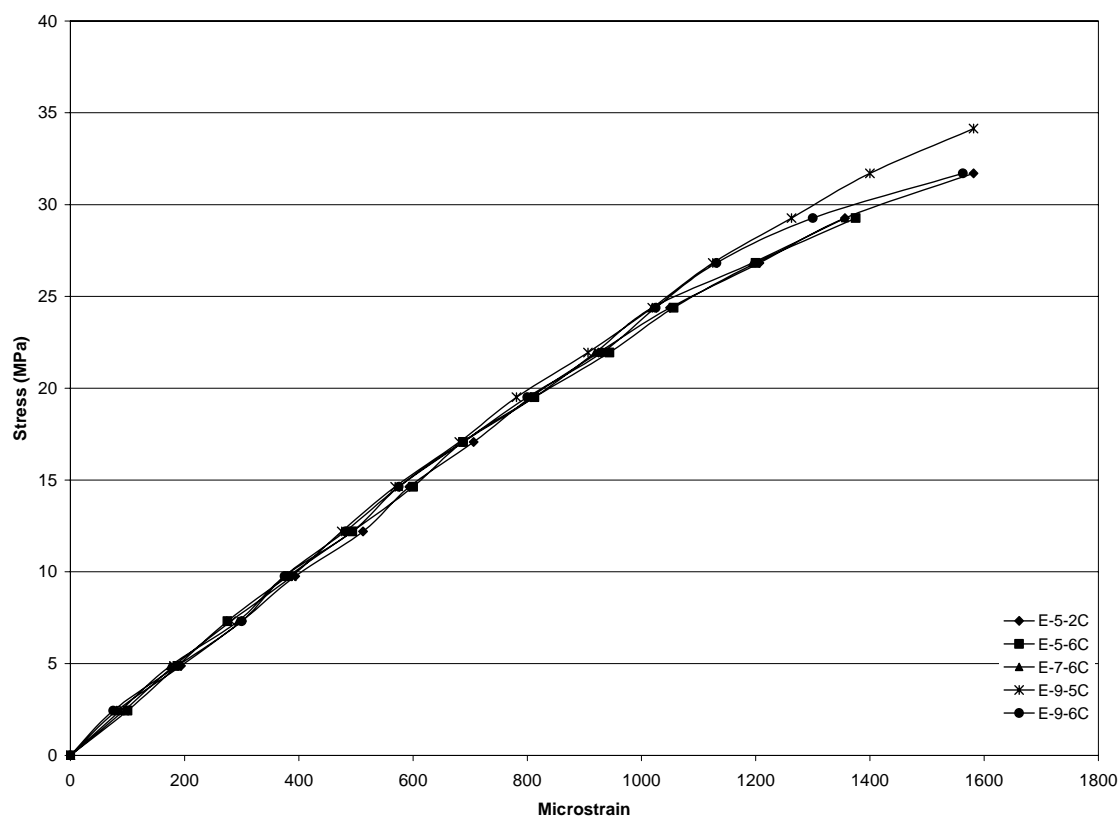


Figure A-4: Concrete Stress/Strain Plots for the Empirical Bridge Deck (Live-Load 1)

Table A-5: Concrete Rupture Beam Summary Data for the Empirical Deck from WTI

Truck	Specimen Number	Specimen Type	Size (in)	Curing	Test Type	Time to Test	Age (days)	Stress (psi)	Stress (Mpa)
E-5	1R	rupture beam	6x6x20	with deck	bending	live load 1	63	484	3.3
	2R	rupture beam	6x6x20	with deck	bending	live load 1	63	484	3.3
E-7	1R	rupture beam	6x6x20	with deck	bending	live load 1	63	487	3.4
	2R	rupture beam	6x6x20	with deck	bending	live load 1	63	484	3.3
	3R	rupture beam	6x6x20	with deck	bending	live load 2			
	4R	rupture beam	6x6x20	with deck	bending	live load 2			
	5R	rupture beam	6x6x20	with deck	bending	extra			
E-9	1R	rupture beam	6x6x20	with deck	bending	live load 2			
	2R	rupture beam	6x6x20	with deck	bending	live load 2			

Table A-6: Concrete Cylinder Summary Data for the HPC Deck from WTI

Truck	Specimen Number	Specimen Type	Size (in)	Curing	Test Type	Time to Test	Age (days)	Stress (psi)	Stress (Mpa)	Notes:
H-5	1C	cylinder	6x12	moist	compression	28 days	28	7,236	49.9	See Figure 5
	2C	cylinder	6x12	with deck	compression	live load 1	69	7,748	53.4	See Figure 6
	3C	cylinder	6x12	with deck	compression	live load 1	69	8,079	55.7	See Figure 6
	4C	cylinder	6x12	with deck	split cylinder	live load 1	69	577	4.0	
	5C	cylinder	6x12	with deck	split cylinder	live load 1	69	589	4.1	
	6C	cylinder	6x12	with deck	compression	live load 2				
	7C	cylinder	6x12	with deck	compression	live load 2				
	8C	cylinder	6x12	with deck	split cylinder	live load 2				
	9C	cylinder	6x12	with deck	split cylinder	live load 2				
H-7	1C	cylinder	6x12	moist	compression	28 days	28	6,420	44.3	See Figure 5
	2C	cylinder	6x12	moist	compression	28 days	28	6,813	47.0	See Figure 5
	3C	cylinder	6x12	with deck	compression	live load 1	69	6,404	44.2	See Figure 6
	4C	cylinder	6x12	with deck	compression	live load 1	69	6,979	48.1	See Figure 6
	5C	cylinder	6x12	with deck	compression	live load 2				
	6C	cylinder	6x12	with deck	compression	live load 2				
H-9	1C	cylinder	6x12	moist	compression	28 days	28	6,238	43.0	See Figure 5
	2C	cylinder	6x12	with deck	compression	live load 1	69	6,785	46.8	See Figure 6
	3C	cylinder	6x12	with deck	compression	live load 1	69	6,819	47.0	See Figure 6
	4C	cylinder	6x12	with deck	compression	live load 2				
	5C	cylinder	6x12	with deck	compression	live load 2				

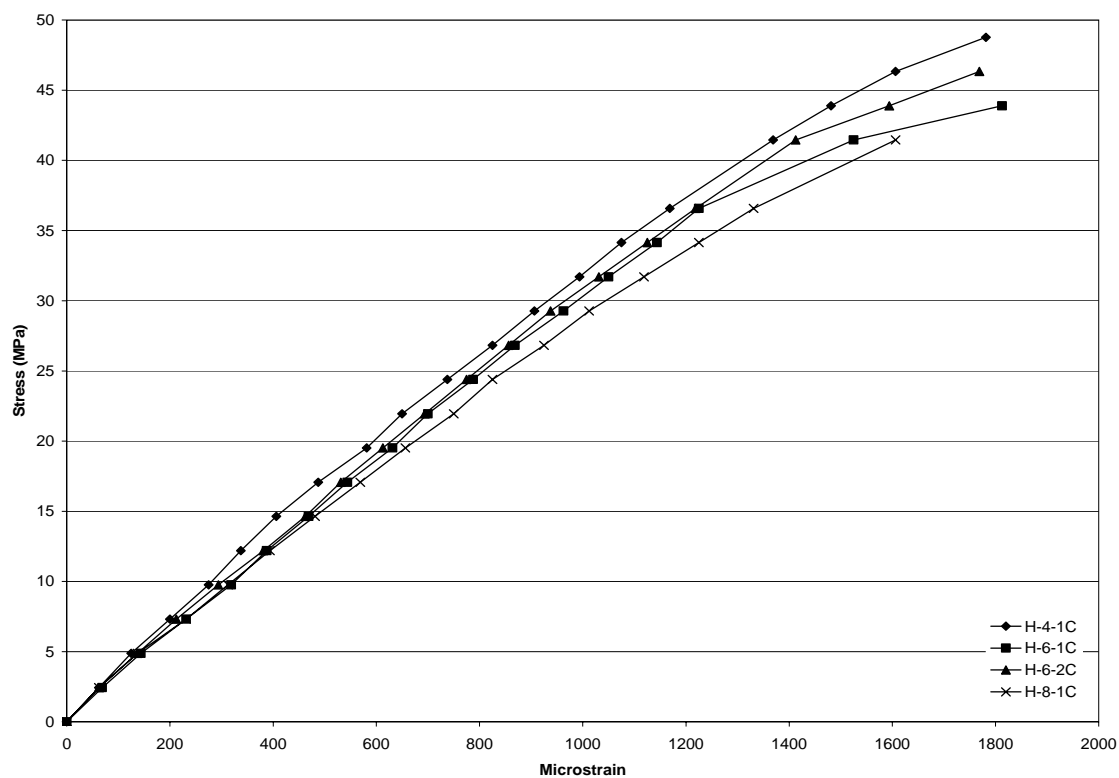


Figure A-5: Concrete Stress/Strain Plots for the HPC Bridge Deck (28-Day)

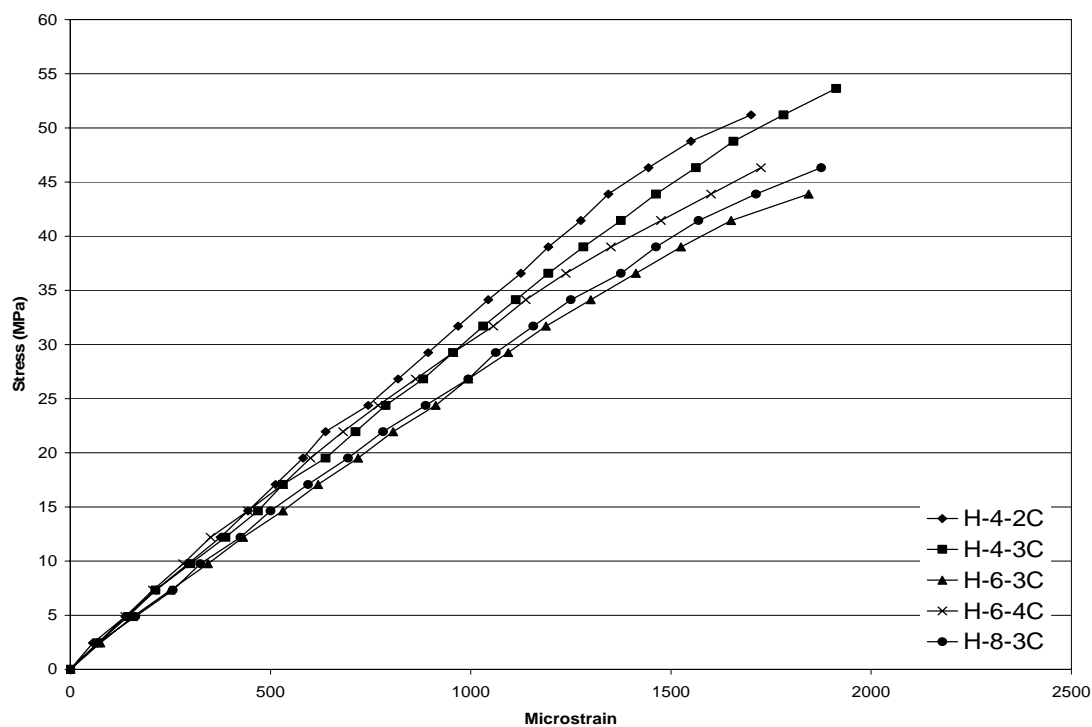
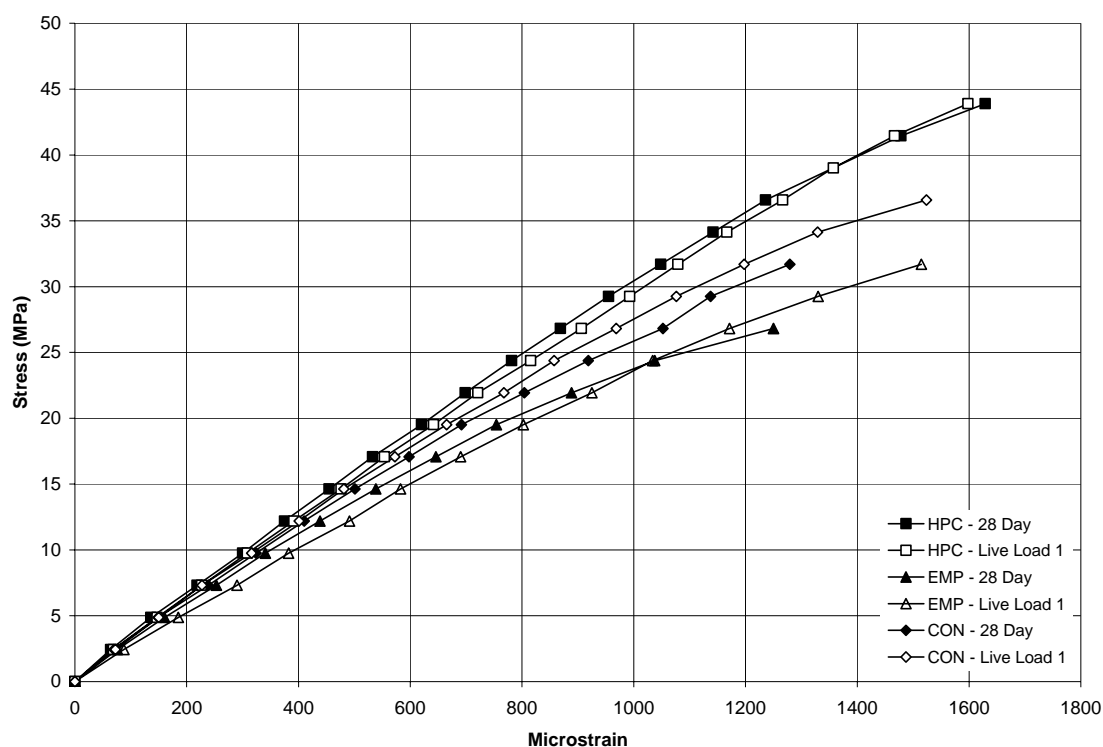


Figure A-6: Concrete Stress/Strain Plots for the HPC Bridge Deck (Live-Load 1)

Table A-7: Concrete Rupture Beam Summary Data for the HPC Deck from WTI

Truck	Specimen Number	Specimen Type	Size (in)	Curing	Test Type	Time to Test	Age (days)	Stress (psi)	Stress (Mpa)
H-4	1R	rupture beam	6x6x20	with deck	bending	live load 1	68	561	3.9
	2R	rupture beam	6x6x20	with deck	bending	live load 1	68	633	4.4
	3R	rupture beam	6x6x20	with deck	bending	live load 2			
H-6	1R	rupture beam	6x6x20	with deck	bending	live load 1	68	610	4.2
	2R	rupture beam	6x6x20	with deck	bending	live load 1	68	603	4.2
	3R	rupture beam	6x6x20	with deck	bending	live load 2			
H-8	1R	rupture beam	6x6x20	with deck	bending	live load 1	68	565	3.9
	2R	rupture beam	6x6x20	with deck	bending	live load 2			
	3R	rupture beam	6x6x20	with deck	bending	live load 2			

**Figure A-7: Average Stress/Strain Plots for All Bridge Decks**

Appendix B – ASTM Specification References

1. ASTM C 31-00: “Standard Practice for Making and Curing Concrete Test Specimens in the Field.”
2. ASTM C 39-01: “Standard Test Method for Compressive Strengths of Cylindrical Concrete Specimens.”
3. ASTM C 78-00: “Standard Test Method for Flexural Strength of Concrete (Using Simple Beam with Third Point Loading).”
4. ASTM C 172-99: “Standard Practice for Sampling Freshly Mixed Concrete.”
5. ASTM C 173-01: “Standard Test Method for Air content of Freshly Mixed Concrete by the Volumetric Method.”
6. ASTM C 192-00: “Standard Practice for Making and Curing Concrete Test Specimens in the Laboratory.”
7. ASTM C 231-97: “Standard Test Method for Air Content of Freshly Mixed Concrete by the Pressure Method.”
8. ASTM C 452-95: “Standard Test Method for Static Modulus of Elasticity and Poisson’s Ratio of Concrete in Compression.”
9. ASTM C 496-96: “Standard Test Method for Splitting Tensile Strength of Cylindrical Concrete Specimens.”
10. ASTM C 876-91 (1999): “Standard Test Method for Half-Cell Potentials of Uncoated Reinforcing of Steel in Concrete.”
11. ASTM C 4580-86 (1997): “Standard Test Method for Measuring Delaminations in Concrete Bridge Decks by Sounding.”

Appendix C – Deck Rebar Material Properties

Table C-1: Mill Test Data for Deck Reinforcing Steel

North Star Steel											
Certificate #	Sales Order	Purchase Order	Product	Size (mm)	Grade	Heat #	Yield (Mpa)	Yield (ksi)	Tensile (Mpa)	Tensile (ksi)	% Elongation
31124	Z030421	1205-A	Rebar	13	60	50719603	477.7	69.28	731.88	105.15	14.40
31374	Z031693	115-B	Rebar	16	60	11565270	494.1	71.66	747.94	108.46	14.75
31404	Z031174	102-B	Rebar	13	60	420224396	475.5	68.96	742.57	107.70	13.70
SMI - Texas			Product	Size (mm)	Grade	Heat #	Yield (Mpa)	Yield (ksi)	Tensile (Mpa)	Tensile (ksi)	% Elongation
			Rebar	19	60	225533	466.8	67.7	738.2	105.9	15

Table C-2: Other Test Data for Deck Reinforcing Steel

Date Sampled	Date Checked & Approved	Quantity (kg)	Name of Material	Grade	Manufacturer	Paint	Thickness	Holidays	Bend Test
3/10/2003	3/26/2003	17,992	Epoxy Reinforcing Steel, # 13 bar	60	North Star & SMI	7	10	OK	OK
						8	9		
						9	12		
3/10/2003	3/26/2003	13,850	Epoxy Reinforcing Steel, #19 bar	60	North Star & SMI	11	8	OK	OK
						8	10		
						8	10		

Table C-3: Coating Properties as Reported by Manufacturers

ABC Coating Co., Inc. of Colorado						
Job #	Work Order #	Invoice #	Size	Weight (lbs)	Heat(s)	Powder Lot(s)
029-MT	3330	3330	#4 / 13M	2,858	420224396	3141901809
			#5 / 16M	1,858	11565270	3141901809
			#6 / 19M	25,818	225533	3141901809
029-MT	3332	3332	#4 / 13M	20,602	50719603	2T41901527
			#5 / 16M	5,030	11565270	3141901809
			#6 / 19M	14,034	225533	3141901993
Valspar Corporation						
Date	Specification	Valspar Product Code		Batch Number	Production Date	Batch Size (lbs)
12/5/2003	ASTM A775 & ASHTO M284	720A009 Greenbar Fusion Bond Epoxy Powder Coating		2T41901527	10/18/2002	41,400
1/27/2003	ASTM A775 & ASHTO M284	720A009 Greenbar Fusion Bond Epoxy Powder Coating		3141901809	1/13/2003	41,540
2/25/2003	ASTM A775 & ASHTO M284	720A009 Greenbar Fusion Bond Epoxy Powder Coating		3141901993	1/23/2003	41,400

Appendix D – Prestressed Girder Material Properties

Table D-1: Concrete Cylinder Summary Data for Conventional Deck Girders

Beam Numbers			Lab No.	Date Cast	Age	Load	Individual Cylinders		3 Cylinder Avg		Spread	% Spread
							psi	MPa	psi	MPa		
25	29	33	824267	10/9/2002	28	84320	6710	46.3	8302	57.2	2737	33.0%
			824268	10/9/2002	28	109940	8749	60.3				
			824269	10/9/2002	28	118720	9447	65.1				
26	30	34	824270	10/11/2002	28	120680	9603	66.2	9659	66.6	94	1.0%
			824271	10/11/2002	28	121600	9677	66.7				
			824272	10/11/2002	28	121860	9697	66.9				
27	31	35	824273	10/14/2002	28	105960	8432	58.1	9047	62.4	1261	13.9%
			824274	10/14/2002	28	121800	9693	66.8				
			824275	10/14/2002	28	113320	9018	62.2				
28	32	36	824300	10/15/2002	28	122740	9767	67.3	9572	66.0	404	4.2%
			824301	10/15/2002	28	117660	9363	64.6				
			824302	10/15/2002	28	120440	9584	66.1				

Table D-2: Concrete Cylinder Summary Data for Empirical Deck Girders

Beam Numbers			Lab No.	Date Cast	Age	Load	Individual Cylinders		3 Cylinder Avg		Spread	% Spread
							psi	MPa	psi	MPa		
13	17	21	823985	10/3/2002	28	108860	8663	59.7	9079	62.6	766	8.4%
			823986	10/3/2002	28	114920	9145	63.1				
			823987	10/3/2002	28	118480	9428	65.0				
14	18	22	823988	10/4/2002	28	100320	7983	55.0	8428	58.1	711	8.4%
			823989	10/4/2002	28	109260	8695	59.9				
			823990	10/4/2002	28	108160	8607	59.3				
15	19	23	824092	10/7/2002	28	113520	9034	62.3	8577	59.1	780	9.1%
			824093	10/7/2002	28	106100	8443	58.2				
			824094	10/7/2002	28	103720	8254	56.9				
16	20	24	824095	10/8/2003	28	115260	9172	63.2	9283	64.0	294	3.2%
			824096	10/8/2003	28	118960	9467	65.3				
			824097	10/8/2003	28	115740	9210	63.5				

Table D-3: Concrete Cylinder Summary Data for HPC Deck Girders

Beam Numbers			Lab No.	Date Cast	Age	Load	Individual Cylinders		3 Cylinder Avg		Spread	% Spread
							psi	MPa	psi	MPa		
2	6	10	823636	9/27/2002	28	115000	9151	63.1	9314	64.2	902	9.7%
			823637	9/27/2002	28	123740	9847	67.9				
			823638	9/27/2002	28	112400	8945	61.7				
3	7	11	823639	9/30/2002	28	121500	9669	66.7	8990	62.0	1049	11.7%
			823640	9/30/2002	28	108320	8620	59.4				
			823641	9/30/2002	28	109100	8682	59.9				
1	5	9	823780	10/1/2002	28	125780	10009	69.0	9791	67.5	729	7.4%
			823781	10/1/2002	28	126240	10046	69.3				
			823782	10/1/2002	28	117080	9317	64.2				
4	8	12	823783	10/2/2002	28	118580	9436	65.1	9123	62.9	673	7.4%
			823784	10/2/2002	28	110120	8763	60.4				
			823785	10/2/2002	28	115240	9171	63.2				

Table D-4: Saco Bridge Girder Layout

Conventional	36	32	28
	35	31	27
	34	30	26
	33	29	25
Empirical	24	20	16
	23	19	15
	22	18	14
	21	17	13
HPC	12	8	4
	11	7	3
	10	6	2
	9	5	1

Note: North is to the left of the Table

Appendix E: Instrumentation Plan

Table of Contents

Introduction.....	A-3
HPC Deck	A-4
Section A-1: General bridge deck layout	A-5
Section B-1: Detailed rebar layout	A-6
Section C-1: Plan view of gage locations.....	A-8
Section D-1: Cable-exiting plan	A-11
Section E-1: Detailed instrumentation list.....	A-12
Section F-1: Detailed drawings of reinforcing bars instrumented with bonded strain gages.....	A-16
Empirical Deck	A-21
Section A-2: General bridge deck layout	A-22
Section B-2: Detailed rebar layout	A-23
Section C-2: Plan view of gage locations.....	A-25
Section D-2: Cable-exiting plan	A-28
Section E-2: Detailed instrumentation list.....	A-29
Section F-2: Detailed drawings of reinforcing bars instrumented with bonded strain gages.....	A-33
Conventional Deck.....	A-38
Section A-3: General bridge deck layout	A-39
Section B-3: Detailed rebar layout	A-40
Section C-3: Plan view of gage locations.....	A-42
Section D-3: Cable-exiting plan	A-45
Section E-3: Detailed instrumentation list.....	A-46
Section F-3: Detailed drawings of reinforcing bars instrumented with bonded strain gages.....	A-50

Introduction

This instrumentation plan is for the Saco bridges located at station 11+57.24, 16+81.74 and 19+23.24, which correspond to the HPC, Empirical and Conventional bridges, respectively. The instrumentation for each bridge deck includes 35 reinforcing strain gages, 9 embedded strain gages, and 20 vibrating wire gages.

The position referencing nomenclature described in Section 3.2 of the body of the report was used throughout this instrumentation plan. This plan details the following information for each bridge:

Section A: General bridge deck layout

Section B: Detailed rebar layout

Section C: Plan view of gage locations

Section D: Cable-exiting plan

Section E: Detailed instrumentation list

Section F: Detailed drawings of reinforcing bars instrumented with bonded strain gages

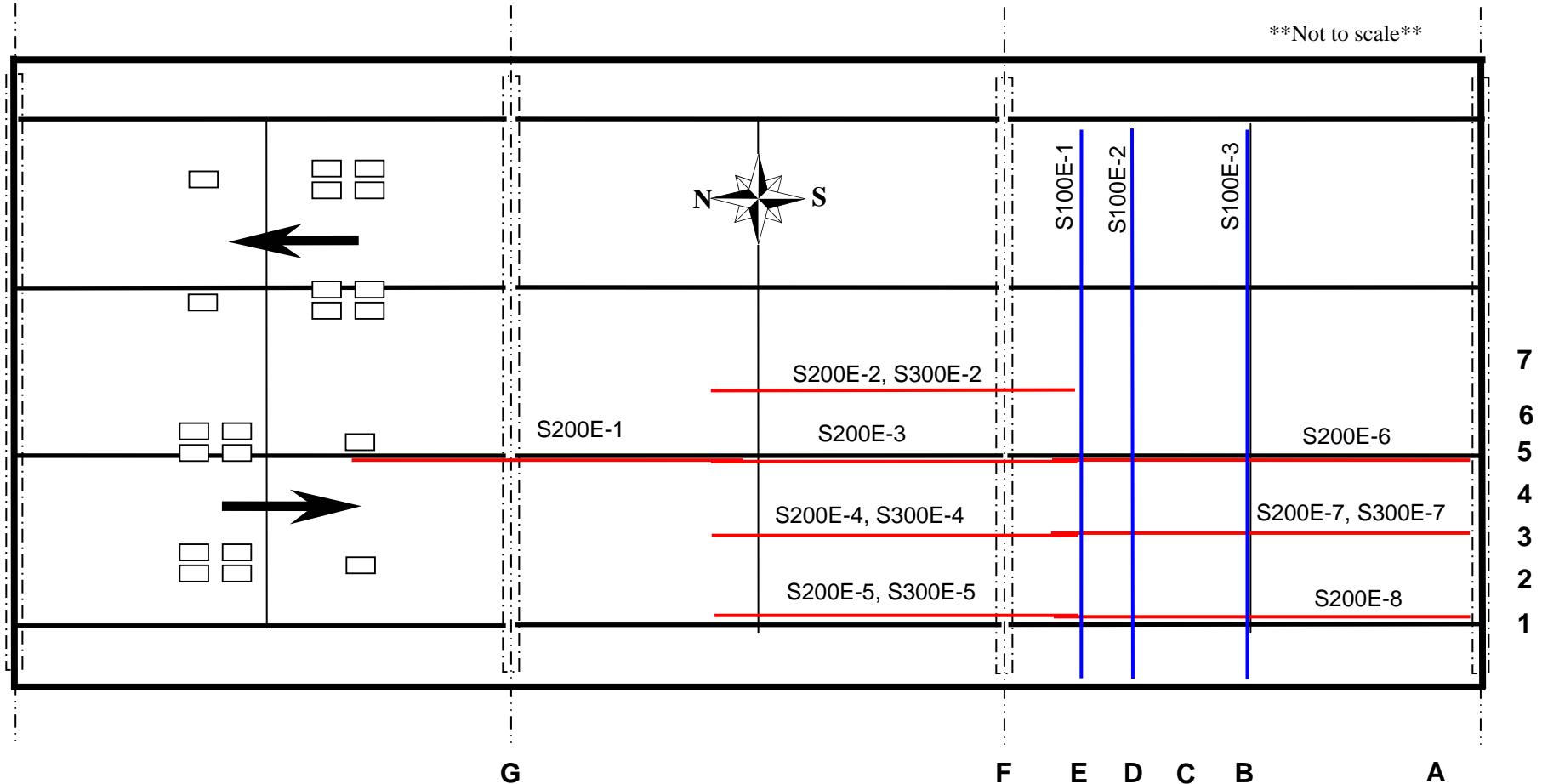
Part 1: HPC Deck @11+57.24

Section A-1: General Bridge Deck Layout

High Performance Concrete Deck at 11+57.24

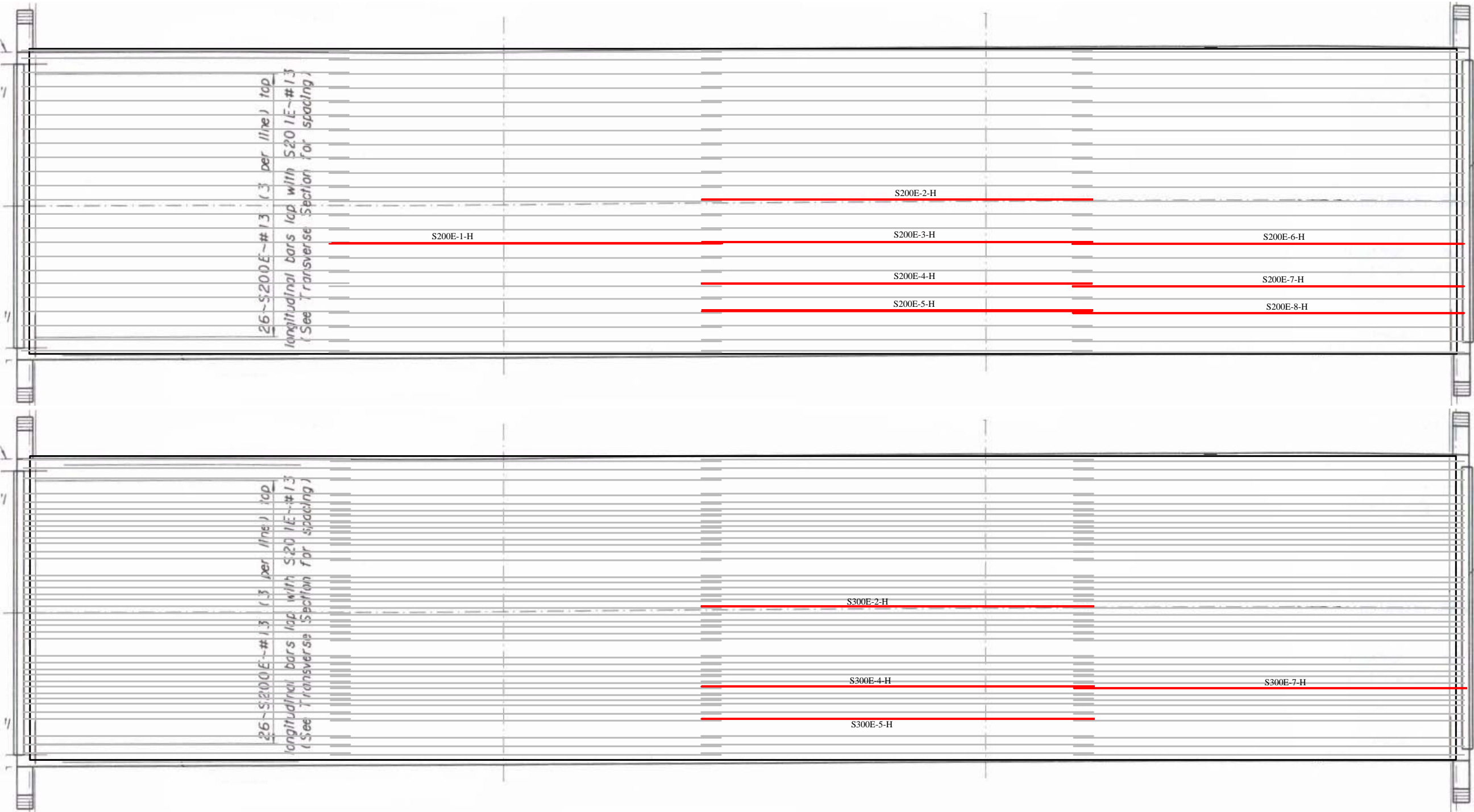
The series of numbers along the bottom of the bridge correspond to the longitudinal gage positions used in the reference number system described above. Likewise, the numbers along the right edge correspond to the transverse position of the gages used in the reference number system. The arrows on the left side show the direction of travel across the bridge of a typical truck.

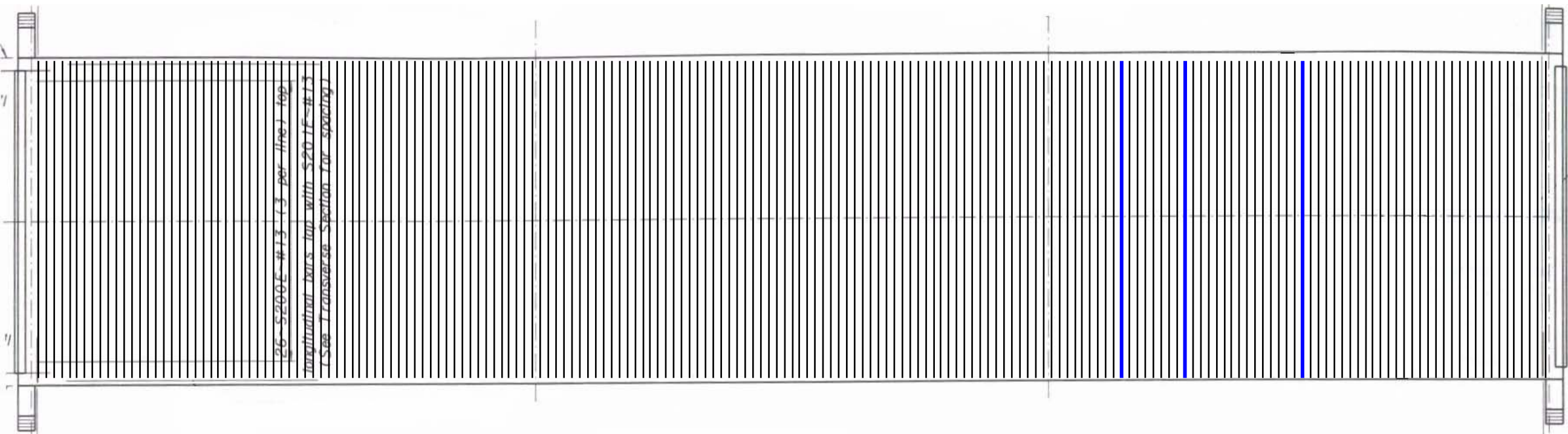
The S200E bars numbered 1 through 8 are the S200E ~ # 13 bars called out in the bridge plans for the top longitudinal reinforcement. The S300E bars numbered 2,4,5, and 7 are the S300E ~ #13 bars called out in the plans for the Bottom longitudinal reinforcement. Each of the longitudinal bars is 12.19 meters in length. The S100E bars numbered 1 through 3 are the S100E ~ # 19 bars called out in the plans as the top and bottom transverse reinforcement. Each transverse bar is 8.95 meters long.



Section B-1: Detailed Rebar Layout

High Performance Concrete Deck at 11+57.24





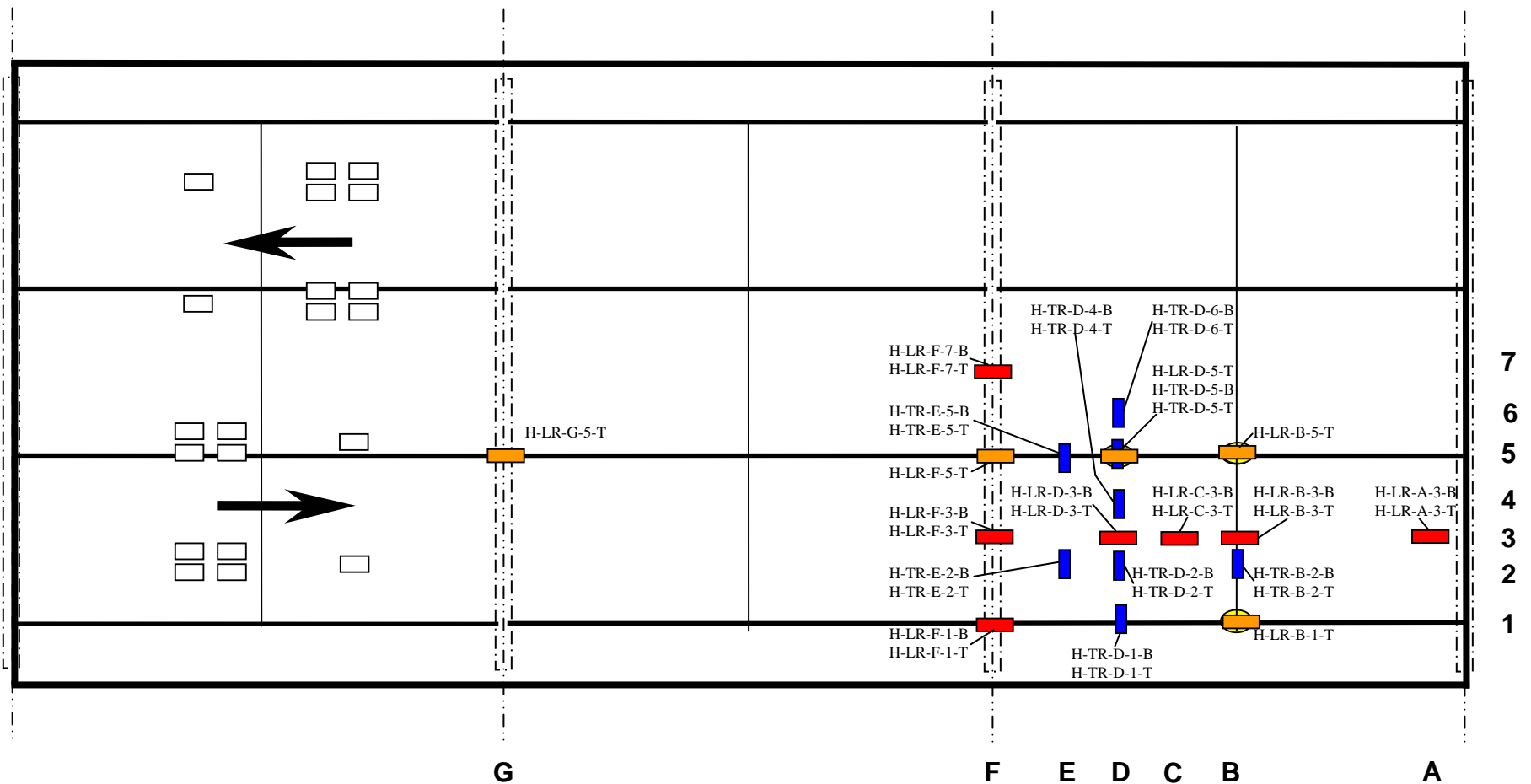
Section C-1: Plan View of Gage Locations

High Performance Concrete Deck at 11+57.24

Bonded Strain Gage Layout

6 transverse bars (16 gage locations)
12 longitudinal bars (19 gage locations)

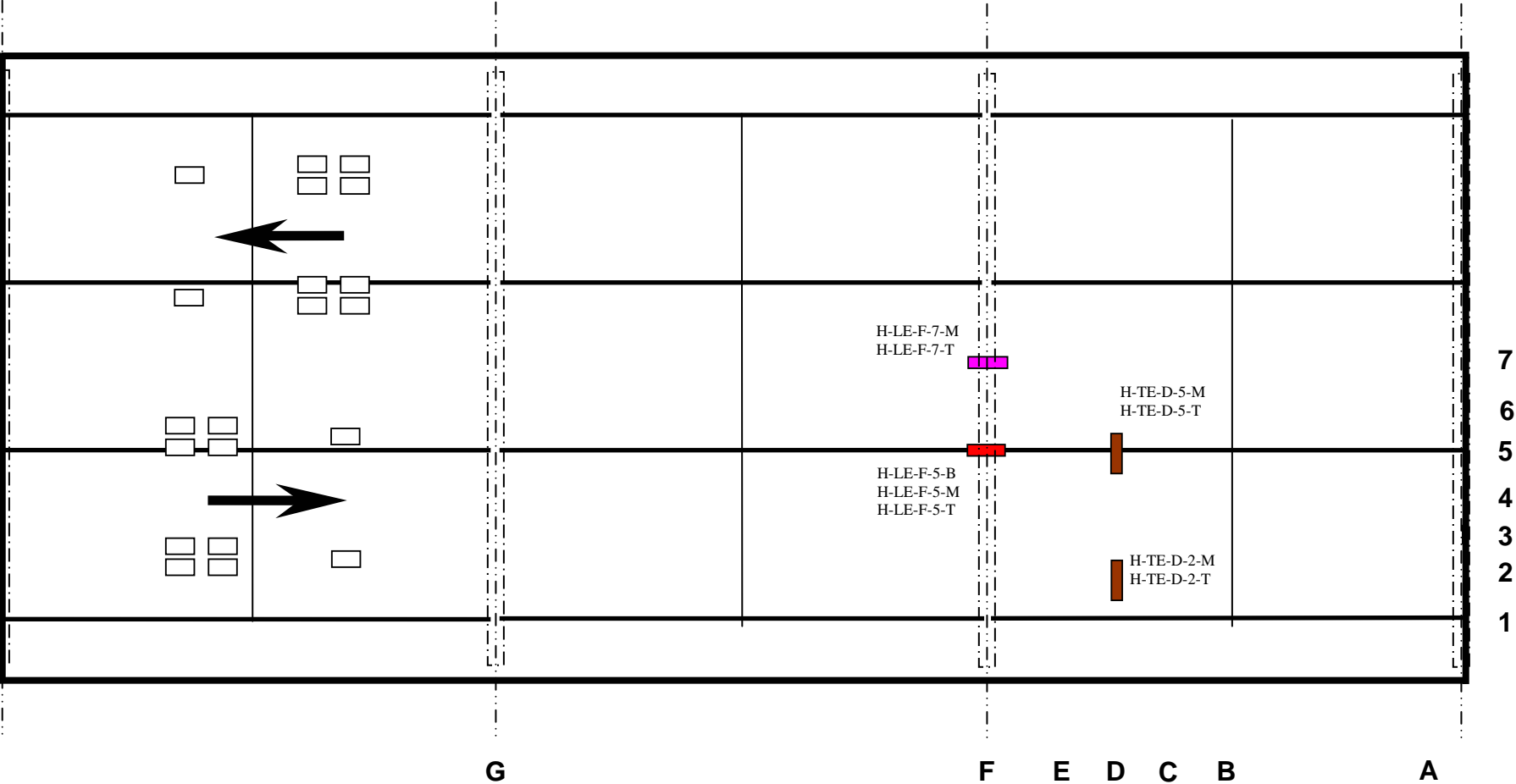
- Transverse gage, top and bottom mat
- Longitudinal gage, top and bottom mat
- Longitudinal gage, top mat only
- Longitudinal gage, bottom of stringer



Embedded Strain Gage Layout

9 locations

- Transverse gage, mid and near surface
- Longitudinal gage, mid and near surface
- Longitudinal gage, bottom, mid, and near surface


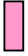




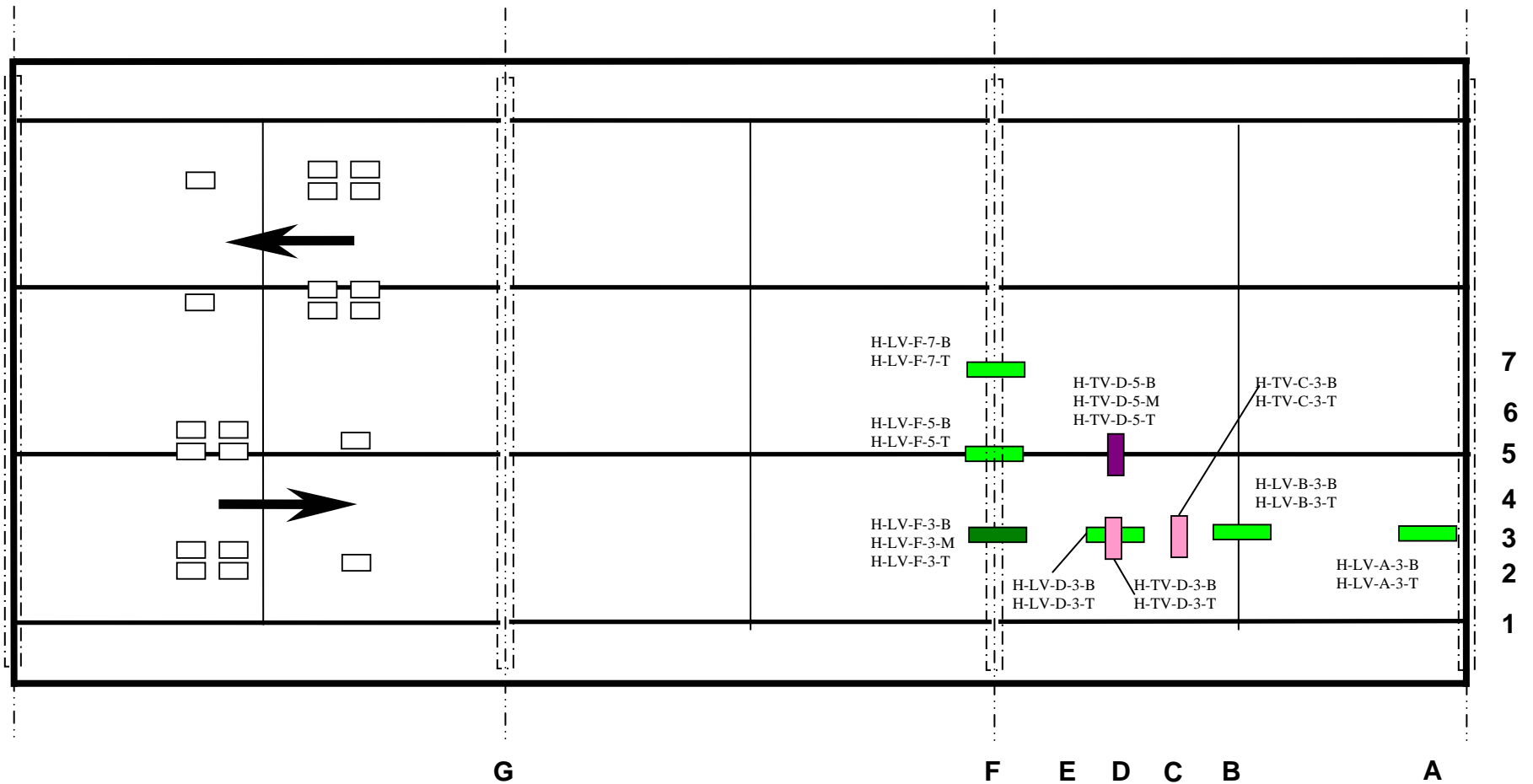
Section C-1: Plan View of Gage Locations

High Performance Concrete Deck at 11+57.24

Vibrating Wire Gage Layout

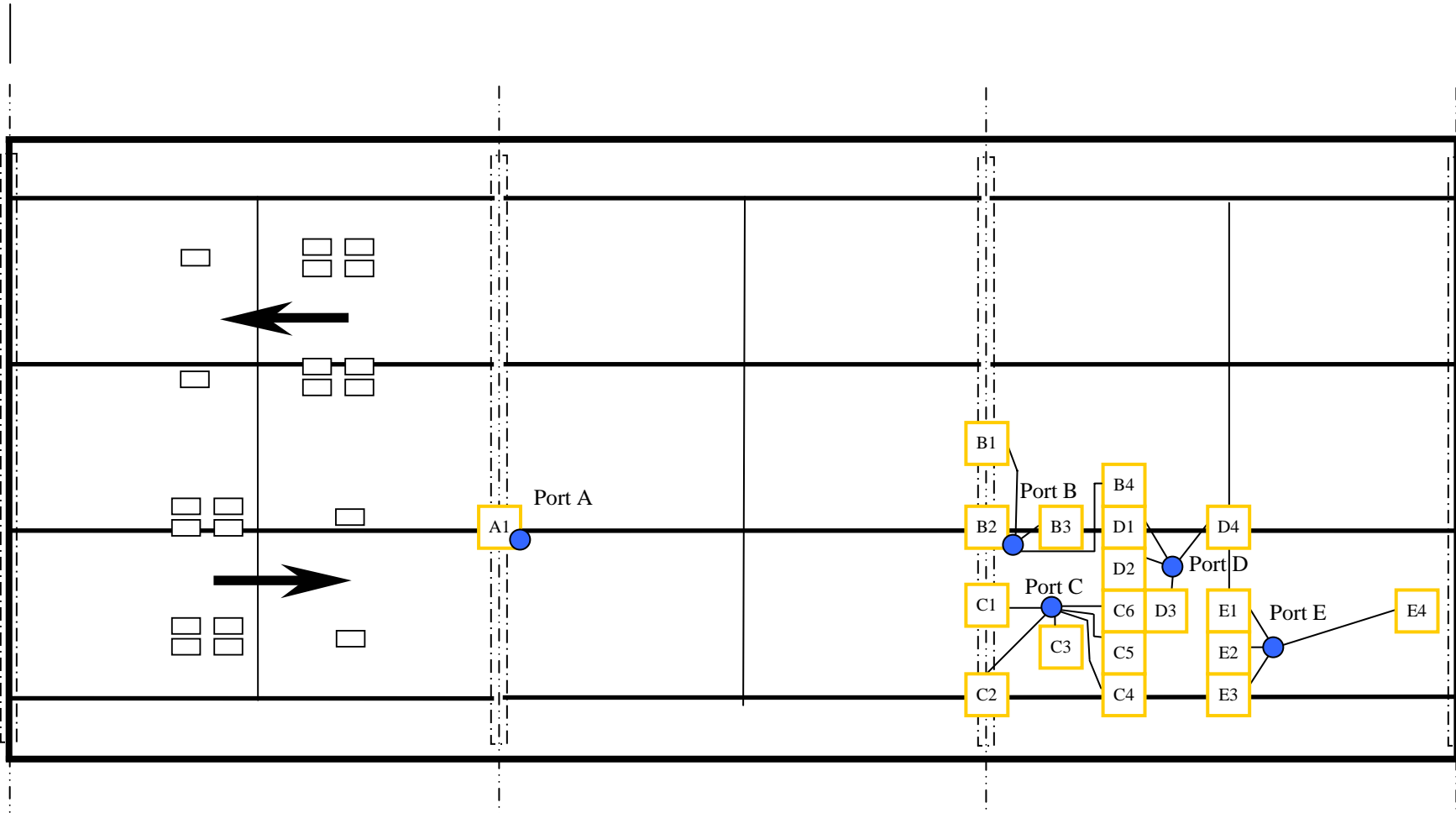
20 locations

-  Transverse gage, top, mid, and bottom
-  Transverse gage, top and bottom
-  Longitudinal gage, top and bottom
-  Longitudinal gage, top, mid and bottom



Cable Exit Layout Showing Gage Clusters

- Gage Cluster
- Exit Location
Each exit is 1½" in diameter



Longitudinal Reinforcement Strain Gages

Table 1-1: Detailed list of strain gages bonded to longitudinal reinforcement in bridge @ 11+57.24 (HPC)

Reference No.	General Position			Expected Response ($\mu\epsilon$)	Cable Exit Port	Approx. Lead Wire Length (m)	Bar Number	Purpose
	X	Y	Z					
H-LR-G-5-T	Over 2 nd bent	Over stringer B	Top mat	-53.8	A1	25	S200E-1	Effect of saw cut
H-LR-F-5-T	Over 3 rd bent	Over Stringer B	Top mat	-53.8	B2	4	S200E-3	String-Bent interaction
H-LR-F-1-T	Over 3 rd bent	Over Stringer A	Top mat	-86.9	C2	7	S200E-5	String-Bent interaction
H-LR-F-1-B	Over 3 rd bent	Over Stringer A	Bot mat	-86.9	C2	7	S300E-5	String-Bent interaction
H-LR-F-3-T	Over 3 rd bent	Btwn stringer A&B	Top mat	-10.3	C1	7	S200E-4	Bending across bent
H-LR-F-3-B	Over 3 rd bent	Btwn stringer A&B	Bot mat	-10.3	C1	7	S300E-4	Bending across bent
H-LR-F-7-T	Over 3 rd bent	Btwn stringer B&C	Top mat	-6.21	B1	7	S200E-2	Bending across bent
H-LR-F-7-B	Over 3 rd bent	Btwn stringer B&C	Bot mat	-6.21	B1	7	S300E-2	Bending across bent
H-LR-D-3-T	Btwn bent & dia	Btwn stringer A&B	Top mat	6.21	C6	9	S200E-7	Local deck behavior
H-LR-D-3-B	Btwn bent & dia	Btwn stringer A&B	Bot mat	6.21	C6	9	S300E-7	Local deck behavior
H-LR-C-3-T	Btwn bent & dia	Btwn stringer A&B	Top mat	5.86	D3	11	S200E-7	Local deck behavior
H-LR-C-3-B	Btwn bent & dia	Btwn stringer A&B	Bot mat	5.86	D3	11	S300E-7	Local deck behavior
H-LR-B-3-T	Over dia 3 to 4	Btwn stringer A&B	Top mat	4.83	E1	12.5	S200E-7	Effect of diaphragm
H-LR-B-3-B	Over dia 3 to 4	Btwn stringer A&B	Bot mat	4.83	E1	12.5	S300E-7	Effect of diaphragm
H-LR-A-3-T	Over 4 th bent	Btwn stringer A&B	Top mat	-1.03	E4	20	S200E-7	Continuity effects
H-LR-A-3-B	Over 4 th bent	Btwn stringer A&B	Bot mat	-1.03	E4	20	S300E-7	Continuity effects
H-LR-B-1-T	Over dia 3 to 4	Over Stringer A	Top mat	-12.1	E3	12.5	S200E-8	Global bending
H-LR-D-5-T	Btwn bent & dia	Over stringer B	Top mat	4.14	D1	12	S200E-6	Global bending
H-LR-B-5-T	Over dia 3 to 4	Over Stringer B	Top mat	-0.345	D4	12	S200E-6	Global bending

Transverse Reinforcement Strain Gages

Table 1-2: Detailed list of strain gages bonded to transverse reinforcement in bridge @ 11+57.24 (HPC)

Reference No.	General Position			Expected Response ($\mu\epsilon$)	Cable Exit Port	Approx. Lead Wire Length (m)	Bar Number	Purpose
	X	Y	Z					
H-TR-D-1-T	Btwn bent & dia	Over stringer A	Top mat	6.21	C4	9	S100E-2	Stringer effects
H-TR-D-1-B	Btwn bent & dia	Over stringer A	Bot mat	6.21	C4	9	S100E-2	Stringer effects
H-TR-E-2-T	Btwn bent & dia	Btwn stringers A&B	Top mat	7.93	C3	7	S100E-1	Local deck behavior
H-TR-E-2-B	Btwn bent & dia	Btwn stringers A&B	Bot mat	7.93	C3	7	S100E-1	Local deck behavior
H-TR-D-2-T	Btwn bent & dia	Btwn stringers A&B	Top mat	6.9	C5	9	S100E-2	Local deck behavior
H-TR-D-2-B	Btwn bent & dia	Btwn stringers A&B	Bot mat	6.9	C5	9	S100E-2	Local deck behavior
H-TR-B-2-T	Over diaphragm	Btwn stringers A&B	Top mat	-2.07	E2	11	S100E-3	Effect of diaphragm
H-TR-B-2-B	Over diaphragm	Btwn stringers A&B	Bot mat	-2.07	E2	11	S100E-3	Effect of diaphragm
H-TR-D-4-T	Btwn bent & dia	Btwn stringers A&B	Top mat	7.24	D2	10.5	S100E-2	Local deck behavior
H-TR-D-4-B	Btwn bent & dia	Btwn stringers A&B	Bot mat	7.24	D2	10.5	S100E-2	Local deck behavior
H-TR-E-5-T	Btwn bent & dia	Over stringer B	Top mat	5.86	B3	5	S100E-1	Stringer effects
H-TR-E-5-B	Btwn bent & dia	Over stringer B	Bot mat	5.86	B3	5	S100E-1	Stringer effects
H-TR-D-5-T	Btwn bent & dia	Over stringer B	Top mat	4.83	D1	12	S100E-2	Stringer effects
H-TR-D-5-B	Btwn bent & dia	Over stringer B	Bot mat	4.83	D1	12	S100E-2	Stringer effects
H-TR-D-6-T	Btwn bent & dia	Btwn stringers B&C	Top mat	6.9	B4	10.5	S100E-2	Local deck behavior
H-TR-D-6-B	Btwn bent & dia	Btwn stringers B&C	Bot mat	6.9	B4	10.5	S100E-2	Local deck behavior

Section E-1: Detailed Instrumentation List

High Performance Concrete Deck at 11+57.24

Embedded Strain Gages

Table 1-3: Detailed list of embedded strain gages in bridge @ 11+57.24 (HPC)

Reference No.	Orientation	General Position			Expected Response ($\mu\epsilon$)	Cable Exit Port	Approx. Lead Wire Length (m)	Purpose
		X	Y	Z				
H-LE-F-5-B	Longitudinal	Over 2 nd bent	Over stringer B	Bot	-15.6	B2	4	Stringer – Bent interaction
H-LE-F-5-M	Longitudinal	Over 2 nd bent	Over stringer B	Mid	-15.6	B2	4	Stringer – Bent interaction
H-LE-F-5-T	Longitudinal	Over 2 nd bent	Over stringer B	Top	-15.6	B2	4	Stringer – Bent interaction
H-TE-D-5-M	Transverse	Btwn bent & dia	Over stringer B	Mid	-1.8	D1	12	Stringer effects
H-TE-D-5-T	Transverse	Btwn bent & dia	Over stringer B	Top	-1.8	D1	12	Stringer effects
H-LE-F-7-M	Longitudinal	Over 2 nd bent	Btwn stringers B & C	Mid	-1.8	B1	7	Bending across bent
H-LE-F-7-T	Longitudinal	Over 2 nd bent	Btwn stringers B & C	Top	-1.2	B1	7	Bending across bent
H-TE-D-2-M	Transverse	Btwn bent & dia	Btwn stringers A & B	Mid		C5	9	Local bending effects
H-TE-D-2-T	Transverse	Btwn bent & dia	Btwn stringers A & B	Top		C5	9	Local bending effects

Section E-1: Detailed Instrumentation List

High Performance Concrete Deck at 11+57.24

Vibrating Wire Strain Gages

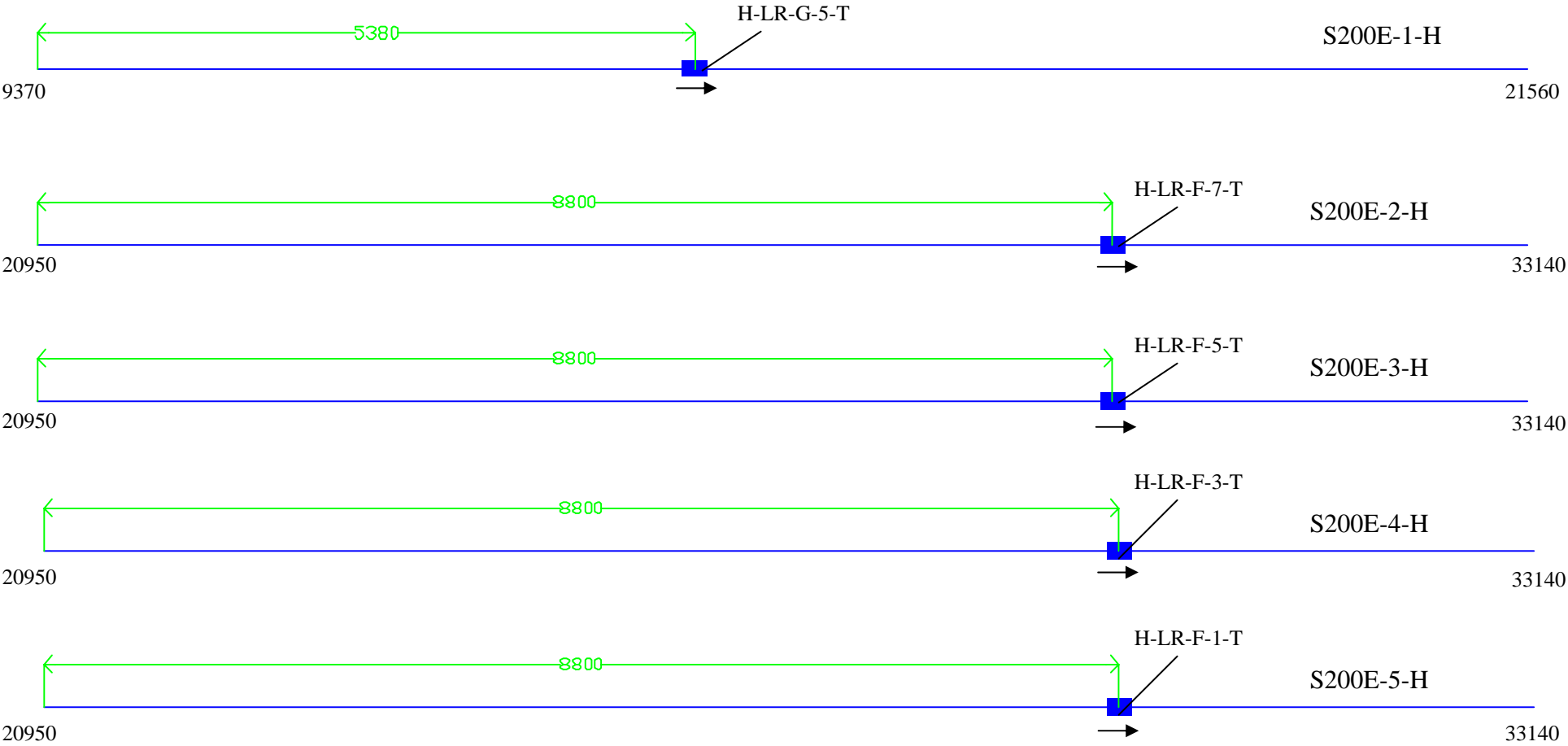
Table 1-4: Detailed list of vibrating wire strain gages in bridge @ 11+57.24 (HPC)

Reference No.	Orientation	General Position			Expected Response ($\mu\epsilon$)	Cable Exit Port	Approx Lead Wire Length (m)	Purpose
		X	Y	Z				
H-LV-F-3-B	Longitudinal	Over bent	Btwn stringers A & B	Bot	-3.0	C1	7	Bending across bent
H-LV-F-3-M	Longitudinal	Over bent	Btwn stringers A & B	Mid	-3.0	C1	7	Bending across bent
H-LV-F-3-T	Longitudinal	Over bent	Btwn stringers A & B	Top	-3.0	C1	7	Bending across bent
H-LV-F-5-B	Longitudinal	Over bent	Over stringer B	Bot	-15.6	B2	4	Stringer – bent interaction
H-LV-F-5-T	Longitudinal	Over bent	Over stringer B	Top	-15.6	B2	4	Stringer – bent interaction
H-LV-F-7-B	Longitudinal	Over bent	Btwn stringers B & C	Bot	-1.8	B1	7	Bending across bent
H-LV-F-7-T	Longitudinal	Over bent	Btwn stringers B & C	Top	-1.8	B1	7	Bending across bent
H-LV-D-3-B	Longitudinal	Btwn bent & dia	Btwn stringers A & B	Bot	1.8	C6	9	Local deck behavior
H-LV-D-3-T	Longitudinal	Btwn bent & dia	Btwn stringers A & B	Top	1.8	C6	9	Local deck behavior
H-LV-B-3-B	Longitudinal	Over dia	Btwn stringers A & B	Bot	-1.4	E1	12.5	Diaphragm effects
H-LV-B-3-T	Longitudinal	Over dia	Btwn stringers A & B	Top	-1.4	E1	12.5	Diaphragm effects
H-LV-A-3-B	Longitudinal	Over 4 th bent	Btwn stringers A & B	Bot	-0.3	E4	20	Effects of end Bent
H-LV-A-3-T	Longitudinal	Over 4 th bent	Btwn stringers A & B	Top	-0.3	E4	20	Effects of end bent
H-TV-D-3-B	Transverse	Btwn bent & dia	Btwn stringers A & B	Bot	2.3	C6	9	Local deck behavior
H-TV-D-3-T	Transverse	Btwn bent & dia	Btwn stringers A & B	Top	2.3	C6	9	Local deck behavior
H-TV-C-3-B	Transverse	Btwn dia & bent	Btwn stringers A & B	Bot	2.7	D3	11	Local deck behavior
H-TV-C-3-T	Transverse	Btwn dia & bent	Btwn stringers A & B	Top	2.7	D3	11	Local deck behavior
H-TV-D-5-B	Transverse	Btwn bent & dia	Over stringer B	Bot	1.4	D1	12	Stringer effects
H-TV-D-5-M	Transverse	Btwn bent & dia	Over stringer B	Mid	1.4	D1	12	Stringer effects
H-TV-D-5-T	Transverse	Btwn bent & dia	Over stringer B	Top	1.4	D1	12	Stringer effects

Section F-1: Detailed Drawings of Reinforcement with Bonded Strain Gages

*High Performance Concrete
Deck at 11+57.24*

Longitudinal Bars – Top Mat

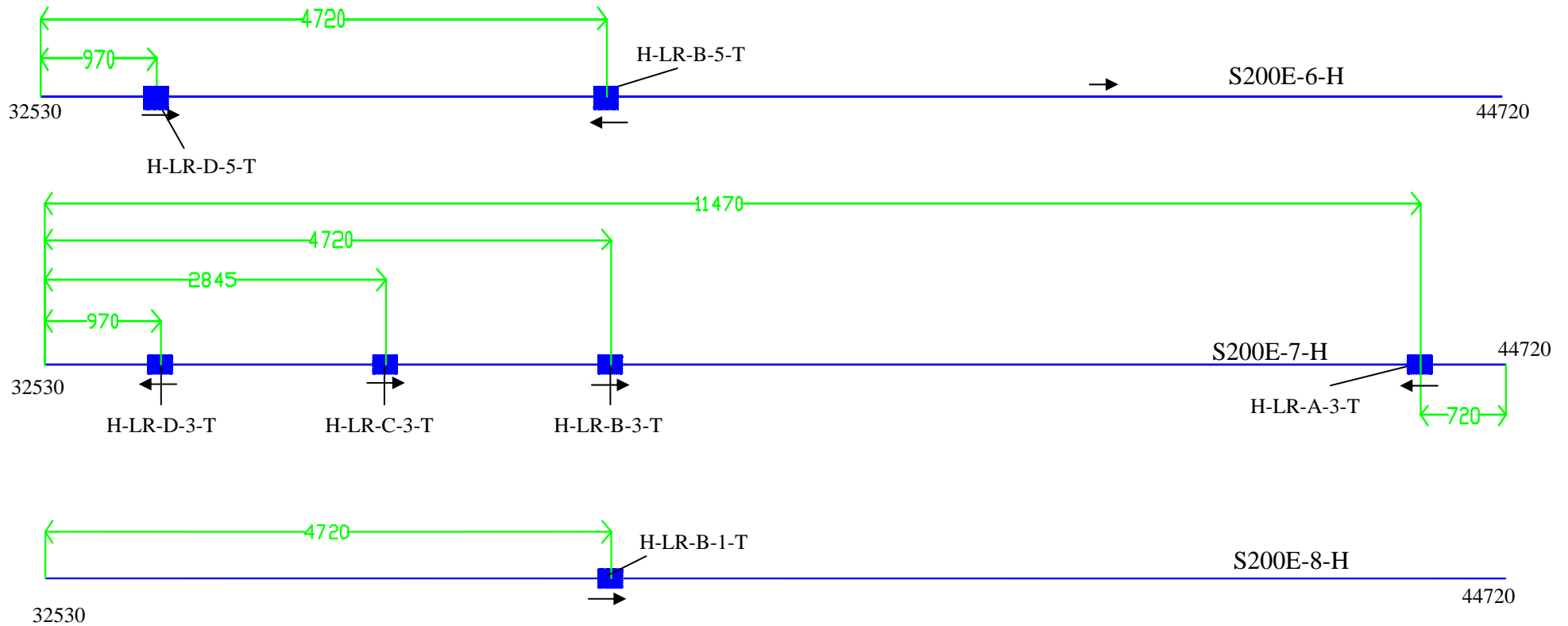


*Numbers at either end of the bar represent the longitudinal beginning and ending positions (in mm) with respect to the bridge deck.

Section F-1: Detailed Drawings of Reinforcement with Bonded Strain Gages

*High Performance Concrete
Deck at 11+57.24*

Longitudinal Bars – Top Mat (continued)



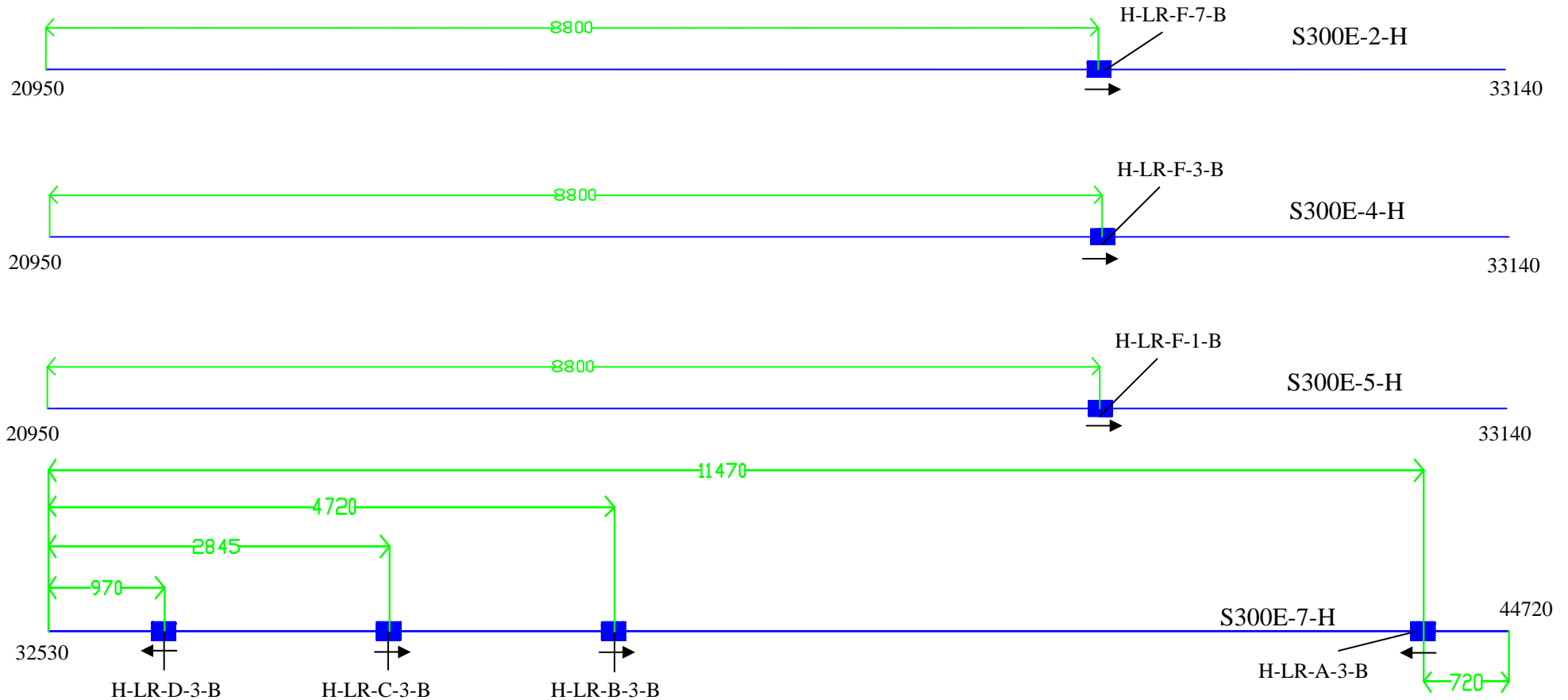
*Numbers at either end of the bar represent the longitudinal beginning and ending positions (in mm) with respect to the bridge deck.

**A total of 8 S200E ~ #13 bars of length 12.19 m are needed for instrumentation from the top mat.

Section F-1: Detailed Drawings of Reinforcement with Bonded Strain Gages

*High Performance Concrete
Deck at 11+57.24*

Longitudinal Bars – Bottom Mat



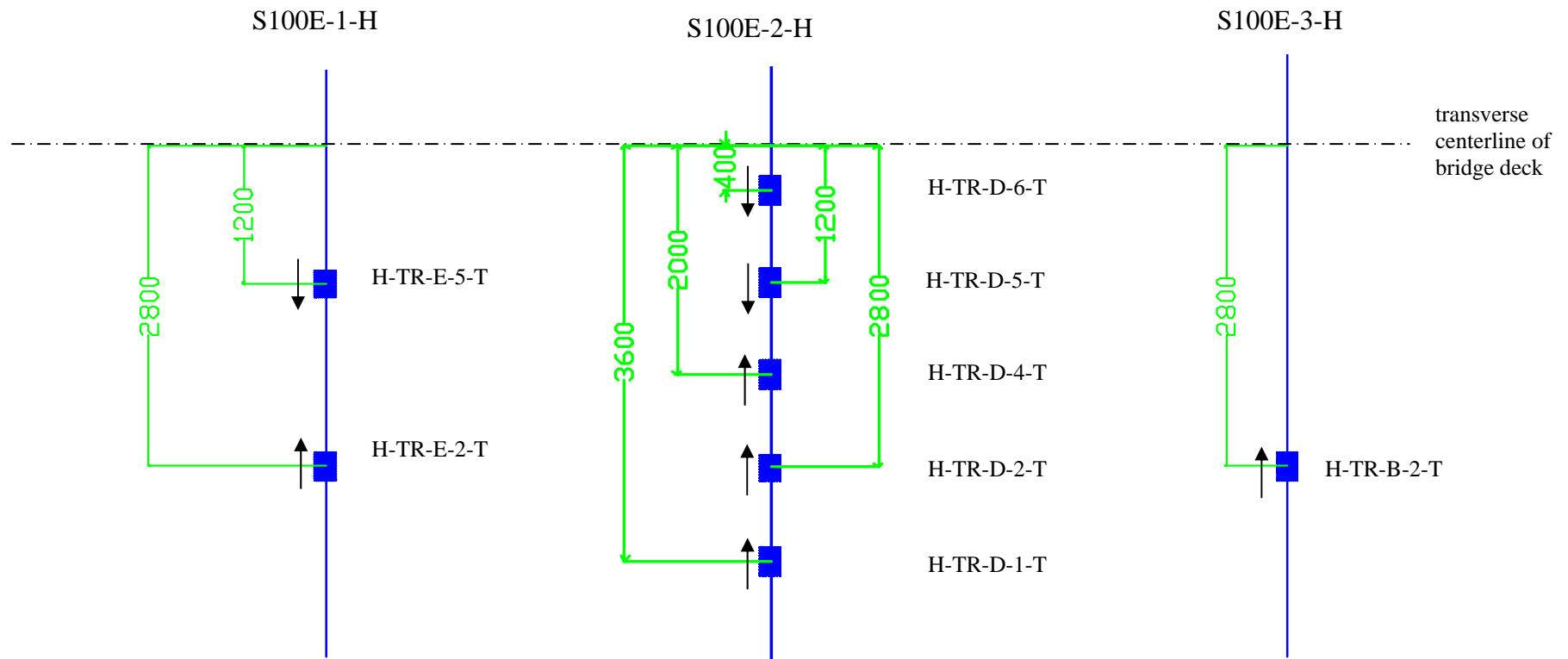
*Numbers at either end of the bar represent the longitudinal beginning and ending positions (in mm) with respect to the bridge deck.

**A total of 4 S300E ~ # 19 bars of length 12.19 m are needed for instrumentation from the bottom mat.

Section F-1: Detailed Drawings of Reinforcement with Bonded Strain Gages

*High Performance Concrete
Deck at 11+57.24*

Transverse Bars – Top Mat

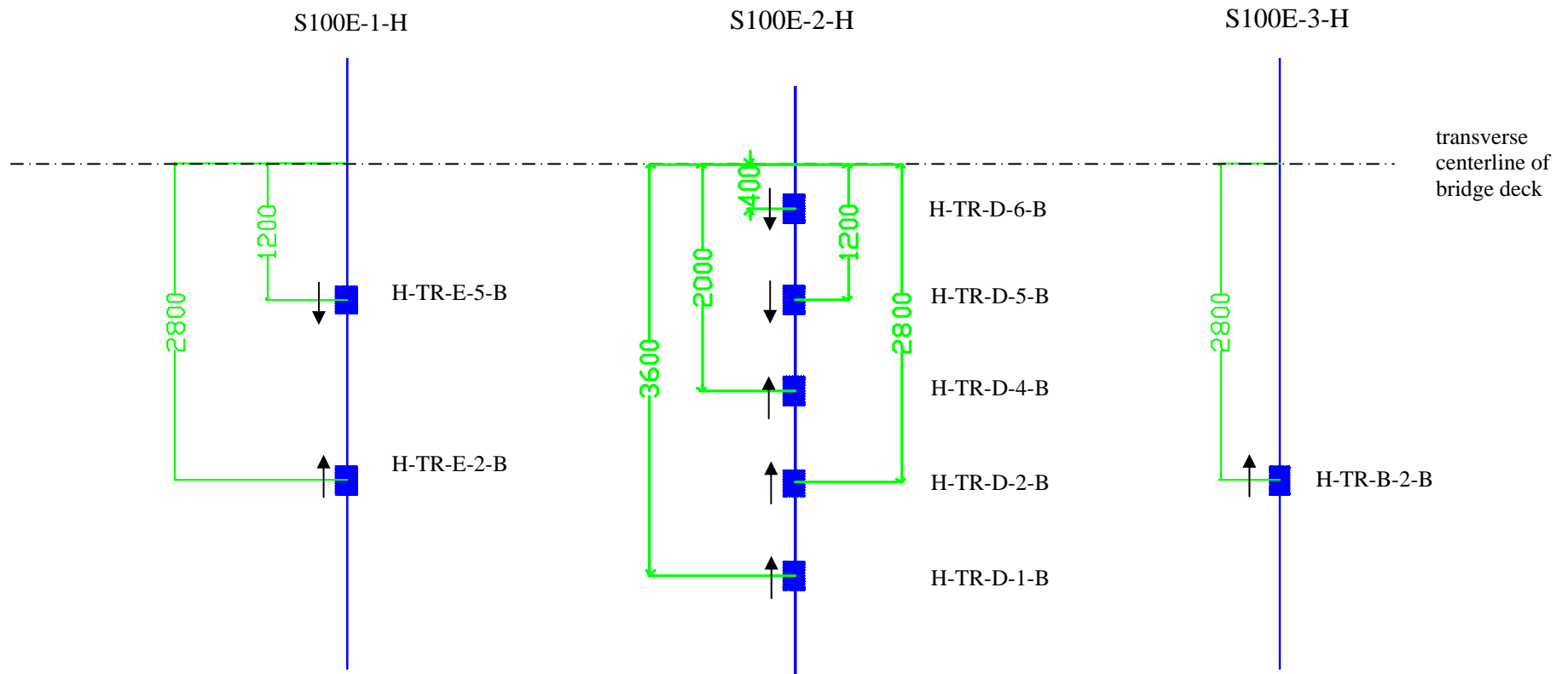


* A total of 3 S100E ~ # 19 bars of length 8.95 m are needed for instrumentation from the top mat

Section F-1: Detailed Drawings of Reinforcement with Bonded Strain Gages

*High Performance Concrete
Deck at 11+57.24*

Transverse Bars – Bottom Mat



* A total of 3 S100E ~ # 19 bars of length 8.95 m are needed for instrumentation from the bottom mat

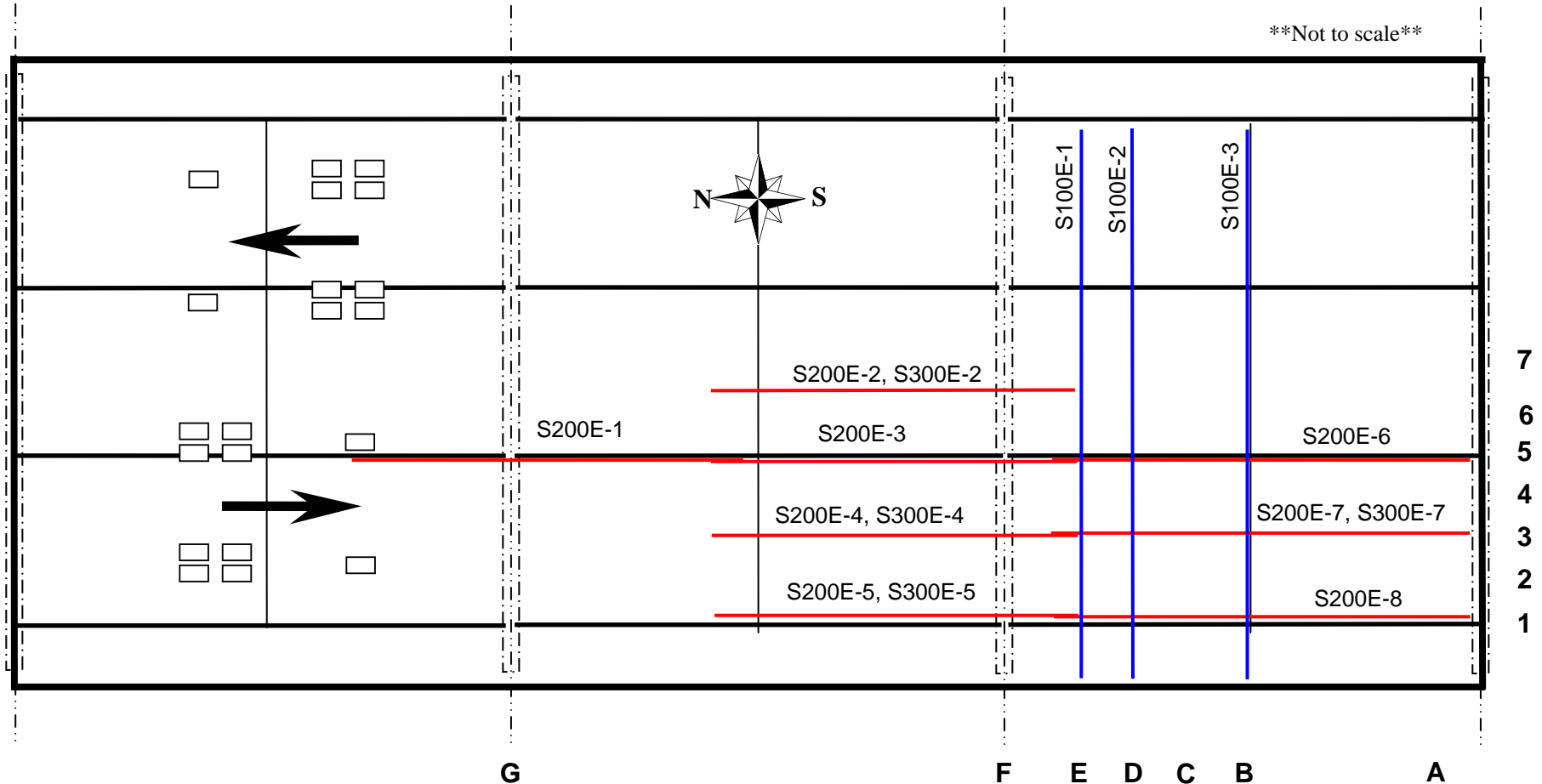
Part 2: Empirical Deck @16+81.74

Section A-2: General Bridge Deck Layout

Empirical Deck at 16+81.74

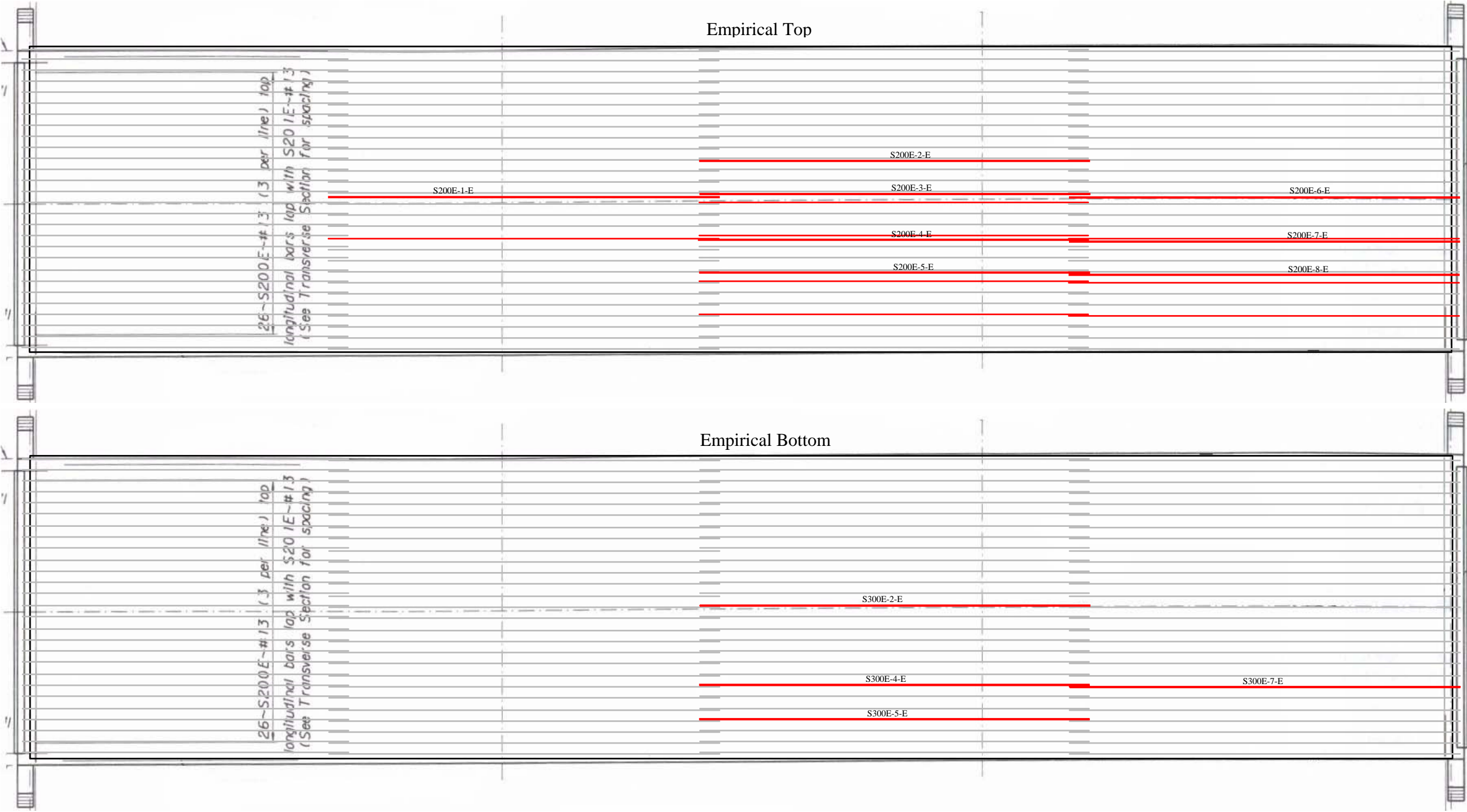
The series of numbers along the bottom of the bridge correspond to the longitudinal gage positions used in the reference number system described above. Likewise, the numbers along the right edge correspond to the transverse position of the gages used in the reference number system. The arrows on the left side show the direction of travel across the bridge of a typical truck.

The S200E bars numbered 1 through 8 are the S200E ~ # 13 bars called out in the bridge plans for the top longitudinal reinforcement. The S300E bars numbered 2,4,5, and 7 are the S300E ~ #13 bars called out in the plans for the Bottom longitudinal reinforcement. Each of the longitudinal bars is 12.19 meters in length. The S100E bars numbered 1 through 3 are the S100E ~ # 19 bars called out in the plans as the top and bottom transverse reinforcement. Each transverse bar is 8.95 meters long.



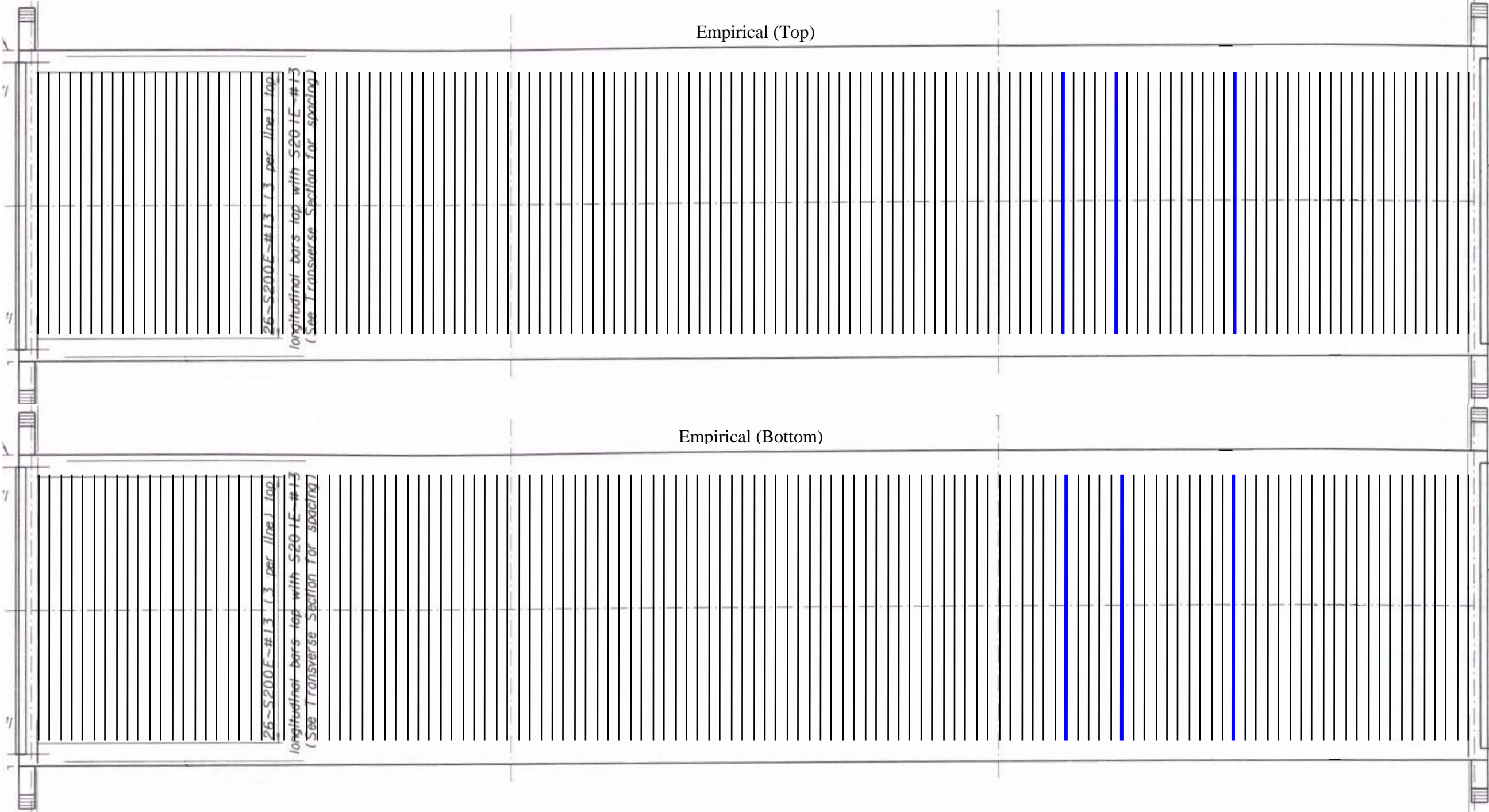
Section B-2: Detailed rebar layout

Empirical Deck at 16+81.74



Section B-2: Detailed rebar layout

Empirical Deck at 16+81.74



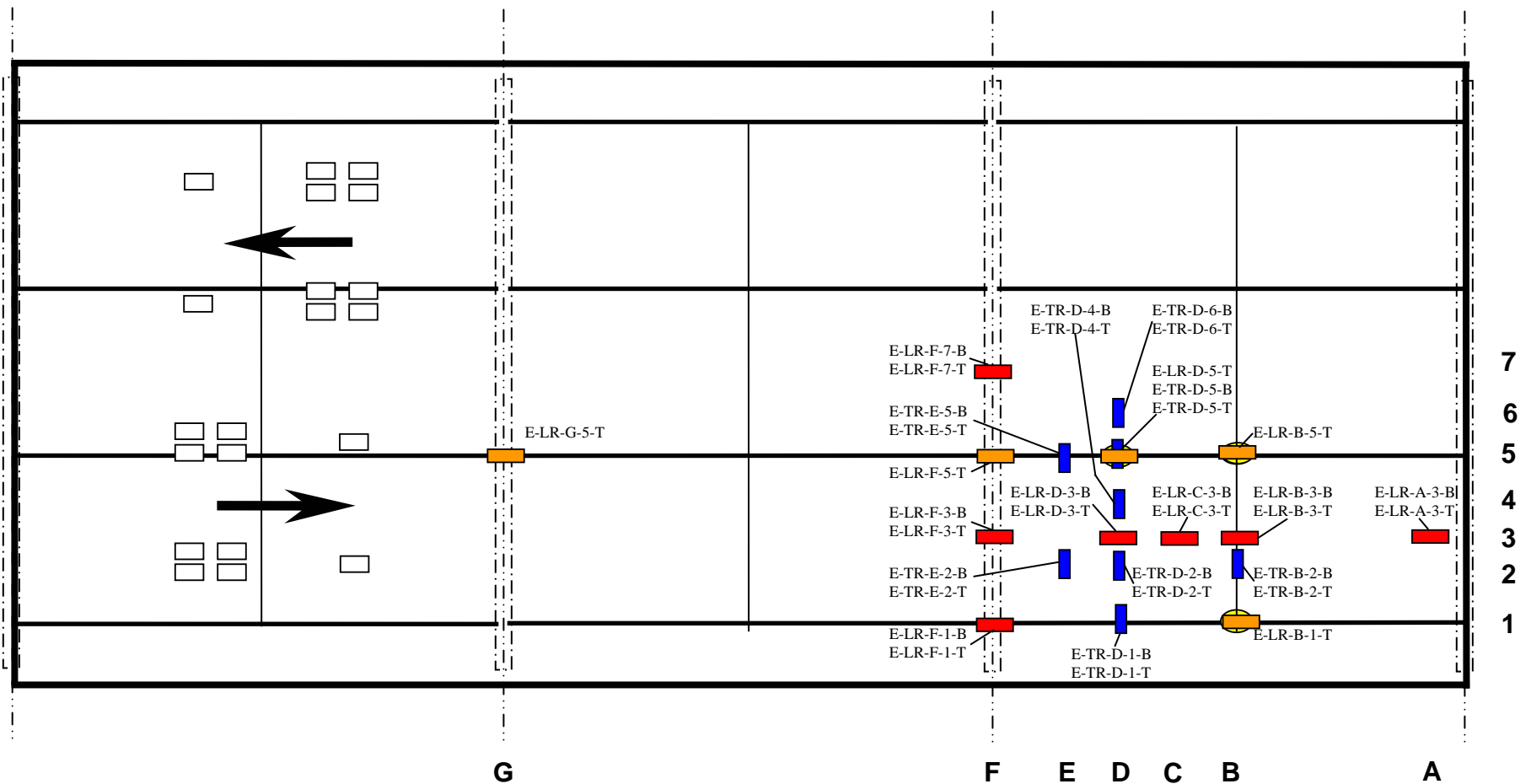
Section C-2: Plan View of Gage Locations

Empirical Deck at 16+81.74

Bonded Strain Gage Layout




6 transverse bars (16 gage locations)
12 longitudinal bars (19 gage locations)

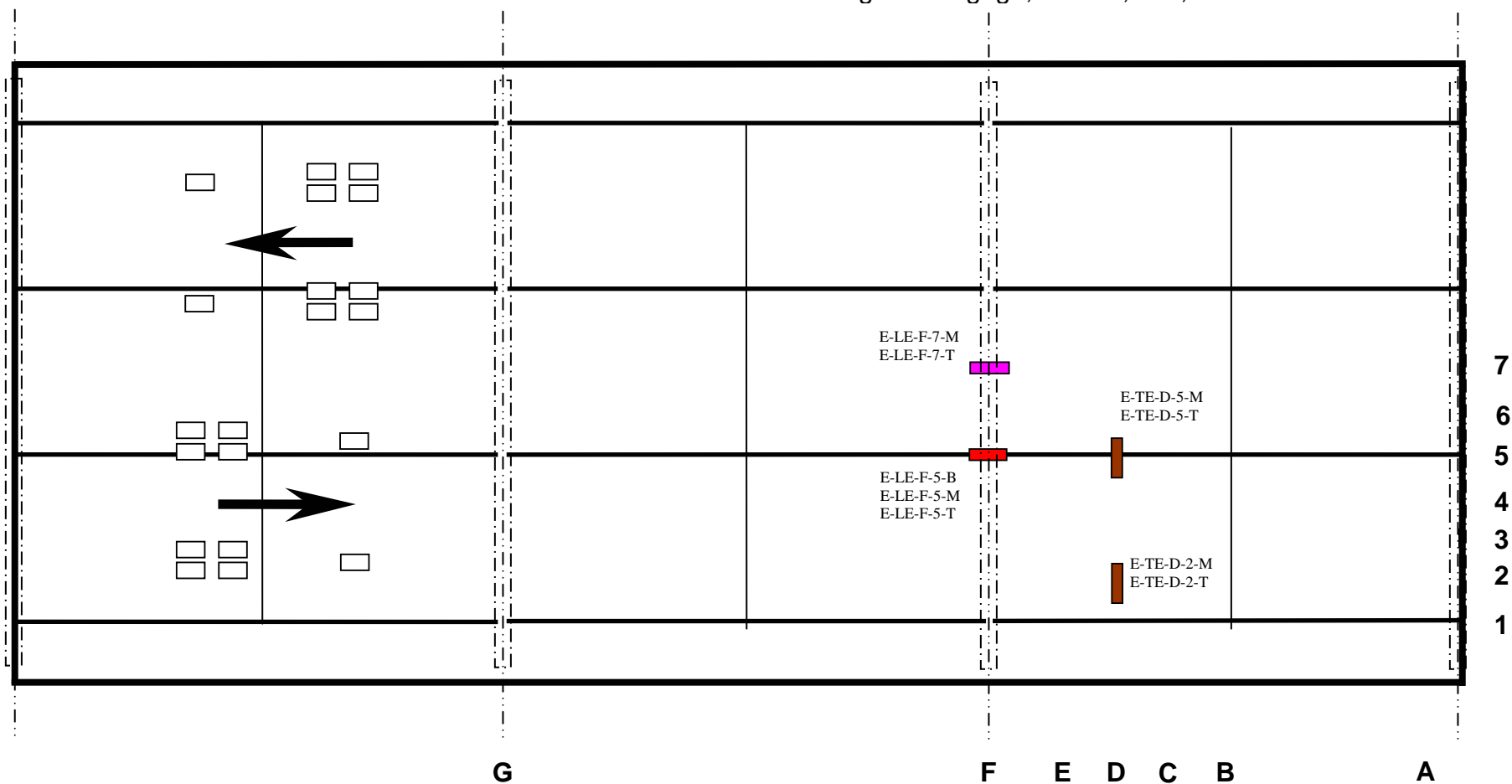
- Transverse gage, top and bottom mat
- Longitudinal gage, top and bottom mat
- Longitudinal gage, top mat only
- Longitudinal gage, bottom of stringer



Embedded Strain Gage Layout

9 locations

-  Transverse gage, mid and near surface
-  Longitudinal gage, mid and near surface
-  Longitudinal gage, bottom, mid, and near surface


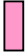




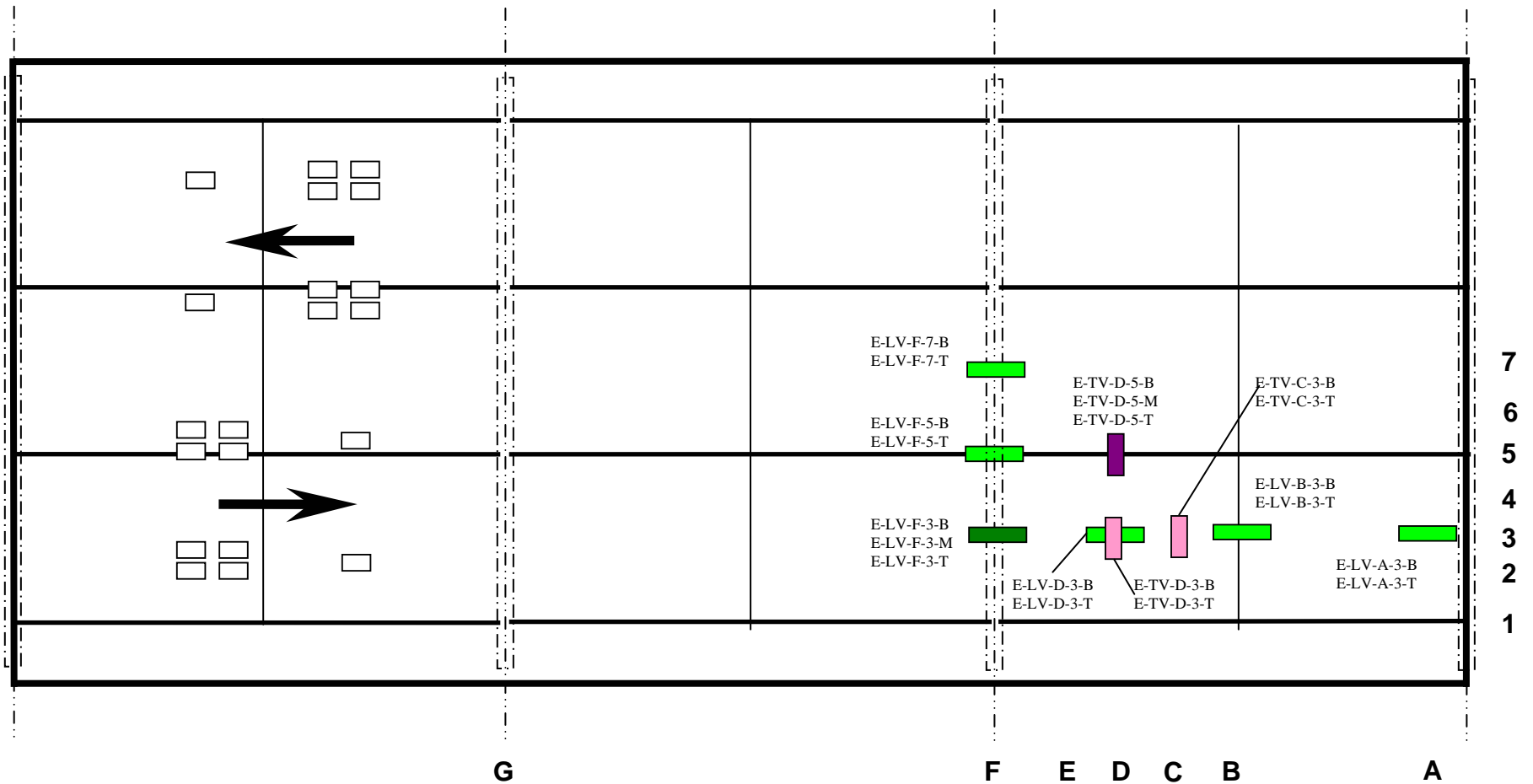
Section C-2: Plan View of Gage Locations

Empirical Deck at 16+81.74

Vibrating Wire Gage Layout

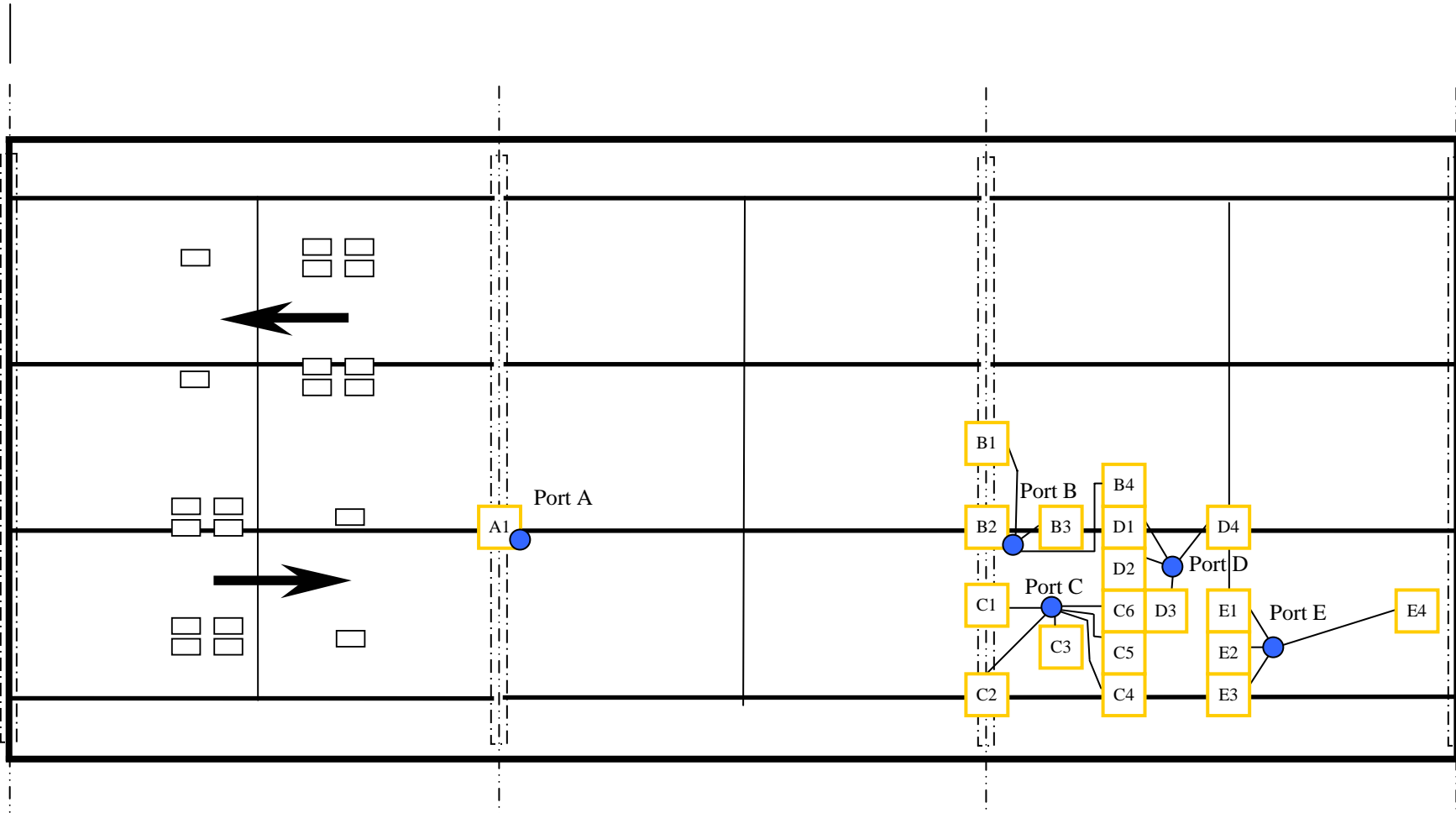
20 locations

-  Transverse gage, top, mid, and bottom
-  Transverse gage, top and bottom
-  Longitudinal gage, top and bottom
-  Longitudinal gage, top, mid and bottom



Cable Exit Layout Showing Gage Clusters

- Gage Cluster
- Exit Location
Each exit is 1½" in diameter



Section E-2: Detailed Instrumentation List

Empirical Deck at 16+81.74

Longitudinal Reinforcement Strain Gages

Table 2-1: Detailed list of strain gages bonded to longitudinal reinforcement in bridge @ 16+81.74 (empirical deck)

Reference No.	General Position			Expected Response ($\mu\epsilon$)	Cable Exit Port	Approx. Lead Wire Length (m)	Bar Number	Purpose
	X	Y	Z					
E-LR-G-5-T	Over 2 nd bent	Over stringer B	Top mat	-53.8	A1	25	S200E-1	Effect of saw cut
E-LR-F-5-T	Over 3 rd bent	Over Stringer B	Top mat	-53.8	B2	4	S200E-3	String-Bent interaction
E-LR-F-1-T	Over 3 rd bent	Over Stringer A	Top mat	-86.9	C2	7	S200E-5	String-Bent interaction
E-LR-F-1-B	Over 3 rd bent	Over Stringer A	Bot mat	-86.9	C2	7	S300E-5	String-Bent interaction
E-LR-F-3-T	Over 3 rd bent	Btwn stringer A&B	Top mat	-10.3	C1	7	S200E-4	Bending across bent
E-LR-F-3-B	Over 3 rd bent	Btwn stringer A&B	Bot mat	-10.3	C1	7	S300E-4	Bending across bent
E-LR-F-7-T	Over 3 rd bent	Btwn stringer B&C	Top mat	-6.21	B1	7	S200E-2	Bending across bent
E-LR-F-7-B	Over 3 rd bent	Btwn stringer B&C	Bot mat	-6.21	B1	7	S300E-2	Bending across bent
E-LR-D-3-T	Btwn bent & dia	Btwn stringer A&B	Top mat	6.21	C6	9	S200E-7	Local deck behavior
E-LR-D-3-B	Btwn bent & dia	Btwn stringer A&B	Bot mat	6.21	C6	9	S300E-7	Local deck behavior
E-LR-C-3-T	Btwn bent & dia	Btwn stringer A&B	Top mat	5.86	D3	11	S200E-7	Local deck behavior
E-LR-C-3-B	Btwn bent & dia	Btwn stringer A&B	Bot mat	5.86	D3	11	S300E-7	Local deck behavior
E-LR-B-3-T	Over dia 3 to 4	Btwn stringer A&B	Top mat	4.83	E1	12.5	S200E-7	Effect of diaphragm
E-LR-B-3-B	Over dia 3 to 4	Btwn stringer A&B	Bot mat	4.83	E1	12.5	S300E-7	Effect of diaphragm
E-LR-A-3-T	Over 4 th bent	Btwn stringer A&B	Top mat	-1.03	E4	20	S200E-7	Continuity effects
E-LR-A-3-B	Over 4 th bent	Btwn stringer A&B	Bot mat	-1.03	E4	20	S300E-7	Continuity effects
E-LR-B-1-T	Over dia 3 to 4	Over Stringer A	Top mat	-12.1	E3	12.5	S200E-8	Global bending
E-LR-D-5-T	Btwn bent & dia	Over stringer B	Top mat	4.14	D1	12	S200E-6	Global bending
E-LR-B-5-T	Over dia 3 to 4	Over Stringer B	Top mat	-0.345	D4	12	S200E-6	Global bending

Transverse Reinforcement Strain Gages

Table 2-2: Detailed list of strain gages bonded to transverse reinforcement in bridge @ 16+81.74 (empirical deck)

Reference No.	General Position			Expected Response ($\mu\epsilon$)	Cable Exit Port	Approx. Lead Wire Length (m)	Bar Number	Purpose
	X	Y	Z					
E-TR-D-1-T	Btwn bent & dia	Over stringer A	Top mat	6.21	C4	9	S100E-2	Stringer effects
E-TR-D-1-B	Btwn bent & dia	Over stringer A	Bot mat	6.21	C4	9	S100E-2	Stringer effects
E-TR-E-2-T	Btwn bent & dia	Btwn stringers A&B	Top mat	7.93	C3	7	S100E-1	Local deck behavior
E-TR-E-2-B	Btwn bent & dia	Btwn stringers A&B	Bot mat	7.93	C3	7	S100E-1	Local deck behavior
E-TR-D-2-T	Btwn bent & dia	Btwn stringers A&B	Top mat	6.9	C5	9	S100E-2	Local deck behavior
E-TR-D-2-B	Btwn bent & dia	Btwn stringers A&B	Bot mat	6.9	C5	9	S100E-2	Local deck behavior
E-TR-B-2-T	Over diaphragm	Btwn stringers A&B	Top mat	-2.07	E2	11	S100E-3	Effect of diaphragm
E-TR-B-2-B	Over diaphragm	Btwn stringers A&B	Bot mat	-2.07	E2	11	S100E-3	Effect of diaphragm
E-TR-D-4-T	Btwn bent & dia	Btwn stringers A&B	Top mat	7.24	D2	10.5	S100E-2	Local deck behavior
E-TR-D-4-B	Btwn bent & dia	Btwn stringers A&B	Bot mat	7.24	D2	10.5	S100E-2	Local deck behavior
E-TR-E-5-T	Btwn bent & dia	Over stringer B	Top mat	5.86	B3	5	S100E-1	Stringer effects
E-TR-E-5-B	Btwn bent & dia	Over stringer B	Bot mat	5.86	B3	5	S100E-1	Stringer effects
E-TR-D-5-T	Btwn bent & dia	Over stringer B	Top mat	4.83	D1	12	S100E-2	Stringer effects
E-TR-D-5-B	Btwn bent & dia	Over stringer B	Bot mat	4.83	D1	12	S100E-2	Stringer effects
E-TR-D-6-T	Btwn bent & dia	Btwn stringers B&C	Top mat	6.9	B4	10.5	S100E-2	Local deck behavior
E-TR-D-6-B	Btwn bent & dia	Btwn stringers B&C	Bot mat	6.9	B4	10.5	S100E-2	Local deck behavior

Section E-2: Detailed Instrumentation List

Empirical Deck at 16+81.74

Embedded Strain Gages

Table 2-3: Detailed list of embedded strain gages in bridge @ 16+81.74 (empirical deck)

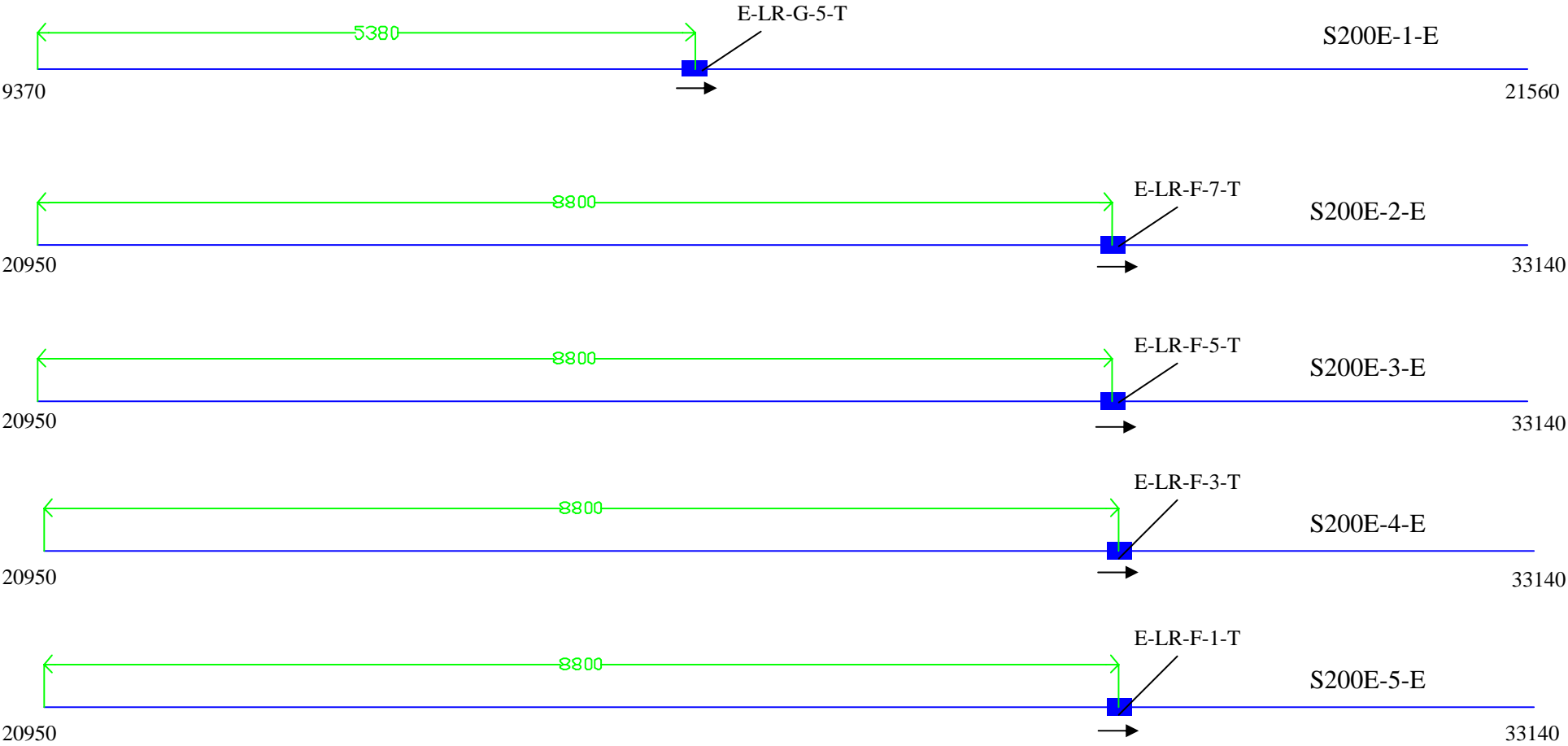
Reference No.	Orientation	General Position			Expected Response ($\mu\epsilon$)	Cable Exit Port	Approx. Lead Wire Length (m)	Purpose
		X	Y	Z				
E-LE-F-5-B	Longitudinal	Over 2 nd bent	Over stringer B	Bot	-15.6	B2	4	Stringer – Bent interaction
E-LE-F-5-M	Longitudinal	Over 2 nd bent	Over stringer B	Mid	-15.6	B2	4	Stringer – Bent interaction
E-LE-F-5-T	Longitudinal	Over 2 nd bent	Over stringer B	Top	-15.6	B2	4	Stringer – Bent interaction
E-TE-D-5-M	Transverse	Btwn bent & dia	Over stringer B	Mid	-1.8	D1	12	Stringer effects
E-TE-D-5-T	Transverse	Btwn bent & dia	Over stringer B	Top	-1.8	D1	12	Stringer effects
E-LE-F-7-M	Longitudinal	Over 2 nd bent	Btwn stringers B & C	Mid	-1.8	B1	7	Bending across bent
E-LE-F-7-T	Longitudinal	Over 2 nd bent	Btwn stringers B & C	Top	-1.2	B1	7	Bending across bent
E-TE-D-2-M	Transverse	Btwn bent & dia	Btwn stringers A & B	Mid		C5	9	Local bending effects
E-TE-D-2-T	Transverse	Btwn bent & dia	Btwn stringers A & B	Top		C5	9	Local bending effects

Vibrating Wire Strain Gages

Table2- 4: Detailed list of vibrating wire strain gages in bridge @ 19+23.24 (conventional deck)

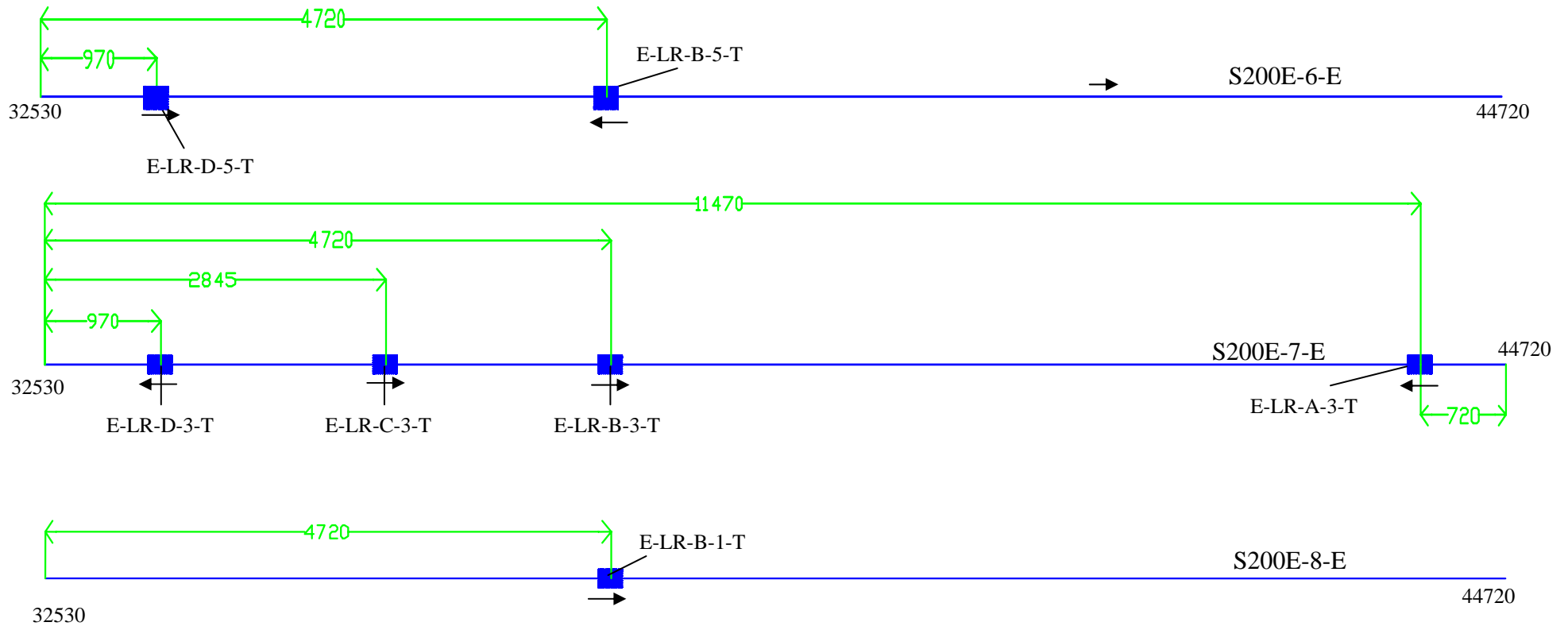
Reference No.	Orientation	General Position			Expected Response ($\mu\epsilon$)	Cable Exit Port	Approx Lead Wire Length (m)	Purpose
		X	Y	Z				
E-LV-F-3-B	Longitudinal	Over bent	Btwn stringers A & B	Bot	-3.0	C1	7	Bending across bent
E-LV-F-3-M	Longitudinal	Over bent	Btwn stringers A & B	Mid	-3.0	C1	7	Bending across bent
E-LV-F-3-T	Longitudinal	Over bent	Btwn stringers A & B	Top	-3.0	C1	7	Bending across bent
E-LV-F-5-B	Longitudinal	Over bent	Over stringer B	Bot	-15.6	B2	4	Stringer – bent interaction
E-LV-F-5-T	Longitudinal	Over bent	Over stringer B	Top	-15.6	B2	4	Stringer – bent interaction
E-LV-F-7-B	Longitudinal	Over bent	Btwn stringers B & C	Bot	-1.8	B1	7	Bending across bent
E-LV-F-7-T	Longitudinal	Over bent	Btwn stringers B & C	Top	-1.8	B1	7	Bending across bent
E-LV-D-3-B	Longitudinal	Btwn bent & dia	Btwn stringers A & B	Bot	1.8	C6	9	Local deck behavior
E-LV-D-3-T	Longitudinal	Btwn bent & dia	Btwn stringers A & B	Top	1.8	C6	9	Local deck behavior
E-LV-B-3-B	Longitudinal	Over dia	Btwn stringers A & B	Bot	-1.4	E1	12.5	Diaphragm effects
E-LV-B-3-T	Longitudinal	Over dia	Btwn stringers A & B	Top	-1.4	E1	12.5	Diaphragm effects
E-LV-A-3-B	Longitudinal	Over 4 th bent	Btwn stringers A & B	Bot	-0.3	E4	20	Effects of end Bent
E-LV-A-3-T	Longitudinal	Over 4 th bent	Btwn stringers A & B	Top	-0.3	E4	20	Effects of end bent
E-TV-D-3-B	Transverse	Btwn bent & dia	Btwn stringers A & B	Bot	2.3	C6	9	Local deck behavior
E-TV-D-3-T	Transverse	Btwn bent & dia	Btwn stringers A & B	Top	2.3	C6	9	Local deck behavior
E-TV-C-3-B	Transverse	Btwn dia & bent	Btwn stringers A & B	Bot	2.7	D3	11	Local deck behavior
E-TV-C-3-T	Transverse	Btwn dia & bent	Btwn stringers A & B	Top	2.7	D3	11	Local deck behavior
E-TV-D-5-B	Transverse	Btwn bent & dia	Over stringer B	Bot	1.4	D1	12	Stringer effects
E-TV-D-5-M	Transverse	Btwn bent & dia	Over stringer B	Mid	1.4	D1	12	Stringer effects
E-TV-D-5-T	Transverse	Btwn bent & dia	Over stringer B	Top	1.4	D1	12	Stringer effects

Longitudinal Bars – Top Mat



*Numbers at either end of the bar represent the longitudinal beginning and ending positions (in mm) with respect to the bridge deck.

Longitudinal Bars – Top Mat (continued)

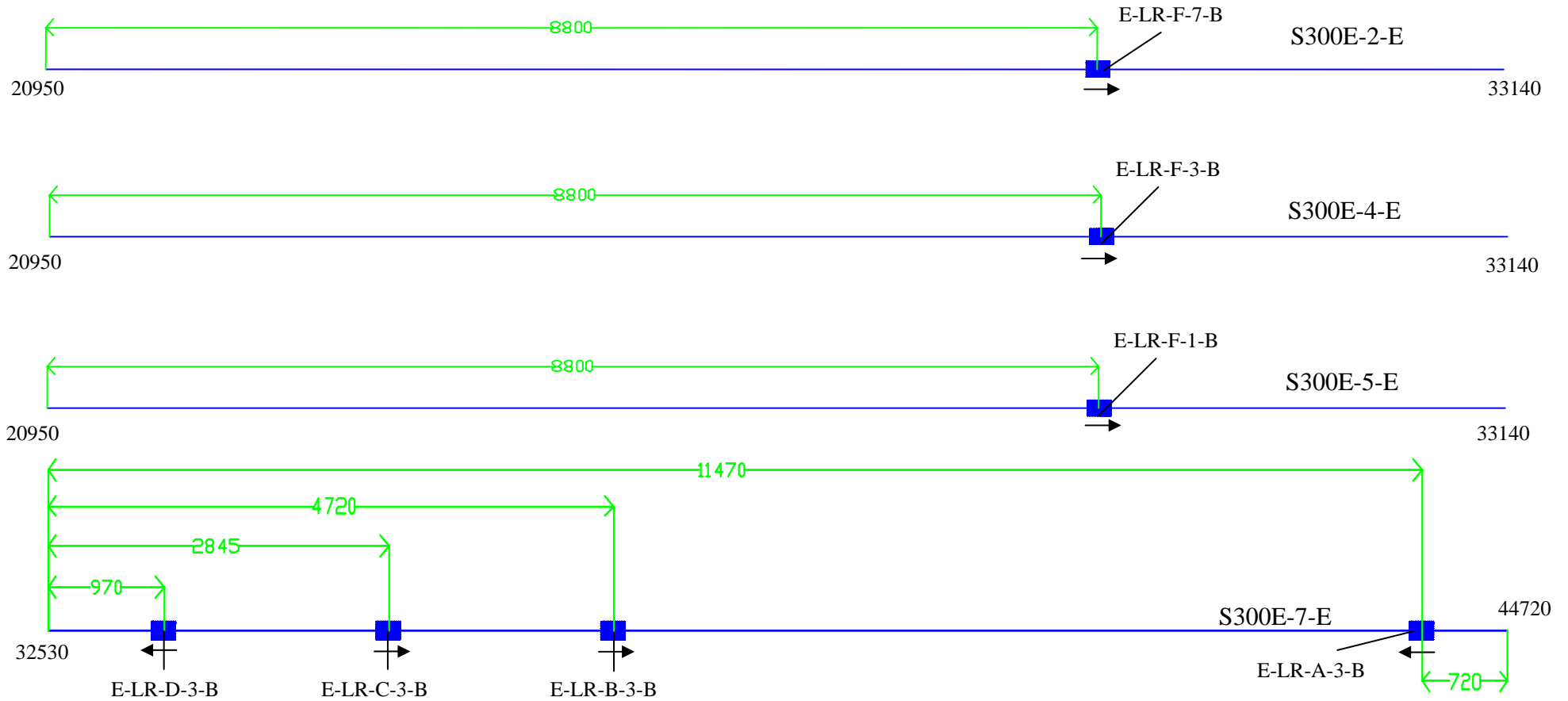


*Numbers at either end of the bar represent the longitudinal beginning and ending positions (in mm) with respect to the bridge deck.

**A total of 8 S200E ~ #13 bars of length 12.19 m are needed for instrumentation from the top mat.

Section F-2: Detailed Drawings of Reinforcement with Bonded Strain Gages *Empirical Deck at 16+81.74*

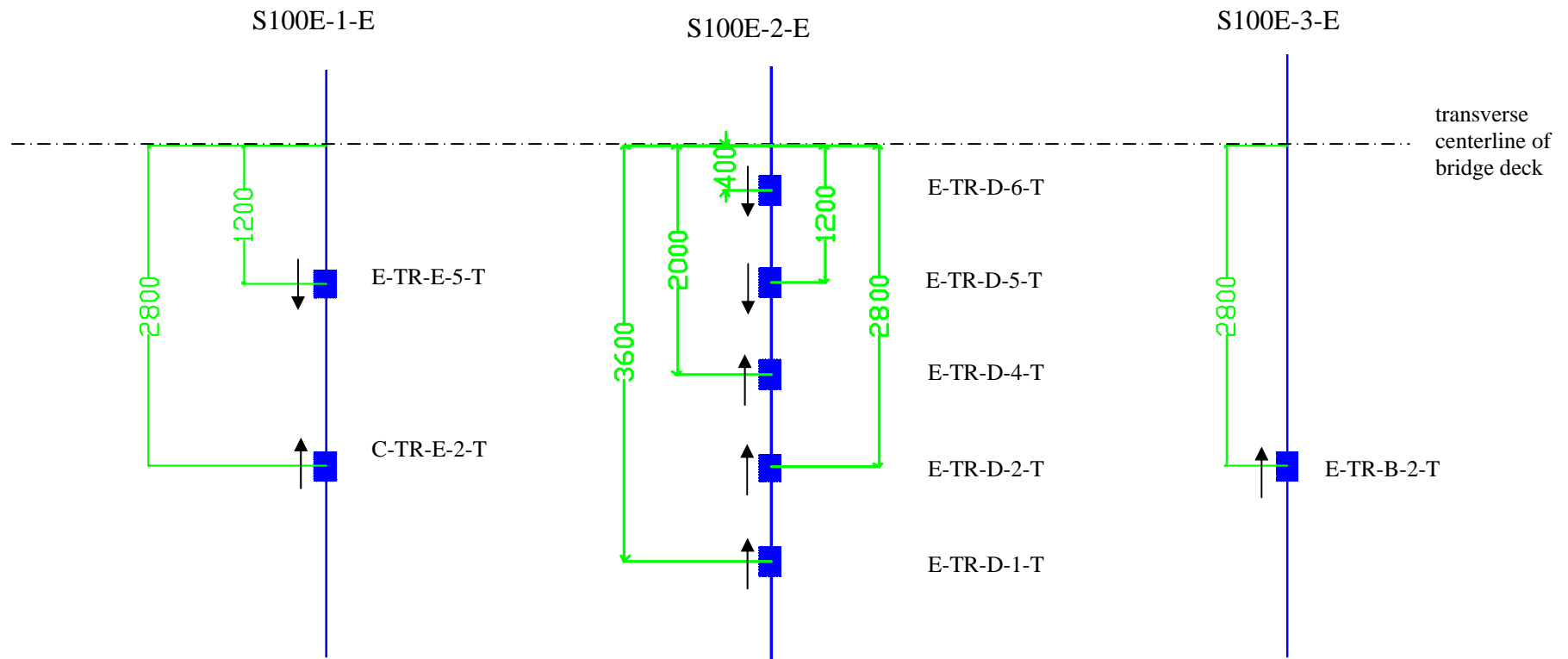
Longitudinal Bars – Bottom Mat



*Numbers at either end of the bar represent the longitudinal beginning and ending positions (in mm) with respect to the bridge deck.

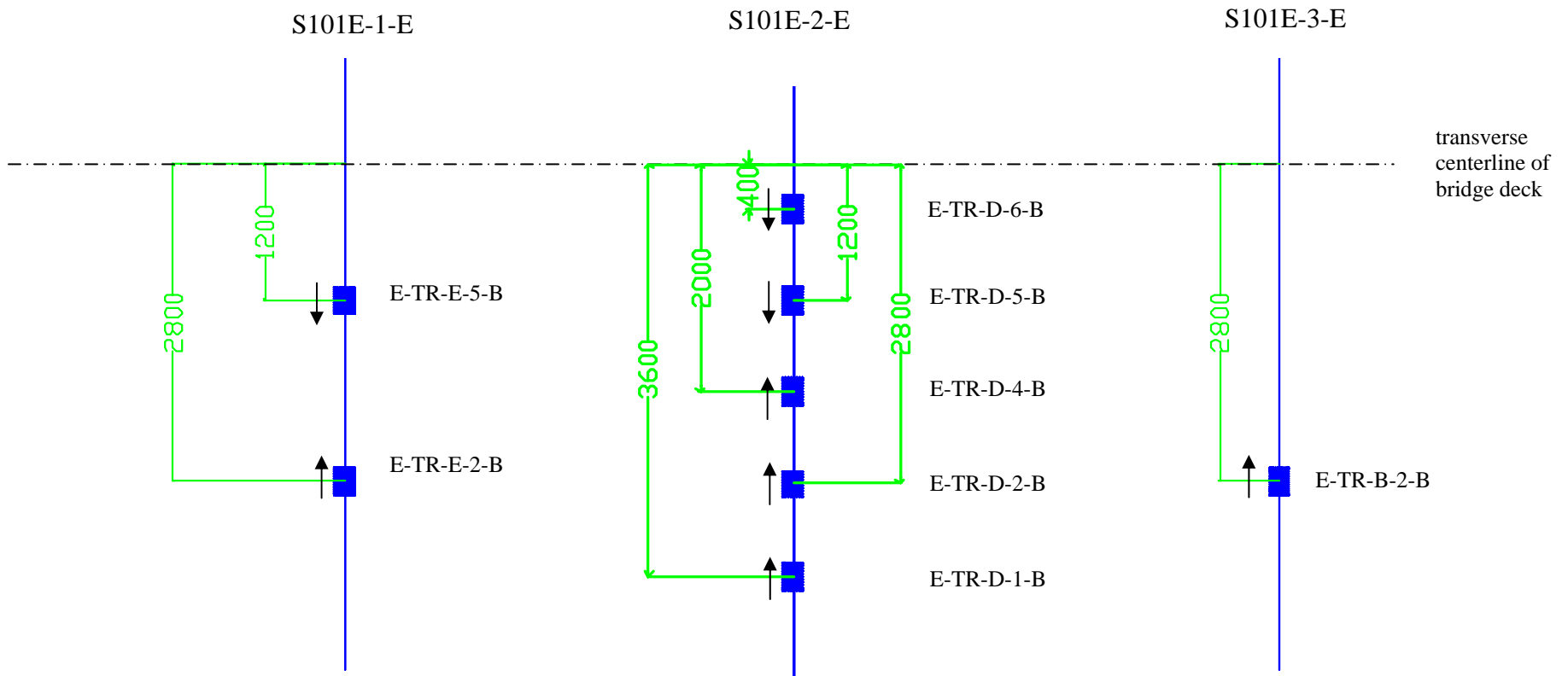
**A total of 4 S300E ~ # 19 bars of length 12.19 m are needed for instrumentation from the bottom mat.

Transverse Bars – Top Mat



* A total of 3 S100E ~ # 13 bars of length 7.64 m are needed for instrumentation from the top mat

Transverse Bars – Bottom Mat



* A total of 3 S101E ~ # 16 bars of length 7.82 m are needed for instrumentation from the bottom mat

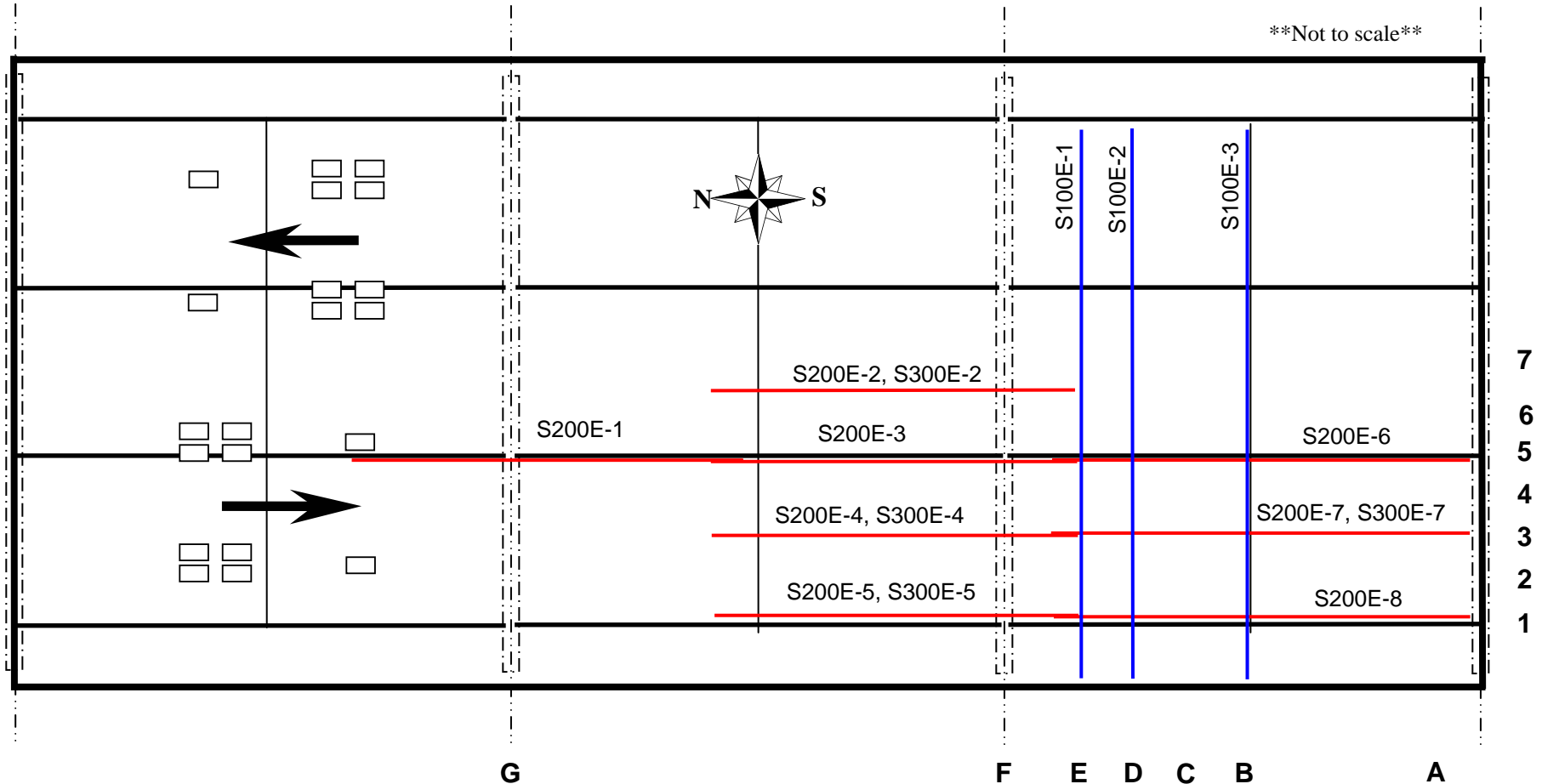
Part 3: Conventional Deck @19+23.24

Section A-3: General Bridge Deck Layout

Conventional Deck at 19+23.24

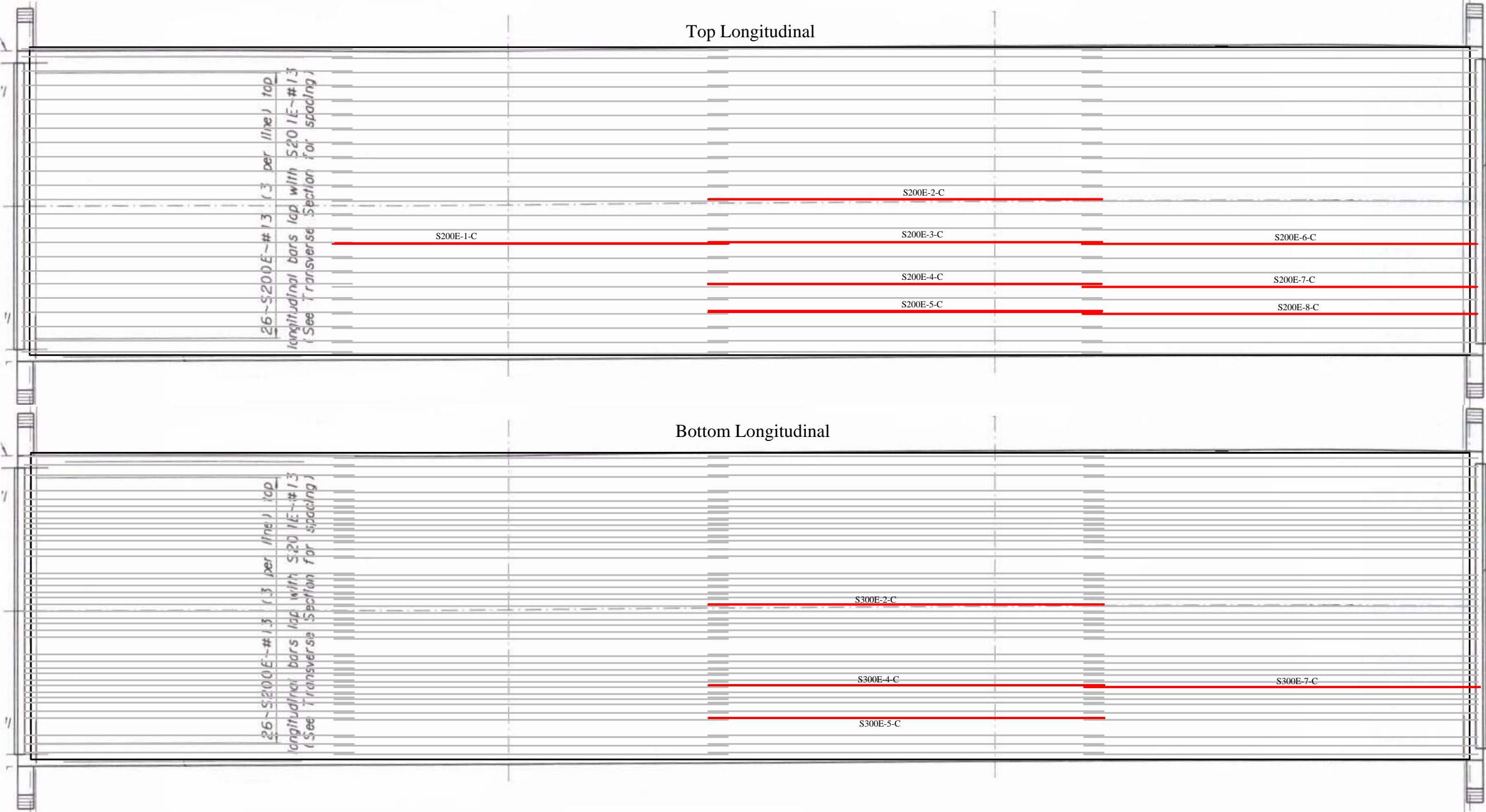
The series of numbers along the bottom of the bridge correspond to the longitudinal gage positions used in the reference number system described above. Likewise, the numbers along the right edge correspond to the transverse position of the gages used in the reference number system. The arrows on the left side show the direction of travel across the bridge of a typical truck.

The S200E bars numbered 1 through 8 are the S200E ~ # 13 bars called out in the bridge plans for the top longitudinal reinforcement. The S300E bars numbered 2,4,5, and 7 are the S300E ~ #13 bars called out in the plans for the Bottom longitudinal reinforcement. Each of the longitudinal bars is 12.19 meters in length. The S100E bars numbered 1 through 3 are the S100E ~ # 19 bars called out in the plans as the top and bottom transverse reinforcement. Each transverse bar is 8.95 meters long.



Section B-3: Specific Rebar Layout

Conventional Deck at 19+23.24





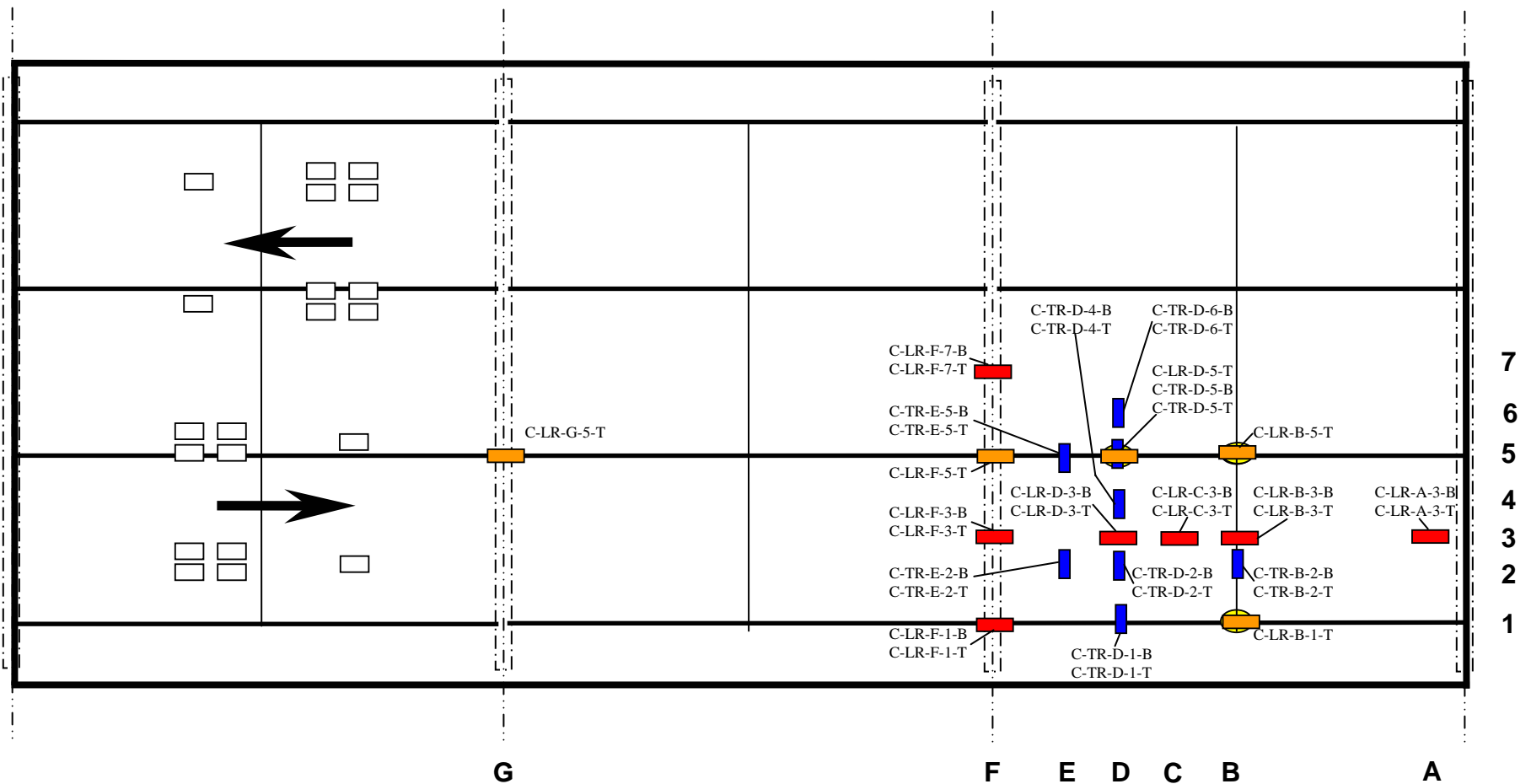
Section C-3: Plan View of Gage Locations

Conventional Deck at 19+23.24

Bonded Strain Gage Layout

6 transverse bars (16 gage locations)
12 longitudinal bars (19 gage locations)

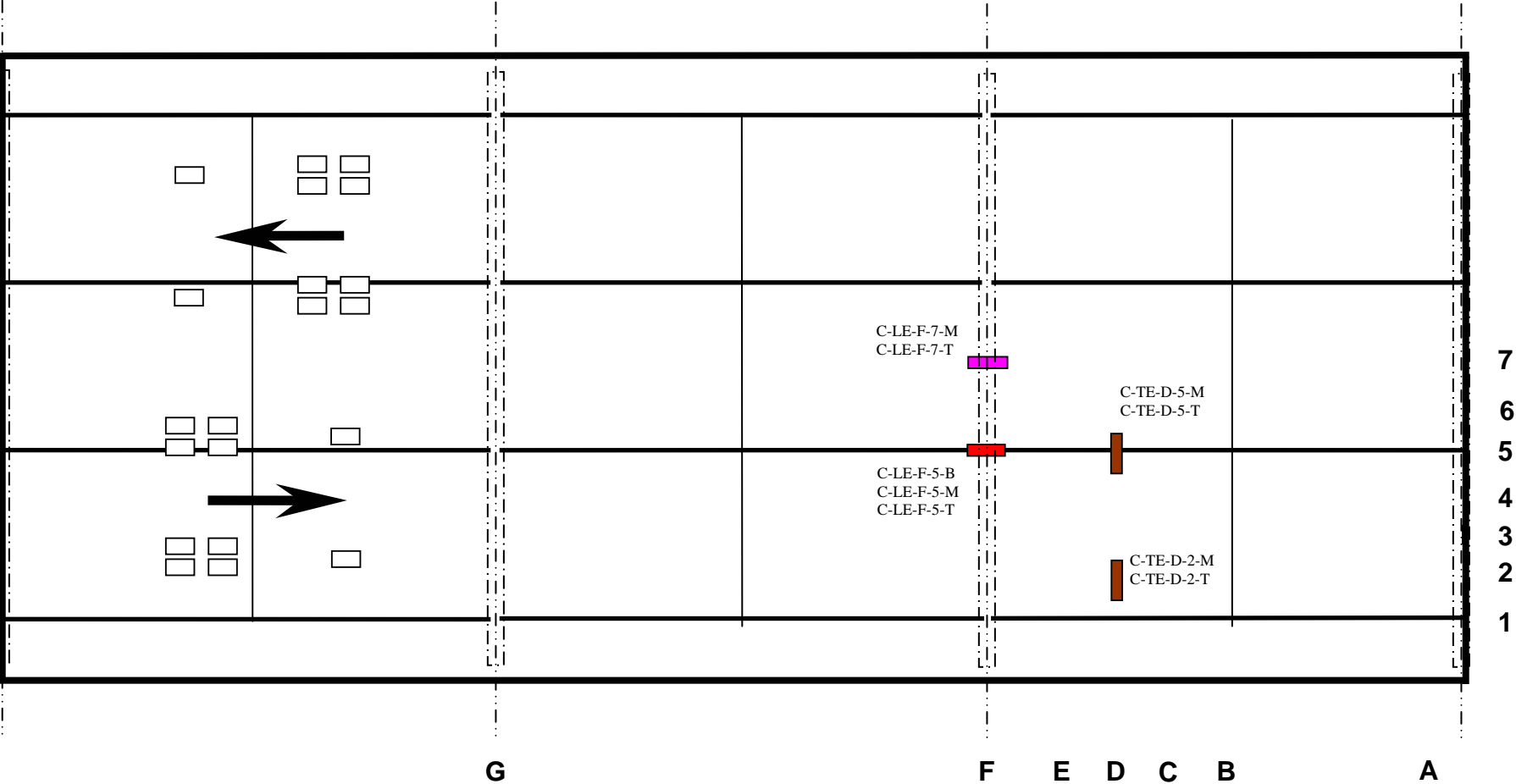
- Transverse gage, top and bottom mat
- Longitudinal gage, top and bottom mat
- Longitudinal gage, top mat only
- Longitudinal gage, bottom of stringer



Embedded Strain Gage Layout

9 locations

- Transverse gage, mid and near surface
- Longitudinal gage, mid and near surface
- Longitudinal gage, bottom, mid, and near surface


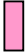




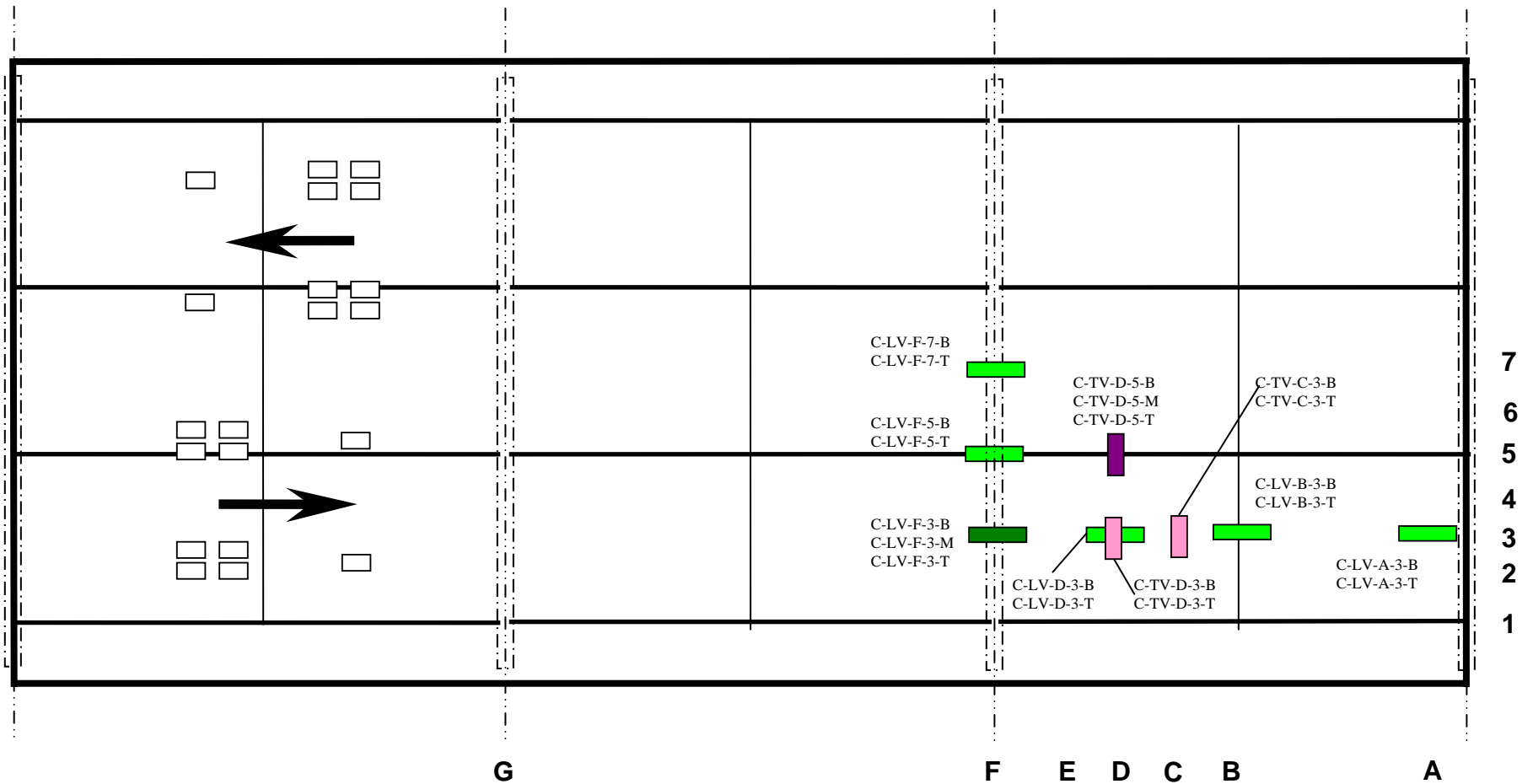
Section C-3: Plan View of Gage Locations

Conventional Deck at 19+23.24

Vibrating Wire Gage Layout

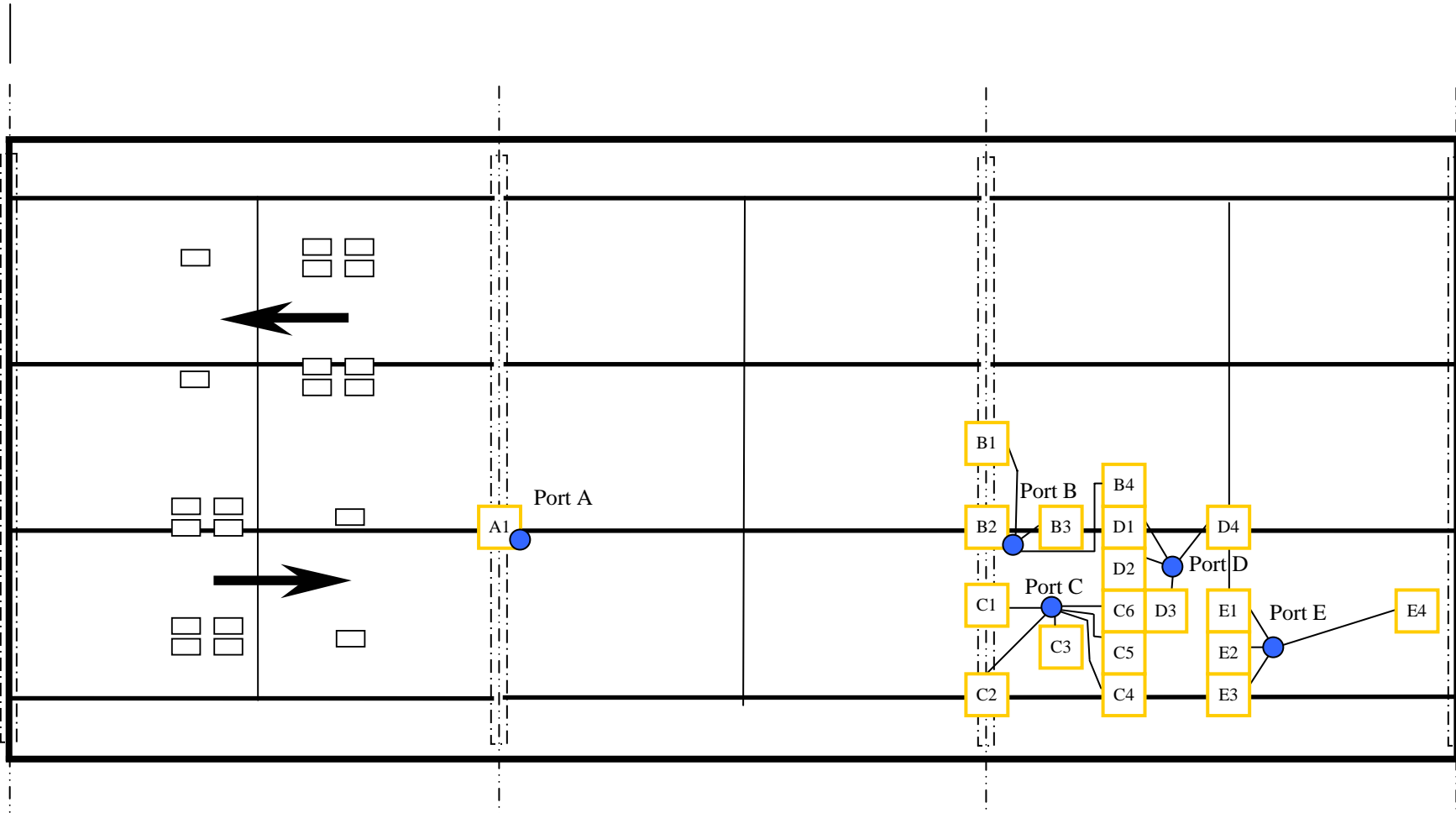
20 locations

-  Transverse gage, top, mid, and bottom
-  Transverse gage, top and bottom
-  Longitudinal gage, top and bottom
-  Longitudinal gage, top, mid and bottom



Cable Exit Layout Showing Gage Clusters

- Gage Cluster
- Exit Location
Each exit is 1½" in diameter



Section E-3: Detailed Instrumentation List

Conventional Deck at 19+23.24

Longitudinal Reinforcement Strain Gages

Table 3-1: Detailed list of strain gages bonded to longitudinal reinforcement in bridge @ 19+23.24 (conventional deck)

Reference No.	General Position			Expected Response ($\mu\epsilon$)	Cable Exit Port	Approx. Lead Wire Length (m)	Bar Number	Purpose
	X	Y	Z					
C-LR-G-5-T	Over 2 nd bent	Over stringer B	Top mat	-53.8	A1	25	S200E-1	Effect of saw cut
C-LR-F-5-T	Over 3 rd bent	Over Stringer B	Top mat	-53.8	B2	4	S200E-3	String-Bent interaction
C-LR-F-1-T	Over 3 rd bent	Over Stringer A	Top mat	-86.9	C2	7	S200E-5	String-Bent interaction
C-LR-F-1-B	Over 3 rd bent	Over Stringer A	Bot mat	-86.9	C2	7	S300E-5	String-Bent interaction
C-LR-F-3-T	Over 3 rd bent	Btwn stringer A&B	Top mat	-10.3	C1	7	S200E-4	Bending across bent
C-LR-F-3-B	Over 3 rd bent	Btwn stringer A&B	Bot mat	-10.3	C1	7	S300E-4	Bending across bent
C-LR-F-7-T	Over 3 rd bent	Btwn stringer B&C	Top mat	-6.21	B1	7	S200E-2	Bending across bent
C-LR-F-7-B	Over 3 rd bent	Btwn stringer B&C	Bot mat	-6.21	B1	7	S300E-2	Bending across bent
C-LR-D-3-T	Btwn bent & dia	Btwn stringer A&B	Top mat	6.21	C6	9	S200E-7	Local deck behavior
C-LR-D-3-B	Btwn bent & dia	Btwn stringer A&B	Bot mat	6.21	C6	9	S300E-7	Local deck behavior
C-LR-C-3-T	Btwn bent & dia	Btwn stringer A&B	Top mat	5.86	D3	11	S200E-7	Local deck behavior
C-LR-C-3-B	Btwn bent & dia	Btwn stringer A&B	Bot mat	5.86	D3	11	S300E-7	Local deck behavior
C-LR-B-3-T	Over dia 3 to 4	Btwn stringer A&B	Top mat	4.83	E1	12.5	S200E-7	Effect of diaphragm
C-LR-B-3-B	Over dia 3 to 4	Btwn stringer A&B	Bot mat	4.83	E1	12.5	S300E-7	Effect of diaphragm
C-LR-A-3-T	Over 4 th bent	Btwn stringer A&B	Top mat	-1.03	E4	20	S200E-7	Continuity effects
C-LR-A-3-B	Over 4 th bent	Btwn stringer A&B	Bot mat	-1.03	E4	20	S300E-7	Continuity effects
C-LR-B-1-T	Over dia 3 to 4	Over Stringer A	Top mat	-12.1	E3	12.5	S200E-8	Global bending
C-LR-D-5-T	Btwn bent & dia	Over stringer B	Top mat	4.14	D1	12	S200E-6	Global bending
C-LR-B-5-T	Over dia 3 to 4	Over Stringer B	Top mat	-0.345	D4	12	S200E-6	Global bending

Transverse Reinforcement Strain Gages

Table 3-2: Detailed list of strain gages bonded to transverse reinforcement in bridge @ 19+23.24 (conventional deck)

Reference No.	General Position			Expected Response ($\mu\epsilon$)	Cable Exit Port	Approx. Lead Wire Length (m)	Bar Number	Purpose
	X	Y	Z					
C-TR-D-1-T	Btwn bent & dia	Over stringer A	Top mat	6.21	C4	9	S100E-2	Stringer effects
C-TR-D-1-B	Btwn bent & dia	Over stringer A	Bot mat	6.21	C4	9	S100E-2	Stringer effects
C-TR-E-2-T	Btwn bent & dia	Btwn stringers A&B	Top mat	7.93	C3	7	S100E-1	Local deck behavior
C-TR-E-2-B	Btwn bent & dia	Btwn stringers A&B	Bot mat	7.93	C3	7	S100E-1	Local deck behavior
C-TR-D-2-T	Btwn bent & dia	Btwn stringers A&B	Top mat	6.9	C5	9	S100E-2	Local deck behavior
C-TR-D-2-B	Btwn bent & dia	Btwn stringers A&B	Bot mat	6.9	C5	9	S100E-2	Local deck behavior
C-TR-B-2-T	Over diaphragm	Btwn stringers A&B	Top mat	-2.07	E2	11	S100E-3	Effect of diaphragm
C-TR-B-2-B	Over diaphragm	Btwn stringers A&B	Bot mat	-2.07	E2	11	S100E-3	Effect of diaphragm
C-TR-D-4-T	Btwn bent & dia	Btwn stringers A&B	Top mat	7.24	D2	10.5	S100E-2	Local deck behavior
C-TR-D-4-B	Btwn bent & dia	Btwn stringers A&B	Bot mat	7.24	D2	10.5	S100E-2	Local deck behavior
C-TR-E-5-T	Btwn bent & dia	Over stringer B	Top mat	5.86	B3	5	S100E-1	Stringer effects
C-TR-E-5-B	Btwn bent & dia	Over stringer B	Bot mat	5.86	B3	5	S100E-1	Stringer effects
C-TR-D-5-T	Btwn bent & dia	Over stringer B	Top mat	4.83	D1	12	S100E-2	Stringer effects
C-TR-D-5-B	Btwn bent & dia	Over stringer B	Bot mat	4.83	D1	12	S100E-2	Stringer effects
C-TR-D-6-T	Btwn bent & dia	Btwn stringers B&C	Top mat	6.9	B4	10.5	S100E-2	Local deck behavior
C-TR-D-6-B	Btwn bent & dia	Btwn stringers B&C	Bot mat	6.9	B4	10.5	S100E-2	Local deck behavior

Section E-3: Detailed Instrumentation List

Conventional Deck at 19+23.24

Embedded Strain Gages

Table 3-3: Detailed list of embedded strain gages in bridge @ 19+23.24 (conventional deck)

Reference No.	Orientation	General Position			Expected Response ($\mu\epsilon$)	Cable Exit Port	Approx. Lead Wire Length (m)	Purpose
		X	Y	Z				
C-LE-F-5-B	Longitudinal	Over 2 nd bent	Over stringer B	Bot	-15.6	B2	4	Stringer – Bent interaction
C-LE-F-5-M	Longitudinal	Over 2 nd bent	Over stringer B	Mid	-15.6	B2	4	Stringer – Bent interaction
C-LE-F-5-T	Longitudinal	Over 2 nd bent	Over stringer B	Top	-15.6	B2	4	Stringer – Bent interaction
C-TE-D-5-M	Transverse	Btwn bent & dia	Over stringer B	Mid	-1.8	D1	12	Stringer effects
C-TE-D-5-T	Transverse	Btwn bent & dia	Over stringer B	Top	-1.8	D1	12	Stringer effects
C-LE-F-7-M	Longitudinal	Over 2 nd bent	Btwn stringers B & C	Mid	-1.8	B1	7	Bending across bent
C-LE-F-7-T	Longitudinal	Over 2 nd bent	Btwn stringers B & C	Top	-1.2	B1	7	Bending across bent
C-TE-D-2-M	Transverse	Btwn bent & dia	Btwn stringers A & B	Mid		C5	9	Local bending effects
C-TE-D-2-T	Transverse	Btwn bent & dia	Btwn stringers A & B	Top		C5	9	Local bending effects

Section E-3: Detailed Instrumentation List

Conventional Deck at 19+23.24

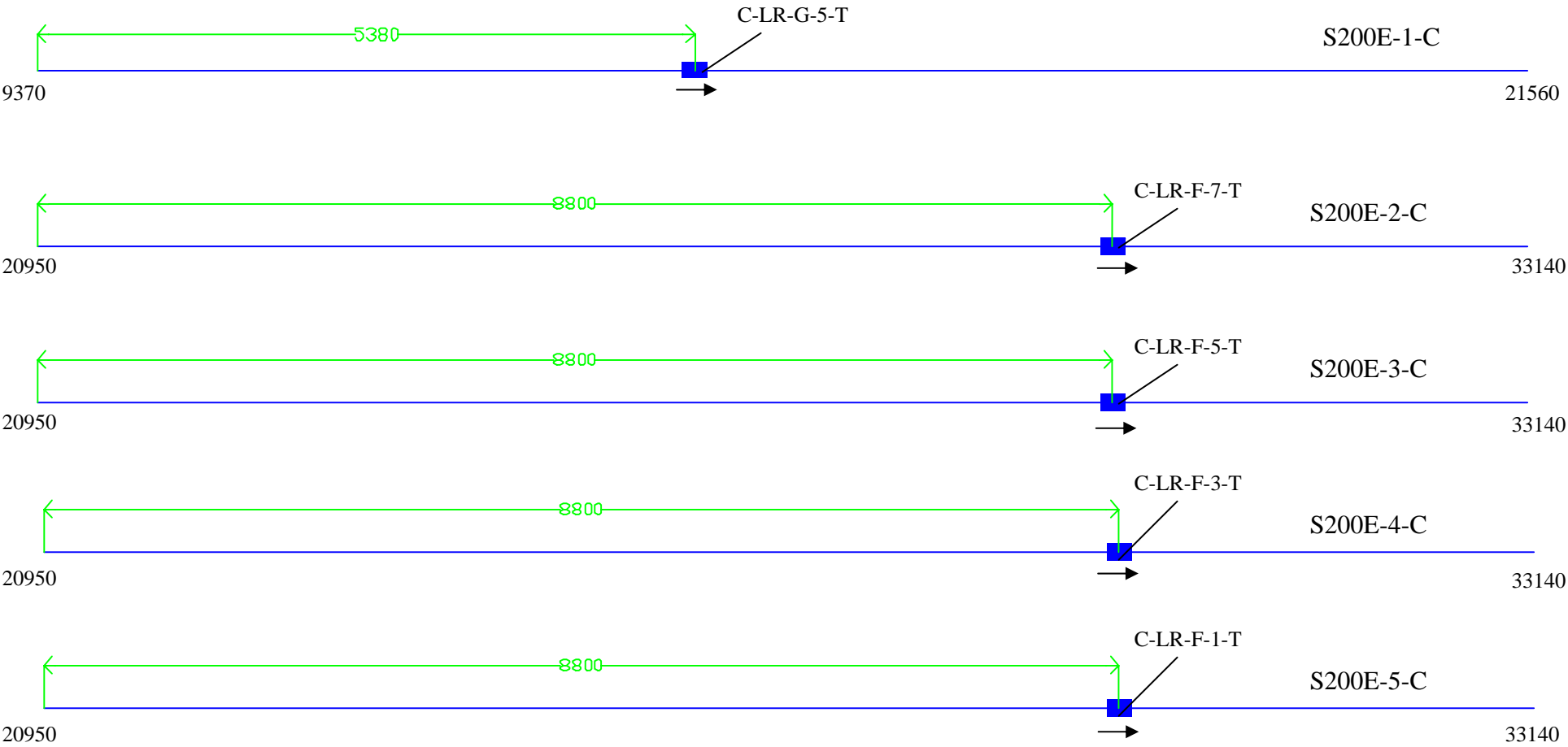
Vibrating Wire Strain Gages

Table 3-4: Detailed list of vibrating wire strain gages in bridge @ 19+23.24 (conventional deck)

Reference No.	Orientation	General Position			Expected Response ($\mu\epsilon$)	Cable Exit Port	Approx Lead Wire Length (m)	Purpose
		X	Y	Z				
C-LV-F-3-B	Longitudinal	Over bent	Btwn stringers A & B	Bot	-3.0	C1	7	Bending across bent
C-LV-F-3-M	Longitudinal	Over bent	Btwn stringers A & B	Mid	-3.0	C1	7	Bending across bent
C-LV-F-3-T	Longitudinal	Over bent	Btwn stringers A & B	Top	-3.0	C1	7	Bending across bent
C-LV-F-5-B	Longitudinal	Over bent	Over stringer B	Bot	-15.6	B2	4	Stringer – bent interaction
C-LV-F-5-T	Longitudinal	Over bent	Over stringer B	Top	-15.6	B2	4	Stringer – bent interaction
C-LV-F-7-B	Longitudinal	Over bent	Btwn stringers B & C	Bot	-1.8	B1	7	Bending across bent
C-LV-F-7-T	Longitudinal	Over bent	Btwn stringers B & C	Top	-1.8	B1	7	Bending across bent
C-LV-D-3-B	Longitudinal	Btwn bent & dia	Btwn stringers A & B	Bot	1.8	C6	9	Local deck behavior
C-LV-D-3-T	Longitudinal	Btwn bent & dia	Btwn stringers A & B	Top	1.8	C6	9	Local deck behavior
C-LV-B-3-B	Longitudinal	Over dia	Btwn stringers A & B	Bot	-1.4	E1	12.5	Diaphragm effects
C-LV-B-3-T	Longitudinal	Over dia	Btwn stringers A & B	Top	-1.4	E1	12.5	Diaphragm effects
C-LV-A-3-B	Longitudinal	Over 4 th bent	Btwn stringers A & B	Bot	-0.3	E4	20	Effects of end Bent
C-LV-A-3-T	Longitudinal	Over 4 th bent	Btwn stringers A & B	Top	-0.3	E4	20	Effects of end bent
C-TV-D-3-B	Transverse	Btwn bent & dia	Btwn stringers A & B	Bot	2.3	C6	9	Local deck behavior
C-TV-D-3-T	Transverse	Btwn bent & dia	Btwn stringers A & B	Top	2.3	C6	9	Local deck behavior
C-TV-C-3-B	Transverse	Btwn dia & bent	Btwn stringers A & B	Bot	2.7	D3	11	Local deck behavior
C-TV-C-3-T	Transverse	Btwn dia & bent	Btwn stringers A & B	Top	2.7	D3	11	Local deck behavior
C-TV-D-5-B	Transverse	Btwn bent & dia	Over stringer B	Bot	1.4	D1	12	Stringer effects
C-TV-D-5-M	Transverse	Btwn bent & dia	Over stringer B	Mid	1.4	D1	12	Stringer effects
C-TV-D-5-T	Transverse	Btwn bent & dia	Over stringer B	Top	1.4	D1	12	Stringer effects

Section F-3: Detailed Drawings of Reinforcement with Bonded Strain Gages *Conventional Deck at 19+23.24*

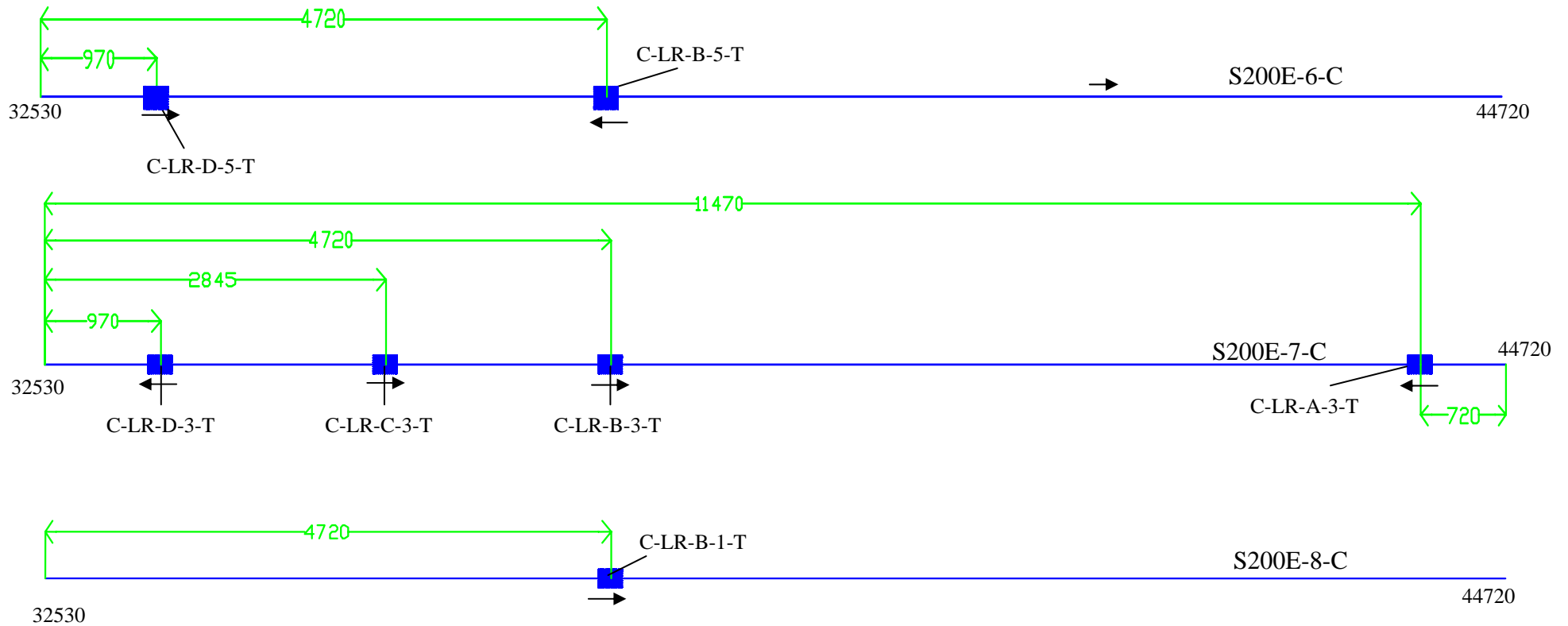
Longitudinal Bars – Top Mat



*Numbers at either end of the bar represent the longitudinal beginning and ending positions (in mm) with respect to the bridge deck.

Section F-3: Detailed Drawings of Reinforcement with Bonded Strain Gages *Conventional Deck at 19+23.24*

Longitudinal Bars – Top Mat (continued)

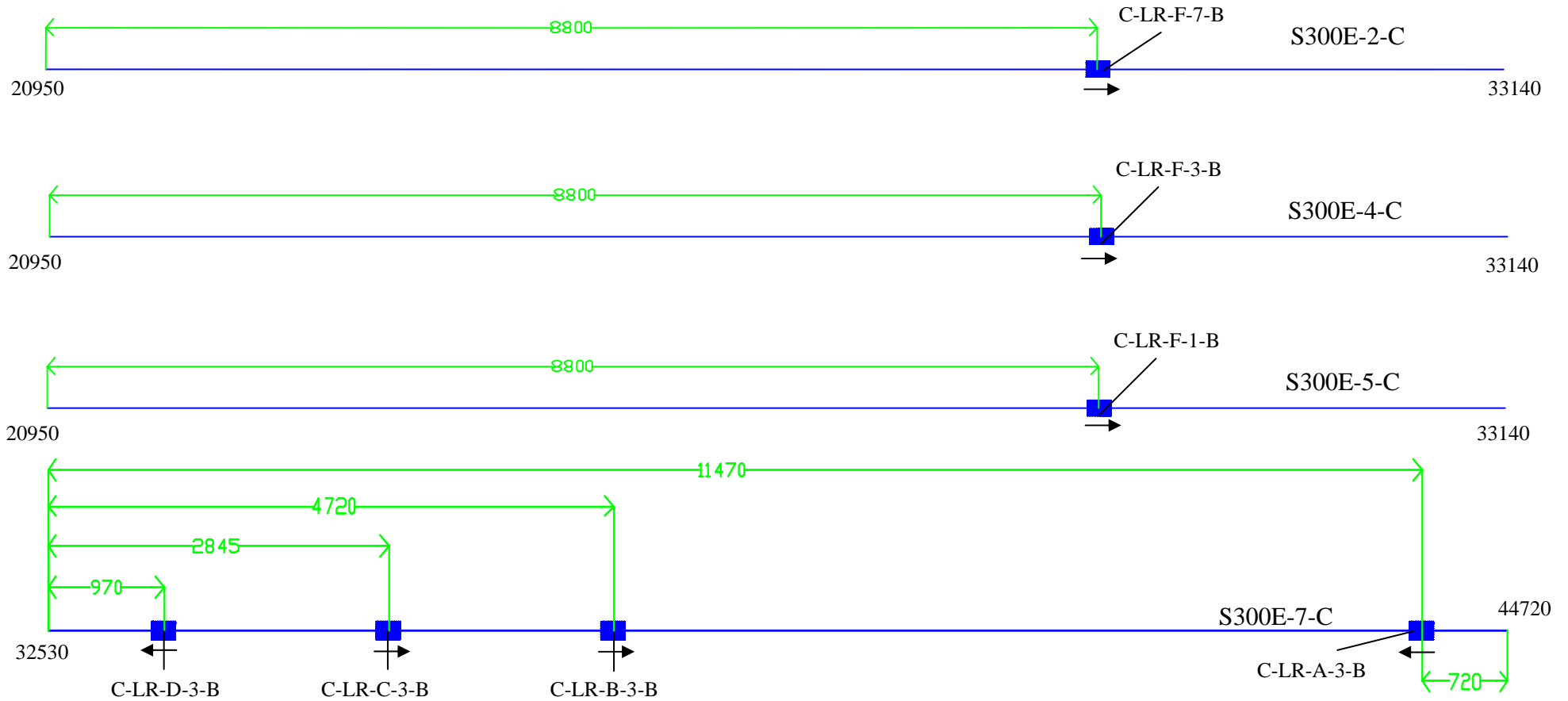


*Numbers at either end of the bar represent the longitudinal beginning and ending positions (in mm) with respect to the bridge deck.

**A total of 8 S200E ~ #13 bars of length 12.19 m are needed for instrumentation from the top mat.

Section F-3: Detailed Drawings of Reinforcement with Bonded Strain Gages *Conventional Deck at 19+23.24*

Longitudinal Bars – Bottom Mat

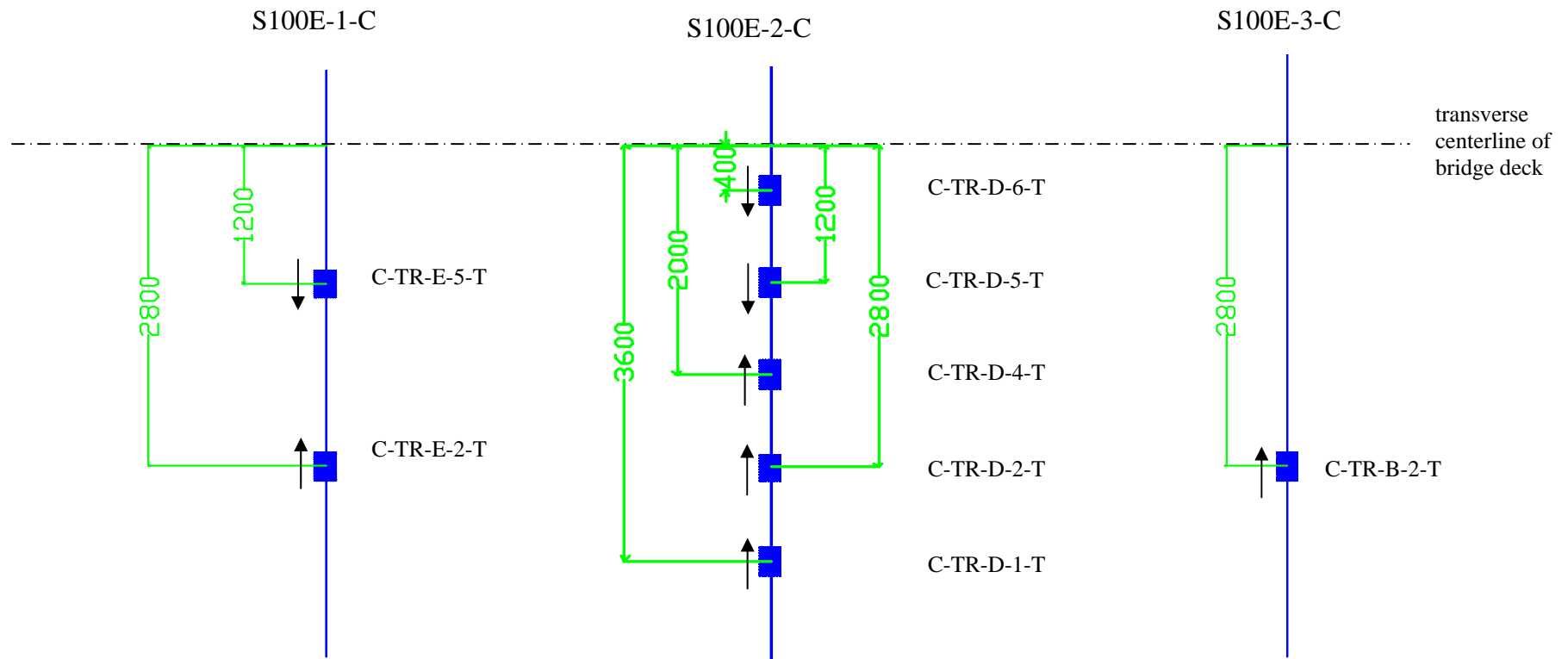


*Numbers at either end of the bar represent the longitudinal beginning and ending positions (in mm) with respect to the bridge deck.

**A total of 4 S300E ~ # 19 bars of length 12.19 m are needed for instrumentation from the bottom mat.

Section F-3: Detailed Drawings of Reinforcement with Bonded Strain Gages *Conventional Deck at 19+23.24*

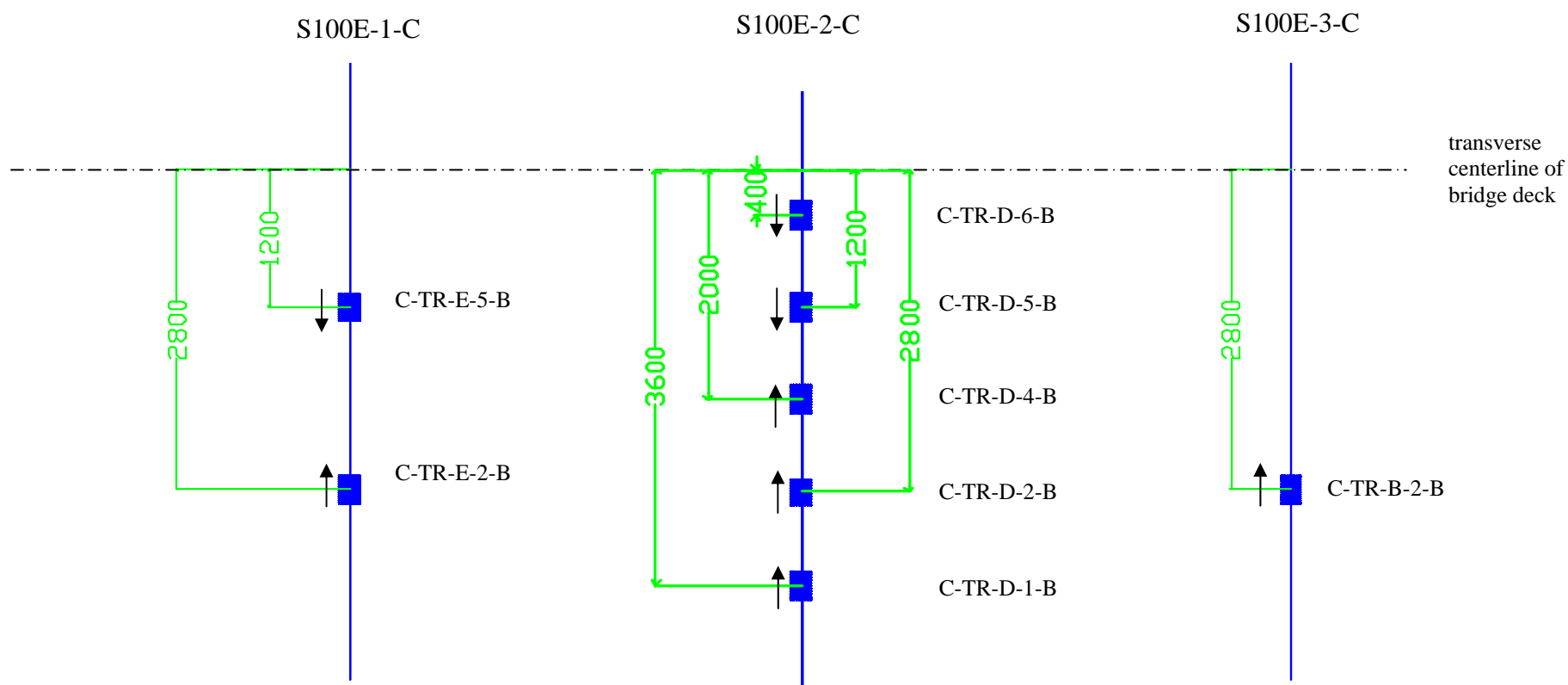
Transverse Bars – Top Mat



* A total of 3 S100E ~ # 19 bars of length 8.95 m are needed for instrumentation from the top mat

Section F-3: Detailed Drawings of Reinforcement with Bonded Strain Gages *Conventional Deck at 19+23.24*

Transverse Bars – Bottom Mat



* A total of 3 S100E ~ # 19 bars of length 8.95 m are needed for instrumentation from the bottom mat

Appendix F – Crack Survey Maps

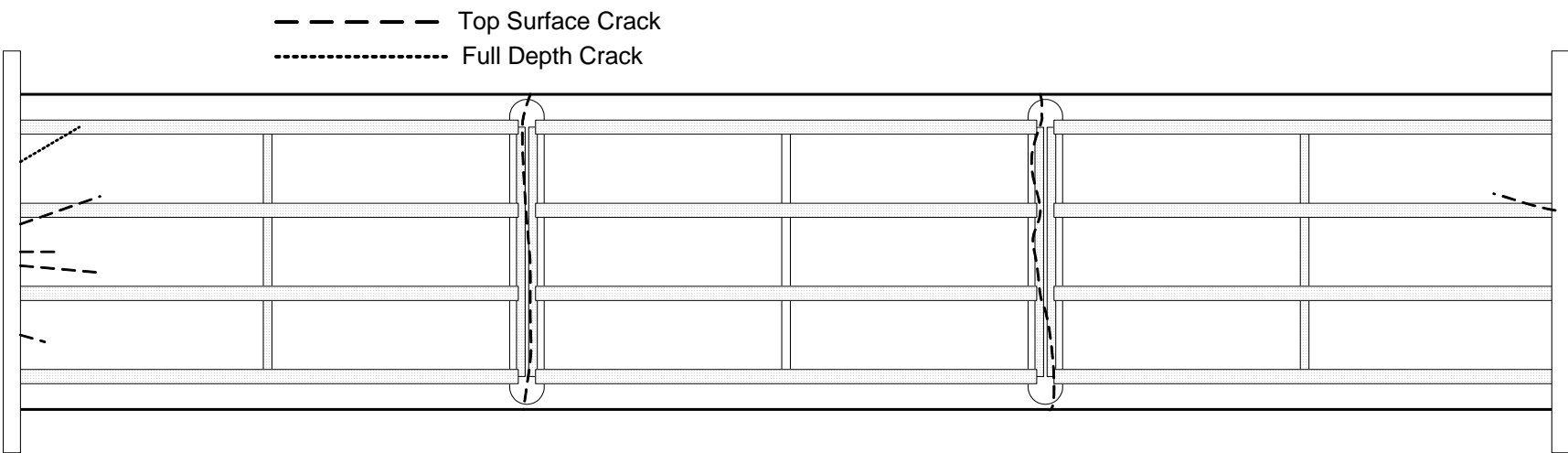


Figure F-1: Detailed Map of Crack Survey on the Conventional Bridge Deck

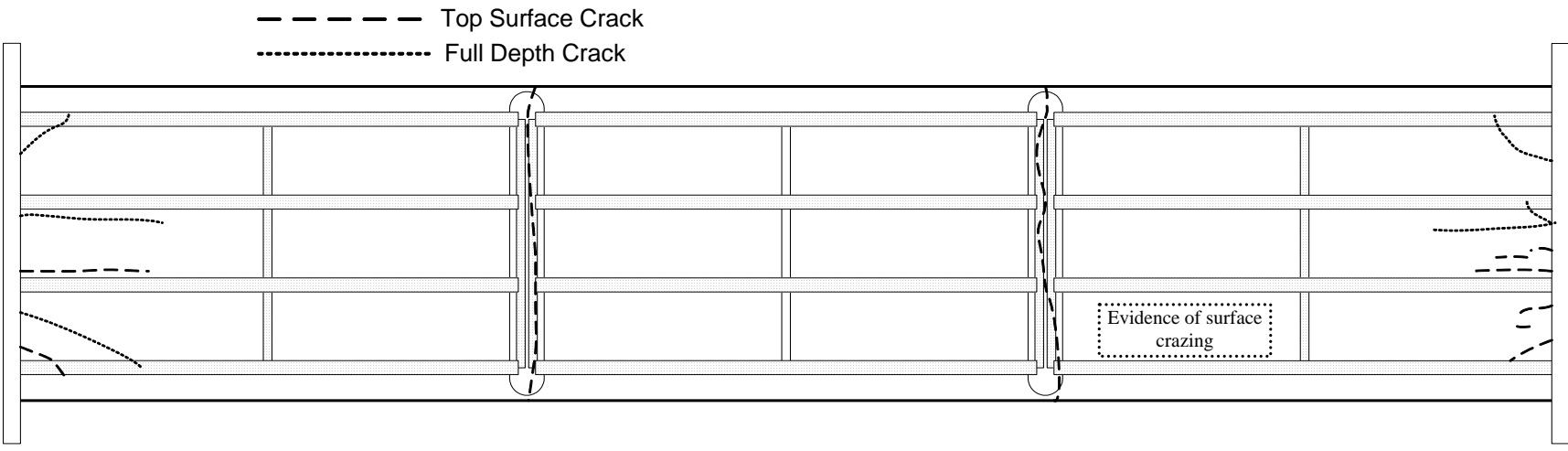


Figure F-2: Detailed Map of Crack Survey on the Empirical Bridge Deck

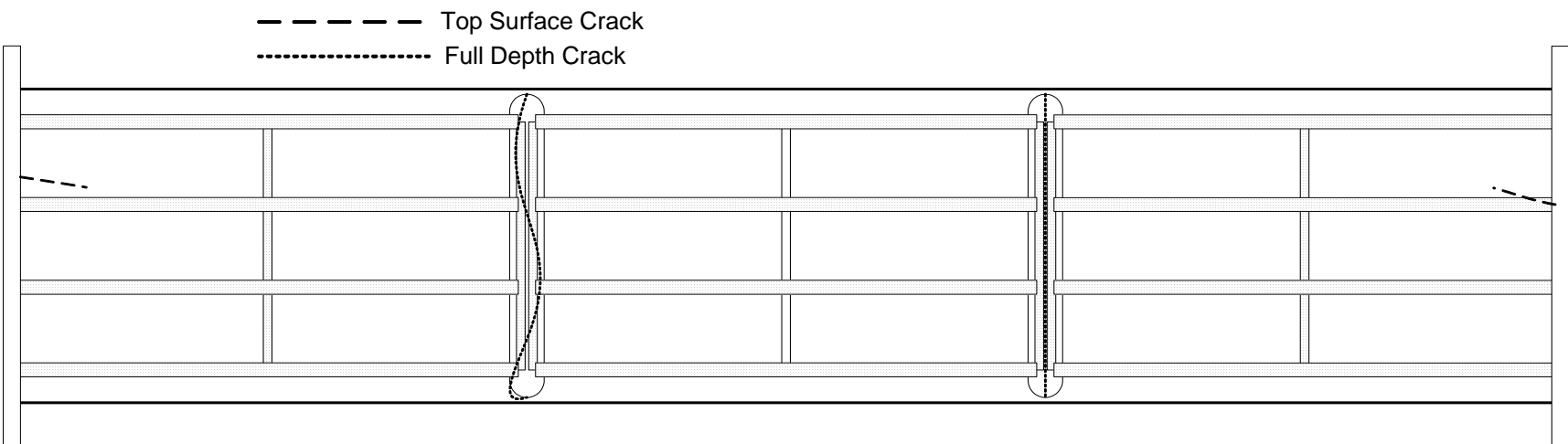


Figure F-3: Detailed Map of Crack Survey on the HPC Bridge Deck